THE GEOLOGICAL EVOLUTION AND SEDIMENTARY DYNAMICS OF HOUT BAY, SOUTH AFRICA

MICHAEL R. MACHUTCHON (B.SC. HONS)

DEPARTMENT OF GEOLOGICAL SCIENCES
UNIVERSITY OF CAPE TOWN

Submitted for the fulfillment of the academic requirements for the degree of Master of Science in the Department of Geological Sciences, University of Cape Town.

August 2012

ABSTRACT

Hout Bay is situated on the Atlantic seaboard of the Cape Peninsula, in the Western Cape Province of South Africa approximately 17 km southwest of Cape Town. Hout Bay is a southward opening bay that hosts a fishing harbour and coastal residential town. This study was initiated to map the marine geology of Hout Bay and to quantify and explain the sediment dynamics of the area. This is important as Hout Bay has the only substantial accumulation of Quaternary sediments on the Atlantic Seaboard of the Cape Peninsula.

The Hout Bay study area was saturated with the latest in cutting-edge geophysical techniques to collect detailed and comprehensive bathymetric, sidescan sonar, magnetic, seismic and beach profiling data. Collectively these data can be used to map offshore geological units as well as infer how Hout Bay has responded to the varying changes in sea-level throughout the Quaternary and allow for the reconstruction of the geological evolution of the Hout Bay seafloor. The bathymetric data collected between 5 and 60 m water depth delineate different lithological outcrops and the extent of sediment accumulation on the seabed in Hout Bay. Six surficial acoustic facies were identified from sidescan sonar data. *In situ* diver observations allowed these acoustic facies to be correlated to the geology with "Prominent Reef[1]" correlated to Cape Granite, "Subdued Reef" to Table Mountain Group Sandstone, "Scattered Reef" to a sub-facies within Subdued Reef and "Shelf Sand" and "Bioclastic Gravel" to the Holocene sediment wedge. Anthropogenic Features identified included two shipwrecks, the breakwater armouring of Hout Bay Harbour and a submarine outfall pipeline.

Seismic data showed the geological succession within Hout Bay to be Cambrian granite basement overlain unconformably by Ordovician mudstone and sandstone and capped by unconsolidated Pleistocene/Holocene sediment. The Cambrian and Ordovician lithologies have been intruded by Cretaceous dolerite dykes associated with the breakup of Gondwana. The seismic data allowed unconsolidated sediment volumes to be approximated at 126 x 10^6 m^3. Magnetic data delineate the sub-bottom orientation and location of numerous dolerite

[1] For the purpose of this dissertation the term "reef" is used to describe any consolidated, lithological outcrop on the seafloor.

dykes, one of which exhibits a slightly different relative intrusion age (intruded during a polarity reversal).

In terms of unconsolidated sediments, crest heights, orientation and wavelengths of the sub-aqueous bedforms and the relative elongation of bedform fields show a predominately bimodal distribution related to the dominant southwest swell and refraction of these waves around the western headland of the Sentinel.

Quaternary sea-level fluctuations have caused Hout Bay to become exposed aerially and completely drowned. This study has shown that the response of marine sediments to these sea-level changes is that the majority of the unconsolidated sediment in Hout Bay can be attributed to Pleistocene sediment which was deposited during sea-level lowstands when the land prograded onto the continental shelf. The dominant source of modern sediment is from biogenic sources related to the reef outcrops (carbonate factories) found in the study area and the primary mechanism for introducing sediment into Hout Bay is from Longshore Drift from the south as it is forced to bifurcate when it encounters the offshore Vulcan Rock – Tafelberg Reef complex of the Sentinel Peak headland. Sediment is also derived from reworked, highstand, coastal Pleistocene deposits, the deposition of sediment during lowstands, coastal erosion from wave action, aeolian derived sediment along the western margin of the Cape Peninsula, chemical weathering of minerals in the exposed lithological outcrops surrounding the study area and terrigenous input from the Disa River. All of which are entrained by the northward flowing longshore drift. Wave and swell action allow sediment to accumulate against the toe of Chapman's Peak and Constantiaberg with fine- to medium grained sediment accumulating along Hout Bay Beach and in the lower energy environments of the study area. A small portion of the accumulated sediment is winnowed off, entrained into the sediment headland bypass corridor as dunes in the Karbonkelberg Dunefield. With increased pressure from the urbanisation of Hout Bay, alien grass species have been introduced to the dunefield as well as the dunes at the head of the bypass on Hout Bay Beach. This introduction has stabilised the dunes and starved the sediment bypass corridor. The majority of unconsolidated sediment continues with the longshore drift vector and tidal pumping around and out of the bay to continue migration towards the north.

PREFACE

The work detailed in this study was carried out as a collaboration between the Marine Geoscience Unit of the Council for Geoscience and the Department of Geological Sciences of the University of Cape Town, under the supervision of Prof. John Compton.

The project was jointly funded by the Council for Geoscience and the Department of Science and Technology (DST). Work started in November 2008 and was completed mid 2011.

I know the meaning of plagiarism and declare that all of the work in this dissertation, save for that which is properly acknowledged, is my own and has not been submitted in any form for a degree at any other tertiary institution.

Name: Michael MacHutchon Signed: Signed by candidate

Date: 8 November 2012

ACKNOWLEGEMENTS

As with most projects there is a whole host of people I am grateful to, for the successful completion of this dissertation. Firstly I must thank my supervisor Prof. John Compton. John thank you for steering and nudging me in the right direction at the appropriate times. I must also apologise for being slack with my progress reports and at the same time thank you for not putting any undue pressure on to me by hounding me to do them.

The next person to whom I am eternally indebted is "Hazel". Thank you for supporting me in all aspects of this project. When things looked like they would never materialise you gave me the encouragement to "vasbyt". Professionally and academically your input and guidance was unrivalled and I truly could not have done this without you.

Then on another level, a plethora of fellow marine professionals need to be thanked. Gordon Rigg and Jonathan Hargraves of Marine Data Consultants (MDC). Thanks guys for all the extra time spent puzzling over software and hardware issues and ultimately fixing them. Gordon, thank you so much for extending yourself and your companies resources well beyond what was originally agreed to. Rio Leuci and the laboratory staff of Environmental Mapping Services (EMS) for processing the sediment samples. Doug Slogrove of Kwazulu Boat Hire for fixing the boomer and bouncing many geophysical ideas off of. Dr. John Rogers for reading and commenting on draft reports and Mike Woodborne for valuable insight into some of the older data.

Lastly I must thank the people that made this possible. Firstly the Department of Science and Technology (DST) for making the necessary funds available to acquire the data. The incredible staff of the Marine Geoscience Unit (MGU). Our manager Dr. Luc Chevallier for all his support and encouragement, the survey and diving team of Hayley Cawthra, Willlem Kupido and Wilhelm Van Zyl and our "lab guy" Clive Botha. Many others have also helped pitch in along the way, Chris Lambert as a helping hand underwater, Willem "Bob" De Wet and Errol Wiles as student/team members and "Boy", "Lizzard" and "KRM" as spare (weekend) crew.

Thank you all I owe you an enormous debt of gratitude!

TABLE OF CONTENTS

1. INTRODUCTION

The aim of this investigation is to provide a qualitative assessment of the nearshore sedimentary dynamics of the Atlantic seaboard in the vicinity of Hout Bay, a south-facing embayment on the Cape Peninsula. The objectives of this investigation are to establish the regional geological evolution based on bedrock geology and structures followed by the determination of the distribution and composition of the overlying, unconsolidated sediment. These objectives are obtained by collecting high resolution geophysical and sedimentological data for the relatively small but representative area of Hout Bay from which the sediment dynamics can be interpreted and estimates derived of the sediment volumes involved.

Hout Bay is situated on the Atlantic seaboard of the Cape Peninsula, in the Western Cape Province of South Africa approximately 17 km southwest of Cape Town. It is the only southward opening bay on the west coast of the Cape Peninsula, nestled between Chapman's Peak on its eastern flank and the peak of The Sentinel (which forms part of Karbonkelberg) on its western margin (Figure 1.1). When viewed in the context of the West Coast of South Africa, Hout Bay can be considered as representative of the coastline between Cape Columbine and Cape Agulhas. There is an active fishing harbour in the northwest corner of the bay which helps support the growing population of Hout Bay and the two informal settlements of Imizamo Yethu and Hangberg on its periphery. A recent topic of debate for the Cape Peninsula is the state of the lucrative tourist beaches; surrounding sediment supply or starvation and any potential pollution threats. This study will help to address these issues by imaging the submarine outfall and the scour associated with its discharge, by quantifying the amount of sediment moving through the study area and into the headland bypass corridor. The study will show how sediment is being starved from this corridor which could have far reaching implications for supply of sediment to the beaches to the north of the study area. On the eastern flank of the study area is the famous Chapman's Peak Drive which connects Hout Bay to Noordhoek. This road is a very popular tourist destination and is for the most part constructed on the nonconformity between the Cape Granites and overlying Table Mountain Group sandstones. The study area extends from Hout Bay Beach towards Noordhoek and from Chapman's Peak to Vulcan Rock covering an area of 13.417 km^2.

The trend for most of the past nearshore and offshore geological mapping off the western margin of South Africa has been to focus on the diamondiferous inner shelf of Namaqualand (De Decker, 1987; Woodborne, 1991) and the various sedimentary inputs into this system (Rogers, 1977). False Bay has also had some scientific interest (Terhorst, 1988; du Plessis and Glass, 1991), however mostly on a regional scale focusing on the False Bay Dyke Swarm (Day, 1986; Backeberg, 2009). The bulk of the scientific investigations, however, focus more on the continental shelf and shelf break (Dingle, 1970; 1971; 1973; Birch *et al.*, 1976; Rogers, 1977; 1980; Dingle *et al.*, 1983; 1987; Rogers and Rau, 2006; Wigley, 2005; Compton and Wiltshire, 2009).

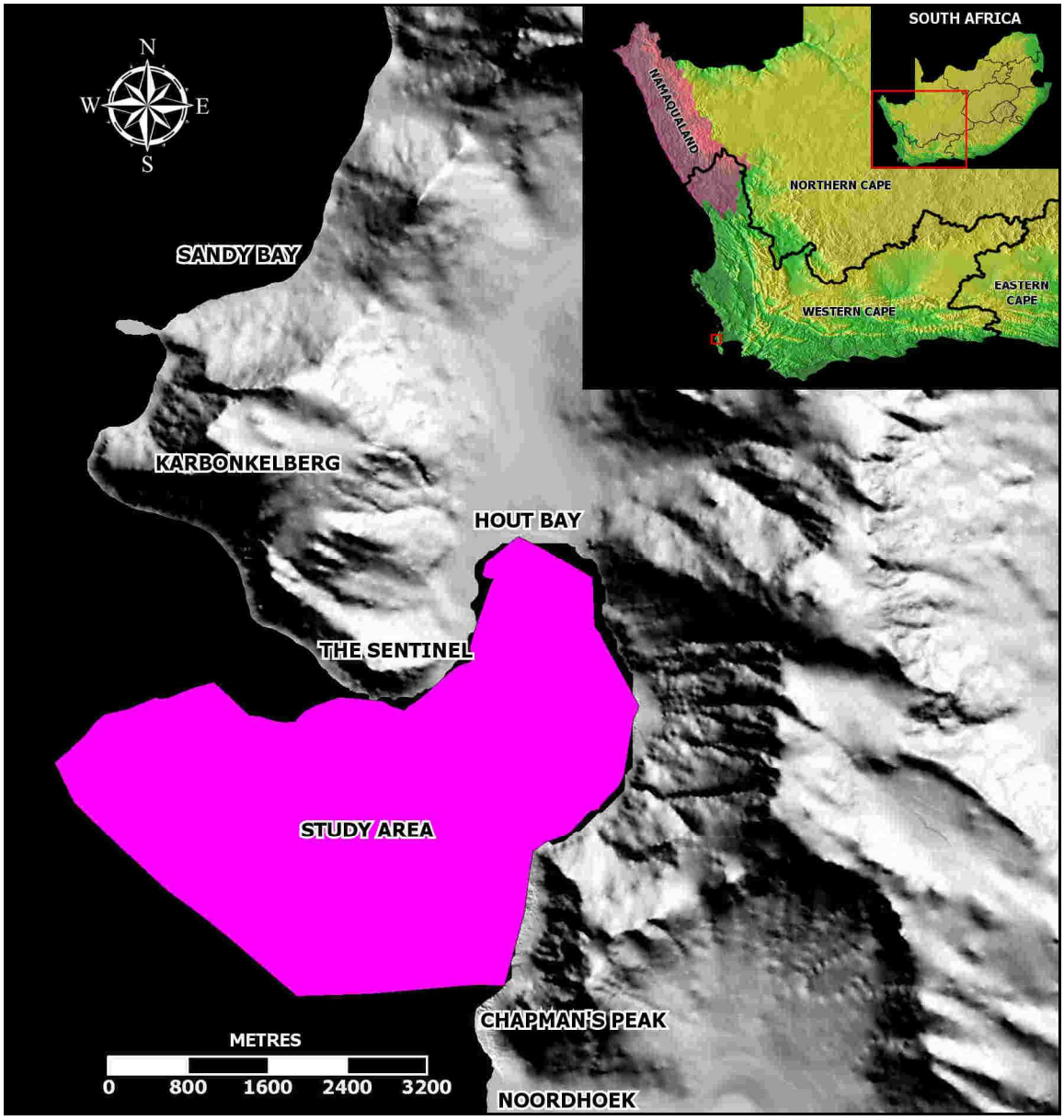

Figure 1.1. Locality map of study area. Image of South Africa courtesy of NOAA Satellite and Information Service (NOAA, 2010).

The geophysical data will be used to infer how Hout Bay responded to the numerous sea level fluctuations of the Quaternary Period and allow for a reconstruction of the complete geological evolution of Hout Bay. Supplementary to the above, the study area serves as a case study to exhibit the value of saturating an area with the latest in cutting-edge geophysical techniques with a view to unravelling the geological evolution of the area and to demonstrate the importance of similar mapping programs along the nearshore zones of our coastline.

These data demonstrate the effectiveness of using geophysical techniques to document submarine geology with the view to reconstruct and better understand the regional geological evolution. These data show that during the Cambrian, Cape Granites intruded the Proterozoic sediments of the Malmesbury Group (Scheepers and Scoch, 2006). These sediments were subsequently eroded off the granitoids and overlain by the Ordovician to Devonian sediments of the Table Mountain Group sandstones under predominantly shallow marine to fluvial depositional environments (Hartnady and Rogers, 1990; Thamm and Johnson, 2006). Once deposited these sediments were deformed during the Cape Orogeny which culminated in the Jurassic as the South American and African plates collided into one another. During the Cretaceous, Gondwana broke apart and the Atlantic Ocean started to open. Tensional rift faulting characterised this period and as a result numerous dolerite dykes intruded the pre-existing lithologies of Hout Bay forming part of the larger False Bay dolerite dyke swarm (Day, 1986). Although the Cretaceous is synonymous with increased offshore sedimentation, Hout Bay falls within a buoyant basement high referred to as the Columbine/Agulhas Arch which shows evidence of being tectonically stable since the Palaeozoic (Dingle *et al.*, 1983). The onset of the Cenozoic is characterised by a marine transgression and the progradation of sediments onto the continental shelf. During the Miocene, however, South Africa experienced uplift and tilting towards the southwest which caused a re-activation of the Columbine/Agulhas Arch (Partridge and Maud, 1987) and effectively planed off all the sediments that had accumulated locally around Hout Bay. Re-activation of the arch again occurred during the Pliocene (Wigley and Compton, 2006). The Quaternary was a relatively stable tectonic environment with the dominant forces at play being the changes in eustatic sea-level directly related to glacial and interglacial cycles. These changes in sea-level are well documented by wave cut terraces at various elevations both above and below current sea-levels.

The sedimentological data when viewed in conjunction with the geophysical data show how the dominant longshore drift vector bifurcates in response to the rugged offshore morphology associated with the offshore reef complex of the Sentinel. Part of the sediment transported by longshore drift is then focused into Hout Bay with the fine- to medium grained fractions ultimately accreting along Hout Bay Beach. A portion of this accumulation is then entrained by aeolian vectors into the headland bypass to be re-introduced into the marine conveyor near Sand Bay yet the majority of the sand continues along the western flank of the bay, most probably by the mechanism of tidal pumping to be reintroduced into the northward migrating longshore drift on the seaward side of the offshore reef complexes. The sediment dynamics within the study area are complex. Any perturbations with this sediment conveyor could have far reaching implications for sediment accumulation or erosion further along the system. The migration of the dunes into the headland bypass dunefield between Hout Bay and Sandy Bay is being arrested by the introduction of invasive dune vegetation and by the city of Cape Town stockpiling the sediment behind the dunes. This starves sediment to the headland bypass and any sediment traps further along the conveyor, manifesting as erosion of important tourist beaches to the north of the Cape Peninsula. Analysis of the sediment volumes and the budgets of Hout Bay have revealed that the core of the sediment is Pleistocene in origin, related to the frequent glacial periods and sea-level lowstands experienced during this time. The other dynamic, modern inputs and outputs, remains fairly balanced.

Anecdotal to the above, an interesting oceanographic phenomenon takes place at the foot of The Sentinel which sets Hout Bay apart globally as one of the premier big wave surfing localities. This surf spot has been nicknamed "Dungeons" and it lives up to its somewhat imposing name (Figure 1.2 & Figure 1.3). During the winter months the South Atlantic experiences severe storm conditions. For large surf at Dungeons a few requirements need to be met, namely a storm needs to develop in the southwest Atlantic and move towards Hout Bay. The storm must then veer eastward and pass to the south of the country, but the swell generated by the storm must continue on its collision course. Once this southwest swell reaches the Sentinel it is funnelled between Vulcan Rock and Tafelberg Reef, further increasing the energy of the wave until it collides with the steeply sloping toe of the Sentinel. Once this occurs the swell is stacked on top of itself with the top of the swell ultimately overtaking the base to produce surf in excess of 30 ft (10 m). The force of such big waves is also key to understanding the formation of the numerous wave cut platforms seen in the

study area and regionally around the coastline of South Africa and the production of bioclastic sediment.

Figure 1.2. An unknown surfer sizing up a wave during the Big Wave Africa, Dungeons, Hout Bay. Photograph by Alan Van Gysen (Red Bull BWA, 2008).

Figure 1.3. Grant "Twiggy" Baker at Dungeons. Photograph by Nick Muzik (Wavescapes, 2009).

2. PHYSICAL SETTING

2.1. Climate

Climatic conditions along the western margin of South Africa (from Cape Point to Namibia) are primarily influenced by meteorological effects originating offshore in the Atlantic and Southern Oceans. Anticyclonic conditions originate at approximately 30ºS as a result of a subtropical high-pressure zone in the Atlantic Ocean, and easterly moving cyclonic cells develop between 35ºS and 40ºS. The relative locations of these features vary seasonally by either a poleward or an equatorward shift of approximately 3º (Schultze, 1965; Nelson and Hutchings, 1983; MacHutchon, 2008; Hutchings *et al.*, 2009).

2.1.1. Wind

In summer the western margin of South Africa is dominated by strong southerly winds. These anticyclonic winds originate from the South Atlantic high and follow the coastline. This pattern results from the arid nature of the hinterland which forms a thermal barrier across which the winds cannot cross (Nelson and Hutchings, 1983; De Decker, 1987; Woodborne, 1991). In winter it is reversed. As a result of the South Atlantic high moving a few degrees northwest, westerly moving circumpolar cyclonic air masses are allowed to collide with the land. Strong gale-force northwesterly and westerly winds predominate during these periods although they are often short lived (Nelson and Hutchings, 1983).

During the autumn and spring seasons it is common for a large high-pressure cell to form over the interior of the country, the net result of which is for air to move catabatically from the interior to the coast heating up as it descends, manifesting as strong (15 m/s) offshore winds commonly referred to as berg winds (Jackson, 1947; De Wet, 1979; Woodborne, 1991). It has been estimated by Shannon and Anderson (1982) that the amount of sediment transported offshore along the Namaqualand coast during one bergwind event, is the same as that of the annual discharge of the Orange River, which in turn was estimated by Rogers (1977) to be in the order of approximately 50 x 10^6 tons. It must be noted that these berg wind conditions are less frequent for the study area.

The wind regime for the Cape Peninsula and the study area of Hout Bay is illustrated in Figure 2.1. These data show that the dominant wind direction is southeast or northwest which agrees with the typical summer/winter pattern.

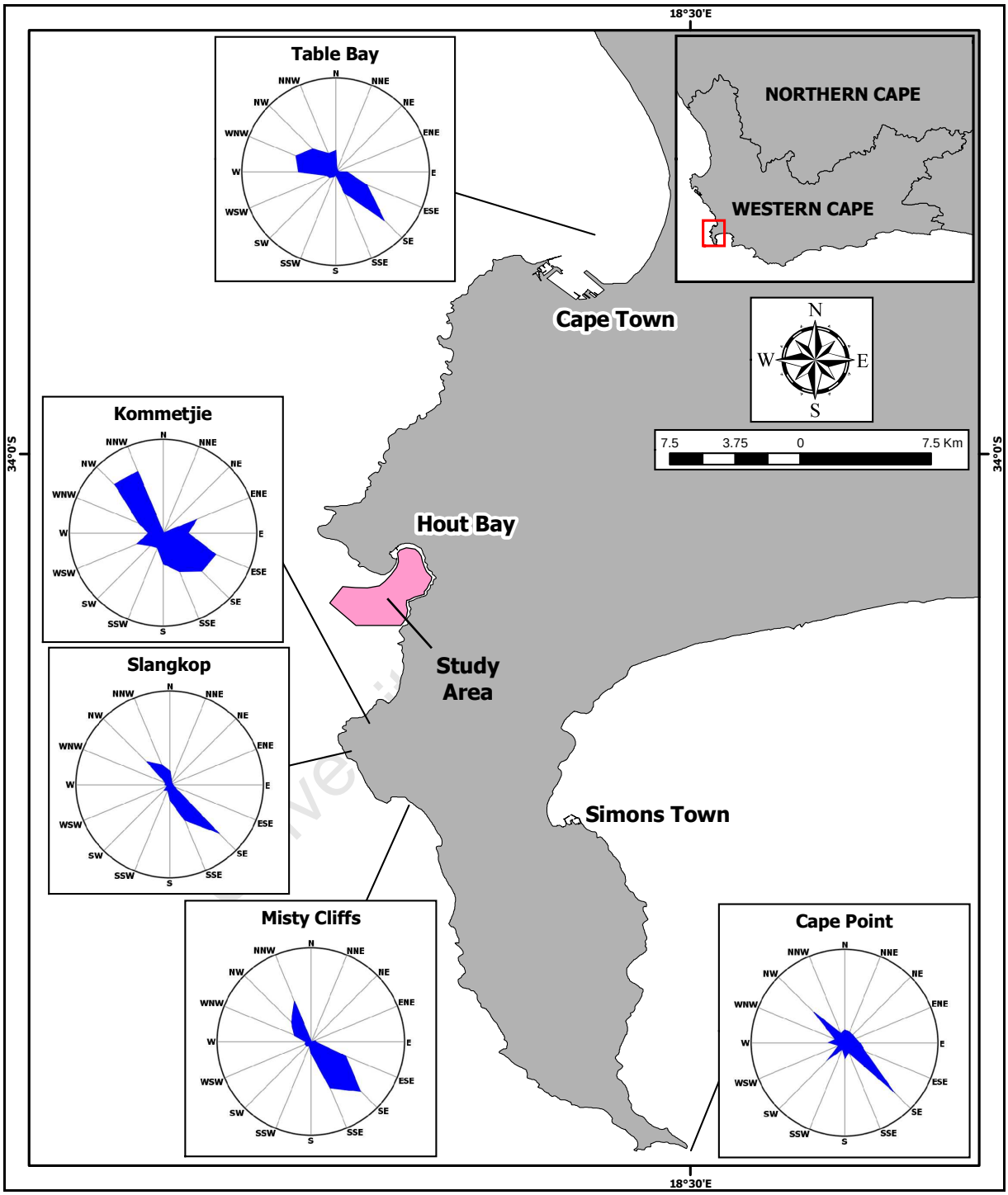

Figure 2.1. Historical wind roses for five stations around the Cape Peninsula between 2002 and 2009. Modified from data recorded by South African Weather Service, accessed through Windfinder (2010).

2.1.2. Precipitation

The Cape Peninsula and Hout Bay experience a typical Mediterranean climate, with dry, hot summers and cold, wet winters. Rainfall data obtained from the South African Weather Service for Kirstenbosch Gardens illustrates this point. These data span 57 years and illustrate that mean summer rainfall is between 36 and 50 mm/month, whilst mean winter rainfall is between 205 and 270 mm/month (Figure 2.2). These data will be slightly higher than that of Hout Bay yet the trend illustrated will remain the same.

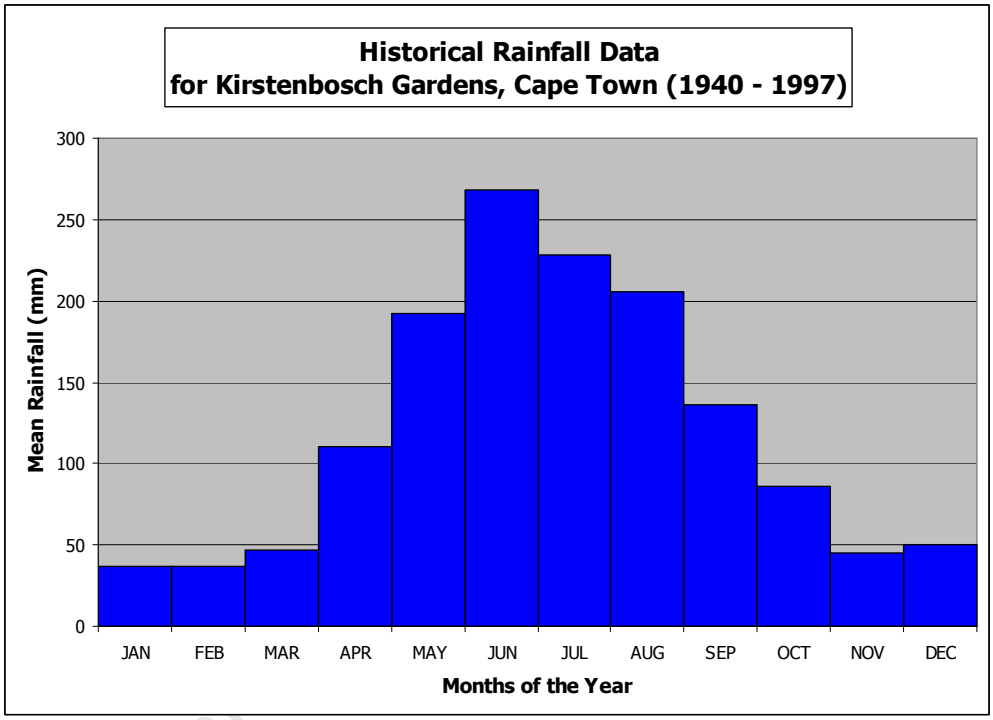

Figure 2.2. Historical rainfall data for Kirstenbosch Gardens, Cape Town from 1940–1997. Data obtained from South African Weather Service, accessed through 1stweather (2010).

2.2. Oceanography

The southern tip of Africa has a unique oceanographic setting as it is the convergence point between two major oceanic currents, namely the Benguela Current which bounds the western margin of southern Africa (Peterson and Stramma, 1991; Wedepohl *et al.*, 2000), and the Agulhas Current which bounds the eastern margin (Gordon, 1985) (Figure 2.3). At the convergence of these currents an interesting oceanographic feature occurs in the form of large anticyclonic circulations of warmer water which "detach" from the Agulhas Current and

propagate into the south Atlantic in a north westerly direction. These features are commonly referred to as Agulhas Rings and have been described by Robinson (1983). An introduction into each oceanographic feature is discussed below.

2.2.1. The Benguela Current

The Benguela Current is part of the large South Atlantic gyre. The Benguela Upwelling System (BUS) is a typical worldwide eastern boundary current system in that it is characterised by the upwelling of cold nutrient-rich water as a response to wind shearing (Skogen, 1999; Boyer *et al.*, 2000; Shannon, 2009). The simplification of this process has been described by Shannon (2009). The displacement of warmer surficial water is equatorwards and offshore according to an Ekman Spiral (Price *et al.*, 1987) which is a combination of longshore winds and the rotation of Earth. The net result of this is a drop in sea-level against the coastline and an upwelling of water from below (and alongshore) to correct the imbalance. Coastal upwelling systems such as the BUS have near the front or shelf-break slow poleward undercurrents and fast equatorward jet currents (Shannon, 2009). On the shelf there is a poleward under current close inshore with velocities of 5 cm/s, whereas in the extreme south the Agulhas Bank surface waters funnel northwards into a shelf-edge frontal jet with speeds ranging from 25 – 75 cm/s (Shannon, 2009).

The water masses that constitute the BUS are Tropical and Subtropical Surface Waters (occurring between water depths of 0 – 50 m), Central Waters (80 – 400 m), Antarctic Intermediate Waters (AAIW) (700 – 800 m), North Atlantic Deep Water (NADW) (1,000 – 3,500 m), and Antarctic Bottom Water (AABW) (< 4,000 m), (Garzoli *et al.*, 1996; Shannon, 2009). It is the Central Waters that upwell along the coastline of southern Africa.

The combined equatorward transport of surface, central and AAIW in the BUS is believed to be in the order of 15 – 25 Sv (where 1 Sv is 10^6 m^3/s), with upper layer speeds of 10 – 30 cm/s (Shannon, 2009). The southern part of the Benguela is fed by the South Atlantic Current and by leakage from the Agulhas Current (Indian Ocean) in the form of Agulhas Rings and filaments. There are typically six rings per year with translation speeds of 5 – 8 cm/s (Shannon, 2009).

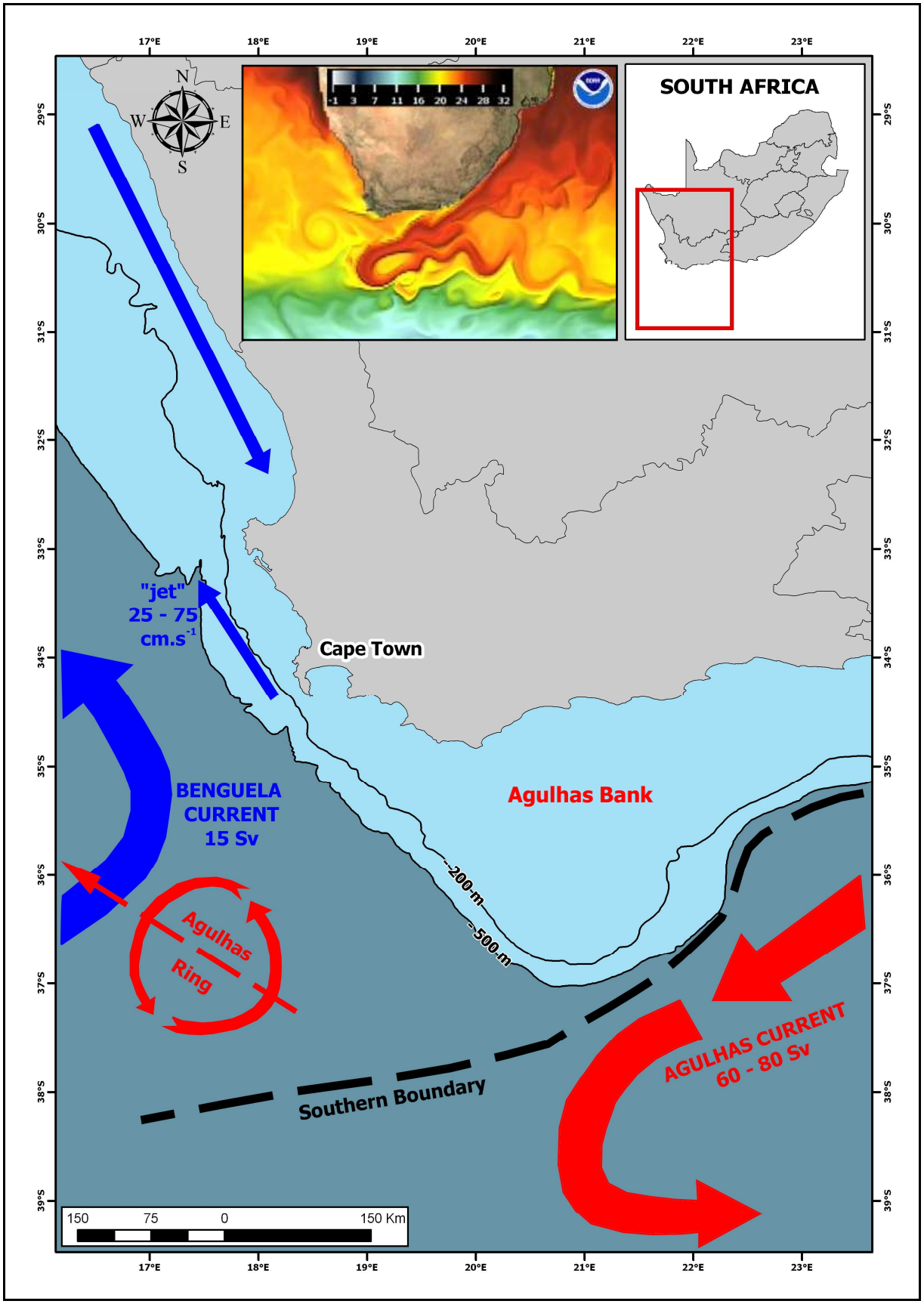

Figure 2.3. Regional oceanographic currents for the southeast Atlantic and southwest Indian Ocean, modified from Shannon (2009). Inset image of sea surface temperatures depicts Agulhas retroflection and ring, modified from NOAA (2011).

2.2.2. The Agulhas Current, Rings and Filaments

The Agulhas Current bounds the east coast of South Africa, originating from the re-circulation of water in the southeast Indian Ocean sub-gyre (Gordon, 1985; Stramma and Lutjeharms, 1997), and to a lesser degree from the warm Moçambique channel eddies (De Ruijter *et al.*, 2002) and the East Madagascar Current. Variability in the current manifests predominantly in the form of Natal pulses (Bryden *et al.*, 2003). The architecture of these pulses is such that they take the form of large solitary meanders with a cold-core cyclone and are found on the inshore margin of the main Agulhas Current (Lutjeharms and Roberts, 1988). Natal pulses typically migrate at speeds of approximately 10 km/day with a frequency of six times per year (Lutjeharms *et al.*, 2003). The significance of these pulses is that after almost every pulse an Agulhas Ring is shed into the south Atlantic (Van Leeuwen *et al.*, 2000).

Surface speeds of the Agulhas Current can be relatively rapid with maximum reported surface velocities of 200 cm/s (Boebel *et al.*, 1998). The current is typically topographically controlled and is found predominantly along the shelf break, although numerous eddies exist along the coastline which are in the opposite direction to the main core (Flemming, 1978; 1980; 1981). Beal and Bryden (1999) and Donohue *et al.* (2000) discovered an undercurrent at 800 m directly beneath the surface core, flowing equatorward with a maximum velocity of 30 – 40 cm/s. The Agulhas Current is one of the largest currents in the world in terms of volume. Over the years many different authors such as Gordon (1985), Toole and Warren (1993), Beal and Bryden (1999), Donohue *et al.* (2000), Bryden *et al.* (2003) and Shannon (2009) have come up with transported water volumes ranging from 60 – 80 Sv.

Unlike other western boundary current separation, the Agulhas extends past the southern tip of Africa before turning out to sea on its own accord (Veronis, 1973; De Ruijter, 1982). Because of this the Agulhas makes an extended elongated loop into the South Atlantic (south of Cape Town, South Africa) before returning back into the Indian Ocean (Bang, 1970; Gründlingh, 1978; Harris *et al.*, 1978; Lutjeharms and van Ballegooyen, 1984; Quartly and Srokosz, 1993). This feature is called the Agulhas Retroflection (Harris *et al.*, 1978) and forms a loop with a diameter of 340 km (Lutjeharms and van Ballegooyen, 1988) from which large anticyclonic rings are shed (Duncan, 1965; Harris *et al.*, 1978; Gordon, 1985). The propagation of the rings is varied with seafloor morphology and the trend of the continental

rise contributing extensively to translation vectors (Olsen and Evans 1986), but in broad terms it can be stated that the rings are formed at the retroflection then move in a northwesterly direction (towards the Vema Seamount) at approximate velocities of 12 cm/s (Lutjeharms and van Ballegooyen, 1988). Each ring is unique in terms of size and internal structure, yet on average most rings exhibit a diameter of between 280 – 320 km (Olsen and Evans, 1986; Gyory *et al.*, 2004) and represent water volumes of 2 – 10 Sv (Shannon, 2009). Coupled with ring formation is the formation of Agulhas filaments (Whittle *et al.*, 2008). These filaments form from the upper layers of the landward border of the Agulhas Current. After initial translation of the water with the shedding of a ring in a northwest direction they are advected southward by the eddy currents which form in the lee of the Agulhas Bank (Whittle *et al.*, 2008). This results in warmer surface water mixing much closer inshore than the Agulhas Rings relatively close to Cape Town and the study area.

2.2.3. Tidal and Wave Regime

From recorded tidal data the tidal range in Hout Bay is 2 m, which means after Davies (1980) that Hout Bay is typical of a microtidal coastline (Cooper, 2001). The general pattern of spring tidal ranges around South Africa is typically between 1.8 – 2.0 m (Cooper, 2001), to which the study area conforms. The wave regime for Hout Bay will be discussed in much more detail in Chapter 10 yet the dominant swell is from the southwest. When these southwesterly swells encounter the submarine extension of the Sentinel they are forced to refract around the headland towards Hout Bay Beach (Figure 2.4). Johnson (1919) first described waves refracting around a headland into a bay yet it was not until Krumbein (1944) that the characteristic shape of the wave fronts and hence the path of the wave crests could be defined. Krumbein (1944) observed that the wave front resembled a logarithmic spiral curve which was first described by French philosopher René Descartes towards the second half of the sixteenth century. Mathematically this means that any point P on the wave crest can be expressed in terms of polar coordinates by the equation:

$$R = R_0 e^{\theta \cot \alpha} \quad \text{.....(2.1)}$$

Where:

R = the length of the radius vector

R_0 = the length of the radius to the origin of angle measurement

Θ = the angle from the origin to the radius vector

α = the constant angle between the tangent to the curve and radius at any point along the spiral.

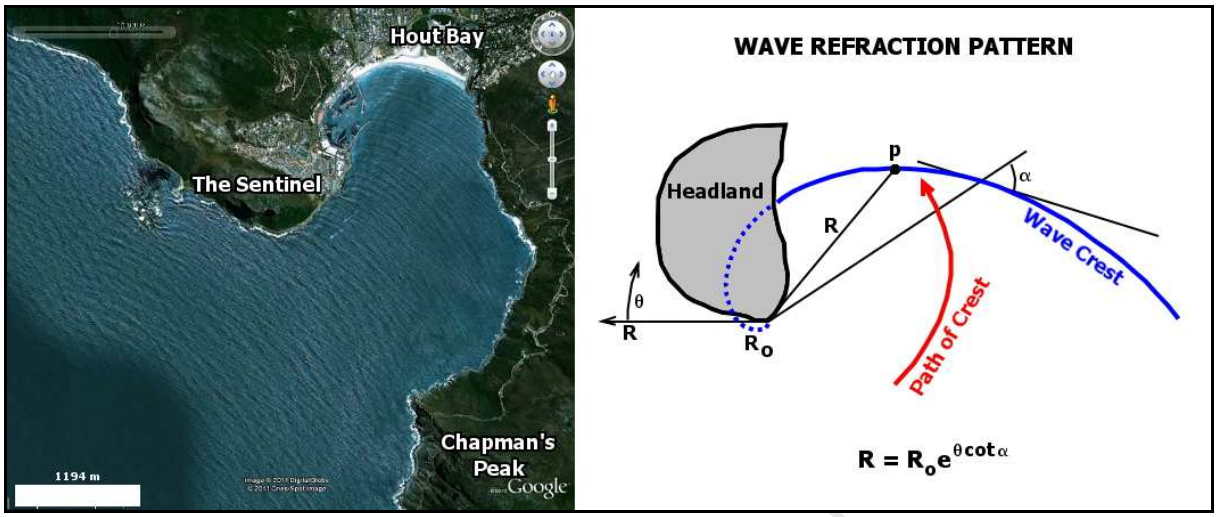

Figure 2.4. The dominant wave refraction pattern for the study area (left) and the mathematical formula and model which defines the shape of the refracted wave crests (right). Image courtesy of Google Earth and wave refraction pattern modified from Schwartz (2005).

2.3. Seafloor Morphology

For this investigation the western margin of South Africa is described from 35ºS to 27.6ºS (Figure 2.5). Traversing the margin in a seaward direction from coastline to abyssal plain, the continental margin has been subdivided into four distinct zones based on morphology. These include: the nearshore rocky platform, the continental shelf, the continental slope and the continental rise (Wigley, 2005; Rogers and Rau, 2006). Parallel to the coastline the margin has been sub-divided by Rogers and Bremner (1991) into the Agulhas Bank (south of 35ºS), the Olifants Shelf (Cape Point Valley to Child's Bank) and the Orange Shelf (Child's Bank to Orange Banks). From 35ºS the slope isobaths have a northwest orientation (approximately coast parallel) (MacHutchon, 2003). North of Cape Columbine the coastline forms the embayment of St Helena Bay, in which the coastline extends eastward, widening the continental margin. The margin remains approximately parallel to the coastline until Kleinzee (latitude 30ºS) where the isobaths turn to a north northeast orientation and the margin narrows across the Orange Shelf (MacHutchon, 2003). Approximate distances to the 500 m isobath from the coastline for Cape Point, Hout Bay and Namaqualand are 53 km, 62 km and 180 km, respectively (Dingle, 1973; Dingle *et al.*, 1987).

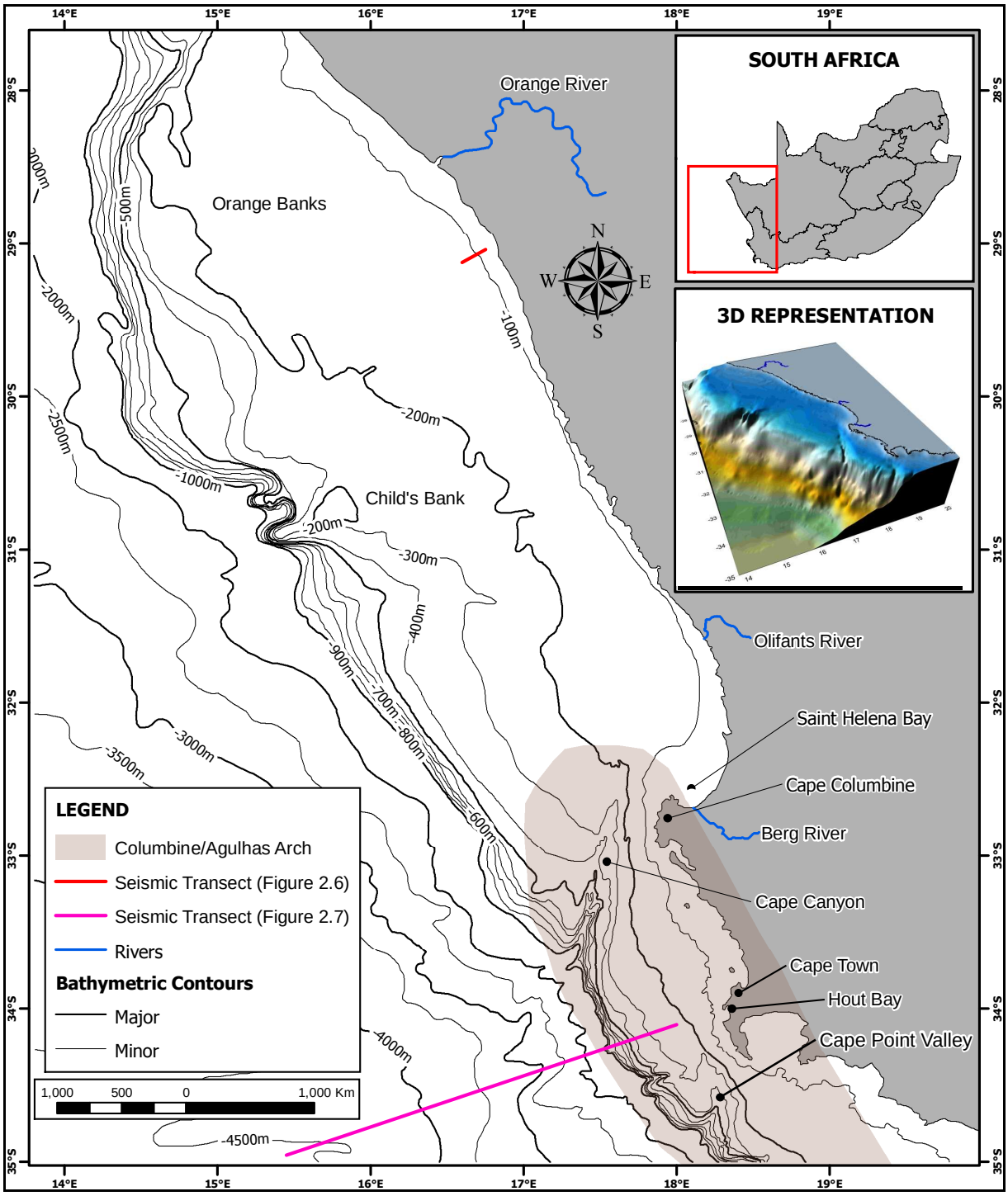

Figure 2.5. Bathymetry for the south east Atlantic, modified from Dingle *et al.* (1987). Columbine/Agulhas Arch after Dingle *et al.* (1983).

There are four topographic anomalies that exist along the continental margin. Two are bathymetric highs formed from Neogene limestone capping (Rogers and Rau, 2006), referred to as Child's Bank and Orange Banks, and two margin-oblique incisions in the form of the Cape Canyon and Cape Point Valley (Dingle *et al.*, 1983). The Cape Canyon is deeply

incised, exhibiting vertical relief of approximately 800 m and can be followed for up to 200 km offshore to water depths of at least 3 600 m (Dingle, 1970; Wigley, 2005).

A characteristic feature of the western margin of South Africa is the double shelf break (Birch *et al.*, 1991; Shannon and Nelson, 1996; Wigley, 2005). The first shelf break exists 200 m below sea-level (BSL) and the second at 500 m BSL (Rogers, 1977; Dingle *et al.*, 1983). It is because of this phenomenon that various authors have sub-divided the shelf into three distinct zones, namely the inner, middle and outer shelf.

The inner shelf has been defined by Dingle (1973), Birch *et al.* (1976), Rogers (1977), De Decker (1987), Woodborne (1991) and Wigley (2005) as a narrow zone along the coastline underlain by pre-Mesozoic basement and characterised by being a rocky, rugged, generally sediment-free platform. It owes its convex shape to the resistant underlying basement (Rogers, 1977) with gradients of approximately 0.5º between 20 – 40 m, steepening to between 1 – 2º at the boundary between the inner and middle shelf (De Decker, 1987).

The middle shelf lies between 70 – 200 m BSL and is characteristically flat with gentle seaward dipping gradients averaging 0.5º. The contact between the middle and inner shelf is masked for the majority of the shelf (between the Orange River and St Helena Bay) by a Holocene mudbelt, which formed primarily from terrigenous sediment from the Orange River. The mudbelt thins and narrows towards the south and is deposited in the inflection point between the two shelf zones which was believed to have formed 18 000 years before present (y. B.P) during the last glacial maximum lowstand that preceded the Flandrian transgression (Murray *et al.*, 1970; Rogers, 1977). Seismic data from the margin illustrates the contact between the inner and middle shelf, the mudbelt which is deposited in the inflection point and the gravel lags associated with the sea-level lowstand (Figure 2.6).

The outer shelf has been defined to lie between 200 and 500 m BSL (Birch *et al.*, 1976; Dingle *et al.*, 1976; Rogers, 1977). It has slightly steeper gradients than those of the middle shelf and it is within this zone that the topographic highs of Child's Bank and Orange Banks (-200 m) occur (Shannon and Nelson, 1996; Wigley 2005). The respective heads of the Cape Canyon and Cape Point Valley also occur within this regional zone. Seaward of the 500 m isobath the shelf drops off rapidly onto the abyssal plain of the Cape Basin.

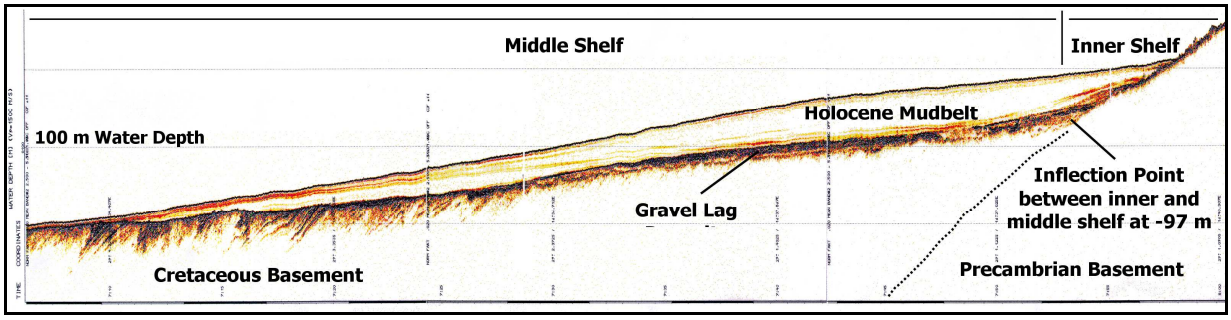

Figure 2.6. Seismic profile from MacHutchon (2003). Locality shown on Figure 2.5.

The study area falls within a relative basement high called the Columbine/Agulhas Arch (Figure 2.7). This arch extends from the edge of the Orange Basin (near Cape Columbine) in a southeasterly direction for approximately 700 km (Dingle *et al.*, 1983) forming the western margin of the Agulhas Plateau. The structure terminates against the Agulhas Fracture Zone. Dingle *et al.* (1983) have shown the arch to have been stable since the Palaeozoic owing its buoyancy to the intrusion of Cambrian granite plutons. As a result of the elevation of the arch with respect to the distal offshore basins only a thin veneer of sediment mantles the basal lithologies with very sparse accumulations of Cenozoic sedimentation along the inner shelf (Dingle *et al.*, 1983). This is due to the re-activation of the feature during the uplift and tilting of the South African landmass during the Neogene (Partridge and Maud, 1987; Wigley and Compton, 2006).

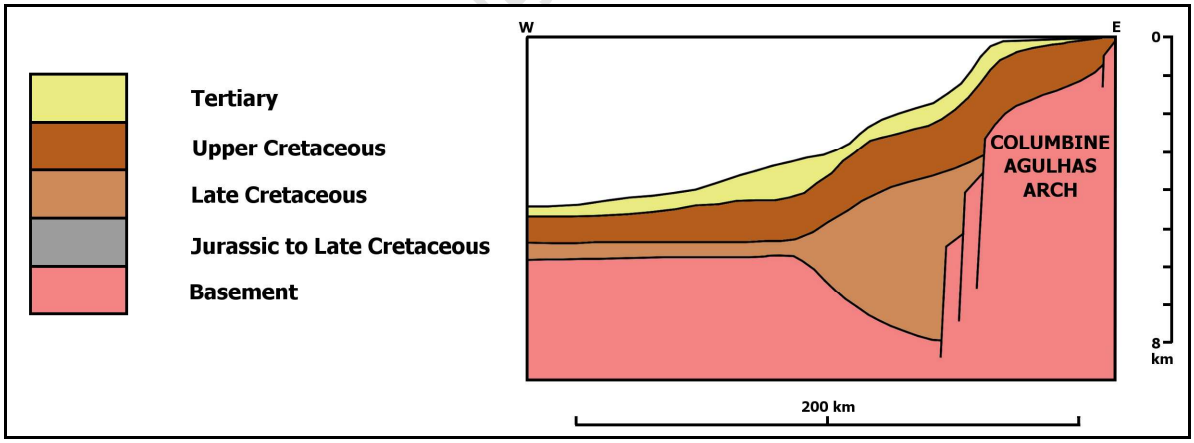

Figure 2.7. Seismic profile showing the western flank of the Columbine/Agulhas Arch, modified from Dingle *et al.* (1983). Locality shown on Figure 2.5.

Now that the regional setting for study area has been discussed the following chapter will look at the regional geology effecting Hout Bay.

3. REGIONAL GEOLOGY

3.1. Neoproterozoic and Cambrian Basement

During the formation of the late Precambrian to Early Cambrian Pan-African Saldania Belt the Cape Granite Suite intruded the existing country rocks (Scholtz, 1946; Schoch *et al.*, 1977). The geochemical composition of the Cape Granite Suite ranges from low to very high silica (~50 – 77% SiO_2), however volumetrically, granitic to granodioritic compositions dominate (Scheepers and Schoch, 2006). The greenschist facies country rocks into which the Cape Granite Suite intruded comprise predominately the metavolcanic and metasedimentary rocks of the Malmesbury Group which are Neoproterozoic in age (Scheepers and Schoch, 2006). In general the granites within the suite are undeformed and show little to no gneissosity.

For ease of description, pluton clusters were geographically subdivided by Scholtz (1946) into the eastern, southwestern and northern plutons. For the purpose of this study only the southwestern plutons have been considered (Figure 3.1). The granite bodies within the southwestern region have been subdivided into three tectonic domains, separated by prominent northwest trending shear zones. The regional distribution reflects the different tectonic constraints within the Malmesbury Group into which these granitic bodies have intruded (Scheepers and Schoch, 2006). The different geographic domains constitute the southwestern domain (Tygerberg terrain), the central domain (Swartland terrain) and northeastern domain (Boland terrain) (Hartnady *et al.*, 1974; Von Veh, 1983).

The different rock types in the southwestern plutons in the Tygerberg terrain have been described by Scheepers and Schoch (2006) to contain large volumes of older, porphyritic granites, medium-grained, equigranular biotite granite, leucocratic, fine-grained granites, discrete bodies of amphibole-bearing quartz syenites and alkali feldspar granites, plutons of gabbroic composition intruded by diorite bodies and rhyolitic to rhyodacitic ignimbrite flows which cover both the underlying granite and Malmesbury metasediments west of the Langebaan Lagoon.

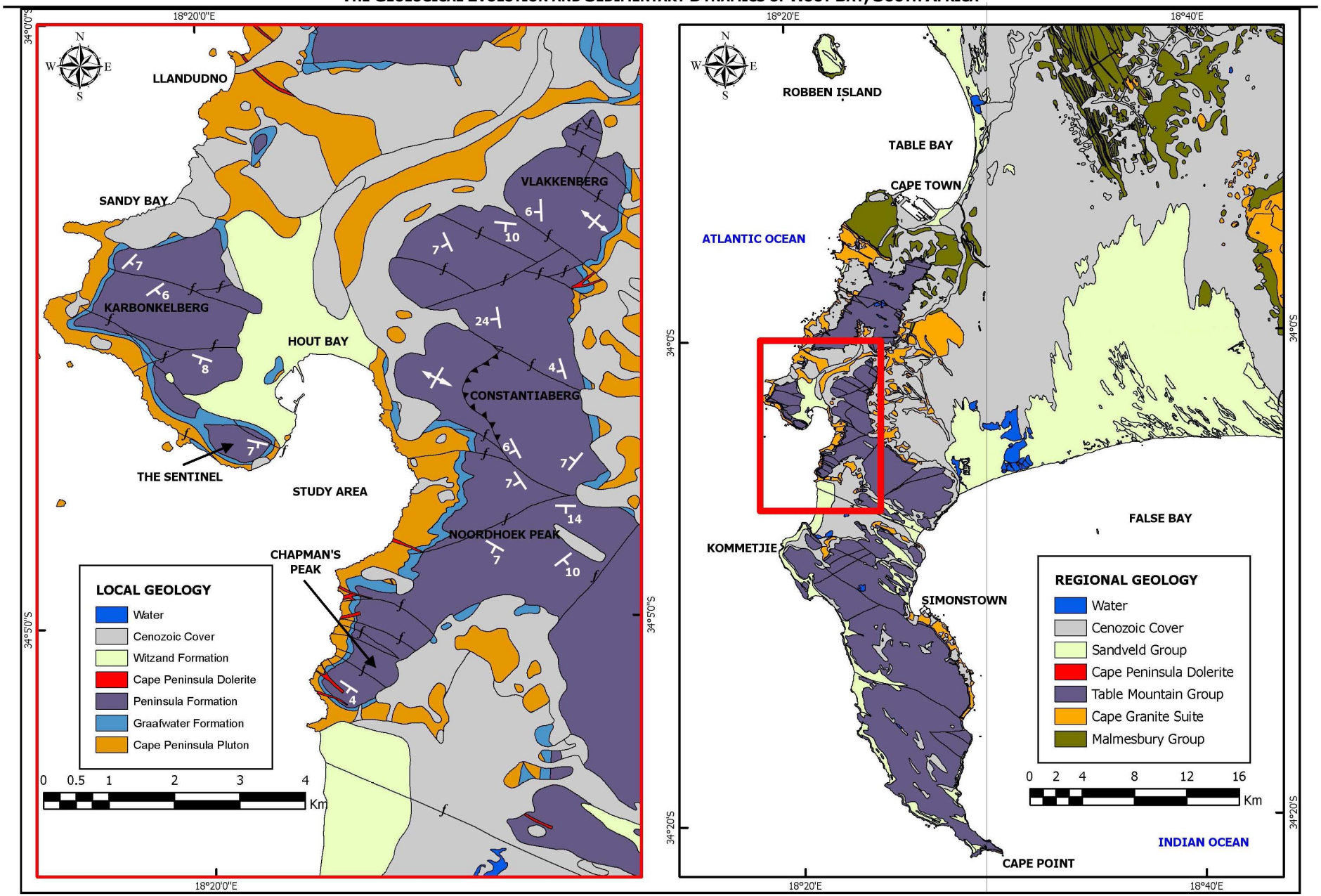

Figure 3.1. Regional and local geology of study area, from 1:50,000 Map Sheets 3318 CD & DC, 3418 AB, AD & BA. Compiled by J.N. Theron (1984).

The granites of the Western Cape can be broadly divided into S-, I- and A-types, based on their overall and enclave mineralogy, accessory minerals and geochemical features (Chappell and White, 1974; Loiselle and Wones, 1979; Eby, 1992; Scheepers, 1990; Scheepers and Cuney, 1992; Scheepers, 1995). A further subdivision into seven associations was made by Scheepers (1995) to give three S-type (Sa_1, Sa_2, Sb_2), two I-types (Ia, Ib) and two A-types (Aa, Ab). Scheepers (1995) was also able to group the southwestern plutons into four consecutive phases (I – IV) based on compositional and mineralogical variations directly related to different source material, field relationships and relative isotopic age constraints (Table 3.1). The intrusives around Hout Bay belong to the Cape Peninsula Batholith which intruded during the first phase of intrusion (around 555 – 540 Ma). This granite is of the Sa_1-type (peraluminous) granite (Schoch, 1975, 1976; Leygonie, 1977; Scheepers, 1995).

Sa_1 and Sa_2 plutons where intruded in a tectonic regime dominated by strike-slip movement. The primary peraluminous melts were derived from crustal material from the deformed Namaqua-Natal metamorphic complex during a period of introduction of basaltic magma into the crust resulting in increased heat flow (Scheepers, 1995). Ages for the first phase of intrusion of Sa_1 association into the folded Malmesbury Group rocks range from 540 – 552 Ma. Determined dates are: 540 ± 4 Ma (Armstrong *et al.*, 1998); 547 ± 6 Ma (Da Silva *et al.*, 1997); 552 ± 3 Ma (Scheepers and Armstrong, 2002). The oldest Sa_1 granitoids intruded along strike-slip shear zones (Von Veh, 1983) and were most likely derived by partial melting of garnet bearing greywackes deep-seated within the Malmesbury Group metasediments (Scheepers, 1995).

Table 3.1. Summary of Cape Granite Suite magmatism in the Saldania Belt, from Scheepers and Schoch (2006). The granite association from the study area is highlighted yellow.

Magmatism	Association	Rock Type	Examples
Phase IV (-515 Ma)	Volcanic	Ignimbrite, tuffisite, quartz porphyry	Postberg Formation (ignimbrite) Saldanha Quartz Porphyry (Saldanha Batholith)
Phase III (-520 Ma)	Aa	Alkali feldspar granite, quartz syenite	Klipberg Granite (Darling Batholith)
	Ab	Alkali feldspar granite	Cape Columbine Granite (Vredenburg Batholith)
Phase II (540 – 520 Ma)	Ib	Granite, alkali feldspar granite	Bathel Dam Granite (Paarl Pluton) Slippers Bay Granite (Vredenburg Batholith)
	Ia	Monzogranite, granite, alkali feldspar granite	Bretagne and Laborie Granites (Paarl Pluton) Vredenburg Granite (Vredenburg Batholith) Greyton Pluton
Phase I (555 – 540 Ma)	Sb	Granite	Trekoskraal and Kamberg Granites (Saldanha Batholith) Darling and Rondeberg Granites (Darling Batholith)
	Sa_2	Granite, alkali feldspar granite	Fine-grained granite (Stellenbosch Batholith) Contraberg Granite (Darling Batholith) Olifantskop Granite (Saldanha Batholith)
	Sa_1	Granite	Sea Point Granite (Cape Peninsula Batholith) Hoedjiespunt and Seeberg Granites (Saldanha Batholith)
(630 Ma ?)		Gabbro, diorite	Gabbro (Malmesbury Batholith)

3.1.1. Cape Peninsula Pluton

The Cape Peninsula Pluton has been described by numerous authors (Theron, 1984; Theron *et al.*, 1992; Cole, 2003). There are slight textural variations within the pluton, yet within the study area the outcrops can be described as a predominantly grey, coarse-grained, porphyritic, biotite granite characterised by large feldspar phenocrysts, xenoliths of Malmesbury metasediments and rounded to oval clots rich in tourmaline (Theron, 1984; Theron *et al.*, 1992; Cole, 2003) (Figure 3.2 A & B).

This lithology crops out as the basal section of Chapman's Peak and the Sentinel (Figure 3.1) and exhibit the "classic" rounded dome-like shape which results from differential cooling and exfoliation weathering (Compton, 2006) (Figure 3.2 C,D). There is a zone of highly weathered granite just below the nonconformity with the upper sediments (Hartnady and Rogers, 1990), indicative of much higher rainfall during this time.

Figure 3.2. Photographs A & B illustrate the coarse grained porhyritic nature of the granite and the large feldspar phenocrysts. B shows the texture at higher magnification, note the tourmaline clot in the upper left corner. C & D illustrate the rounded weathering pattern exhibited by the granite outcrops, C is just below Chapman's Peak Drive near the lookout point and D is at the foot of the Sentinel.

3.2. Early Palaeozoic Deposits

Following the Saldanian Orogeny which spanned the Late Precambrian to Early Cambrian and the various Pan-African depositional events related to the assembly of Gondwana, the siliciclastic Cape Supergroup sediments where deposited over almost 170 million years (from the Early Ordovician to the Early Carboniferous). These sediments accreted in a passive margin basin with a provenance from the north (Figure 3.3), which allowed approximately 10 km of strata to accumulate and be preserved (Thamm and Johnson, 2006). Despite the fact that the consolidated strata were later deformed during the Cape Orogeny, three distinct

lithological subdivisions of primary Cape Supergroup have been identified, all of which show lateral continuity throughout the length of the Cape Fold Belt (some 1000 km) (Thamm and Johnson, 2006). These subdivisions are the Table Mountain, Bokkeveld and Witteberg Groups (Figure 3.4).

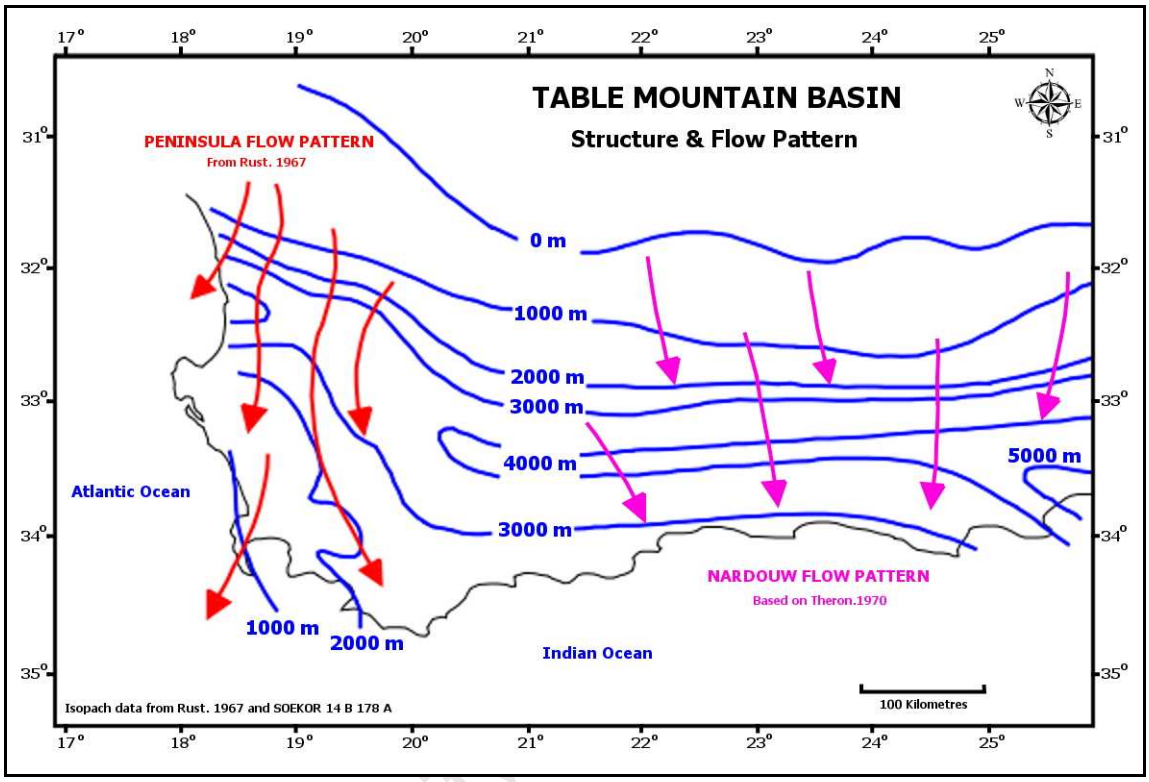

Figure 3.3. Structure and palaeo-flow patterns of Table Mountain Basin, modified from Rust (1973).

The Table Mountain Group (TMG) comprises predominantly sandstone formations that span the Ordovician to the Early Devonian. Depositional environments range from shallow marine to fluvial with a glacial interlude in the middle (Thamm and Johnson, 2006). The Early to Middle Devonian Bokkeveld Group shales overlie the Table Mountain Group sandstones. This group comprises coarsening upward cycles of fossiliferous shales and sandstone units, indicative of basinward progradational cycles characteristic of wave dominated deltas (Theron, 1972). The supergroup succession is capped by Late Devonian to Early Carboniferous Witteberg Group which consists of mudrock and sandstone deposited in a shallow marine, paralic and deltaic environment (Thamm and Johnson, 2006).

For the purposes of this dissertation only selected basal units of the Table Mountain Group which outcrop in the study are will be described in detail (Figure 3.1 & Figure 3.4).

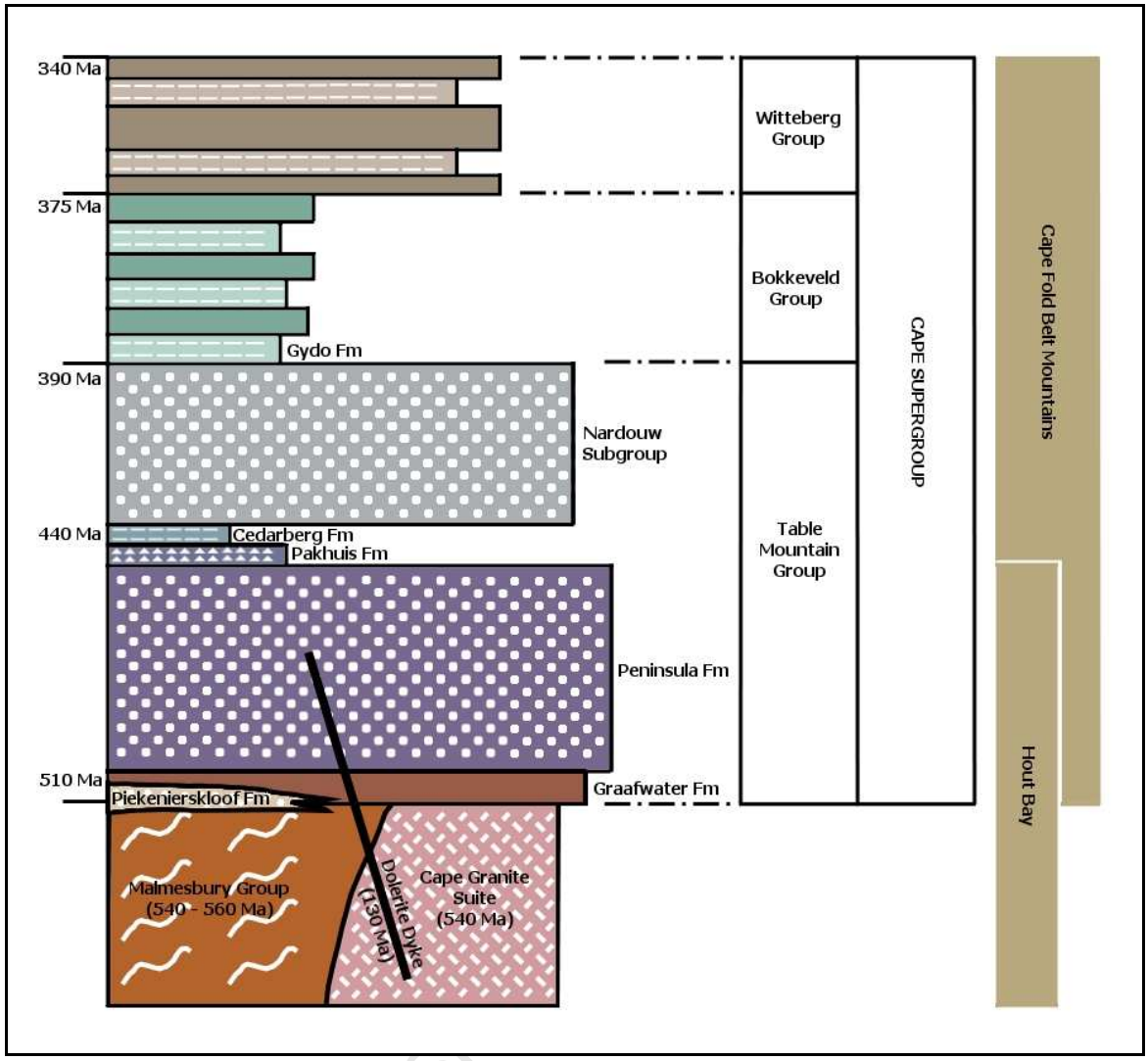

Figure 3.4. Stratigraphy of the Cape Supergroup modified from Compton (2006).

3.2.1. Graafwater Formation

The Graafwater Formation crops out within the study area at the base of the Sentinel and along Chapman's Peak drive. It has been described by Rust (1967) and Theron (1984) as a generally reddish mudstone, siltstone and sandstone formation attaining a maximum thickness of approximately 430 m. Within the study area the thickness is between 60 – 80 m (Figure 3.5). Field evidence in the form of sedimentary structures (wave ripples), mud cracks, bedding geometries, polymodal palaeocurrent directions, vertical sequences and abundant trace fossils have led authors such as Rust (1967, 1977) and Tankard and Hobday (1977) to suggest a depositional environment of either tidal flats or a tidal/shallow marine setting (Figure 3.6). Alternatively Turner (1990) has suggested that the upper and lower portions of the formation are characteristic of low-sinuosity channels draining a low-relief

coastal plain, with the internal portion reflecting alternating sub-aerial and sub-aqueous conditions.

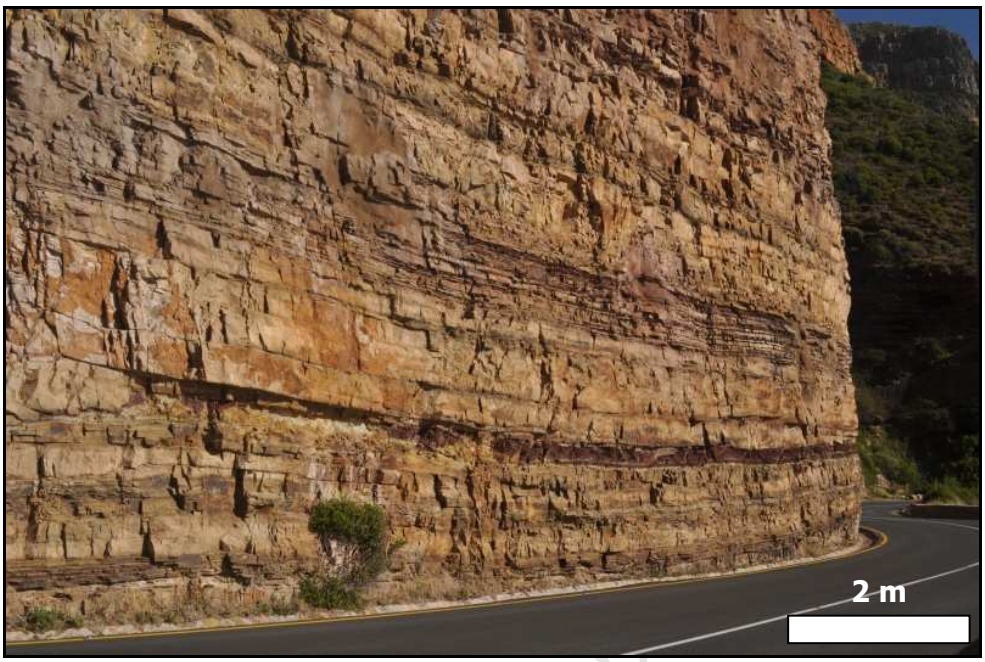

Figure 3.5. Photograph of the Graafwater Formation just south of the Chapman's Peak lookout point. Note the alternating sandstone and reddish mudstone horizons.

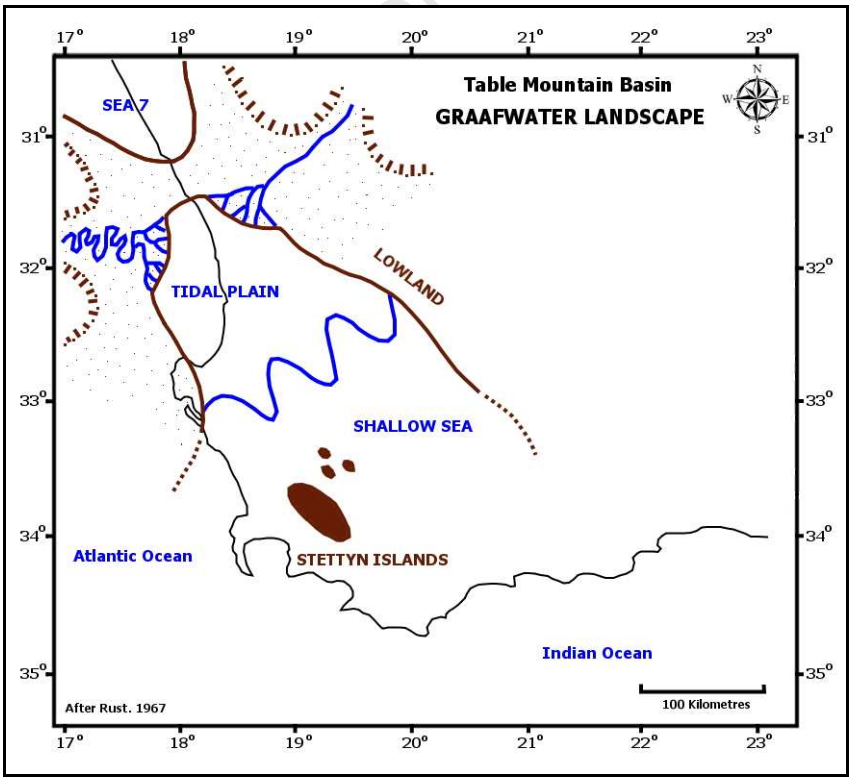

Figure 3.6. Palaeo-landscape and depositional environment of the Graafwater Formation, modified from Rust (1973).

3.2.2. Peninsula Formation

The Peninsula Formation forms the majority of the mountains surrounding Hout Bay. This formation is made up of quartz arenite with minor amounts of conglomerate and shale (Thamm and Johnson, 2006). The Peninsula Formation is the dominant unit of the Cape Supergroup and is thickest towards the eastern part of the basin with a maximum thickness of ~2 700 m (Johnson, 1976), thinning to ~2 000 m in the west (Rust, 1967). Within the study area thicknesses are between 600 – 800 m. The unit thins rapidly to the north of the trough axis (in the proximal part of the basin). Different authors have postulated varying depositional environments for the Peninsula Formation. Rust (1967, 1981) and Hobday and Tankard (1978) proposed a shallow-marine shelf deposit encompassing transgressive barrier, tidal and beach environments (Figure 3.8). Fuller (1985), Fuller and Broquet (1990) and Turner (1990) however have proposed a fluvial braid-plain environment on the basis of overall lithology, cut-and-fill structures, abundant horizontal laminations, planar cross-bedding and a unimodal palaeocurrent pattern. Palaeontological evidence in the form of the *Eurypterid* (trilobite) trace fossil *Cruziana* which has been found in the lower bioturbated zones of the Peninsula formation indicates an Early Ordovician minimum age (older than ~470 Ma) (Cocks and Fortey, 1986; Broquet, 1992).

Figure 3.7. Photograph of Peninsula Formation from the Sentinel. Note the well defined cross-bedding.

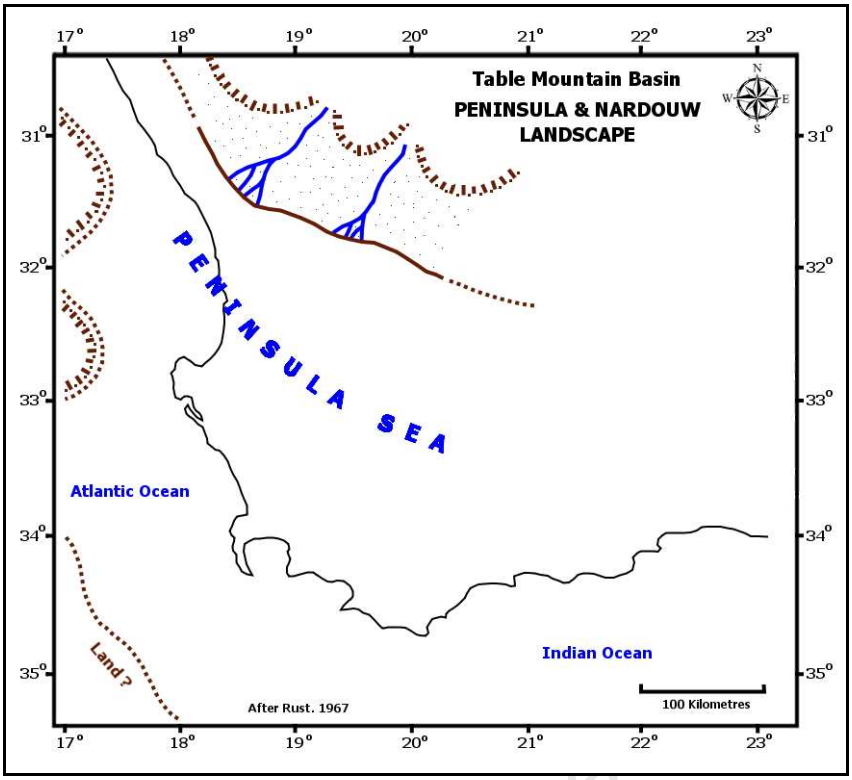

Figure 3.8. Palaeo-landscape and depositional environment of the Peninsula Formation, modified from Rust (1973).

3.3. Cretaceous Deposits and Intrusions

During the Late Jurassic and into the Early Cretaceous the southern margin of South Africa was dominated by tensional rift faulting (Dingle *et al.*, 1983; De Decker, 1987) which resulted in extensive horst and graben development around the cratonic margins and was the onset of the breakup of Gondwana (to form Africa and South America) (Dingle *et al.*, 1983). After the breakup, subsidence occurred which resulted in increased accommodation space on the continental margin and increased sedimentation with a seaward shift of active depocentres and prograding strata onto the continental shelf (Dingle *et al.*, 1983; De Decker, 1987). The downfaulted blocks acted as sediment dams resulting in large offshore sedimentary basins forming along the western margin (Scrutton and Dingle, 1973) (Figure 3.9 C). The two basins which formed along the western margin are that of the Walvis and Orange Basins. The Orange Basin is bounded on either side by buoyant basement highs (arches). The southern arch is referred to as the Columbine/Agulhas Arch and has been buoyant since the Palaeozoic (Dingle *et al.*, 1983) (Figure 3.9 D).

During the Aptian – Albian (Late Cretaceous times) the sedimentary basins fundamentally changed in the way they formed (Dingle *et al.*, 1983). The basins switched from narrow and deep fault bounded basins to becoming regionally downwarped. This caused the basins to become "saucer shaped" with depocentres overstepping the older fault boundaries (Dingle *et al.*, 1983). The seismic characteristics of Upper Cretaceous progradational strata is that of shallow seaward dipping reflectors, typically averaging 3º of dip (Dingle, 1973) (Figure 2.6). Within the study area there is no surficial expression of Cretaceous sediments (neither on- nor offshore). The region does fall within the Columbine/Agulhas Arch described above (Figure 3.9 D). There is however the intrusion of Cape Peninsula Dolerites.

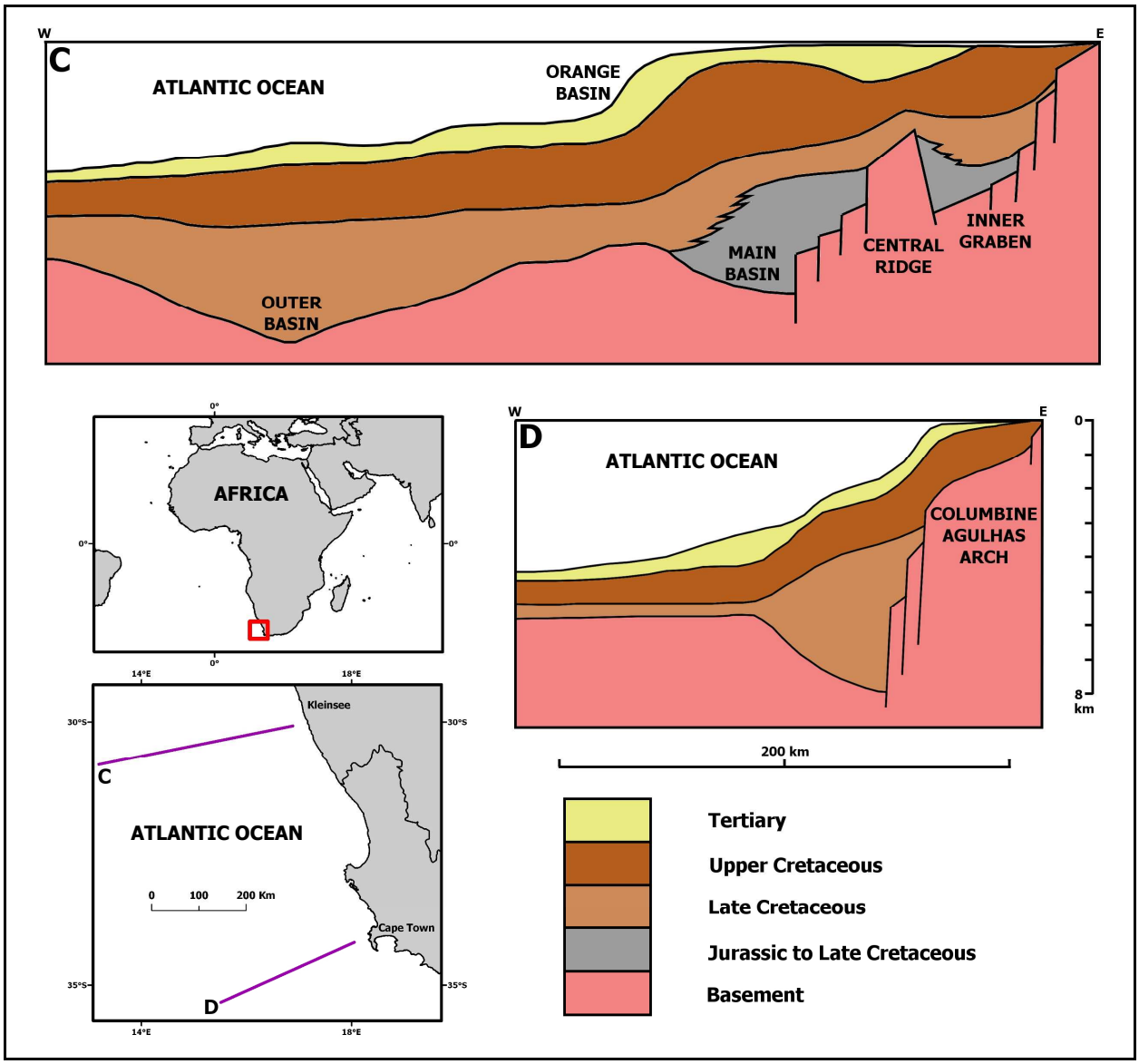

Figure 3.9. Simplified seismic architecture of regional setting. Modified from Dingle *et al.* (1983).

3.3.1. Cape Peninsula Dolerites

The dolerite dykes which intrude the headlands around Hout Bay (Figure 3.10) form part of the Cape Peninsula Dolerite dyke swarm (Day, 1987). These dykes have been described by Nell and Brink (1944), Day (1984) and Theron (1984). From field observations Theron (1984) described the dykes as being intrusive into the metasediments of the Malmesbury Group, the Cape Granite Suite and in some places (such as those seen at Chapman's Peak) intruding at least 30 m into the basal units of the Table Mountain Group. The dykes average approximately 6 m in thickness.

Fresh, relatively unweathered dykes have been described as medium-grained, dark grey melanocratic rocks with augite and plagioclase as dominant minerals. Subordinate minerals include biotite, olivine, quartz, ilmenite, magnetite and glass (Theron, 1984). The dykes regularly have a microporhyritic texture with 1 – 2 mm long feldspar crystals set in a dense dark groundmass. In the main dyke at Chapman's Peak there are large phenocrysts of pyroxene (Theron, 1984).

Figure 3.10. Dolerite dyke intruding the Cape Granite Suite just below Chapman's Peak Drive. Scale bar is 5 m wide. Photograph courtesy of Ms. Hayley Cawthra.

3.4. Palaeogene & Neogene Deposits

The onset of the Palaeogene is marked by a major marine transgression (Dingle, 1971; Dingle *et al.* 1983). During the Palaeocene – Eocene the shelf exhibited predominantly an

upward direction of construction, as a result of which the middle shelf started to sag and a thick succession of marine sediments accumulated (Dingle, 1971). The end of the Palaeogene is marked by a major regression and the onset of the Middle- to Late Oligocene erosional hiatus (Dingle, 1971; Siesser and Dingle, 1981; Cramez and Jackson, 2000; Lavier *et al.* 2001). During the Early Miocene the subcontinent experienced uplift (Partridge and Maud, 1987, 2000; Partridge, 1998) resulting in a slightly westward tilt of the subcontinent. As a result of this uplift the palaeodrainage was re-activated and sedimentation rates onto the shelf increased, resulting in progradation and seaward thickening of marine sediments (Dingle, 1971) and ultimately in triggering the major offshore slumps described by Dingle *et al.* (1983). The end of the Neogene is marked by a major marine regression (Dingle, 1971). No Palaeo- Neogene sediments are present in the study area. With the uplift events experienced during this period the Columbine/Agulhas Arch was re-activated, causing downwarping to the southwest and removing most of the sediment cover (Partridge and Maud, 1987; Wigley and Compton, 2006).

3.5. Pleistocene Sea-Level Changes

The Quaternary period is characterised as being a relatively stable tectonic period for the study area (Partridge and Maud, 2000; Wigley and Compton, 2006). The dominant forces effecting the period are the dynamic interplay between glacially driven eustatic sea-levels as a result of dramatic changes within deep ocean current circulations which allowed the formation of regional ice sheets which locked up more freshwater causing sea-levels to fall or rise if these ice sheets melted (Compton, 2001; Waelbroeck *et al.* 2002; Ogg *et al.*, 2008; Compton and Wiltshire, 2009; Cawthra, 2010). Waelbroeck *et al.* (2002) established a robust regression between relative sea-level and ratios of oxygen isotopes in benthic foraminifera to establish a relative sea-level curve for the last 430 kyr (Middle Pleistocene to Present) (Figure 3.11). These data agree with sea-levels derived from U-Th ratios in corals from various authors for the last 20 kyr (Waelbroeck *et al.* 2002). These data, although conclusive, are representative of a global relative sea-level with most of the data obtained from the Pacific Ocean. Compton and Wiltshire (2009) derived sea-level curves for the west coast of South Africa which span an equivalent period to the curve of Waelbroeck *et al.* (2002). These curves have been superimposed relative to one another in Figure 3.11 to show that both exhibit the same general trends, differing primarily in amplitude. Higher resolution sea-level curves have been derived for the west coast (Compton, 2001) and east

coast (Ramsay, 1995; Ramsay and Cooper, 2001) of South Africa. The Ramsay (1995) and Compton (2001) data span a relatively short time period of the last 9 kyr (since the most recent deglaciation transgression) (Compton, 2001) and the Ramsay and Cooper (2001) curve tentatively extends to 150 kyr. The curve of Compton (2001) (Figure 3.12) was derived from Langebaan Lagoon (less than 100 km north of Hout Bay) and the Compton and Wiltshire (2009) curve from cores taken in the vicinity of the Cape Canyon.

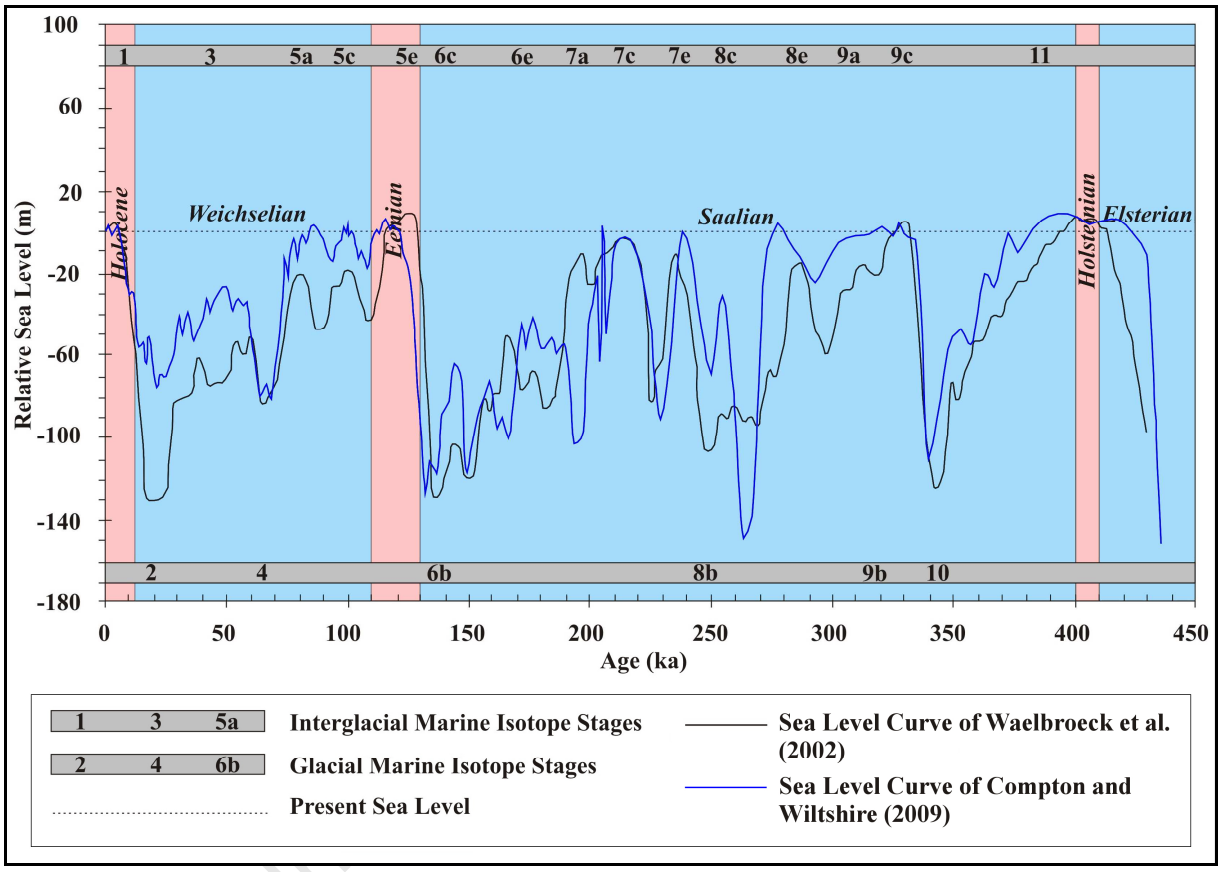

Figure 3.11. Composite image of Waelbroeck *et al.* (2002) and Compton and Wiltshire (2009) relative sea-level curves, with glacial/interglacial cycles 1-11 superimposed (grey bands). North Western European stratigraphic terminology for these periods is shown in pink and blue blocks. All data synthesised by Cawthra (2010) from Gibbard and Kolfschoten (2004); Haq (2007) and Gibbard *et al.* (2008).

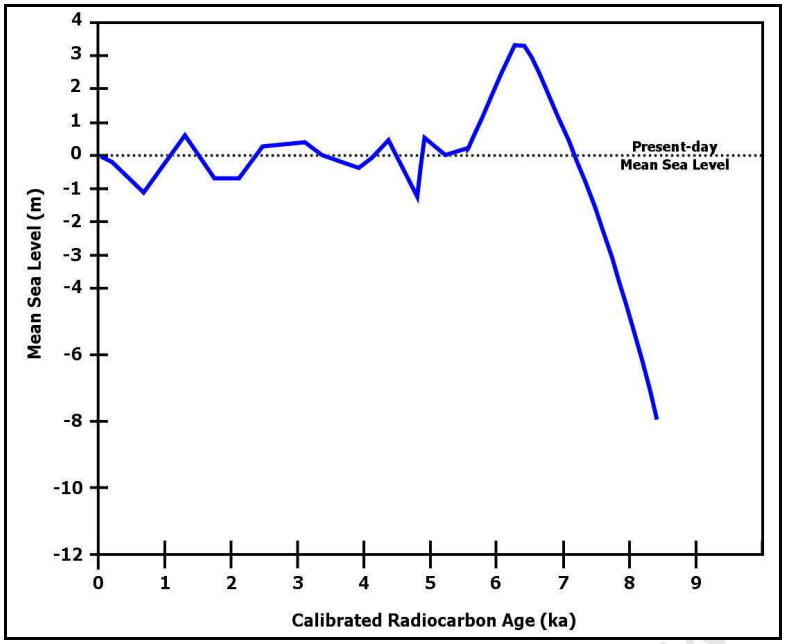

Figure 3.12. Holocene sea-level curve, modified from Compton (2001).

3.6. Pleistocene Deposits

Quaternary outcrops in the study area are confined to the Holocene Witzand Formation. In the offshore sediments there exists the possibility that Pleistocene sediments could be encountered therefore all the local Pleistocene deposits are described below (Figure 3.13).

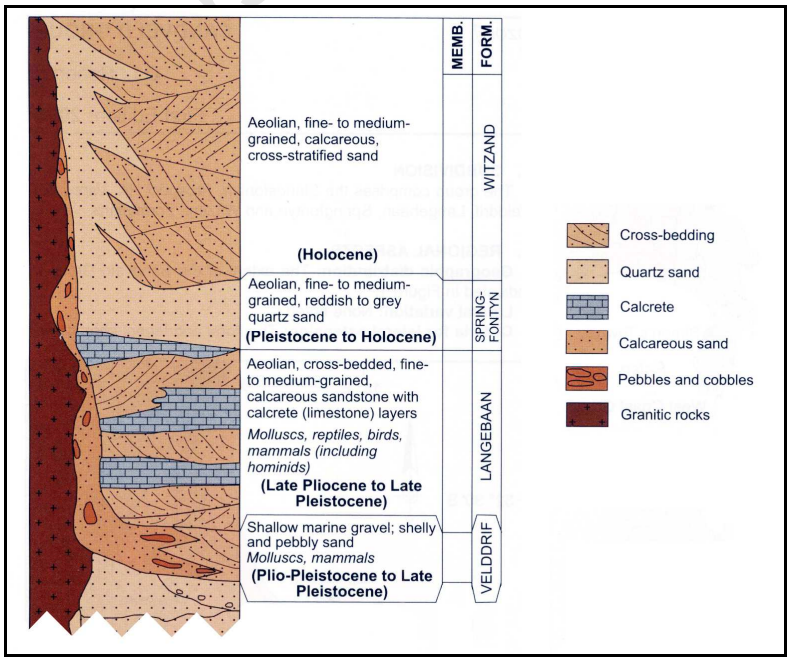

Figure 3.13. Stratigraphic column of Pleistocene- to Recent sediments of the Sandveld Group. Modified from Roberts (2006).

3.6.1. Velddrif Formation

The Velddrif Formation has been described as a cobble-bearing shelly limestone and sandstone which in places is capped by calcrete horizons (Rogers *et al.*, 1990). Stratigraphically the formation is bound below by the Varswater Formation and above by the Langebaan Formation (Rogers *et al.*, 1990). The depositional environment for these sediments has been proposed by Hartnady and Rogers (1990) to be estuarine and intertidal.

3.6.2. Langebaan Formation

The Langebaan Formation has been described by Rogers *et al.* (1990) to be a crossbedded aeolian deposit of fine- to medium grained calcretised shelly sand and calcarenite, containing terrestrial gastropod shells. The formation is bounded below by the Veddrif Formation and above by the Springfontein Formation.

3.6.3. Springfontein Formation

The Springfontein Formation has been described by Rogers *et al.* (1990) and Roberts (2006) as a light reddish decalcified, unconsolidated structureless aeolian quartzose sand which is peaty in places and comprised of well rounded and sorted grains. The formation is stratigraphically positioned between the older Langebaan Formation and the Recent Witzand Formation. The sand from this formation is believed to represent the leached aeolian sands of the underlying calcareous Langebaan Formation (Roberts *et al.*, 2011)

3.6.4. Witzand Formation

Sediments of the Witzand Formation constitute the beach and surrounding dunes of Hout Bay and the unconsolidated shelf sand within the study area (Figure 3.14). It has been described as unconsolidated, moderately to well-sorted, fine- to medium grained, quartzose sand containing comminuted shell fragments of predominantly marine organisms (Rogers, 1980; Theron *et al.*, 1992; Roberts, 1999; Cole 2003). The formation overlies pre-Cenozoic

bedrock and Tertiary and Pleistocene sediments unconformably (Geological Survey, 1990; Roberts, 1999; Cole and Roberts, 2000). The sediments are derived from aeolian processes, often experiencing several phases of onshore deflation (Rogers, 1980, 1982; Roberts, 1999). The Holocene age constraint of the formation has been derived from the occurrence of Late Stone Age artefacts and dwelling structures within the formation (Roberts, 1999).

Figure 3.14. Photograph of dunes (Witzand Formation) which border north western sector of Hout Bay Beach. Photograph courtesy of Mr. Willem De Wet.

3.7. Structural Setting

Theron (1984) describes a south-westwards-plunging broad, open, synclinal trough as the dominant feature associated with Table Mountain. The extension of the fold axis towards Hout Bay is clearly evident from the eastward dipping beds of Karbonkelberg and the westward dips of Vlakkenberg (Figure 3.1). To the east of this fold axis is a broad, open anticline which plunges in the same direction as the syncline. Towards the eastern front of Vlakkenberg there are a series of parallel, sharp monoclinal to kink folds (Theron, 1984). The kink fold zones can be followed along strike to the immediate west of Constantiaberg where ten metre amplitude folds can be observed. It is usual that faults with similar strike orientations to that of the fold axis develop laterally to these monoclines and kink folds which are supported by the numerous southeast – northwest faults seen locally around Hout Bay. Another set of fault orientations is northeast – southwest. These faults share a similar orientation to the Cape Peninsula Dyke Swarm and were formed during the breakup of

Gondwana (Day, 1986). The fault blocks associated with the latter orientation exhibit larger displacements regionally, the best example of this is the Sun Valley Fault just to the south of Chapman's Peak with a throw of several hundred metres to the south (Theron, 1984). The Sentinel is also downfaulted to the south which is clearly evident by the height above sea-level of the nonconformity between the granites and overlying TMG strata when compared to its equivalent on Chapman's Peak. The large majority of the faults in the study area are normal with one exception of a thrust fault on the western flank of Constantiaberg (Theron, 1984). Hartnady and Rogers (1990) have shown that compressional tectonism is responsible for the thrust deformation observed and extensional for those of the normal faults.

Having adequately defined the regional geology and physical setting of the study area the next chapter will discuss the methods and principles employed by the various geophysical instruments used to collect the relevant data for this dissertation.

4. METHODS & PRINCIPLES

4.1. Introduction

Since mariners started going to sea there has been a need to understand the morphology of the seafloor so as to enable safe passage of vessels and their cargo and ultimately to facilitate trade. The first recorded techniques for "accurately" determining the depth of water below ones keel was to use a lead line (Figure 4.1), (a weighted line with known increments marked on the line). The line was periodically dropped until it came to rest on the seafloor and the depth measured on the graduated line. This method was slow, cumbersome and heavily influenced by sea-state. The need for a faster, more accurate measuring system arose and thus sonar imaging of the seafloor was born. Even nowadays almost half a century after the first sonars where introduced, we know less about the relief of our ocean floors than the topography of Mars and Venus (Smith, 1993; Smith and Sandwell, 1994).

A brief summary of sonar principles, sonar equipment and specific equipment settings for the data acquisition is presented here.

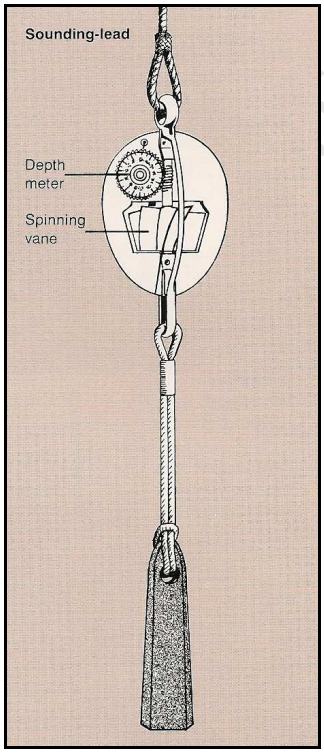

Figure 4.1. A sketch of a lead line from Turner (1997). This particular model is very sophisticated, with a spinning vane to turn a meter. It also has a locking device which stops the meter when the lead shot comes to rest on the bottom.

4.2. Basic Sonar Principles

The basic elements of any active sonar system, from a simple depth sounder to sophisticated sidescan sonar, are essentially the same (Mazel, 1985). The system's heart is the transducer, which converts electrical energy into a pressure wave. For most systems this commonly takes place via a piezoelectric crystal (a ceramic material which physically changes shape when a voltage is applied across it) (Ingham, 1975; Mazel, 1985; Jones, 1999). It converts the electrical signal (oscillation) from the transmitter into a mechanical vibration, which is transferred into the water as an oscillating pressure wave. This pressure wave propagates away from the transducer, in a manner determined by the acoustic properties of the water until it strikes a target in the water or the seafloor. Some of the incident sound is reflected back to the transducer as backscatter. This backscatter is recorded by the transducer, transformed back into an electrical pulse and amplified by the receiver portion of the sonar (Mazel, 1985). Finally there must be a control (master) unit which regulates the precise timing that is required for the various elements to synchronise their operations. This master unit is also normally connected to or one of its own components is a graphical display of the recorded data.

Sonar systems measure depth or distance by recording and displaying the time it takes for a transmitted sonar pulse to travel from the transducer to the target and return (McQuillan and Ardus, 1977; Mazel, 1985; Jones, 1999). The distance to the target is half the product of the two-way transit time and the mean vertical sounding velocity, with a small correction added for the draft (depth) of the transducer (Jones, 1999).

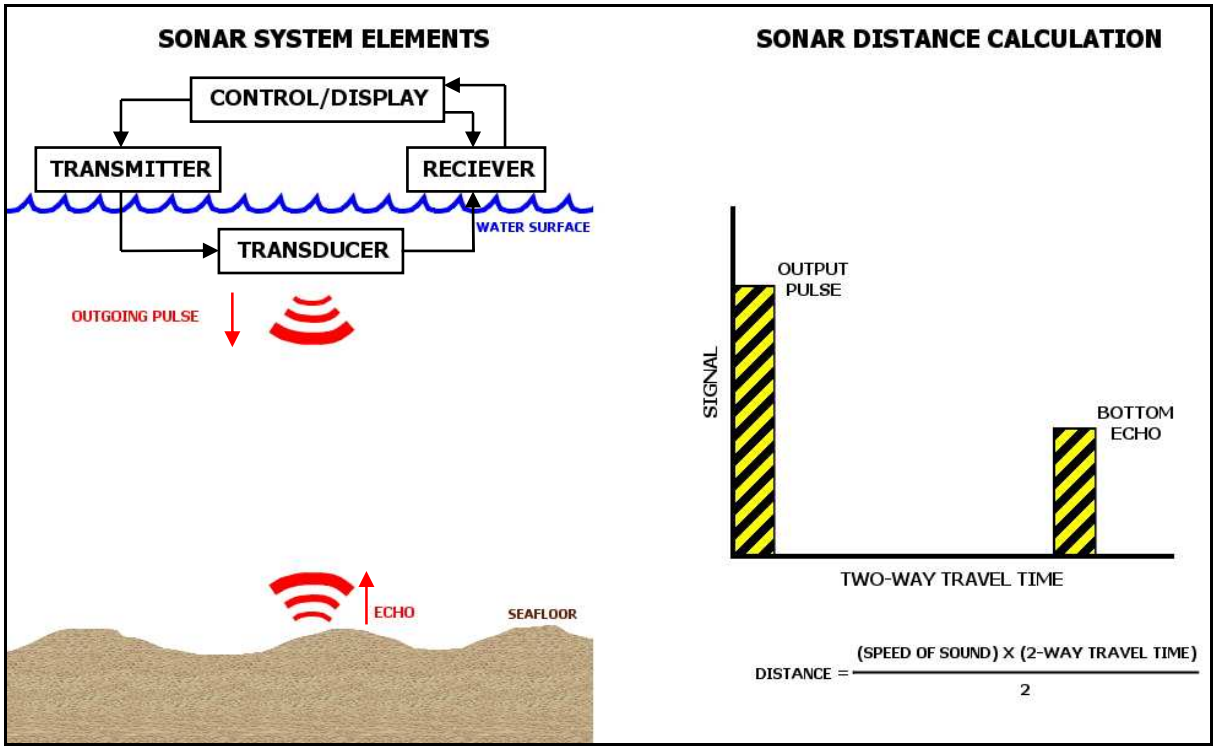

Figure 4.2. Illustration of basic sonar elements (left) and distance calculation from two-way travel time (right). Modified from Mazel (1985).

4.2.1. Singlebeam Echosounders

Singlebeam echosounders are typically hull mounted and special care is taken to mount the device to minimise acoustic interference (Jones, 1999). They are usually circular transducers with diameter five times the wavelength of sound in water at the transmitted frequency (Horton, 1959). The main beam of the echosounder is usually cone-shaped with a half angle at the 6 dB power point of 1º - 40º (Jones, 1999). The geometry of the beam is crucial to the resolution of the system with narrow beams providing more accurate data.

As previously noted, raw singlebeam bathymetric data need to be corrected for tidal variations, static transducer draft, vessel instability (heave, pitch and roll) and sound velocity changes with depth. Each depth reading also needs to be accurately positioned and then reduced to an acceptable datum. It is therefore imperative that the relative offsets between the devices used is noted and applied either real-time or in post processing. Figure 4.3 illustrates the various equipment offsets and vertical corrections that need to be applied for accurate depth values.

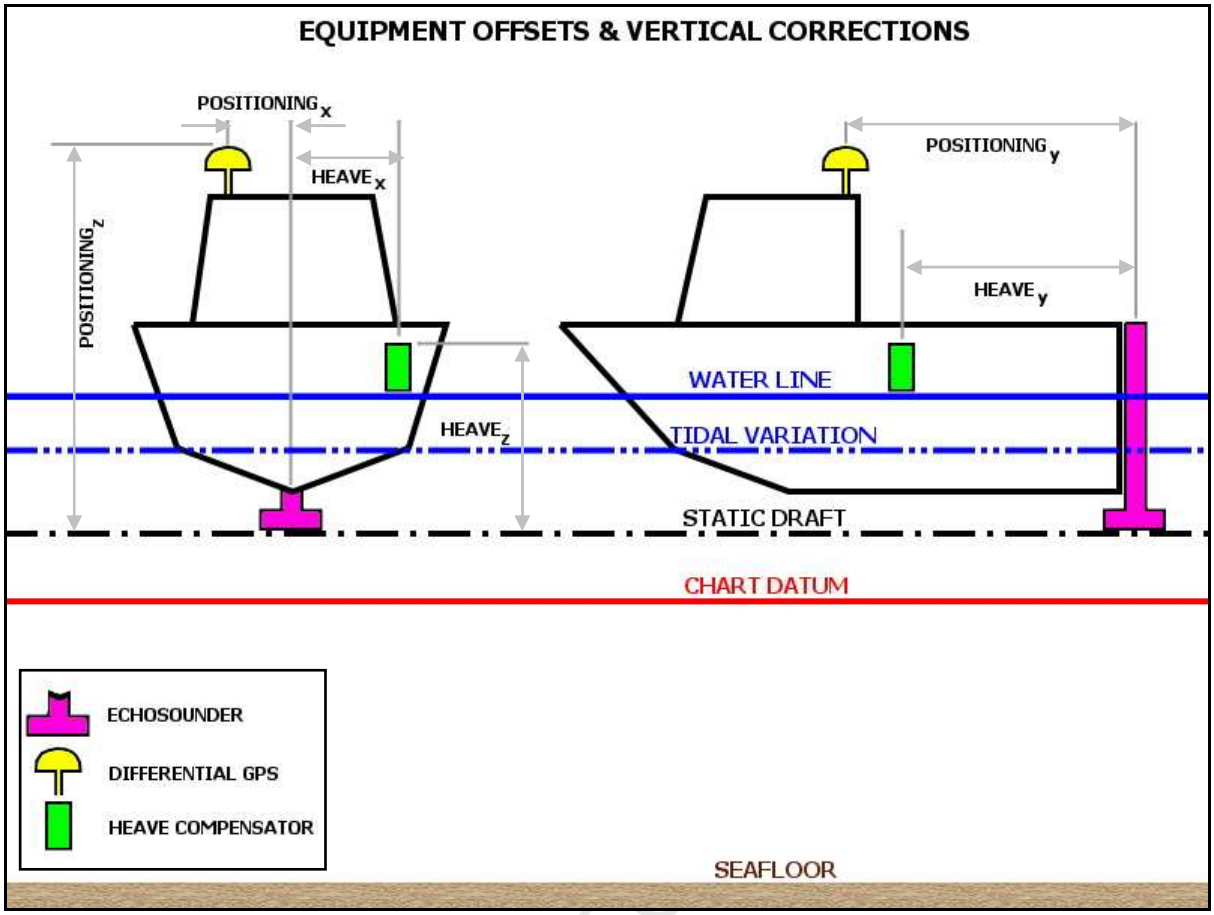

Figure 4.3. Illustration of relative equipment offsets and the different vertical corrections that need to be applied to singlebeam echosounder data.

4.2.2. Multibeam Echosounders

One of the limitations of singlebeam echosounders is that they are only able to provide reliable depth data from directly below their transducers, therefore any relatively small-scale target between adjacent survey lines is not detected by the sonar (Galway, 2000). It was because of this that multibeam echosounders (MBES) were developed, so that 100% bottom coverage could be achieved, even though the meaning of 100% bottom coverage is still poorly defined (Hughes-Clark, 1999).

MBES systems measure the oblique slant range to the seafloor of distances beyond the first arrival of echoes directly below the transducer (Galway, 2000). The systems are usually hull mounted (Jones, 1999) and based on a cross fan beam geometry generated by two transducer arrays orthogonally mounted to each other in an L or T configuration (de Moustier, 1988). The transmit array is placed parallel to the vessel's keel and projects a

vertical fan beam that is narrow along track (1º - 3º) and broad across track (150º and more) (Farr, 1980). Galway (2000) and Jones (1999) describe the receiver array as consisting of a series of hydrophones mounted orthogonally to the vessel's direction of travel. This array generates a series of fan-shaped beams that are in planes parallel to the vessel's direction of travel, and is sensitive to the narrow rectangular window on the seafloor that intersects the transmit and receive beams (Figure 4.4). The receive beamwidths are typically 1º - 3º across track and 20º along track.

Conventionally echosounders determine the travel time of the acoustic pulse by detecting the sharp leading edge of the return echo (Mayer and Hughes-Clark, 1995). This method of bottom detection is referred to as amplitude detection. As the angle of incidence increases, the return echo loses this sharp leading edge and the accurate determination of depth via amplitude detection becomes more difficult (Galway, 2000). MBES systems overcome this problem by determining the phase difference between two beams pointing in the same direction over the duration of the return echo envelope (Galway, 2000). The point at which there is no phase difference, corresponds to the maximum response axis of the beam, providing a measure of two-way travel time for a known angle from which a depth to the seafloor can be determined (Mayer and Hughes-Clark, 1995). Most MBES systems will compute both amplitude and phase bottom detection for each beam and then the software will select the better of the two for that specific beam (Galway, 2000).

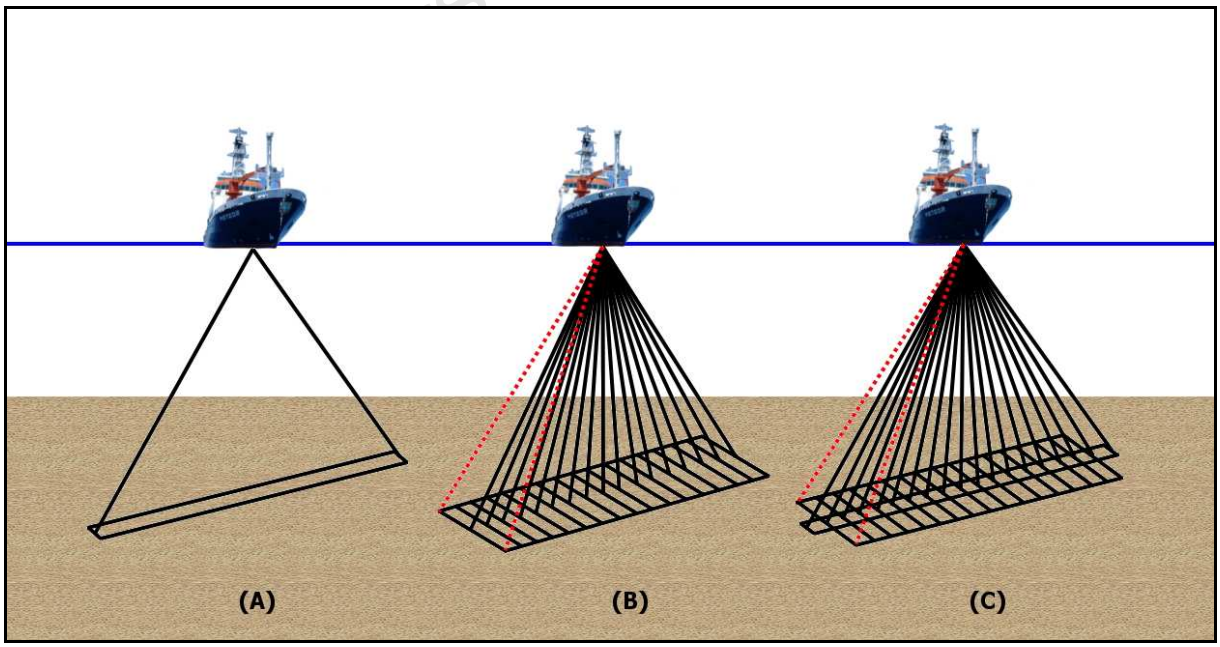

Figure 4.4. Relationship of the transmit and receive beams for MBES. (A) Area of seafloor insonified by transmission pulse, (B) Area of seafloor covered by receiving hydrophones, (C) Received acoustic energy. Modified from Renard and Allenou (1979).

4.2.3. Sidescan Sonars

In the 1950's researchers realised it was possible to turn conventional sonars on their sides and look at a series of echoes along the seafloor as apposed to a single echo from a discrete target (Mazel, 1985). It was at this time that a team from the National Institute of Oceanography in Britain used this technique for studying continental shelves, finding that bottom irregularities at distances of several hundreds of metres produce clear echoes which could be used to determine their shape and position (Belderson *et al.*, 1972).

In contrast to the cone-shaped transmission pattern of conventional echosounders, the main beam of a sidescan sonar is very narrow fore-aft (~1º - 2º) and wide in the transverse direction (Jones, 1999). The narrowness of the beam allows for very high resolution imagery along a strip of seafloor (Mazel, 1985). Other differences cited by Mazel (1985) include the fact that the transducers are angled to the side, that the system consists of two channels and that it is normally tethered to and towed behind the survey vessel. The reason for towing the sidescan is that it helps decouple the vessel motion from that experienced by the towfish, greatly enhancing image quality (Mazel, 1985).

To correctly understand sidescan sonar imagery one needs to understand sidescan sonar geometry. Typically the towfish is towed at an elevation above the seafloor that is equal to ~10% of the scan range (Jones, 1999). Mazel (1985) explains the geometry as follows: the transmitted pulse produces a very dark mark at the start of the display for each channel. Next there will be a period of time when the sonar pulse is moving through the water column and not returning any echoes. The first return should be that of the seafloor and then targets spanning the scan range of the sonar (as the pulse moves outwards). The distances seen on the record are in fact slant ranges and not true distances, although the true distance can be easily calculated, as shown in Figure 4.5.

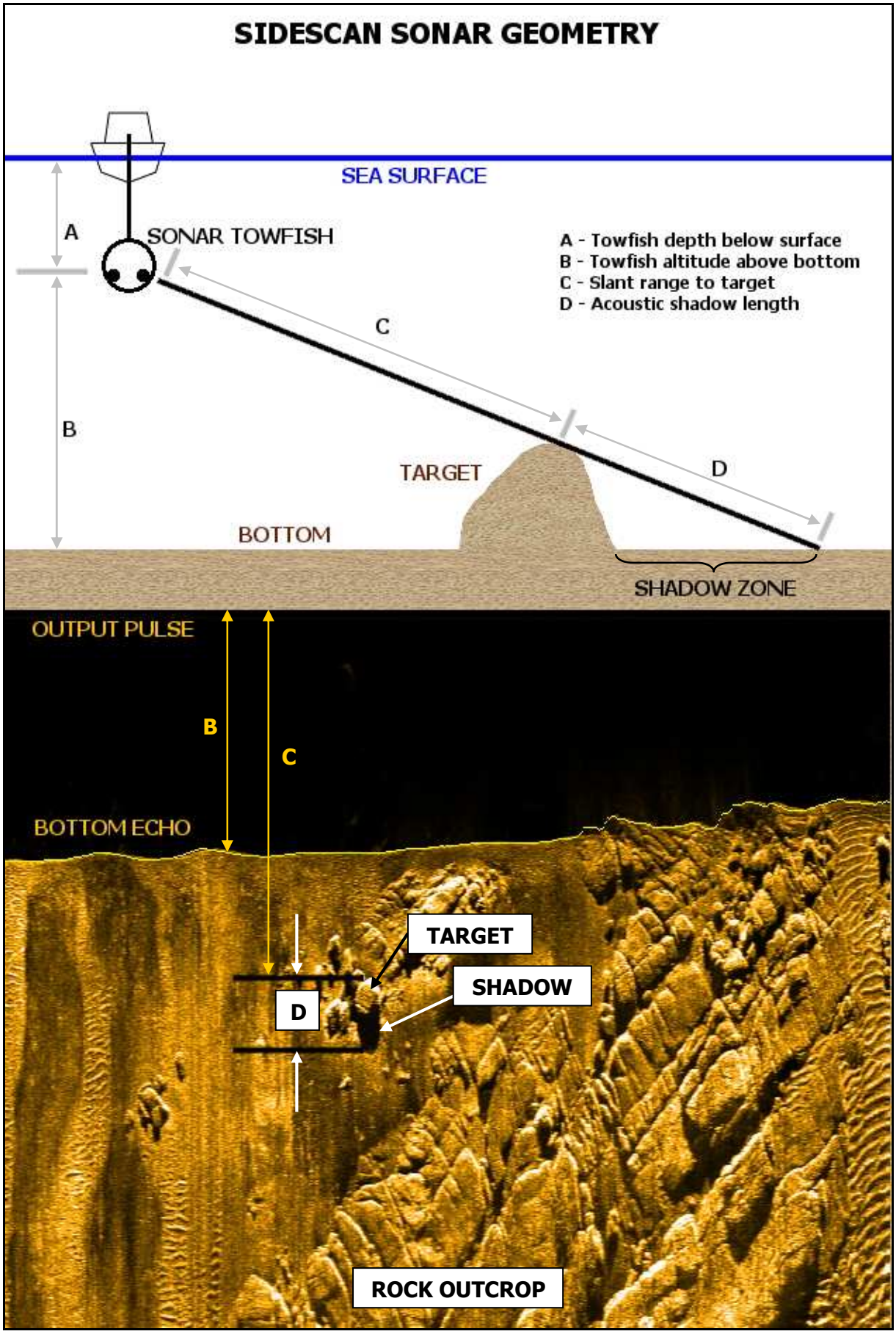

Figure 4.5. Illustration of sidescan sonar geometry, modified from Mazel (1985).

4.2.4. Seismic Profilers

Marine seismic exploration (after Jones, 1999) uses a seismic energy source; a means of detecting elastic waves travelling through the water column or in the seabed; and a method of recording and displaying seismic waves in an interpretable form.

Ideally the outgoing signal should be a spike with an infinite bandwidth of frequencies, but in practice, energy stored in the source cannot be transferred instantaneously. The nature of the transducer, the frequency-dependent absorption of elastic waves and the presence of nearby boundaries all serve to make the outgoing waveform more complex than a simple spike (Jones, 1999).

Seismic waves are detected by hydrophones which are sensitive to the pressure variations in the medium. They are normally configured in arrays and can be either fixed, free-floating or towed (Jones, 1999).

An electromagnetic seismic source (boomer) was developed during the early 1960's (Edgerton and Haywood, 1964). The source is generated from the sudden separation of an aluminium plate from a flat copper coil embedded in a hard epoxy resin (Jones, 1999). The plate is repelled from the copper coil when large capacitor banks are discharged through the coil. An initial pressure wave is formed as the plate is repelled followed by a subsequent wave from the implosion of the cavitation volume. Most boomer systems are capable of resolving reflectors less than 0.3 m apart in near-shore sediments (Simpkin and Davis, 1993), although as a result of this relatively high vertical resolution the system is restricted in terms of depth penetration to a maximum of a few hundred metres (Keary *et al.*, 2002).

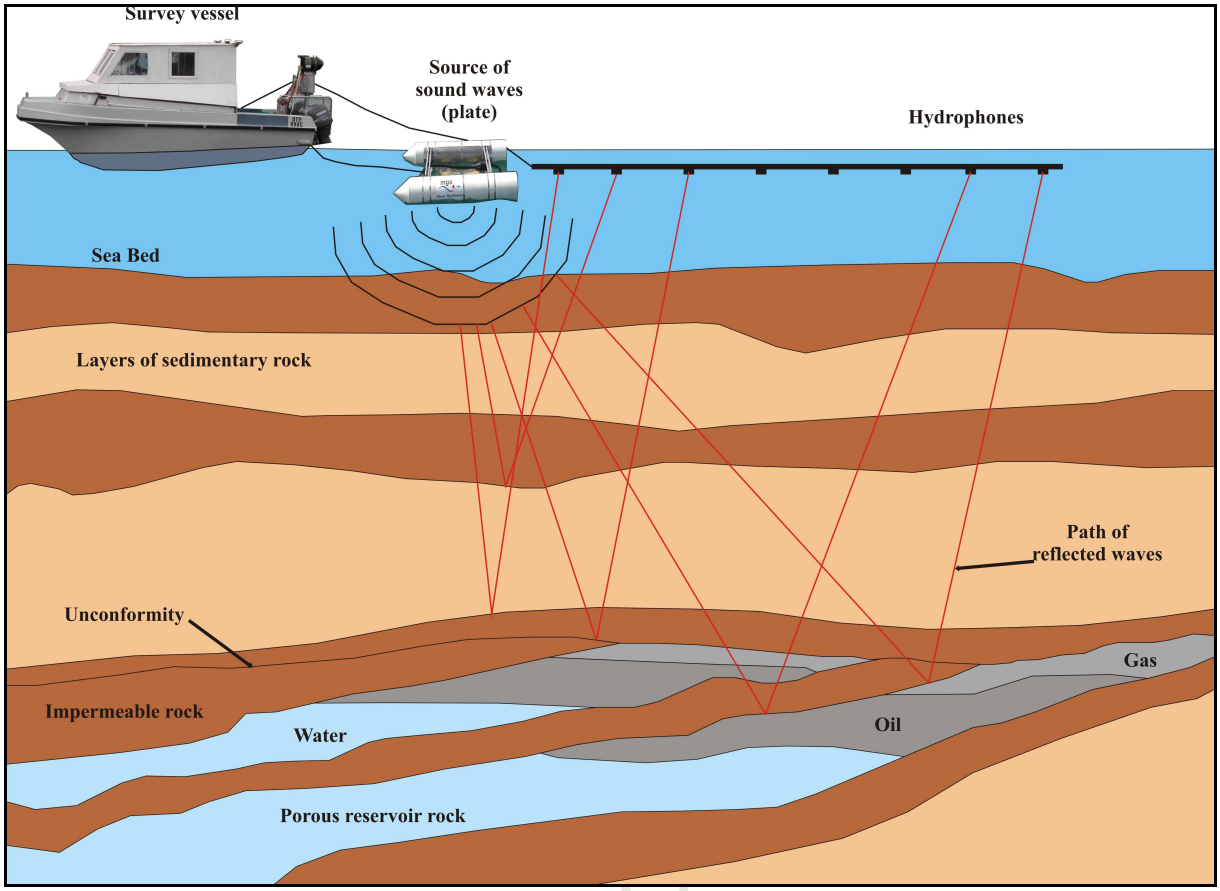

Figure 4.6. Illustration of the principles of reflection seismics as used by the boomer system (Cawthra, 2010).

4.3. Principles of Magnetics

To effectively understand the principles behind marine magnetometer surveys a few principles of magnetics need to be discussed. These principles will help to describe how magnetic fields are modelled and the terms that are needed to effectively understand the model (Hrvoic, 2007).

4.3.1. The Nature of Magnetic Fields

Because magnetic fields cannot be directly perceived by humans the concept of magnetic flux has been invented to help visualise these fields and help in the understanding of how they interact. If one considers a bar magnet the contour lines that flow around the magnet are known as flux lines, the relative concentration of which in space is referred to as the magnetic flux density and is measured in Tesla (T). Magnetic field intensity is measured in A/m and is represented by the symbol H (Hrvoic, 2007).

In a vacuum a magnetic field produces magnetic flux B according to the following relationship:

$$B = \mu_0 \cdot H$$

Where μ_0 is defined as the permeability of free space (Keary *et al.*, 2002; Hrvoic, 2007). Therefore, should an object be placed within a pre-existing magnetic field it will alter the distribution of the magnetic flux because it will have a different magnetic permeability to that of a vacuum.

A further property of magnetic flux according to Gauss' Law, is that the flux must flow in "closed loops", which means that all magnetic fields must exist as dipoles (have positive and negative poles) (Hrvoic, 2007).

4.3.2. Magnetic Permeability of Materials

When an object is placed in a magnetic field, the magnetic flux density for the object is described by:

$$B = \mu_0 \cdot \mu_r \cdot H$$

Where μ_r represents the relative magnetic permeability of an object (Keary *et al.*, 2002, Hrvoic, 2007). All of the so called "magnetic" materials have a very high magnetic permeability and are collectively known as being ferromagnetic (Jones, 1999; Keary *et al.*, 2002; Hrvoic, 2007).

The flux density as a result of the object only can be calculated by subtracting the flux density of a vacuum from the flux density of the object. The result of this subtraction can be expressed as $\mu_0 I$ where I is the induced magnetisation of the material, (Hrvoic, 2007). Hrvoic (2007) described this induced magnetisation as the magnetic field created by the interaction of the applied field with the object's magnetic permeability. The total flux density within the object can now be expressed as:

$$B = \mu_0 \cdot H + \mu_0 \cdot I$$

With the magnetic susceptibility of the object being defined as I/H, (Hrvoic, 2007).

4.3.3. Earth's Magnetic Field

Earth's magnetic field is generally accepted to be derived from the dynamo effect of rotation of the Earth's liquid iron-nickel core (Hrvoic, 2007). An electric current is generated by this rotation which has a magnetic field associated with it. This field is not constant and varies from the tropics to the poles (Figure 4.7).

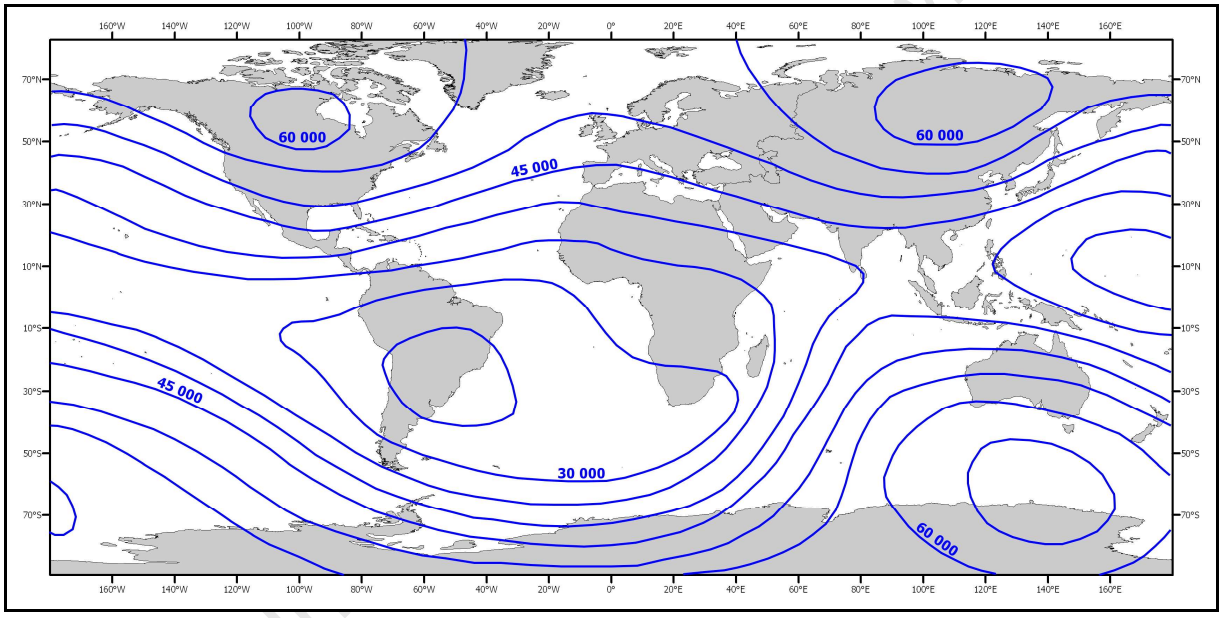

Figure 4.7. Contour map of the total magnetic field intensity over the surface of the Earth, as of 1995. The contour interval is 5 000 nT. Modified from Hrvoic (2007).

4.3.4. The Marine Magnetometer

A proton-spin magnetometer is one of the variants of magnetometers and its operational principles are described below. The device contains a small volume of proton-rich fluid, typically kerosene or methanol (Jones, 1999; Keary *et al.*, 2002; Hrvoic, 2007). A coil is wound around this fluid and when a current is passed through the coil it induces a temporary artificial magnetic field. The result of this magnetic field is that it causes the dipoles of the protons within the liquid to align with the induced magnetic field. This process

is known as polarisation (Jones, 1999; Keary *et al.*, 2002; Hrvoic, 2007). Once the electric field has been applied long enough the fluid will be fully polarised and the proton spin population can be described using the following relationship:

$$\frac{N_+}{N_-} = 1 + \frac{\mu_i \cdot B_p}{k \cdot T}$$

Where N_+ and N_- refer to the number of protons with positive and negative spin polarisations respectively, B_p is the ambient (applied) magnetic flux density, and k the Boltzman's constant. In this equation μ_i represents the magnetic moment of a proton and should not be confused with magnetic permeability (Hrvoic, 2007).

When the induced magnetic field is "turned off" the polarised protons precess (spiral) back to the alignment of the ambient magnetic field (Keary *et al.*, 2002). As this precession takes place an alternating magnetic field is generated which can be detected by a coil and its relative frequency measured by the magnetometer electronics (Keary *et al.*, 2002, Hrvoic, 2007). This frequency is directly proportional to the magnitude of the ambient field vector.

The problem with proton-spin magnetometers is that they require large amounts of power and the proton precession signal cannot be sampled whilst the polarising field is in place. The technique used to get around these inherent problems is to use the Overhauser effect. The primary way this differs from the technique described above is that the Overhauser effect uses electron-proton coupling to achieve polarisation (Hrvoic, 2007).

A chemical that contains a free radical (an unpaired electron in the outer most electron shell) is added to the proton rich fluid. If this free electron is subjected to low radio frequency radiation it can be easily and efficiently stimulated to correspond to a specific energy level transition (Hrvoic, 2007). The electron does not release this energy, it rather transfers it to the protons effectively polarising the population without generating a large magnetic field. Once polarised the proton spin population in an Overhauser magnetometer can now be described by the following (Hrvoic, 2007):

$$\frac{N_+}{N_-} = 1 + \frac{h \cdot (\omega_s - \omega_i)}{k \cdot T}$$

Where h is Plank's constant, ω_i is the proton spin angular frequency and ω_s is the electron spin angular frequency.

The advantages of an Overhauser magnetometer are that it can produce a clear strong proton precession signal using only 1 – 2 W of power (Hrvoic, 2007). Other benefits of using this technique are that the polarising power is applied at a frequency that far exceeds the precession signal bandwidth, therefore the sensor can be polarised at the same time measurements are taking place which effectively doubles the amount of information available to the device (Hrvoic, 2007).

4.4. Geophysical Instrument Suite

The following instrumentation and settings have been modified from internal Council for Geoscience (CGS) reports on the geophysical survey of Hout Bay and surrounds by MacHutchon (2009) and the survey of Simons Town Harbour walls using multibeam echosounder and scuba diving methods by MacHutchon and Cawthra (2009).

4.4.1. Navigational Equipment

The navigation system for the geophysical survey of Hout Bay consisted of a C&C Technologies C-Nav 2050 RTG differential GPS system, which is capable of decimetre accuracy. The sensor consists of a 10-channel dual frequency precision GPS receiver, two additional channels (for receiving Satellite Based Augmentation System (SBAS) signals) and an L-Band demodulator for reception of the StarFire Network APS correction service. With the C-Nav 2050 interfaced, high precision navigation data was output at 5 Hz to the navigational and acquisition software.

Figure 4.8. C-Nav 2050 RTG DGPS.

4.4.2. Multibeam Acquisition System

A Reson SeaBat 7125 multibeam echosounder was used to chart the study area. This is an ultra high resolution system with an operating frequency of 400 kHz. It is a wide sector, wide-band, multibeam sonar utilising 512 dynamically-focused receive beams at 0.5º across-track beamwidth separations. The system measures a 128º swath across the seafloor, detecting the bottom, and delivering the measured ranges at a depth resolution of 5 mm up to 50 times per second. The multibeam system is shown in Figure 4.9.

The SeaBat was interfaced to an Applanix POS MV 320 motion reference unit (MRU) with L1/L2 RTK capability. As an integrated GPS/inertial reference system, the POS MV outputs all motion variables at high rates of up to 200 Hz even in the presence of GPS dropouts or degraded differential GPS corrections. The data output variables include RTK positioning and elevation, velocity, 3D attitude (roll, pitch and true heading), heave (and true heave), acceleration vectors and angular rate vectors. This high-specification system is the highest precision motion reference unit for use with multibeam sonar systems. The multibeam system was calibrated with a Navitronic SVP-15 sound velocity probe (SVP), which can accurately measure the velocity of sound in the water column in 0.5 m increments down to a depth of 200 m.

All data from these devices were acquired and processed using *Qinsy* software.

Figure 4.9. Multibeam acquisition system: Reson SeaBat 7125 sonar (top left), processing unit (top middle), Applanix POS MV motion reference unit (bottom right) and processor (top middle), Navitronic SVP-15 sound velocity probe (top right) and *Qinsy* acquisition and processing software (bottom left).

4.4.3. Singlebeam Acquisition System

For the singlebeam echosounder data collected in the study area, a Navisound 210 single frequency, digital, survey-grade echosounder was used. The Navisound 210 has a narrow beam (9°) 200 kHz transducer and is capable of centimetre scale resolution with a maximum sounding rate of 20 Hz and an effective operating depth of 400 m. The echosounder is calibrated twice daily using a Navitronic SVP-15 sound velocity probe, which can accurately measure the velocity of sound in the water column in 0.5 m increments down to a depth of 200 m. These data are used to accurately correct for changes of sound velocity in the water column, either due to temperature or salinity variations. All hydrographic data was acquired and processed using *HyPack* software.

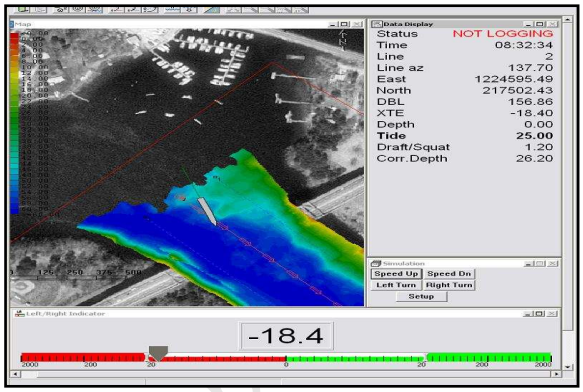

Figure 4.10. Reson Navisound 210 singlebeam echosounder and transducer (top). Navitronic SVP-15 sound velocity probe and *Hypack* acquisition software (bottom).

4.4.4. Heave Compensator

The TSS DMS25 heave sensor is a small portable system for measuring the vertical displacement of a survey vessel. Heave measurements are made by an on board accelerometer and linked via RS232 and analogue BNC to the *Hypack* acquisition laptop.

Figure 4.11. TSS DMS25 Heave Compensator

4.4.5. Sidescan Sonar

A Klein System 3000 dual frequency (100/500 kHz) digital sidescan sonar was used to collect the sonographs. This high-resolution system is based on new transducer technology and advanced circuitry developed for the Klein multi-beam focused sidescan sonar. Acquisition was accomplished using Klein's *SonarPro* PC based system.

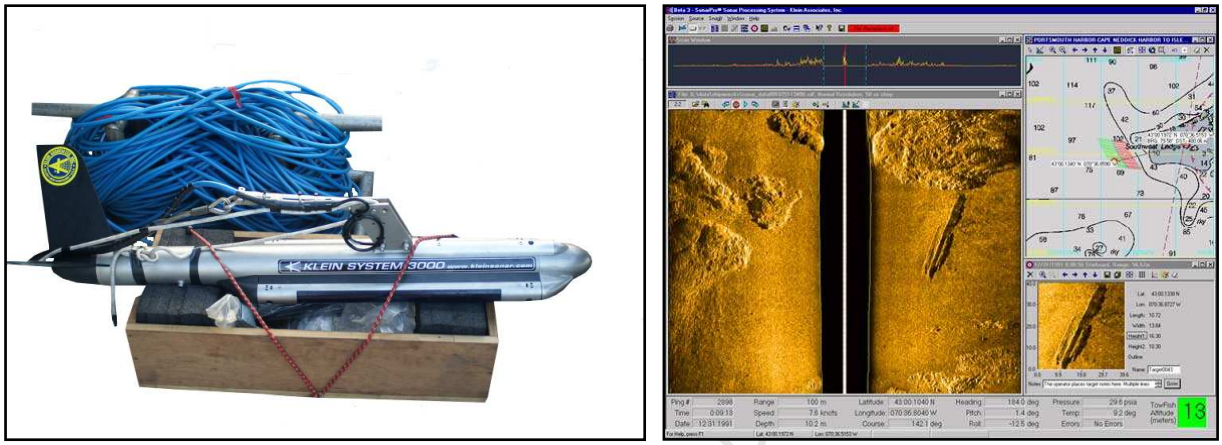

Figure 4.12. Klein 3000 sidescan sonar towfish (left) and *Sonar Pro* acquisition software (right).

4.4.6. Marine Magnetometer

A Marine Magnetics Corporation SeaSPY magnetometer was used for the acquisition of all the magnetic data. This make of magnetometer is an Overhauser magnetometer (Chapter 4.3.4) which allows for faster sampling rates and lower power consumption. The unit has a sensitivity of 0.01 nT and an effective resolution of 0.001 nT. It has no "dead zone", is completely unaffected by any heading offset and is not influenced by ambient temperature. Sampling was performed at a frequency of 1 Hz.

Figure 4.13. Marine Magnetics SeaSpy magnetometer towfish and cable.

4.4.7. Boomer Seismic Profiler

A Design Projects high frequency boomer was used to collect medium penetration seismic profiling data in the survey area. An Applied Acoustic Engineering CSP1000 power supply that produces a maximum energy output of 1 000 J/s was used to power the boomer plate and a Design Projects twenty element hydrophone array was used in conjunction with an Octopus 760D seismic processor to acquire and store the seismic data in SEG-Y format. The Octopus was used for real-time processing, digital recording and as a post-processing workstation. Onboard processing facilities include swell filtering, stacking, water column blanking, time varied band pass filtering, time varied gain, and automatic bottom tracking.

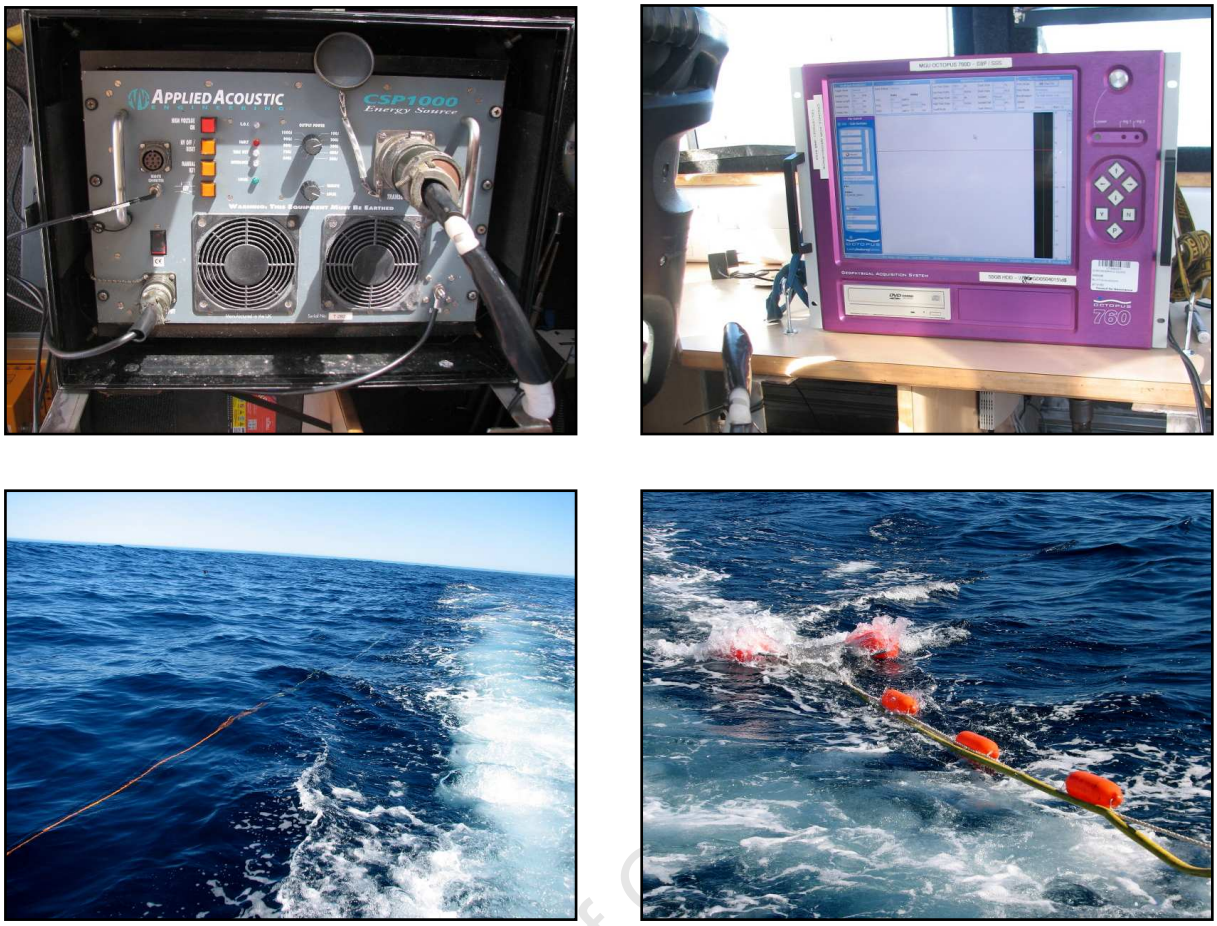

Figure 4.14. Boomer seismic profiling equipment of CSP1000 power supply (top left), Octopus 760D acquisition unit (top right), towed hydrophone array (bottom left) and towed 500J boomer plate in purpose built catamaran float (bottom right).

4.4.8. Pinger Seismic Profiler

A Massa transducer pinger array was used to collect shallow penetration seismic profiling data in the survey area. The unit is powered by a GeoAcoustics 5430A Geopulse transmitter. This unit has a maximum power output of 10 kW and a selectable operating frequency range of 2 – 15 kHz. The amplifier has a signal-to-noise ratio of 20 dB at 100 dB gain, a 1 kHz centre frequency and 1 kHz bandwidth. The transmit repetition rate can be controlled externally or internally and is operator selectable. Pulse length is selected by the number of cycles to improve efficiency of the transducers and to reduce "ringing".

The Octopus 760D seismic processor was used to acquire and store the seismic data in SEG-Y format. It is used for real-time processing, digital recording and as a post-processing workstation. Onboard processing facilities include swell filtering, stacking, water column blanking, time varied band pass filtering, time varied gain, and automatic bottom tracking.

Figure 4.15. Pinger seismic profiling equipment of Octopus 760D acquisition unit (left) and GeoAcoustics Geopulse transmitter (right).

4.4.9. Beach Profiling Equipment

For the beach profiling data two Leica SR20 DGPS units were used. Each unit consists of a handheld Leica GS20 connected to an external Leica AT501 12 channel L-band antenna (Figure 4.16). One unit was set up as a base station, while the other was configured to be a rover collecting realtime kinematic chain data i.e. a data point every second while the unit is moving. In post-processing the base data is used to correct the rover data delivering a baseline root mean square error of 5 – 10 mm in the horizontal and double this in the vertical.

Figure 4.16. Leica SR20 DGPS units.

4.5. Geophysical Survey Procedure

4.5.1. Sidescan Sonar and Singlebeam Bathymetry

The area was surveyed with simultaneous collection of sidescan sonar and singlebeam data. 100% seafloor coverage was achieved with the sidescan sonar, and singlebeam coverage at 130 m line spacing was achieved with the echosounder. A total of one hundred and two lines of sidescan and singlebeam echosounder data were collected.

Survey speed was dependant on sea conditions, prevailing currents and survey direction but was generally kept between 4 – 6 knots. The data coverage achieved during the survey is illustrated by the track chart (Figure 4.17).

One sound velocity profile per day was collected to correct the echosounder data for water column sound velocity changes. This profile measures the velocity at half metre intervals from the water surface down to the seafloor.

The sidescan sonar towfish was "tethered and towed" behind the survey vessel while the singlebeam echosounder was hull mounted. A sidescan sonar scan range of 75 m was used to enable a minimum of 100 % seafloor swath coverage. Four channels of sidescan sonar data (100 and 500 kHz) were stored in SDF format on the acquisition PC hard drives.

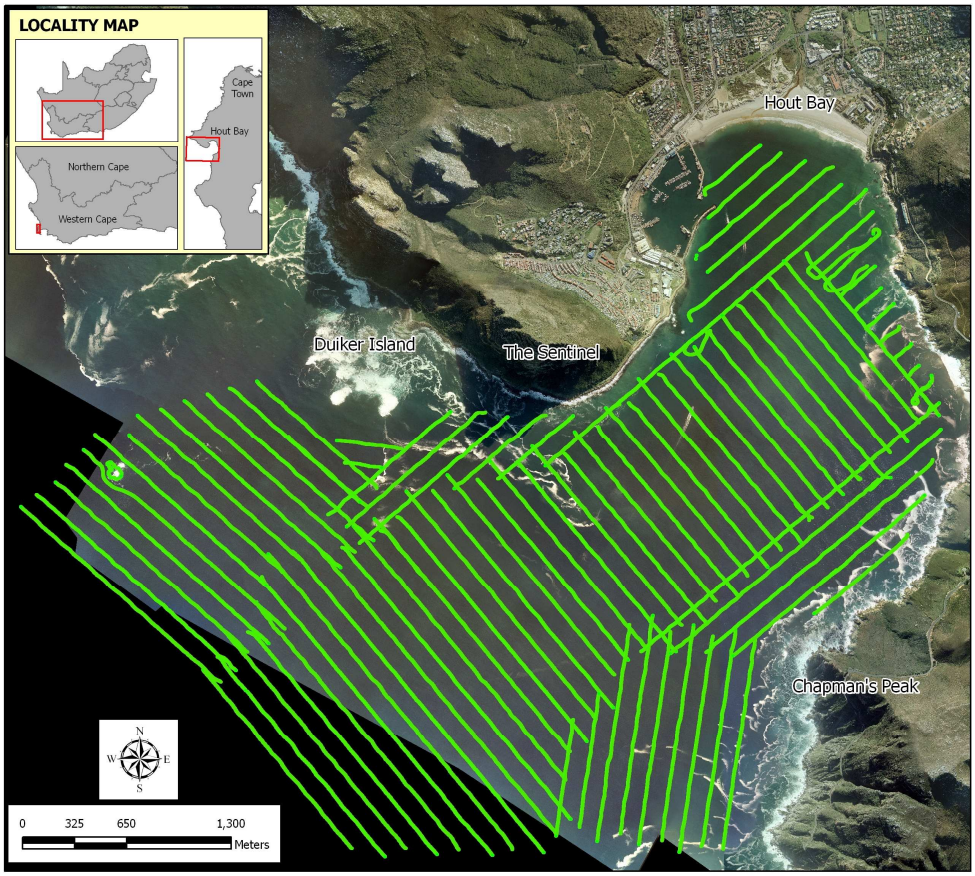

Figure 4.17. Sidescan sonar and singlebeam bathymetry track chart, showing the extent of data coverage.

4.5.2. Multibeam Bathymetric Survey

The Reson SeaBAT 7125 multibeam echosounder used for acquisition was housed in a custom made aluminium shroud so that the transmit and receive arrays were orientated in the correct "Mills Cross" configuration. This shroud in turn was fastened to the end of a stainless steel pole with the projector orientated aft of the vessel. The pole was fabricated to rigidly return to the same mounting position whenever deployed and held firmly in place with stainless steel locking pins.

The inertial motion reference unit used to correct for the dynamic attitude of the vessel during data acquisition was installed inside the cabin of the vessel, slightly to the starboard side of the vessel's centre line. The GPS antennae used by the device were installed on the roof of the vessel (to ensure sufficient "sky" for both receivers). Both antennae were installed on a stainless steel bar ensuring a minimum separation (baseline) of 2 m.

The relative offsets between each device were determined using a Leica total station while the vessel was on the quayside (to eliminate any vessel movement due to sea surface perturbations). These offsets were entered into the relevant device software.

Survey speed was dependant on sea conditions, prevailing currents and survey direction but was generally kept between 4 – 6 knots. The data coverage achieved during the survey is illustrated by the sounding grid (Figure 4.18).

One sound velocity profile per day was collected to correct the echosounder data for water column sound velocity changes. This profile measures the velocity at half metre intervals from the water surface down to the seafloor.

Survey lines were planned to ensure 100% seafloor coverage with adjacent lines overlapping by a minimum of 20%. The spacing between these lines varied depending on the water depth. All data were acquired and processed using *Qinsy* software.

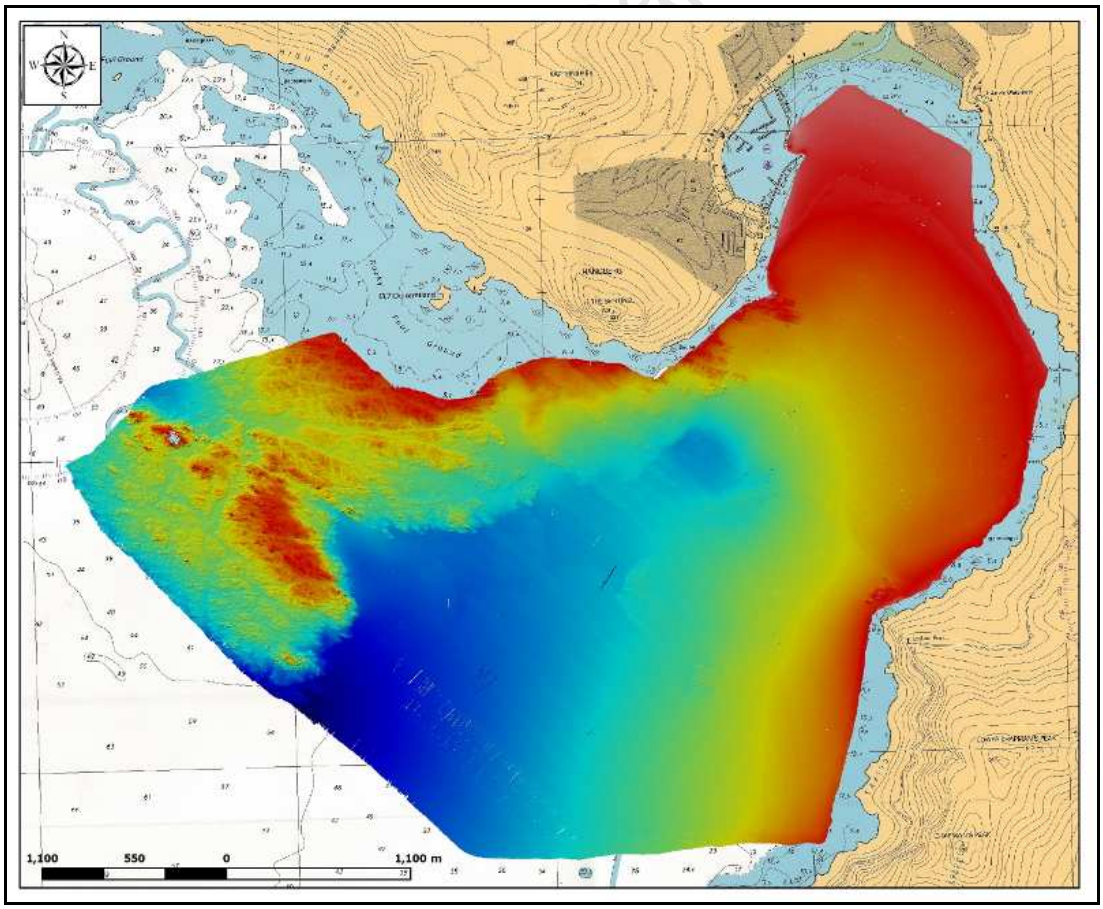

Figure 4.18. Multibeam bathymetry sounding grid. These data are not tidally corrected or cleaned.

The most important aspect of any multibeam survey is to calibrate (align) the minute misalignment of the transducer. This is done by collecting "patch test" lines over an object, sloping or flat seafloor (that is within the study area). These data are then used by the acquisition software to compute the relative corrections (pitch, roll and yaw) to the alignment of the transducer. The following patch test values were determined for the acquisition of multibeam bathymetric data within the study area:

Roll: -1.65°
Pitch: 0.28°
Yaw: 0.39°

4.5.3. Marine Magnetometer Survey

The survey area was surveyed on a regional scale therefore a line spacing of 250 m was utilised. Dolerite dykes were seen outcropping along the foot of Chapman's Peak, so survey lines were planned to run perpendicular to these features. The magnetometer was tethered to and towed 30 m behind the survey vessel. This is done to ensure the magnetic effects of the survey vessel do not in any way interfere with what the magnetometer is recording. Upon startup the device is synchronised with the dGPS time so that the correct position was appended to the correct measurement. The "layback" (how far the towfish was towed behind the vessel) was also input into the software, therefore the resultant position recorded was layback corrected. A sampling frequency of 1 Hz was selected for data acquisition.

Survey speed was dependant on sea conditions, prevailing currents and survey direction but was generally kept between 4 – 6 knots. The data coverage achieved during the survey is illustrated by the coverage chart (Figure 4.19).

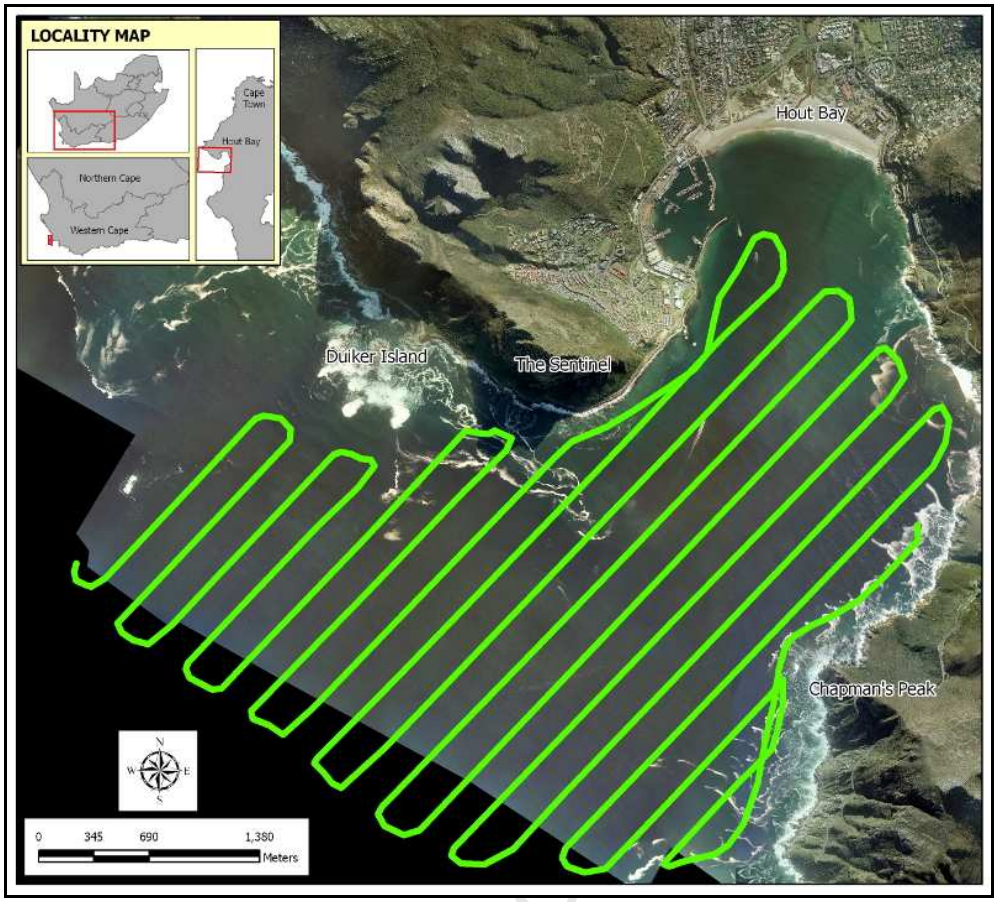

Figure 4.19. Track chart for the magnetometer survey, showing the extent of data coverage.

4.5.4. Boomer Seismic Profiling Survey

The boomer seismic profiling survey was carried out on a regional scale with a line spacing of 500 m within the study area, oriented approximately northwest – southeast. Two seismic lines were run from the study area towards the shelf break to provide a regional continental shelf setting. The length of the lines was determined by the operational range of the survey vessel which is 15 Nm (approximately 27 km) (Figure 4.20).

A 500 J boomer plate was fitted into a catamaran float and towed 10 m behind the vessel off the port side aft bollard. The hydrophone array was secured to a custom built outrigger which extended 3 m from the starboard side of the vessel. Enough cable was let out to ensure that the hydrophone array was positioned opposite the boomer float.

The boomer system was triggered at 600 ms and run on full power at 500 J.

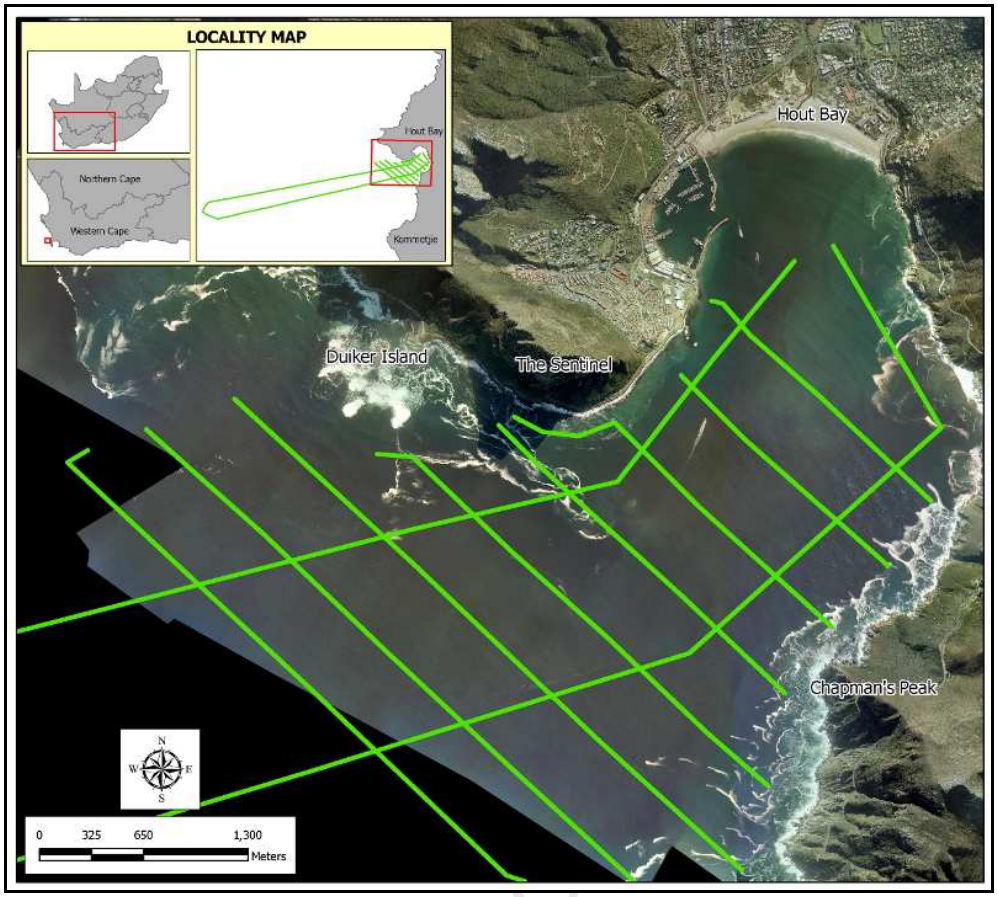

Figure 4.20. Track chart for the boomer seismic survey, showing the extent of data coverage. Locality map shows extent of regional continental shelf lines.

4.5.5. Pinger Seismic Profiling Survey

The pinger seismic profiling survey was carried out on the same lines (within the bay) as those of the boomer approximately northwest – southeast. Because of the limited penetration of the pinger system over consolidated lithologies the lines were shortened to only encompass unconsolidated sediment.

The transducer array was fitted into the same catamaran float (that housed the boomer plate), yet unlike the boomer it was tethered to the starboard gunwale of the vessel.

The pinger system was triggered at 200 ms and run at variable power of between 50 – 30%, optimising penetration versus ringing for the different sediment types.

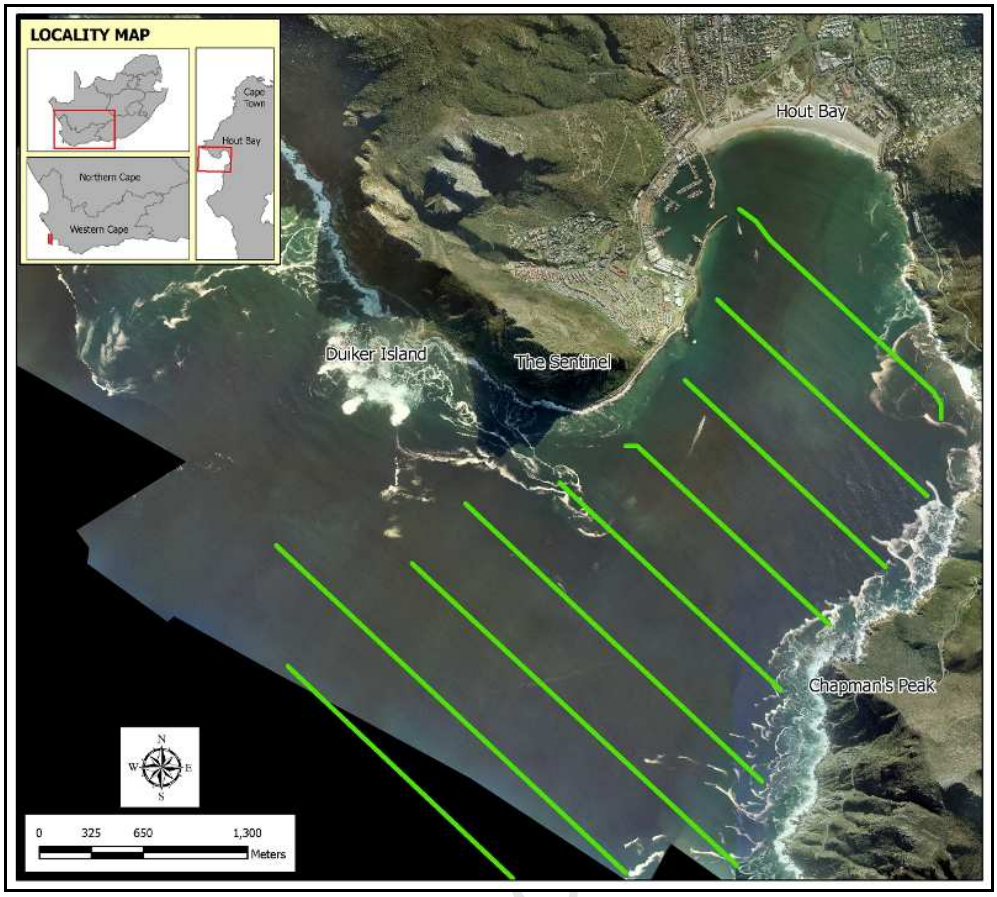

Figure 4.21. Track chart for the pinger seismic survey, showing the extent of data coverage.

4.5.6. Beach Profiling

The days identified to profile the Hout Bay Beach were specifically selected to coincide with spring low tide so as to maximise the effective area that could be surveyed. Lines were walked in a grid configuration where possible, with approximately 10 – 15 m line spacing. The start of each survey focused on the swash zone as this area is the first to become inaccessible as the water level transgresses with the incoming tide (Figure 4.22).

The base station was set up on a tripod positioned on the seaward edge of the Hout Bay Beach parking lot (in the eastern part of the beach). The tripod was levelled with a constant vertical separation of 2 m. The unit was initialised for 8 minutes (so that a suitable horizontal dilution of precision (HDOP) could be achieved). Then data defining the base station position was logged at 1Hz for the duration of the survey period.

The antenna for the roving unit was mounted on a carbon fibre survey pole and rigidly mounted in a backpack. The separation of the antenna from the ground was measured and entered into the rover unit. Like the base station, the rover was first initialised on a stationary spot for 8 min. Once initialised a kinematic chain was allowed to be recorded. Data was logged at 1Hz for the duration of the data acquisition.

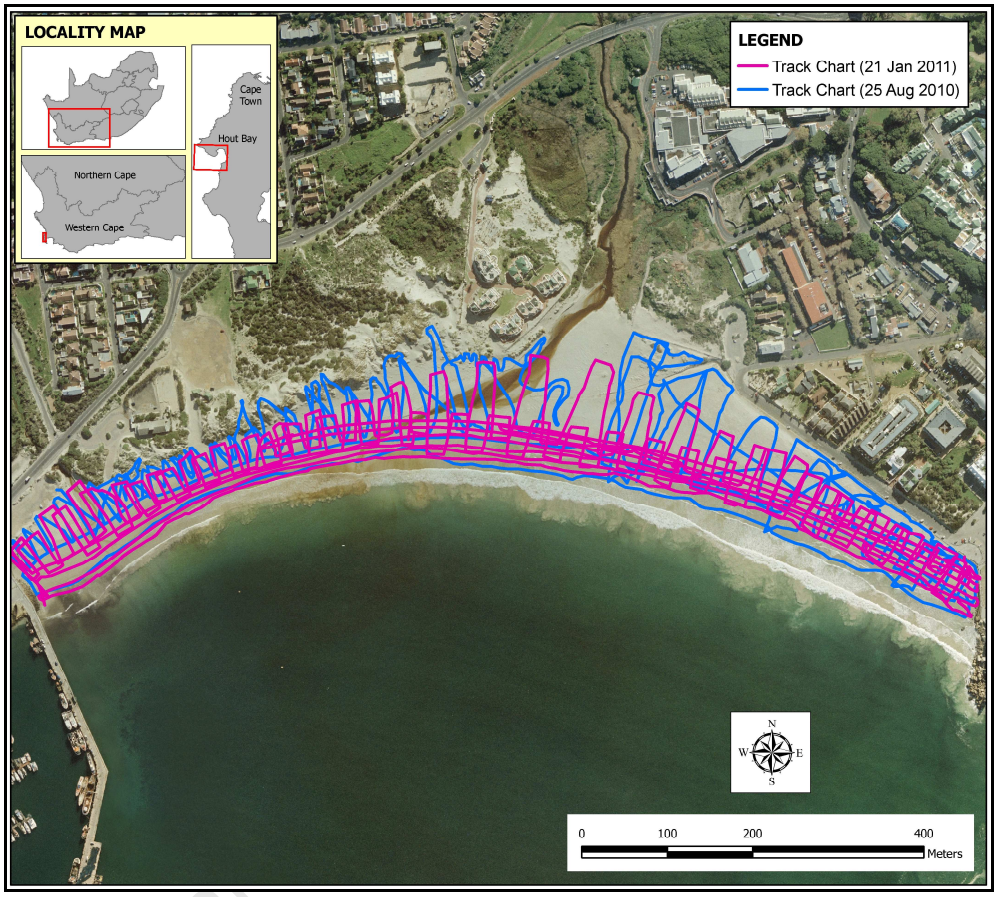

Figure 4.22. Track chart for the beach profiling surveys, showing the extent of data coverage.

4.6. Sediment Statistics

The different sediment statistics reported are mean grain size, median grain size, sorting and skewness after Folk and Ward (1957). The carbonate content of each sample was also calculated using the carbonate bomb method. The sample localities are shown in Figure 4.23. The mean (average) grain size (μ) is calculated using equation (4.1) as defined by Folk and Ward (1957). The calculation uses different percentile ranges for the cumulative weight percentage of the grain size in the sample, expressed as Φ (phi) units. Equation

(4.2) is the relationship between Φ and ξ (grain size in mm). The reported statistic provides an indication of the energy required to transport the sediment (Pethick, 1984).

$$\mu = \frac{(\phi_{16} + \phi_{50} + \phi_{84})}{3} \quad \text{.....(4.1)}$$

$$\xi = 2^{-\Phi} \quad \text{.....(4.2)}$$

The median value (M_d) is that value which separates the lower half of the grain size population from that of the higher half. This value is sometimes the same as the mean (Pethick, 1984). Folk and Ward (1957) define the median as the 50th percentile of Φ (Equation 4.3).

$$M_d = \Phi_{50} \quad \text{.....(4.3)}$$

The sorting (σ) of the sample is equivalent to the standard deviation of the grain size population and is defined by equation (4.4) (Folk and Ward, 1957). The sorting of a sediment sample is an indication of how effective the depositional medium is at separating the grains into their respective size classes (Pethick, 1984). Small values of sorting indicate low standard deviation and selective transport and deposition with the converse holding firm for high values of sorting (Pethick, 1984). Factors influencing sorting include sediment source, transport mode and depositional environment and sorting generally increases from proximal to distal environments (Pethick, 1984).

$$\sigma = \frac{\phi_{84} - \phi_{16}}{4} + \frac{\phi_{95} - \phi_5}{6.6} \quad \text{.....(4.4)}$$

Skewness (sk) is a measure of the symmetry of the grain size distribution within the sample and is related to erosional and depositional processes (Pethick, 1984). The statistic is defined by equation (4.5) (Folk and Ward, 1957). A negative skew (coarse tail) indicates a mode of finer grained sediment with a large coarse tail with the converse holding firm for a positive skew (Pethick, 1984; Boggs, 2001).

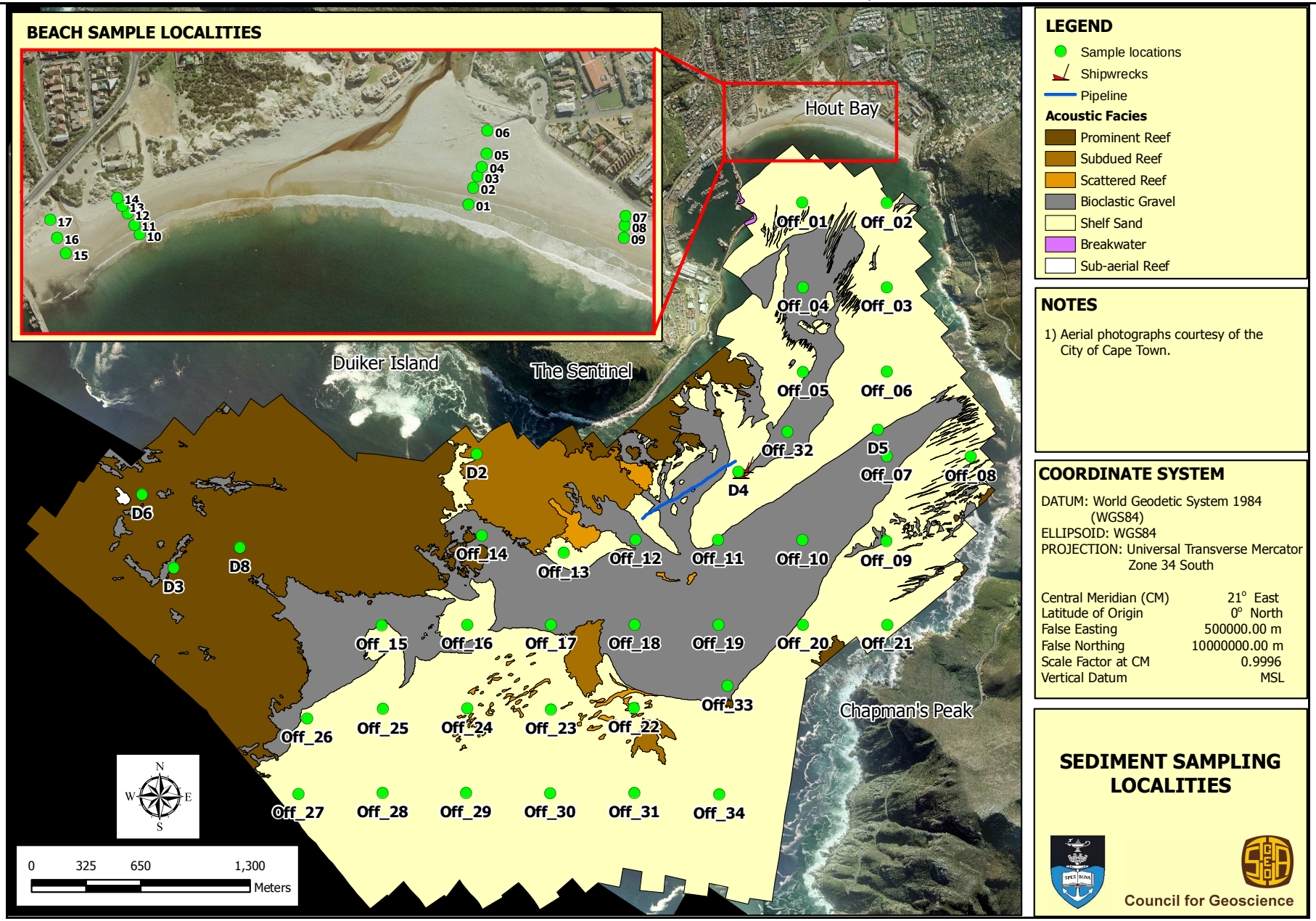

Figure 4.23. Sediment sampling localities in relation to acoustic facies. Inset map depicts beach sampling localities.

$$sk = \frac{\phi_{16} + \phi_{84} - 2\phi_{50}}{2(\phi_{84} - \phi_{16})} + \frac{\phi_5 + \phi_{95} - 2\phi_{50}}{2(\phi_{95} - \phi_5)} \quad \text{.....(4.5)}$$

Carbonate content was determined by the carbonate bomb method, using the technique initially described by Schink *et al*. (1979). The amount of CO_2 liberated from the dissolution of $CaCO_3$ by dilute HCl is measured as a pressure increase. Because this increase is in a closed system it can be directly related to the mass of carbonate in the sample, thereby allowing the weight percent of $CaCO_3$ to be calculated. The accuracy of this test is better than three percent with a precision of two percent for concentrations > 5% $CaCO_3$ (Birch, 1979).

In the laboratory the grab samples collected were stirred to homogenise the sample and two subsamples were collected. A larger 200 g sample from which the sedimentary characteristics would be determined and a smaller 50 g sample for verification of the sidescan sonar facies and to be photographed. An organogram of the analytical laboratory procedures is outlined in Figure 4.24.

The 200 g sample was dialysed for 24hr to remove interstitial salt then split into a larger and smaller subsample with the respective dry weights of each recorded. Carbonate content was determined using the smaller sample whilst the larger sample was wet sieved first through the 2 mm sieve to separate the gravel fraction from the sample and then through the 63 µm sieve to separate the sand and mud fractions. The sand fraction was dried in an oven then passed through a series of sieves defining the various sand fractions. The dry weight of sand retained by each sieve allowed a weight percentage for each fraction to be calculated. A full and detailed description of this methodology is provided by Woodbourne (1991).

This chapter concludes all equipment settings and methodologies; the following chapters will present and discuss the different data types collected for this investigation.

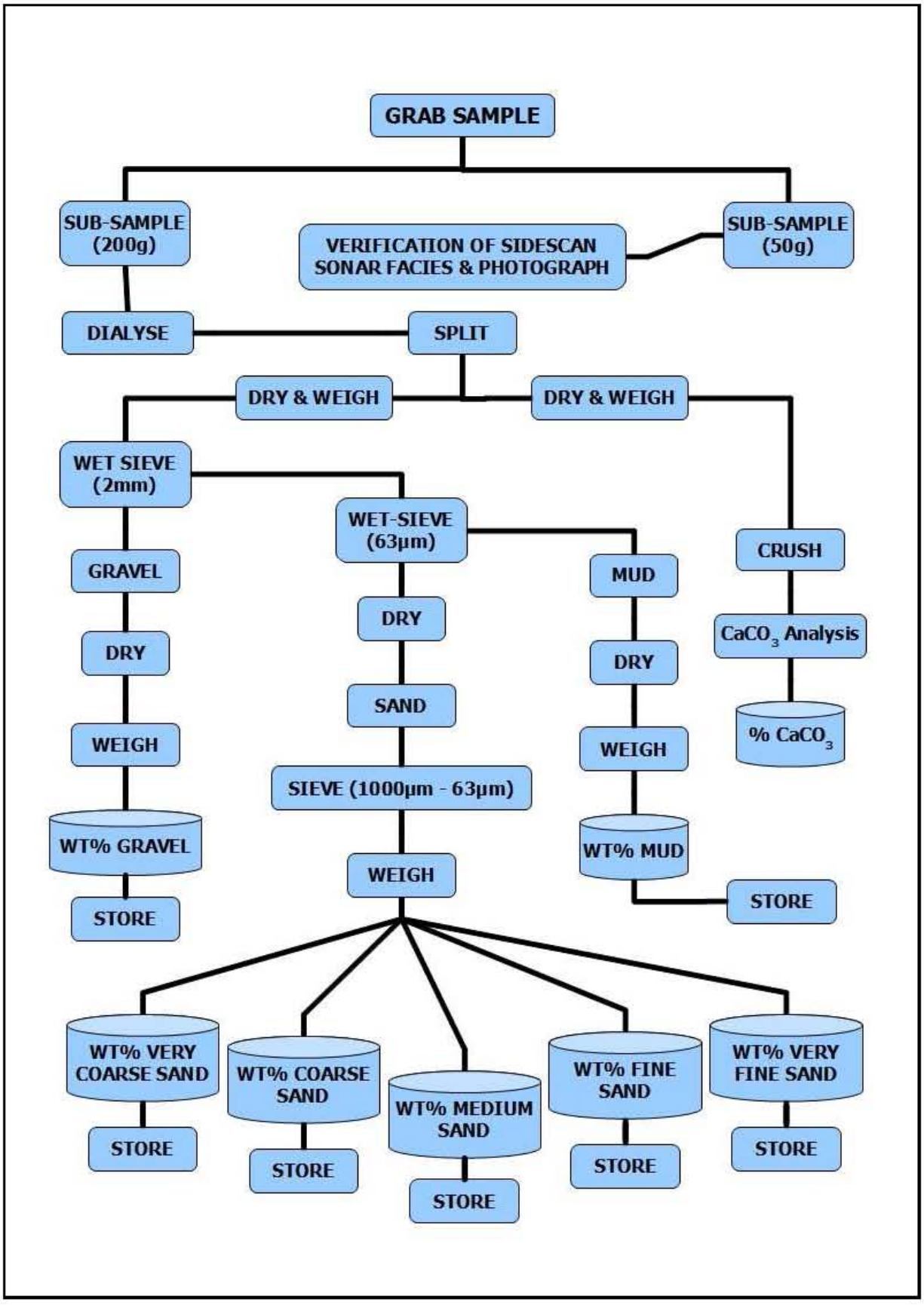

Figure 4.24. Organogram outlining the processing methodology for each sediment sample.

5. BATHYMETRY

5.1. Introduction

Two bathymetric datasets were collected in the study area, the first of which was a singlebeam dataset collected concurrently with sidescan sonar data and the second a multibeam dataset. All depths quoted are reduced to Mean Sea Level (MSL).

5.2. Tidal Analysis

Recorded tidal data were recovered from an atmospherically vented tide gauge which was levelled to MSL and deployed in Hout Bay Harbour. These data were used to reduce the geophysical data to a known datum and span one complete spring high cycle and one full neap cycle (Figure 5.1).

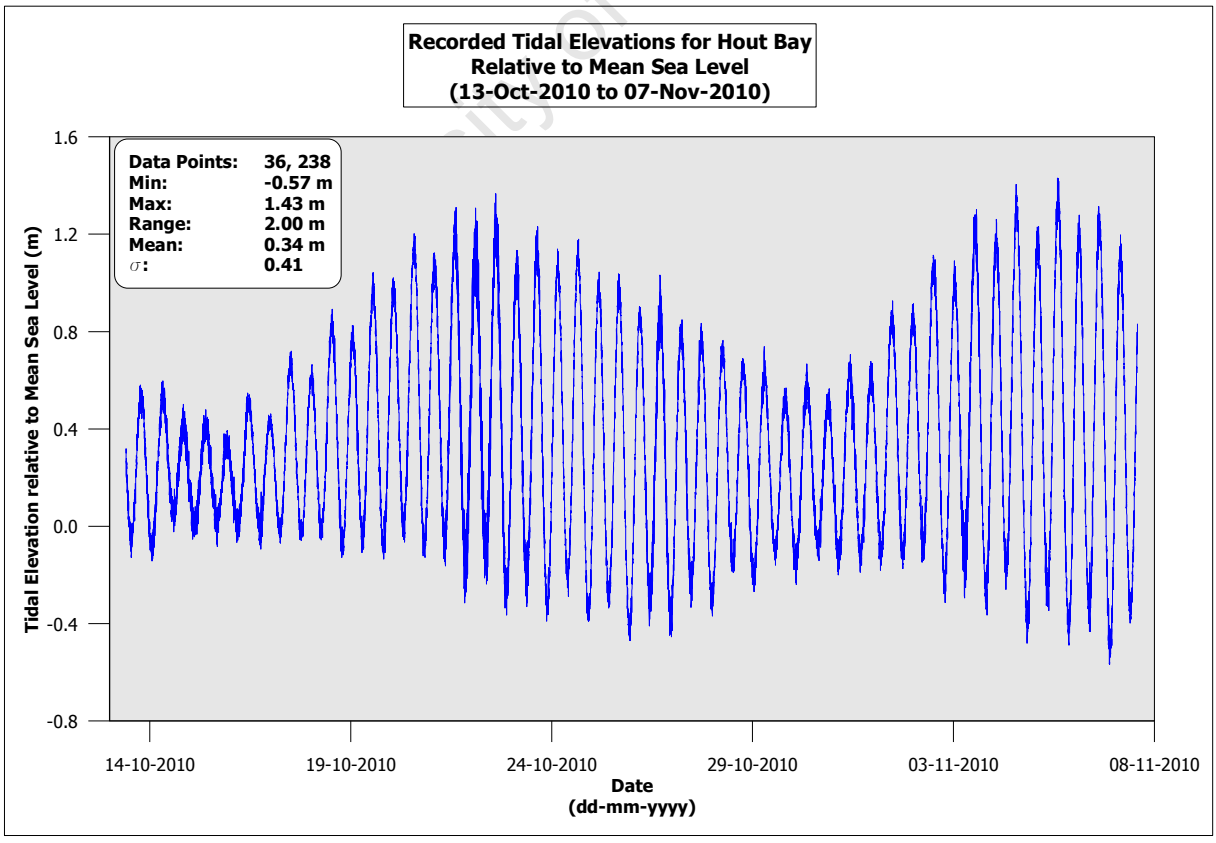

Figure 5.1. Tidal data collected by the author in Hout Bay Harbour.

5.3. Singlebeam Bathymetry

The bathymetry of the surveyed area in Hout Bay ranges from 5 m BSL in the protected north eastern part of the bay to 52 m BSL in the south western portion of the study area (Figure 5.3). The main axis of the embayment trends southwest – northeast (234º/54º) with a generalised slope of between 1 – 1.5º, dipping towards the south west. There is a slight (~3 m) depression in the seafloor bathymetry approximately 740 m SSE of the Sentinel covering an area 0.2 km^2. The northern part of the embayment tends to bulge to the north with Hout Bay beach at its margin.

The area extending away from the Sentinel in a south westerly direction is characterised by an undulose seafloor morphology and represents the sub-marine toe of the sub-aerial outcrops of this headland. The bathymetry adjacent to the Sentinel extends from 0 to 34 m BSL. Approximately 2,1 km southwest of the Sentinel are three localised bathymetric highs of varying shape, although collectively they form a lobe like structure which strikes at 136º. The most prominent of the three is Vulcan Rock, which breaks the waterline at spring low tide (Figure 5.2). It rises from a depth of approximately 20 m BSL with steeply sloping sides of between 15º and 16º. Approximately 300 m dextrally along strike is another unnamed pinnacle which rises from 20 to 10 m BSL. Continuing along strike a further 500 m the largest of the three highs is encountered. The reefs which constitute the largest high are Tafelberg Reef to the west and Klein Tafelberg Reef to the east. Collectively these reefs measure approximately 880 x 430 m and rise from 22 m to 10 m BSL. These bathymetric highs are a contributing factor to the large surf experienced at Dungeons in that they focus the incoming swell via the channels between them onto an area that shoals very rapidly at the base of the Sentinel.

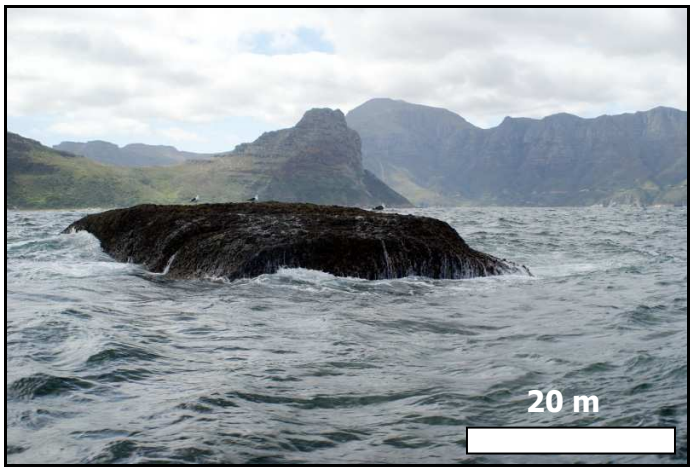

Figure 5.2. Photograph of Vulcan Rock breaking the surface with the Sentinel in the background. Photograph courtesy of Mr. Errol Wiles.

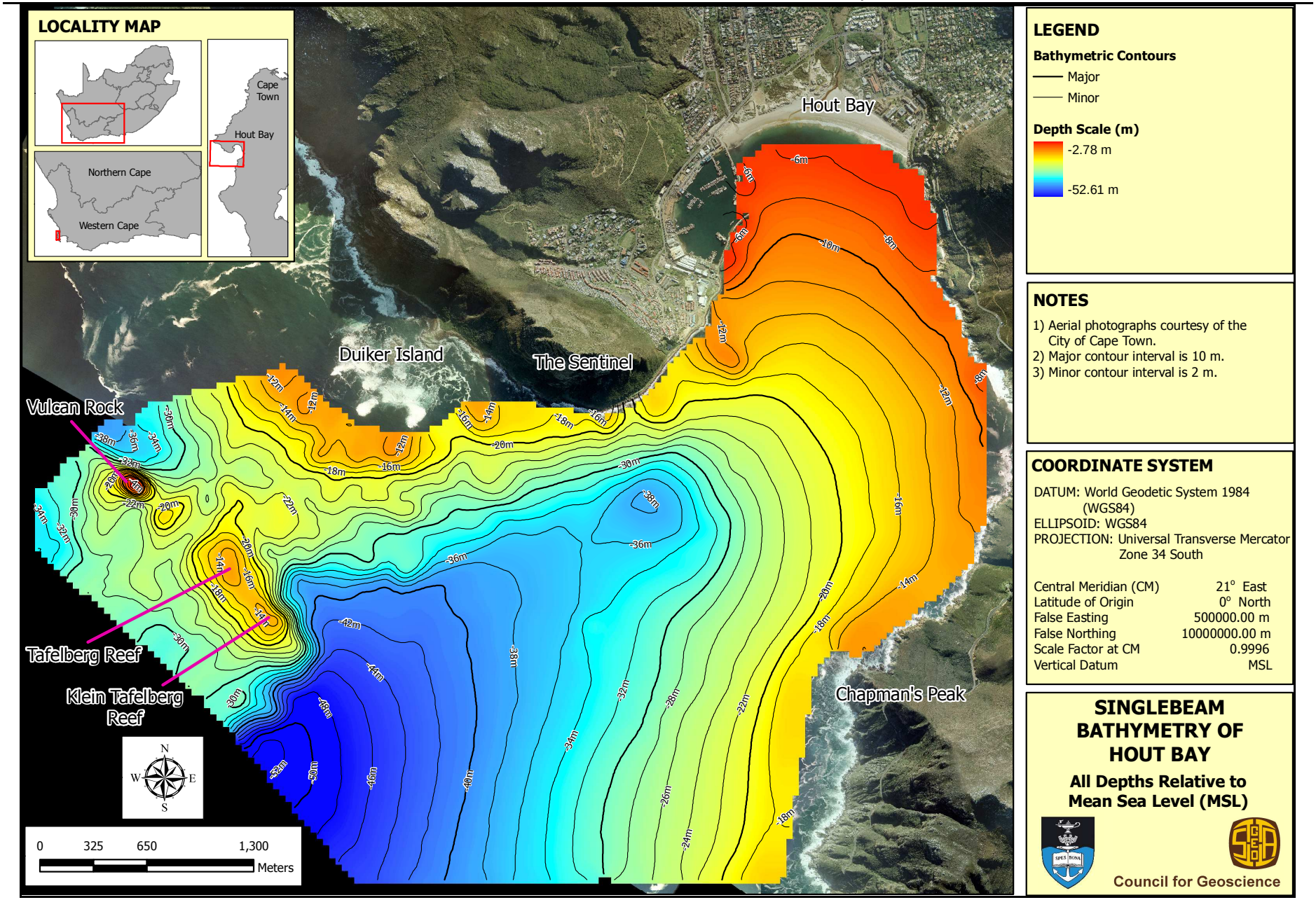

Figure 5.3. Singlebeam bathymetry of the study area.

5.4. Multibeam Bathymetry

The general trends outlined by the singlebeam bathymetry are reinforced by the multibeam data with the only difference being the marked increase in resolution. After each sounding has been corrected for the motion of vessel and alignment of the transducer it can be presented spatially and is collectively referred to point cloud data (Figure 5.6). These data help to visualise the different surficial seafloor facies. Every point on these images is a real sounding and can vary from 5 – 30 cm (across track). It is as a result of this ultra-high resolution that one can delineate fabrics in the reef outcrops, or bedform wavelengths and crest heights.

The first juxtaposition immediately evident when analysing the bathymetry of Hout Bay is the difference in slope and texture of the east side of the bay versus the west. The eastern and northern margin of the bay has a smooth (gentle gradient) slope in the vicinity of Chapman's Peak becoming more convex in nature towards the northern part of the bay (Figure 5.5 C, D). The eastern part of the study area has exposed rock outcrop with subordinate sediment infilling gullies.

The sub-marine toe of the Sentinel extending to the south west has an almost lobe-like morphology when viewed from above. The "lobe" is flattened along an axis trending 226º. Similar sub-marine toes in other parts of the study area exhibit the same trend namely the two reef outcrops directly to the east of the Sentinel and the toe associated with Chapman's Peak lookout point. The outcrop in front of the Sentinel shoals steeply from water depths of approximately 48 to 10 m BSL (Figure 5.5 A, B). From the singlebeam bathymetric results the "lobe" offshore of the Sentinel has three localised highs. The increased resolution of the multibeam data allows four relative bathymetric highs to be identified and the remaining three more clearly defined. The three main highs are separated by gullies which trend approximately 30 – 38º. The width of these gullies varies from approximately 30 to 60 m wide.

The margin of the largest of these highs (which incorporates Tafelberg and Klein Tafelberg Reefs, respectively) exhibits spur and groove topography, which primarily reflects the orthogonal joint sets of the outcrop (Figure 6.3 & Figure 6.4).

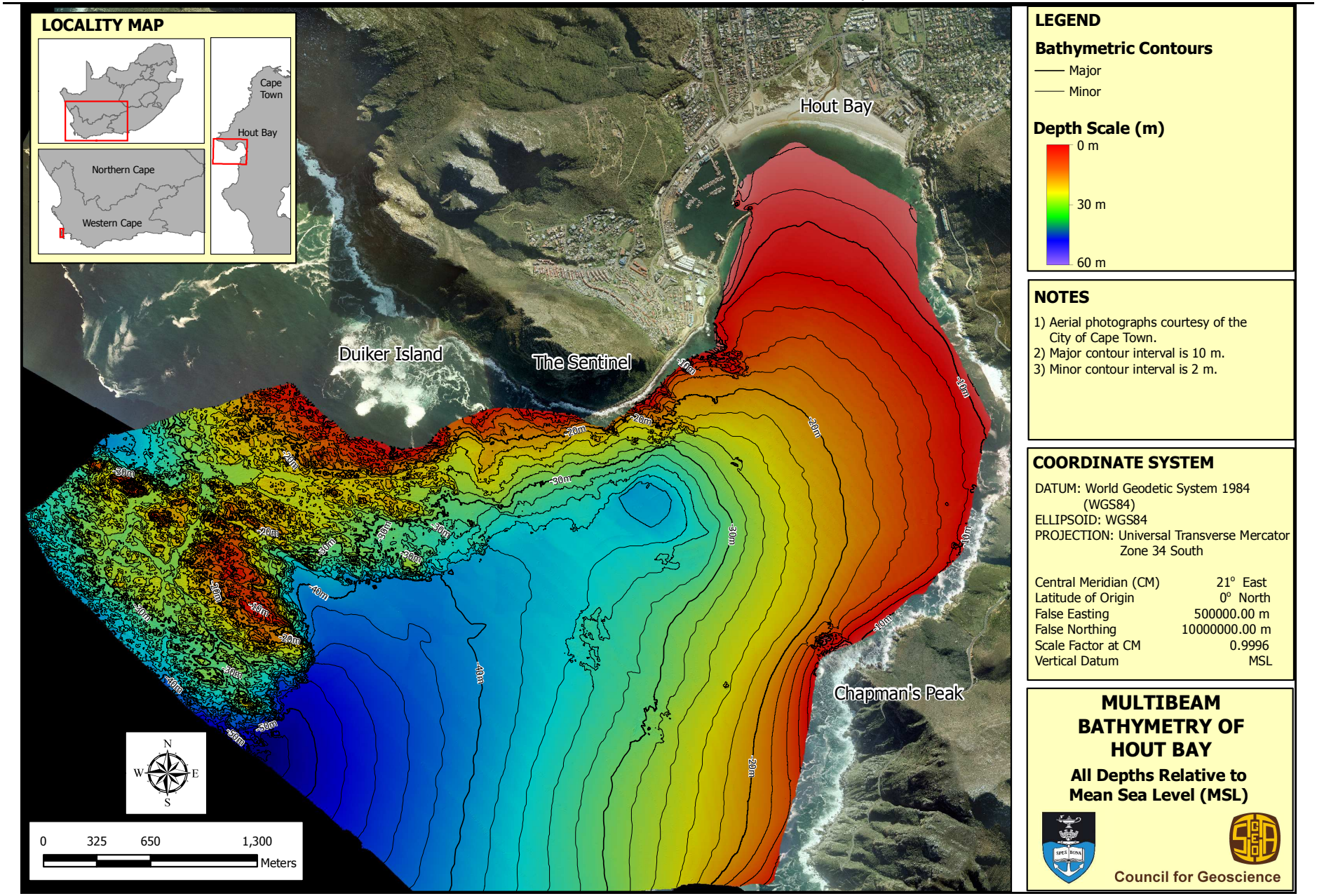

Figure 5.4. Multibeam bathymetry of the study area.

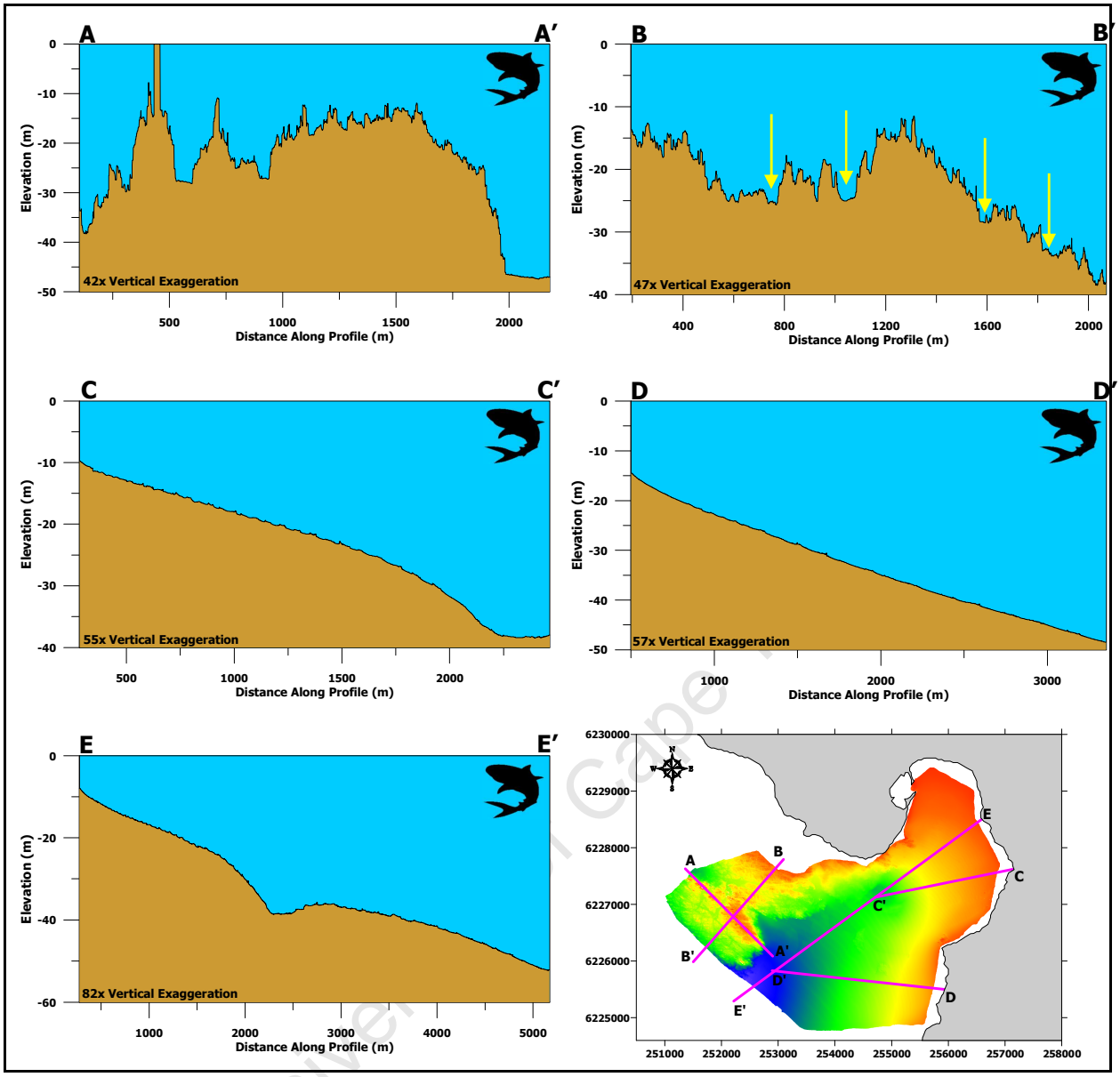

Figure 5.5. Selected bathymetric cross sections. All elevations relative to Mean Sea Level (MSL).

Figure 5.5 presents cross-sectional profiles through the multibeam dataset. In the section from Duiker Island to Tafelberg Reef four lineations are clearly visible (demarcated by arrows in Figure 5.5 B). These lineations are fairly laterally extensive throughout the outcrop with the two most offshore lineations striking at approximately 127º and 131º, respectively, and the most inshore at 112º.

The fabric seen within the offshore reef is repeated in the toe just off Duiker Island, yet around the Sentinel towards the east the morphology of the seafloor differs to that offshore. Although still displaying a rugged microtopography it is more subdued. The margin of this

zone around the base of the Sentinel is characterised by rubble derived from the slopes above.

There are three noticeable erosional depressions in the study area. The first and largest is the depression associated with the sub-marine outfall discharge. The other two are found at the base of the southern breakwater and the end of the northern quay which forms the entrance to Hout Bay Harbour.

There are a few notable anthropogenic bathymetric features. The two shipwrecks in the mouth of Hout Bay (Figure 5.6) form notable bathymetric highs. The more northern of the two is called the *Astor*. She was a South African fishing trawler scuttled 9 August 1997 (Koornhof, 2000; Wikitravel, 2009) and shoals from approximately 26 to 13 m BSL. She rests vertically on the seafloor with an orientation of 130º and rigging still clearly intact. A scour moat of approximately 2.5 m has developed around her with it most pronounced beneath her bow. She measures 27 m long (bow to stern) with a gross tonnage of 340 t (Wikitravel, 2009). The *Astor* is located approximately 1.5 km on a bearing of 182º from the end of the southern breakwater of Hout Bay Harbour. The southern vessel is called the *Katzmaru* . She was an oriental trawler that struck an unidentified object and was holed on her port side. While under tow to Hout Bay she flooded and sank on 7 August 1978 (Koornhof, 2000) and lies 42 m to the southwest of the *Astor* on her starboard side which means she shoals from 26 to 20 m BSL. She has come to rest with an orientation of 117º. From the point cloud data (Figure 5.6) it is clearly evident as to how she met her demise with the impact on her port side clearly visible. It can clearly be seen that her propeller has been salvaged. A prominent scour moat of almost 5 m has developed in her leeward side. She measures 25 m long (bow to stern) with a gross tonnage of 400 t (Wikitravel, 2009).

The other notable anthropogenic bathymetric feature is that of the submarine outfall pipeline (Figure 5.7). The concrete collars that support the pipeline are evident in the point cloud data, with an average spacing of 4.5 m apart. The pipeline is mostly visible with it being partially covered by sediment to fully exposed in its distal sections and completely buried from just inshore of the shipwrecks to the pump station.

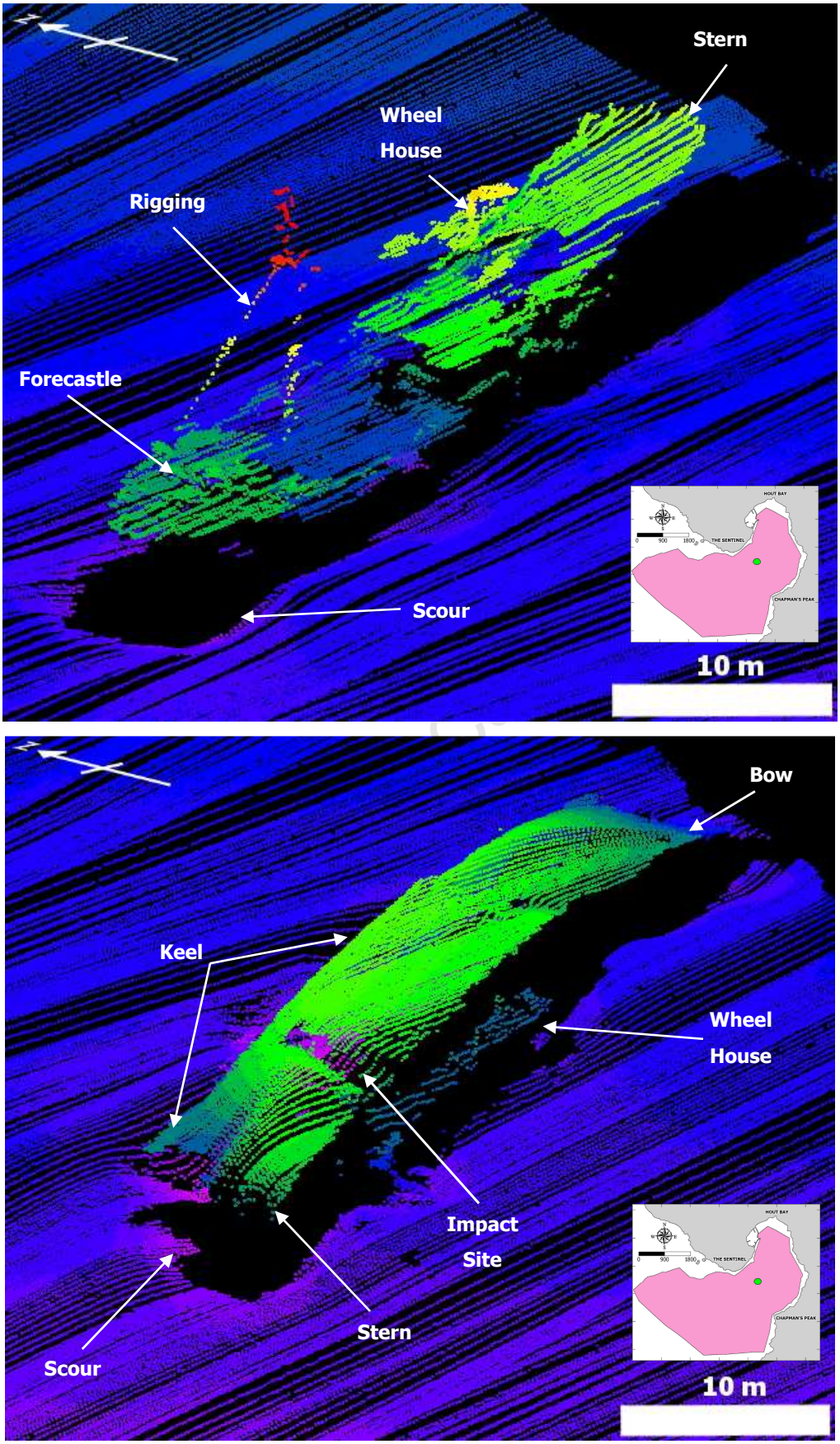

Figure 5.6. Point Cloud images of the *Astor* (top) and *Katzmaru* (bottom). Inset maps shows image location.

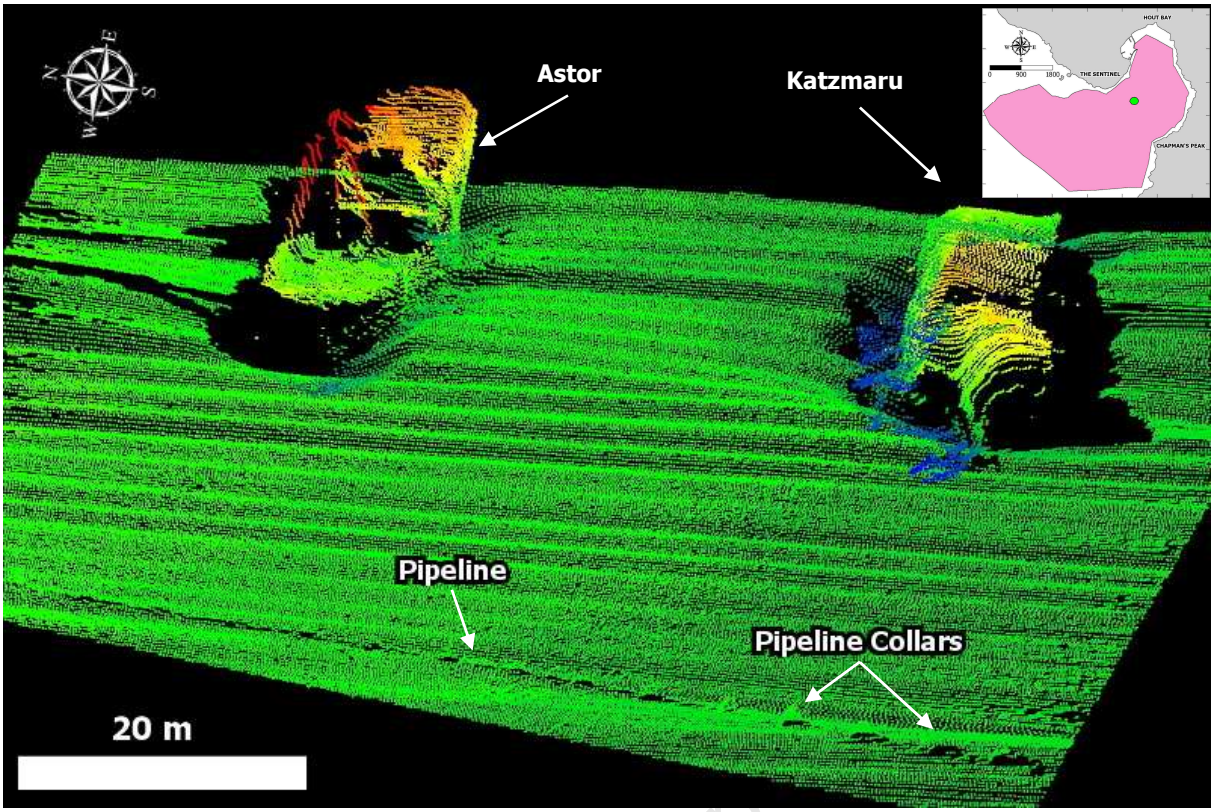

Figure 5.7. Point Cloud image of the submarine outfalls pipeline. Inset map shows image location.

5.5. Discussion

From field observations of the regional geology exposed (sub-aerially) around the flanks of Hout Bay and incorporating where the seafloor exhibits a rugged, undulose morphology, it is possible to tentatively correlate these areas to outcrops of Cape Granite Suite and Table Mountain Group sandstone. The lobe-like structure described in the results is therefore granite outcrops which show a generalised orientation of approximately 226º. Scheepers and Schoch (2006) reported that the granites in the study area were emplaced during the Saldania Orogeny, so the observed orientation would be aligned to weaknesses within the underlying Malmesbury metasediments as a result of the orogenic events.

There is a definite erosional structure (fabric) in the granite exposures which most likely results from the orthogonal joint sets as typical of most granite outcrops. There are however a few linear features which show a slightly different orientation to that of the joints. These linear features can be seen adjacent to Tafelberg Reef. Two of them when described using SCUBA diving revealed themselves to be dolerite dykes.

The contrast in surface texture between the western and eastern margins of Hout Bay may be explained by sediment availability within the study area and prevailing hydrological factors. As has been shown by Rossouw (1984) (Figure 10.4) the dominant wave direction for the study area is from the southwest. The dominant wind directions (Figure 2.1) have been shown to be from the southeast, therefore one would expect an accumulation of fine- to medium grained sediment along the eastern margin extending into Hout Bay entrained by the prevailing wind and hydrological regime. The bathymetric profiles show this trend with a sediment wedge forming along the eastern margin (Figure 5.5 C – E). It must be noted that bathymetric data were not collected in water depths too shallow or too high energy for safe navigation. This equates to the surf zone around Hout Bay. Field observations show that there are no beaches around the eastern margin of the study area which means that although the sediment wedge thickens towards Chapman's Peak and Constantiaberg there is a very narrow high energy zone which prohibits sediment accumulation. The western margin of the study area is dominated by the Vulcan Rock – Tafelberg Reef complex which is far too high an energy environment for fine- to medium grained sediment to accumulate as it is well within the reach of normal wave base as well as storm wave base.

Multibeam bathymetric results show that almost all of the sub-aqueous bedform fields present as negative bathymetric features. This could imply marginally different ages of the sediment comprising the depressions and the sediment surrounding the depression.

The localised depression associated with the termination point of the submarine outfall pipeline is probably caused by the scouring action of the effluent pumped through the pipeline as it discharges out to sea. This depression also affects the convexity from the northern margin towards the middle of the bay (Figure 5.5 E). Were it not for the depression the bathymetric slope would be smoother and not have such a convex morphology. The depressions associated with the shipwrecks in the study area are better developed in the lee of the structures indicating that there are wave induced bottom currents although these currents will only be active for short periods when the sea state is large enough.

The depression associated with the southern breakwater is as a result of sediment being scoured away as high energy swells refract around the breakwater. Conversely the depression at the end of the northern quay is related to the tidal ebb and flow of water going into and coming out of the harbour.

For a holistic view of all of the above the multibeam bathymetric dataset has been merged with topographic elevations (Figure 5.8). Viewed in three dimensions the difference in morphology between the two lithological outcrops is evident. The offshore Vulcan Rock – Tafelberg Reef complex exhibits the rugged nature of granite with the smoother outcrops just inshore of the granites and in the middle of the study area indicative of TMG. The fabric in the granite presents clearly, as do the outfalls pipeline and shipwrecks. Somewhat misleading is the smoothness of the surf zone around Hout Bay below Chapman's Peak Drive. Due to the bathymetric data not terminating against the coastline, gridded (interpolated) singlebeam data has been used to "bridge" the gap and this biases a smooth seafloor from the expected, rugged, exposed granites seen in the field.

The next chapter will deal with the surficial seafloor geology as defined using sidescan sonar.

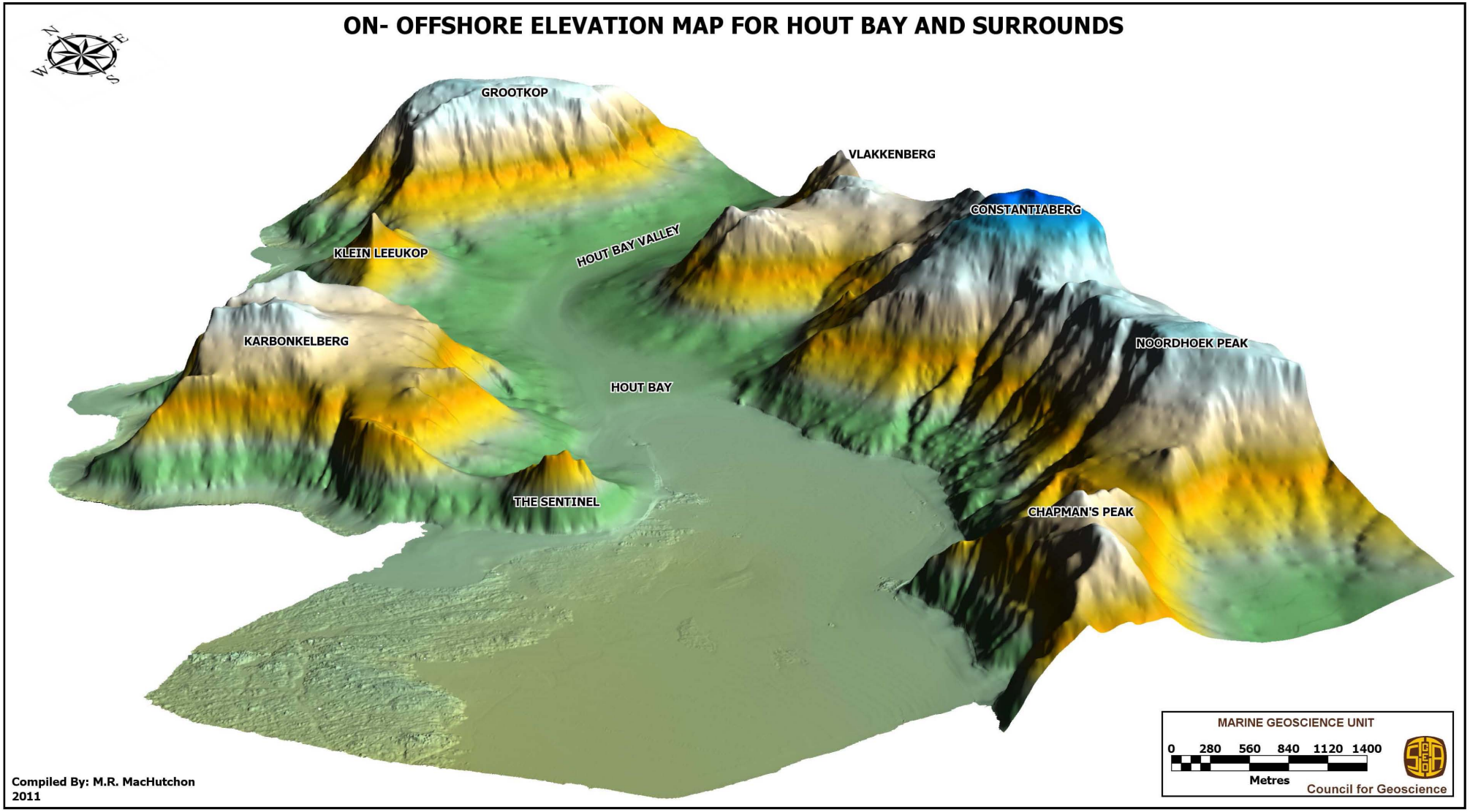

Figure 5.8. On- offshore elevation map of Hout Bay and Surrounds.

6. SIDESCAN SONAR

6.1. Introduction

The surficial seafloor geology was first classified on the basis of discrete sonar facies, imaged using a sidescan sonar. Each facies was ground truthed and described using the SCUBA diving techniques as outlined by Cawthra (2010). Where possible, multibeam echosounder (point cloud) data (Chapter 5) have been included to visualise the facies in three dimensions.

6.2. Results

Using the high-resolution 500 kHz sidescan sonar seafloor mosaic (Figure 6.1) produced for this study, seven different acoustic facies were identified in the study area based on their relative acoustic signatures (Figure 6.2). The difference in sonar properties is directly related to the constituent lithologies on the seafloor and, therefore, can be used as a direct correlation to the surficial seafloor geology (Mazel, 1985). For example rock outcrop has a much harder (darker) acoustic signature than fine- to medium grained sand, and differing lithologies within the rock outcrop have different fabric and textures. The name and extent of each facies in the survey area is summarised in Table 6.1.

Table 6.1. Exposure and coverage of the different acoustic facies.

Interpreted Acoustic Facies	Exposed Area (km^2)	Percentage Coverage (%)
Prominent Reef	3.002	22.37
Subdued Reef	0.558	4.16
Scattered Reef	0.105	0.78
Bioclastic Gravel	3.175	23.66
Shelf Sand	6.569	48.96
Sub-aerial Reef	0.005	0.04
Breakwater & Armouring	0.003	0.03
TOTAL	**13.417**	**100.00**

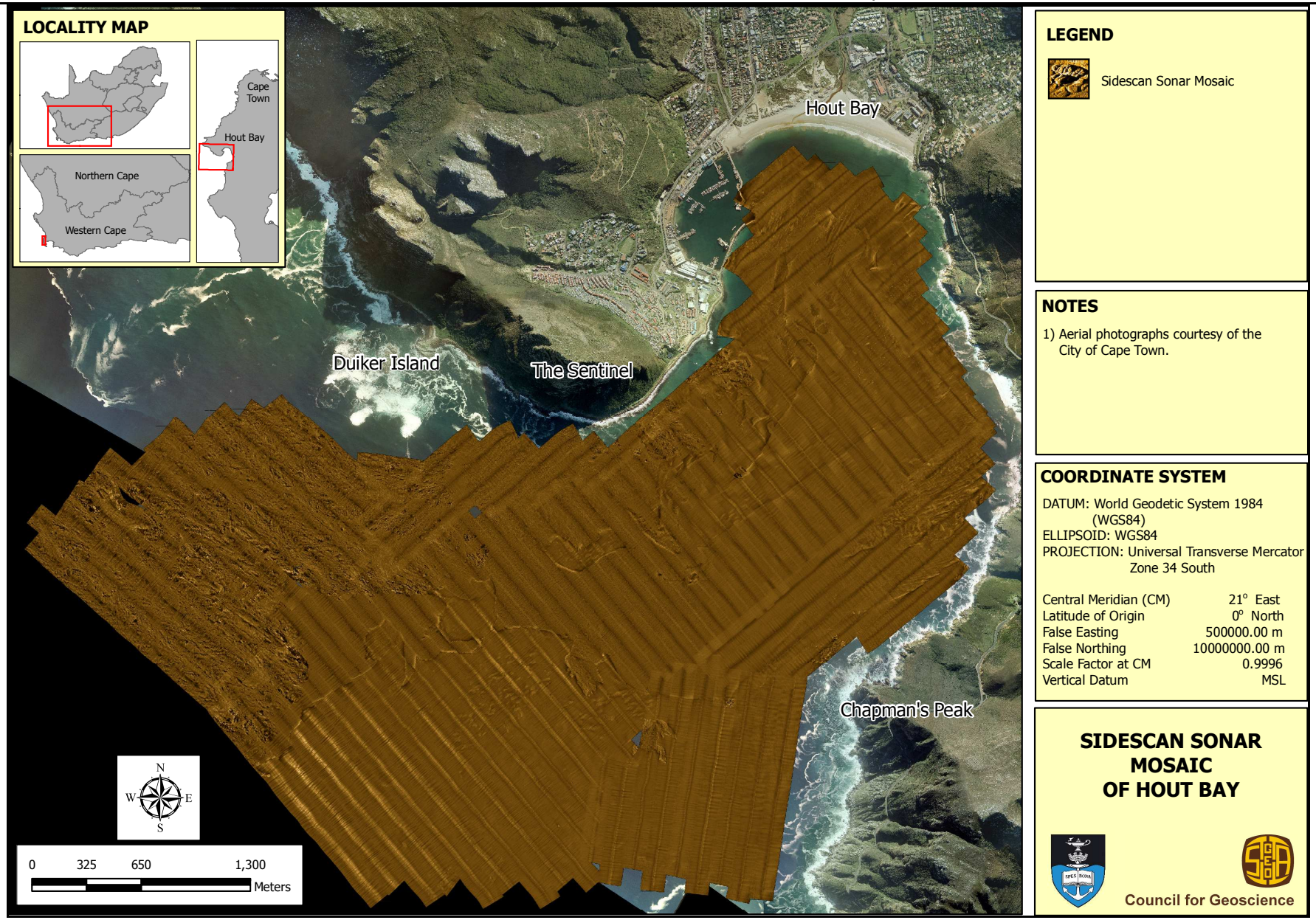

Figure 6.1. Pseudo-coloured high-resolution (500 kHz) sidescan sonar mosaic of study area.

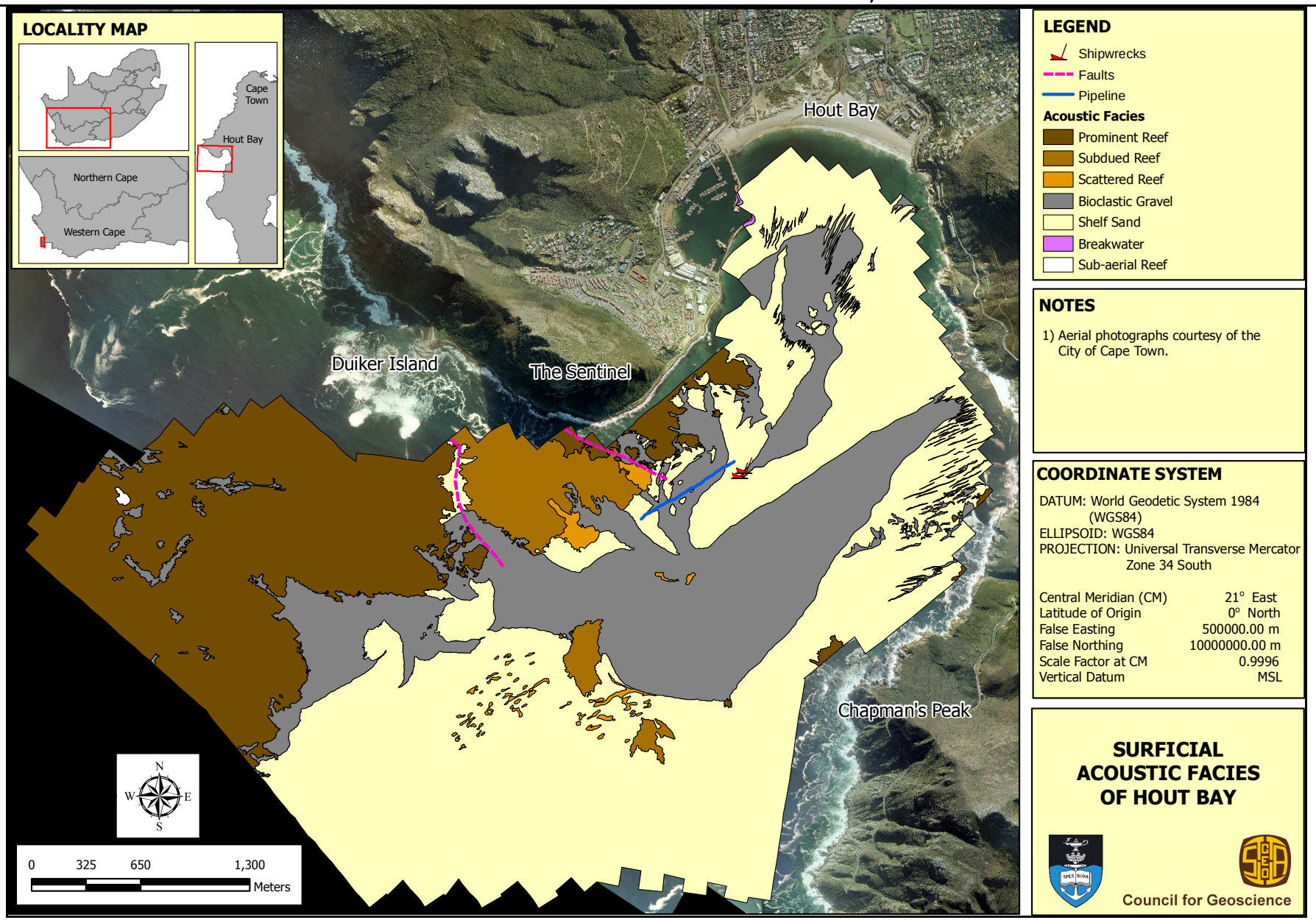

Figure 6.2. Interpreted acoustic facies of study area.

6.2.1. Prominent Reef

The acoustic facies classified as Prominent Reef (Figure 6.2) has a strong reflective pattern with bulbous morphology and numerous well developed, wide, acoustic shadow zones that are indicative of rugged microtopography (Russel-Cargill, 1989) (Figure 6.3). Numerous orthogonal joint sets can be identified within the facies (Figure 6.4), with one set of lineations trending 100º/280º and the other 10º/190º. This facies is the third most dominant covering 3.002 km^2 which equates to 22.37 % of the study area. Prominent Reef crops out predominantly to the southwest of the Sentinel and along the margin of Chapman's Peak.

Diver observations revealed Prominent Reef to be large granite outcrops with feldspar megaphenocrysts clearly visible (Figure 6.5 A). The outcrops are heavily bio-armoured with calcareous and soft-bodied marine organisms (Figure 6.5 B) and *Laminaria pallida* (kelp) holdfasts. The granites are intruded by dolerite dykes samples of which show a zone of alteration (halo) around the exposed dyke outcrops (Figure 6.5 C).

One of the facies related to the prominent reef is the sub-aerial reef facies such as where Prominent Reef (Vulcan Rock) breaks the sea surface (Figure 6.2). Vulcan Rock is an offshore member of Duiker (Seal) Island.

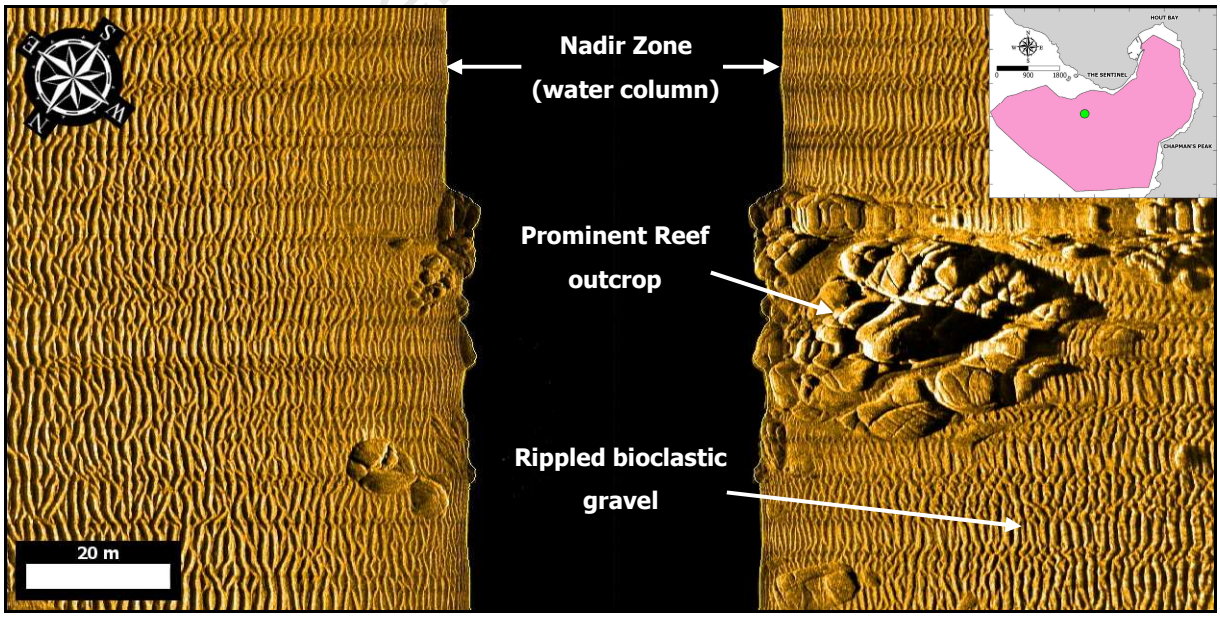

Figure 6.3. A pseudo-coloured sidescan sonograph illustrating an outcrop of Prominent Reef (granite) surrounded by rippled bioclastic gravel. Inset map shows image location.

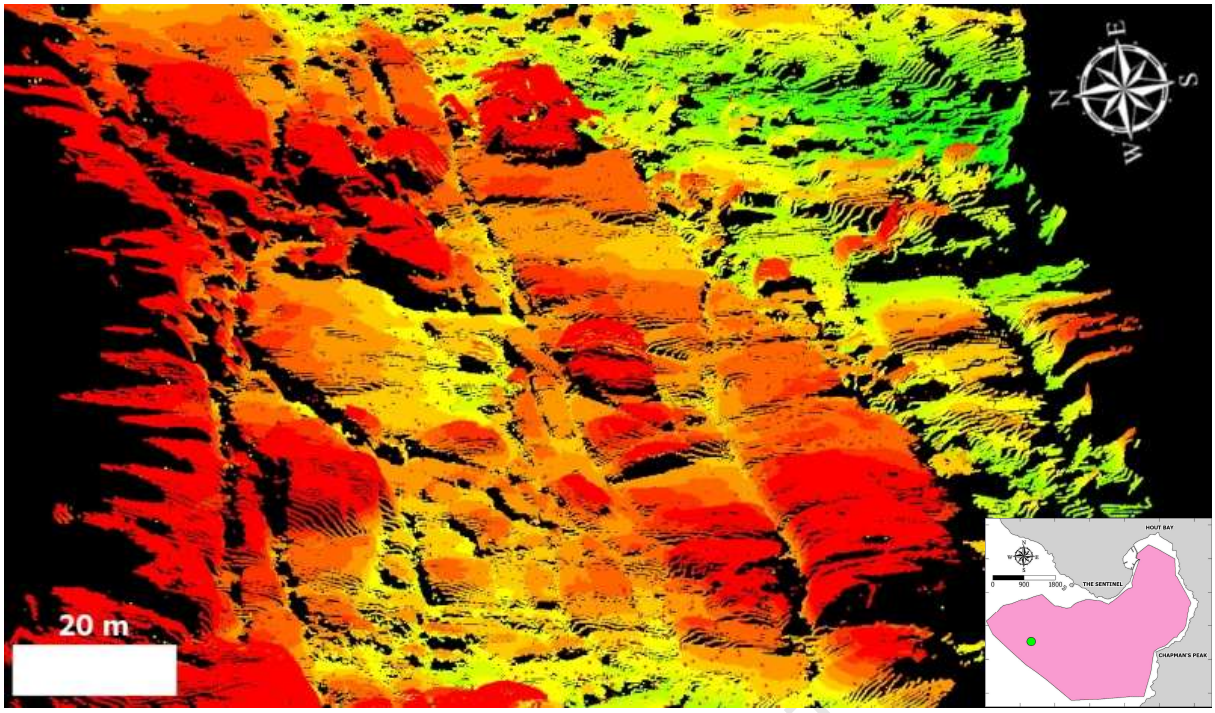

Figure 6.4. A point cloud image illustrating the bulbous morphology and joint patterns of the Prominent Reef facies. Inset map shows image location.

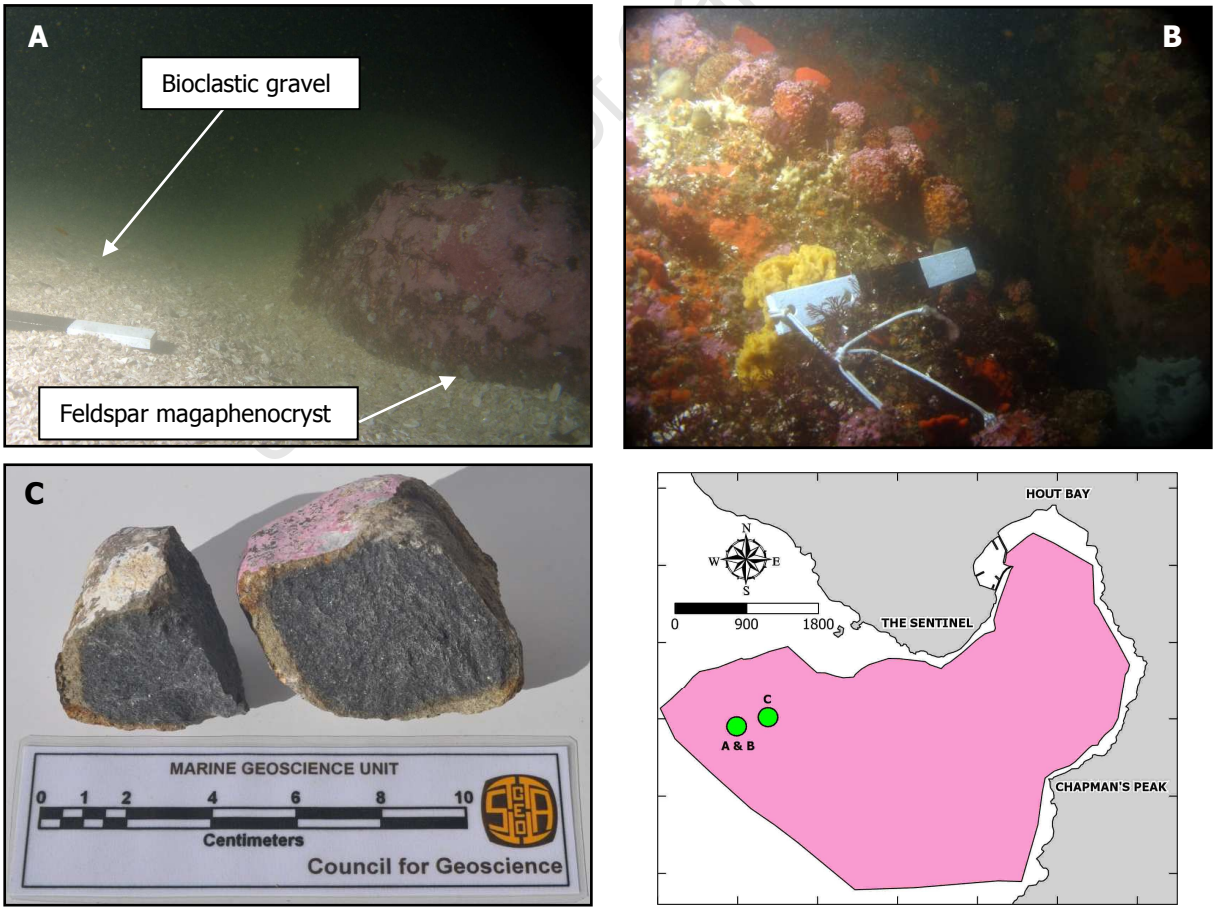

Figure 6.5. Underwater images of granite outcrops (A & B). Sample of dolerite dyke (C). Scale bar divisions are 10 cm. Photographs courtesy of Mr. Wilhelm Van Zyl. Map shows image locations.

6.2.2. Subdued Reef

Subdued Reef (Figure 6.6) has a moderately reflective pattern with regular well developed linear reflectors and associated acoustic shadow zones (Russel-Cargill, 1989). This facies displays a more subdued microtopography in comparison to the bulbous topography of the prominent reef. It represents a much more planed surface with lineations trending approximately 175º/355º. This facies outcrops at the foot of the Sentinel and extends in a southeastern direction into Hout Bay, although the majority of this area is covered by a thin veneer of fine- to medium grained sediment. Subdued reef is the fourth most dominant acoustic facies covering an area of 0.558 km^2, which equates to 4.16 % of the surveyed area.

Diver observations of Subdued Reef revealed it to be outcrops of sandstone. Bedding planes are clearly visible with measured dips of approximately 10 – 15º. In the middle of the study area the edges of the bedding planes are very angular (Figure 6.8 A), whereas below the Sentinel the edges of the bedding planes were rounded (Figure 6.8 B). The outcrops are less intensely bio-armoured than the granite outcrops with less soft-bodied organisms and more abundant *Parechinus angulosus* (sea urchins).

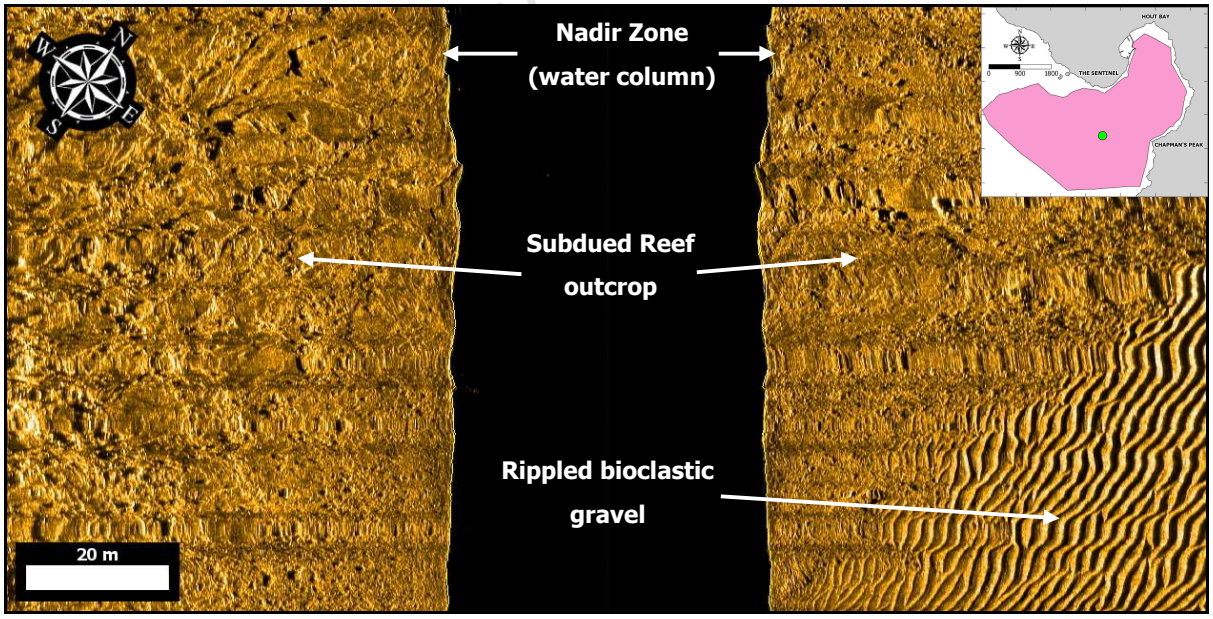

Figure 6.6. A pseudo-coloured sidescan sonograph illustrating an outcrop of Subdued Reef. Inset map shows image location.

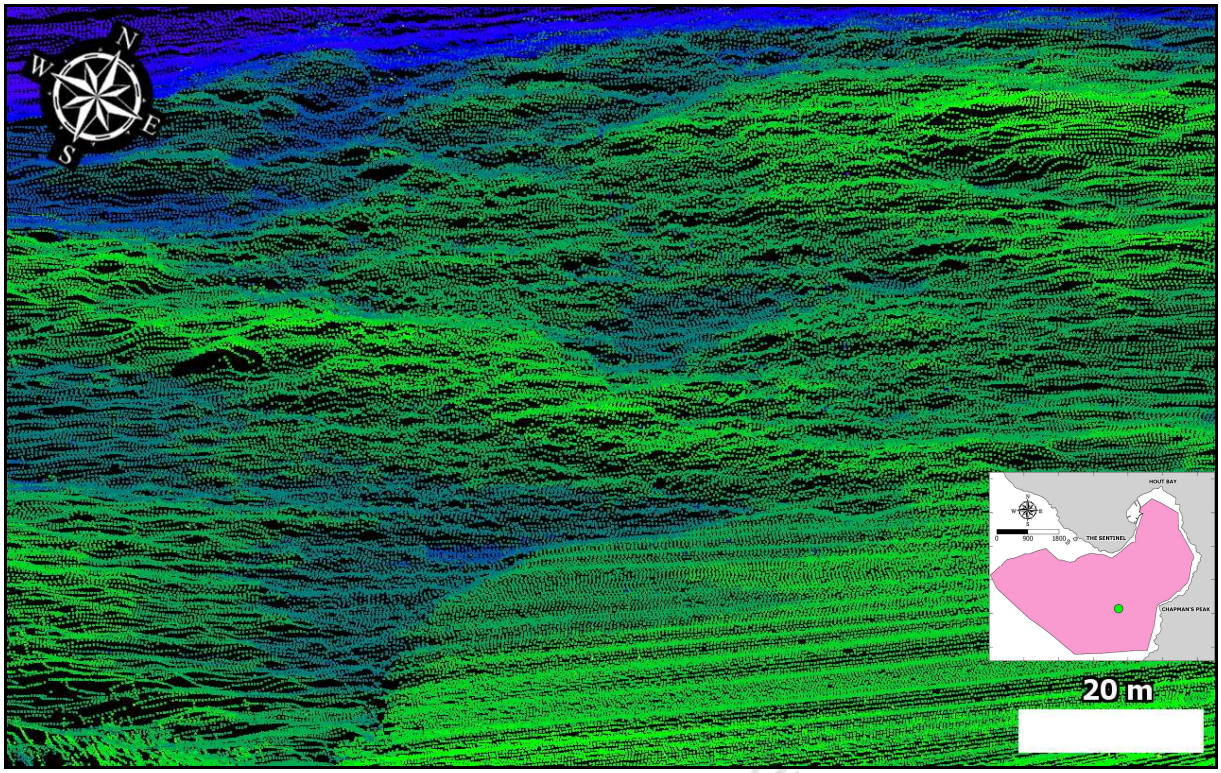

Figure 6.7. A point cloud image illustrating the planed, low relief morphology of the Subdued Reef facies. Inset map shows image location.

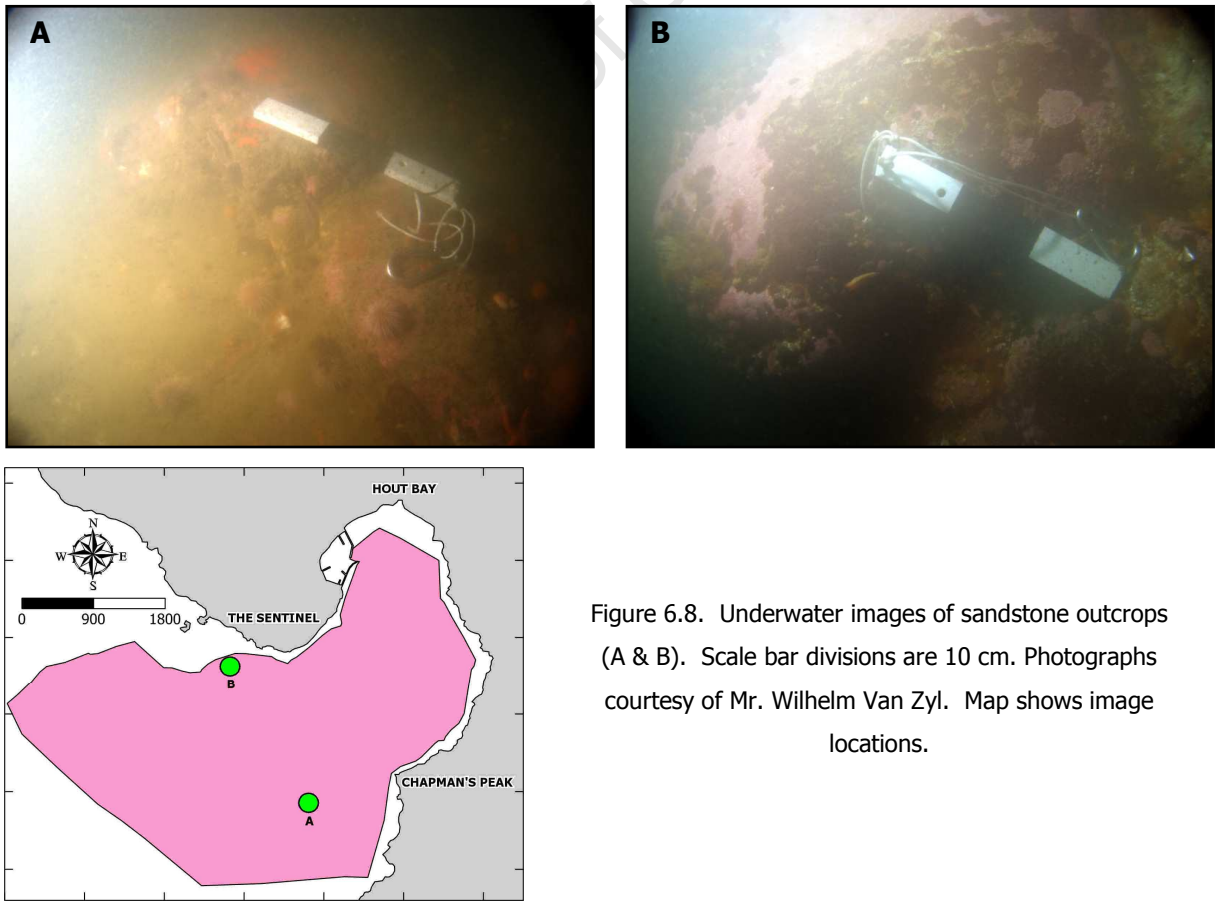

Figure 6.8. Underwater images of sandstone outcrops (A & B). Scale bar divisions are 10 cm. Photographs courtesy of Mr. Wilhelm Van Zyl. Map shows image locations.

6.2.3. Scattered Reef

Scattered reef (Figure 6.9) has a "blotchy" signature on the sonar record and is comprised of a mixture of boulders, cobbles and occasional reef outcrops. There are no discernable lineations or trends within the facies. However, it does appear to be associated with the Subdued Reef facies cropping out either along the facies margin of Subdued Reef or in the immediate vicinity. Scattered reef accounts for 0.78% of the survey area (0.105 km^2), making it the fifth most abundant facies surveyed.

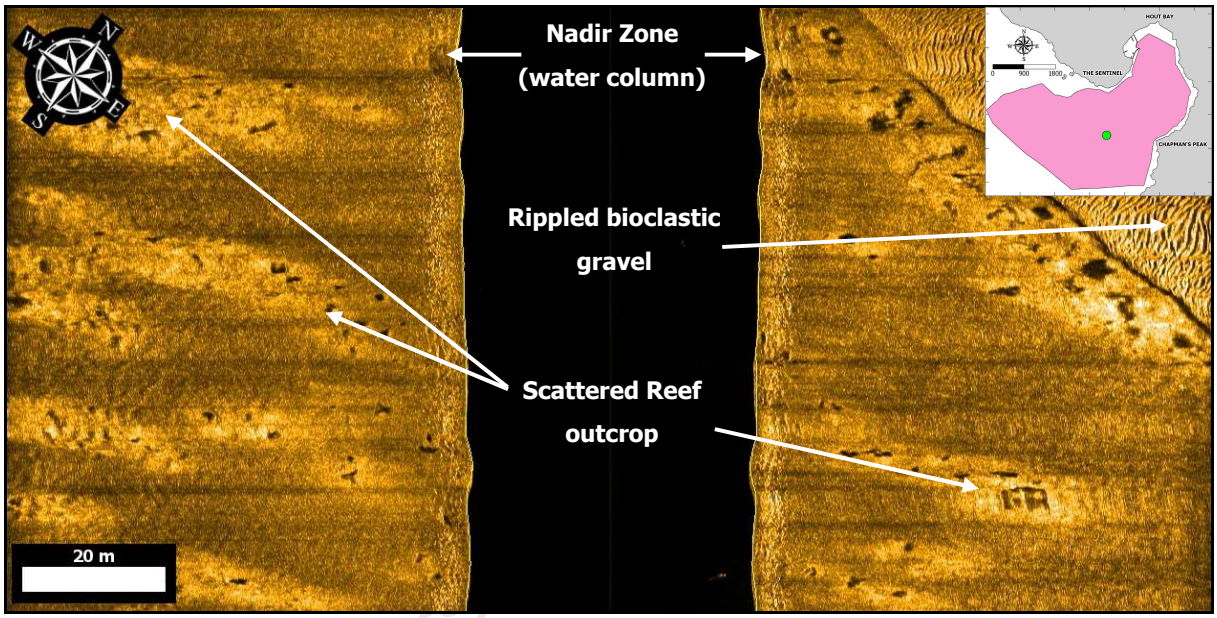

Figure 6.9. A pseudo-coloured sidescan sonograph illustrating outcrops of Scattered Reef. Inset map shows image location.

6.2.4. Bioclastic Gravel

The bioclastic gravel facies has a wavy acoustic signature with symmetrical, bifurcating bedforms. Crest amplitudes are typically between 20 – 30 cm (H) and wavelengths are in the order of 1.7 m (L). The orientation of the ripple crests in the large majority of the bay is 150º/330º, with this trend changing slightly in front of Chapman's Peak to 177º/357º. This facies has a relatively strong acoustic signature and is comprised of a shell hash (Figure 6.12). The bedforms are strongly developed in the deeper part of the survey area. Farther inshore at water depths of 26 to 15 m BSL (towards the higher-energy environment) the ripples grade into more planar coarse-grained sediment and then in the very shallow zones at less than 15 m BSL back into well-developed bedforms. Within the survey area Bioclastic

Gravel is the second most dominant facies accounting for 23.66 % of the total area (3.175 km^2). The facies occurs as a halo around the reef outcrops described in 6.2.1 and 6.2.2 and on the leeward side of high-relief objects.

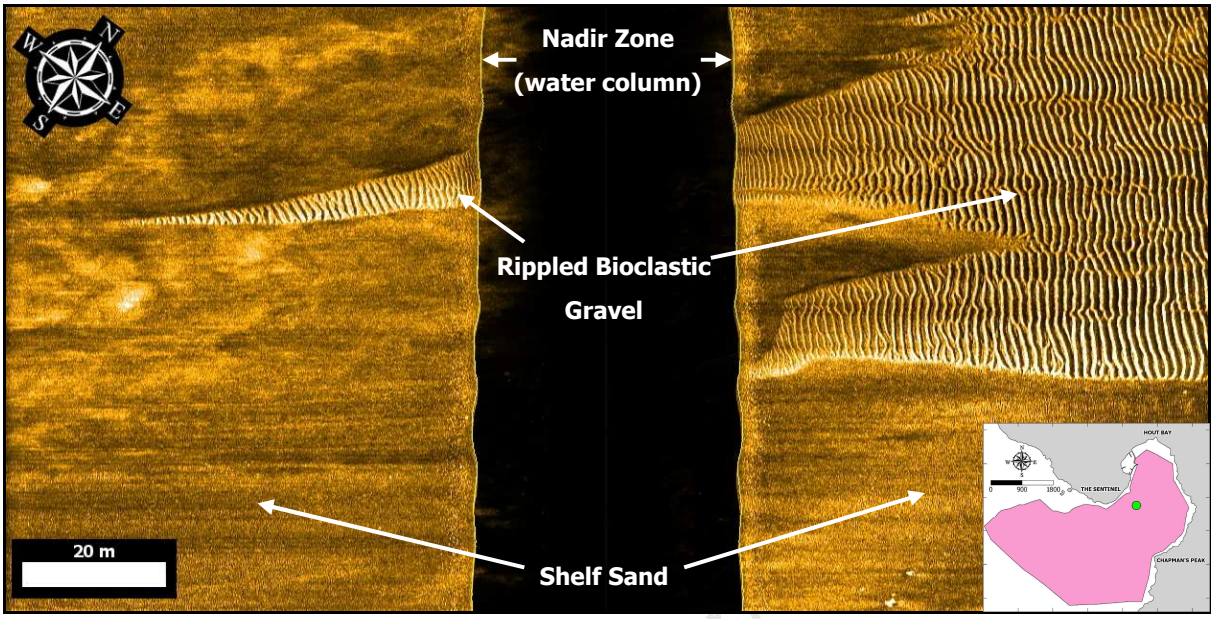

Figure 6.10. A pseudo-coloured sidescan sonograph illustrating sub-aqueous bedform field of the Bioclastic Gravel and Shelf Sand facies. Inset map shows image location.

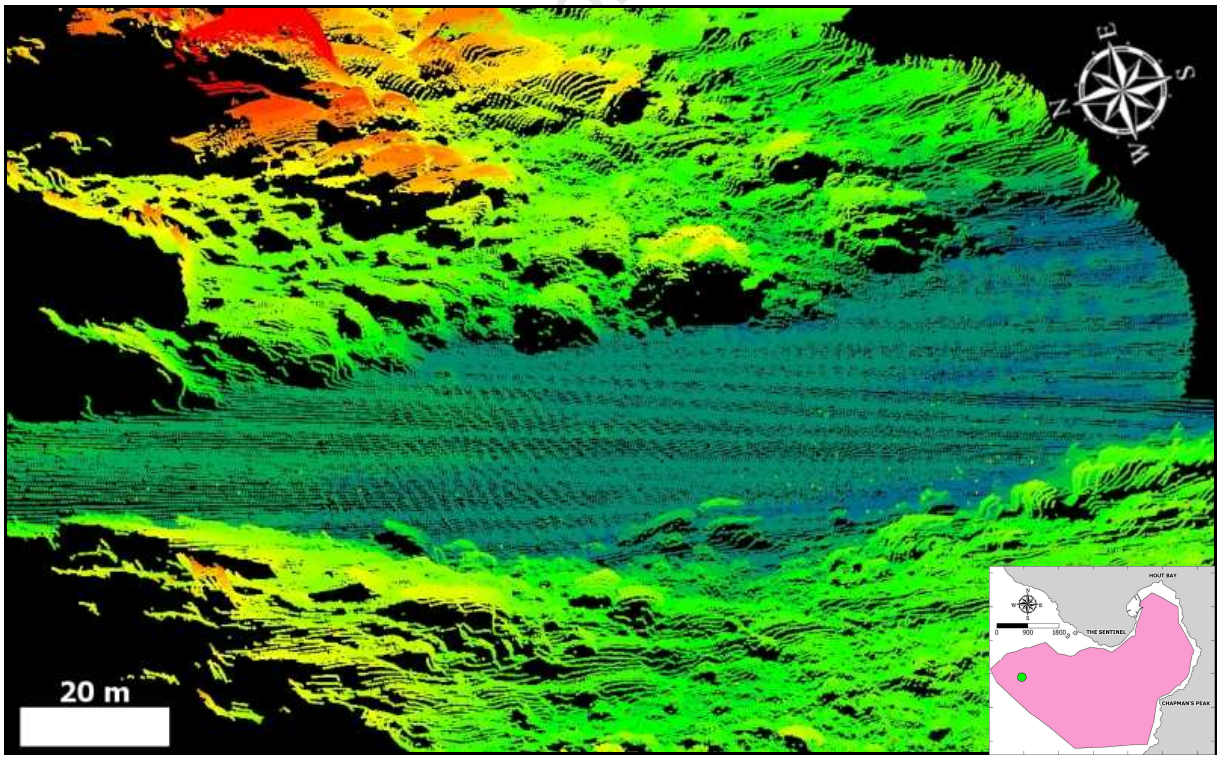

Figure 6.11. Point Cloud image illustrating the Bioclastic facies, which manifests as a bedform field in a gully between Prominent Reef outcrops. Inset map shows image location.

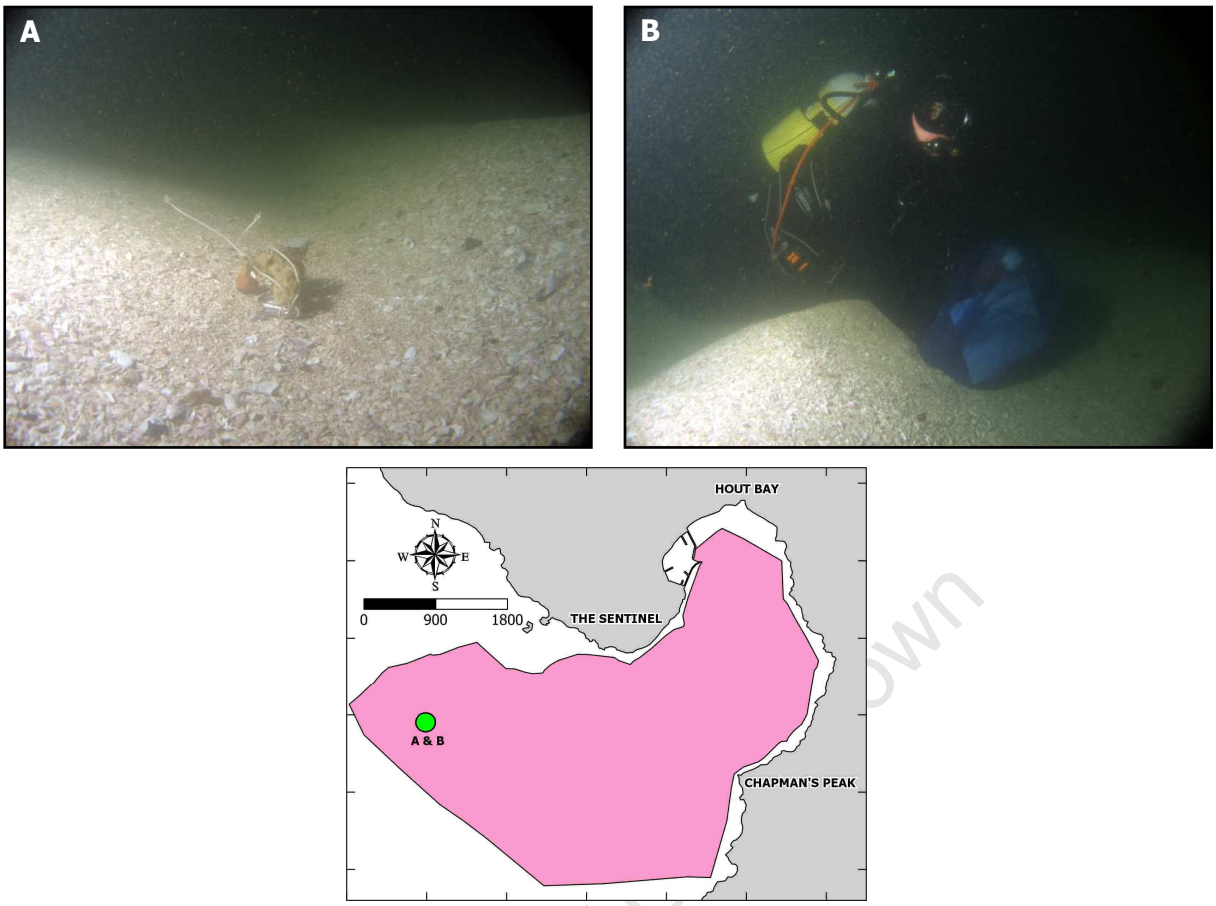

Figure 6.12. Underwater images of bioclastic gravel bedforms (A & B). Carabiner for scale in (A) and author on crest of bedform in (B). Photographs courtesy of Mr. Wilhelm Van Zyl. Map shows image locations.

6.2.5. Shelf Sand

The shelf sand facies consists of fine- to medium grained calcareous quartzose sand which has weak acoustic reflection with no acoustic shadowing (Figure 6.10). It constitutes the largest acoustic facies in the study area covering 6.569 km^2 (48.96 %). The facies displays no bedforms and presents as a flat featureless surface. In the vicinity of the reef outcrops the upper most layers are heavily bioturbated and host a plethora of burrowing infauna. For a concise breakdown of composition, grain size, sorting and skewness statistics for this facies refer to Chapter 9.

6.2.6. Anthropogenic Features

The three distinct anthropogenic features in the study area are the Hout Bay Harbour breakwater and its associated armouring, two shipwrecks in the middle of the bay and a submarine outfall pipeline. The last 84 m (from the harbour mouth) of the southern breakwater and armouring was imaged with the sidescan sonar, as well as the last 70 m (from the harbour mouth) of the northern quay. The southern groin is much more heavily armoured to cope with the high energy regime associated with incoming waves and swells. The multibeam data illustrate that the armouring on the southern breakwater consists of large concrete blocks approximately 3 x 3 m (Figure 6.13). Because the northern quay experiences a more subdued energy regime (to that of the south) it is not armoured. The quay is rather constructed out of caissons and piles, with discarded fender tyres lying on the seafloor (Figure 6.14).

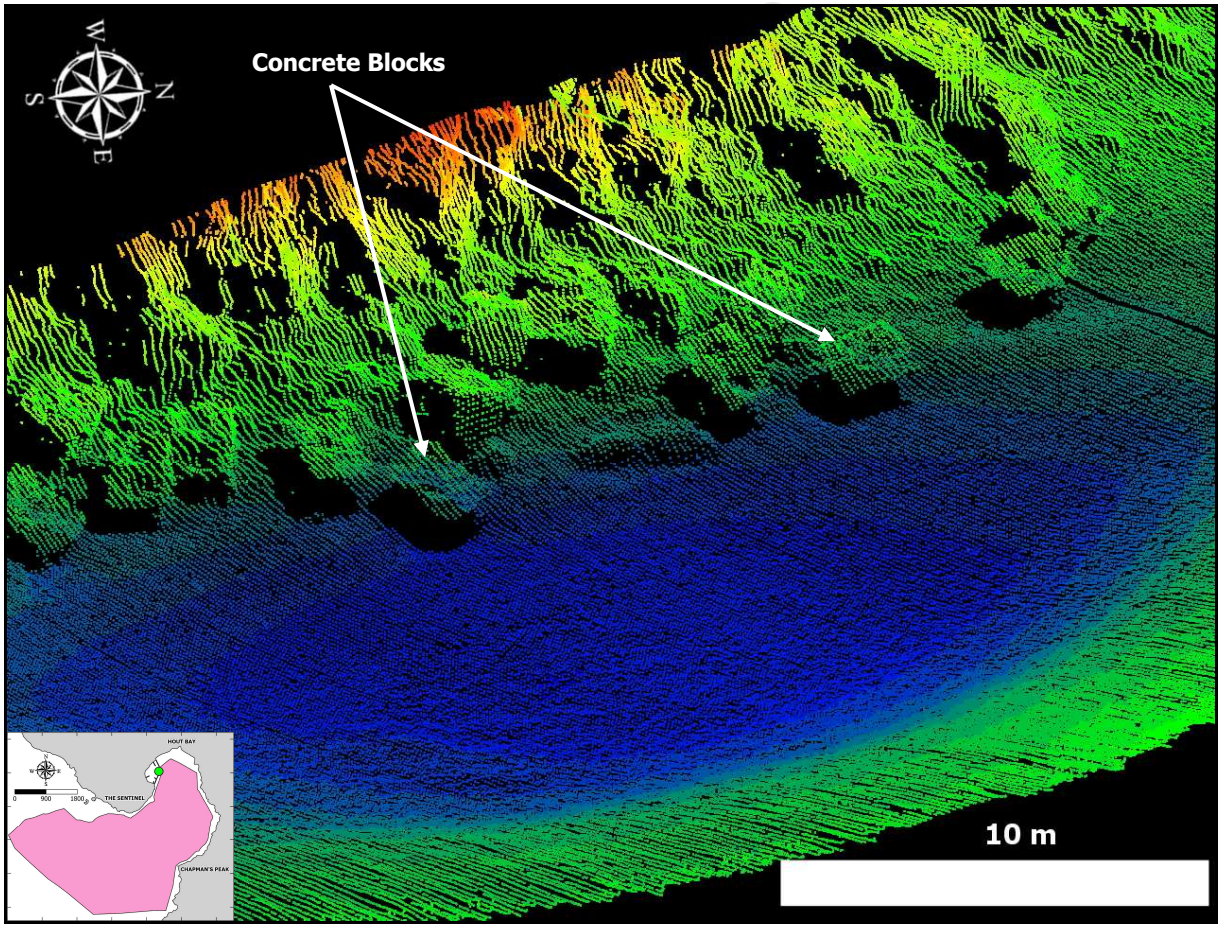

Figure 6.13. A point cloud image illustrating the composition of the southern breakwater armouring. Inset map shows image location.

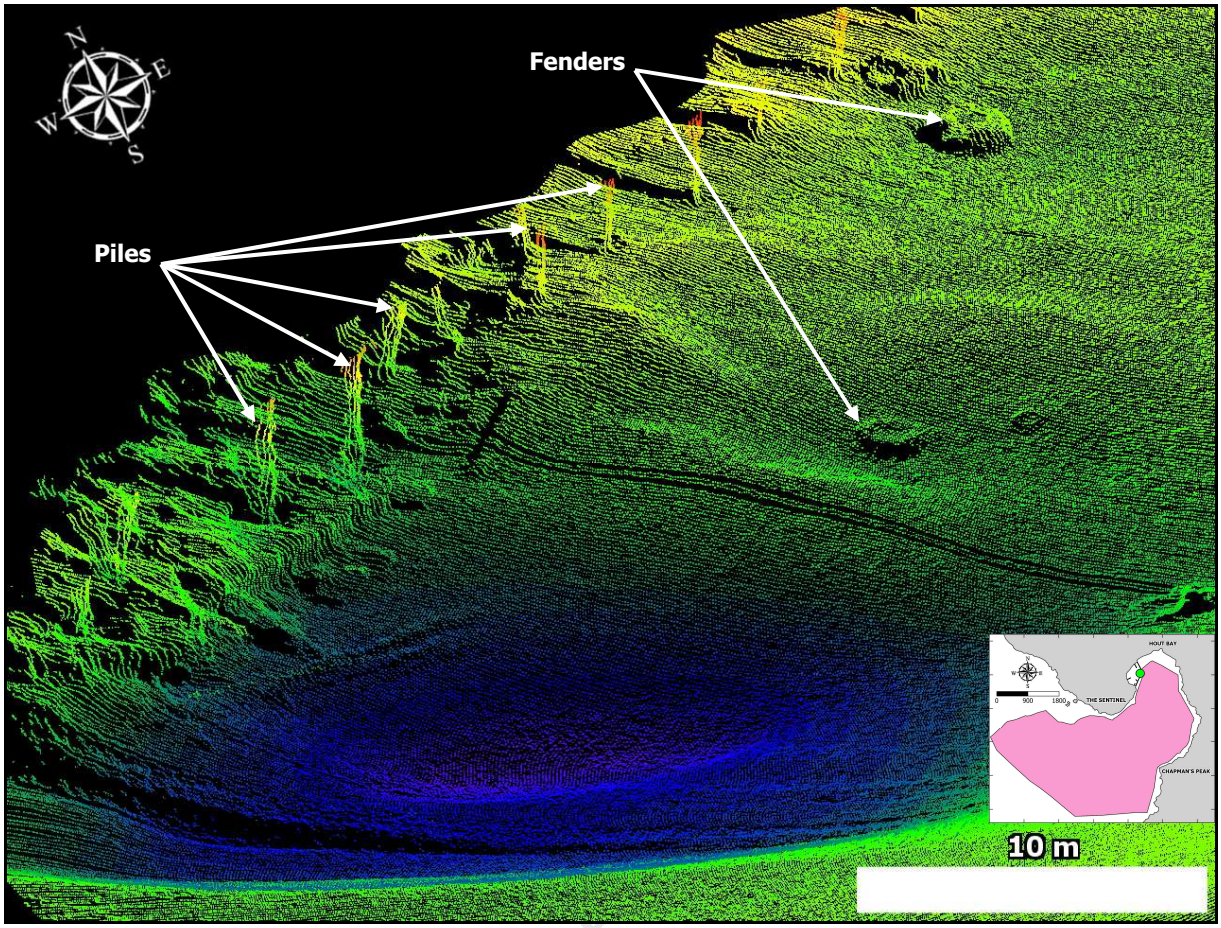

Figure 6.14. A point cloud image illustrating the pile construction of the northern quay. Inset map shows image location.

The two shipwrecks in the study area are referred to by different names in literature as the *Astor* and *Katzmaru* (Koornhof, 2000) or *Aster* and *Katsu Maru* (Wikitravel, 2009). Both vessels form artificial reefs which are extensively utilised by the various recreational diving operators in the area (Figure 6.15 & Figure 6.16). The background and dimensions of the vessels are reported on in Chapter 5.

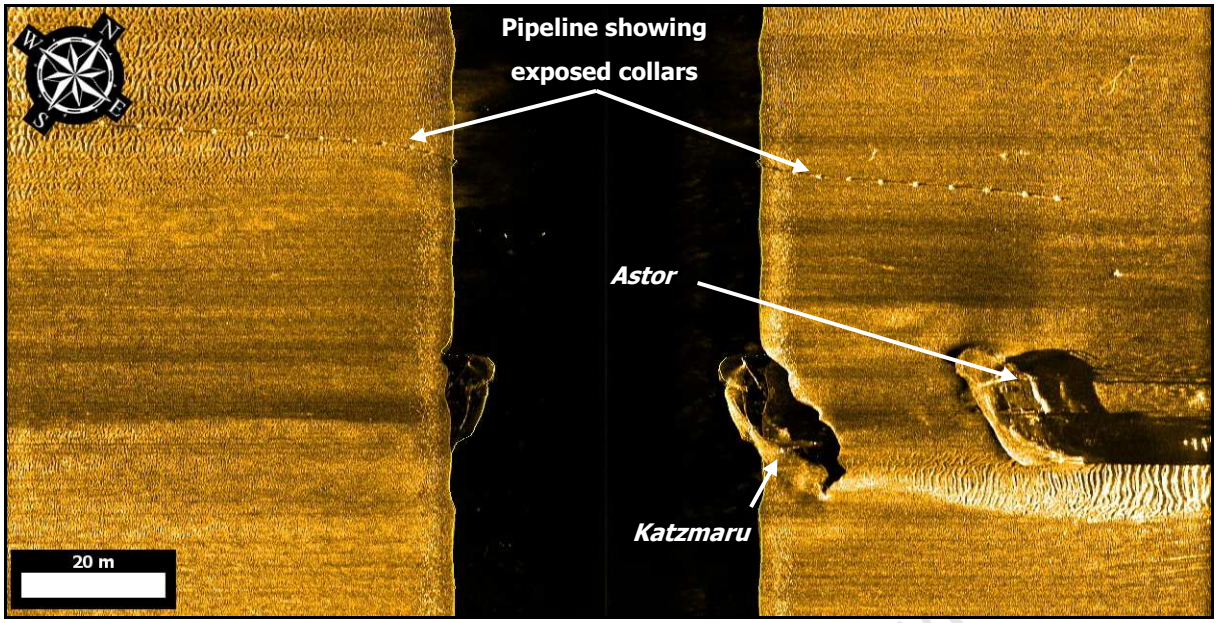

Figure 6.15. A pseudo-coloured sidescan sonograph illustrating the submarine outfall and shipwrecks. See Figure 5.6 for shipwreck locality.

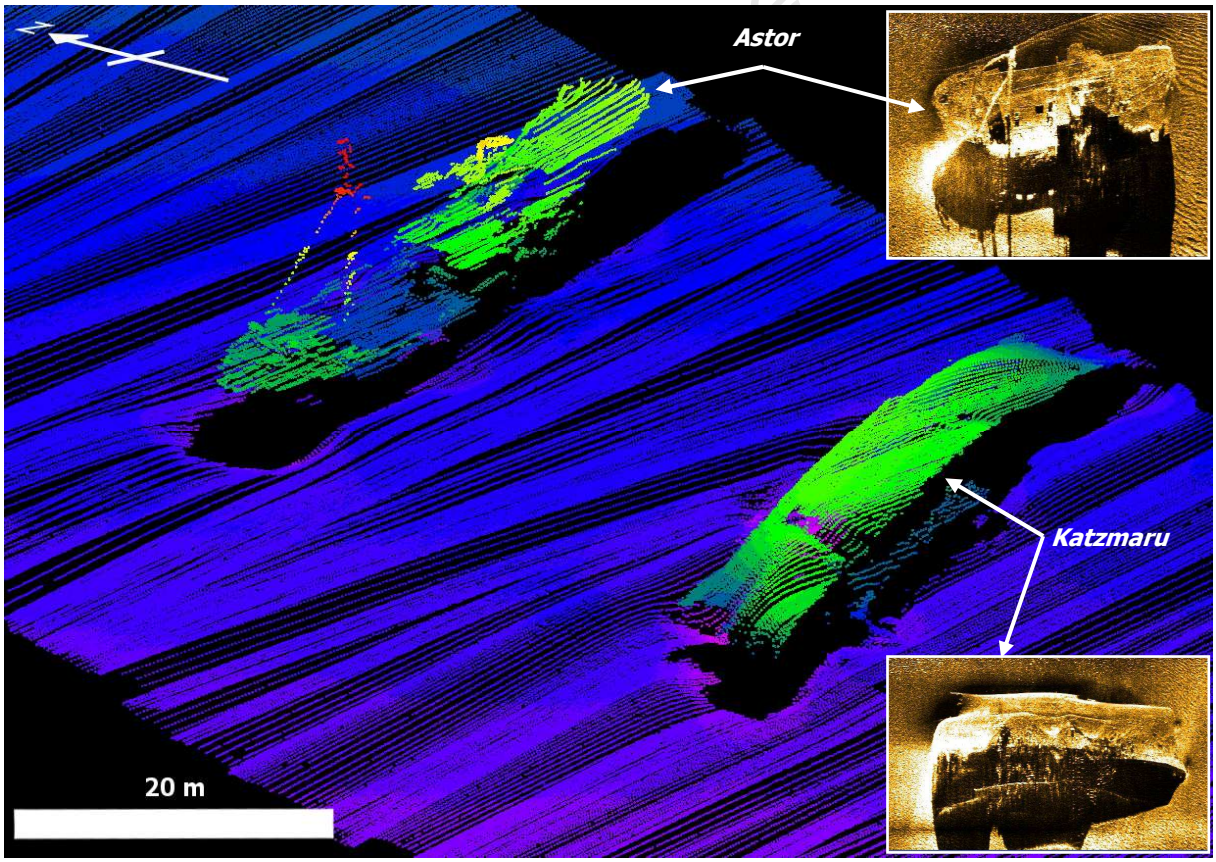

Figure 6.16. A point cloud image illustrating the *Astor* and *Katzmaru*. Inset images are pseudo-coloured sidescan sonographs. See Figure 5.6 for shipwreck locality.

The third anthropogenic feature in the study area is a submarine sewer outfall pipeline (Figure 6.15). The pump station is approximately 265 m south of the southern part of the harbour (E: 255170, N: 6228422). From the pump station the pipeline runs due east and is buried shortly after entering the water. The pipeline then doglegs to the right and runs southwest (parallel to the coastline). It is buried for most of this section and only becomes exposed 82 m northwest of the *Astor*. From this point on it is exposed for 650 m to its termination point (E: 254771, N: 6227192). The outfall discharges a mixture of treated waste water mixed with storm water overflow. From data published by the City of Cape Town the pipeline has a diameter of 600 mm with a discharge capacity of 9.6 Ml/day at 0.7 m/s. Annually the outfall utilises 60% of its hydraulic capacity.

6.3. Discussion

In ground truthing the geophysical data *in situ* underwater observations of the constituent lithologies have allowed the geophysical facies (Prominent- and Subdued Reef) to be correlated to granite and sandstone outcrops, respectively. Based on onshore field evidence these outcrops correlate to submarine exposures of Cape Granite and Table Mountain Group Sandstone (TMG). Due to the lack of sufficient vertical exposure of the sandstone outcrops and the extent of biological growth it is not clear which of the formations the outcrops represent. However, based on underwater observations of the deeper outcrops the surficial exposures appear more similar to the Peninsula Formation based on the lack of interbedded mudstone horizons and the relative purity of the sandstone. The smoothness and rounding of the bedding planes in the area to the south of the Sentinel represent a wave planed terrace formed during a sea-level lowstand of 18 to 20 m BSL (De Decker, 1986; Russel-Cargill, 1989; Woodborne, 1991). In places there is evidence of potholes containing relict cobbles; unfortunately underwater conditions prohibited taking discernable pictures. These cobbles are overgrown by marine algae, supporting their relict nature and confirming the terrace to be wave planed (Russel-Cargill, 1989). The town of Kommetjie (approximately 11 km south of Hout Bay) shows evidence of two wave planed terraces which formed during a relative sea-level highstand, one at approximately 20 m above sea-level and one at present sea-level (Hartnady and Rogers, 1990; Compton, 2006). The scattered reef acoustic facies represent TMG bedrock exposure that has been mantled by a thin veneer of sediment.

Flemming (1980) defined transverse bedforms generated by wave-induced oscillatory flow near the seabed as wave ripples. To describe the ripples more accurately a naming convention has been proposed by Ashley (1990). This convention is primarily for describing large scale sub-aqueous dunes. The author will therefore use the first order descriptors of Ashley (1990) and substitute dunes for ripples after Flemming (1980). Before a final classification can be assigned to the bedforms it must first be ascertained what oceanographic influence formed the ripples. The ripples show evidence of bifurcation and due to their symmetrical form it can be inferred that they are wave ripples as opposed to asymmetrical current ripples. Therefore, the ripples can be classified as two dimensional, straight crested, small sub-aqueous wave ripples.

The composition of the bioclastic gravel varies throughout the study area. Around the granite outcrops it presents as a shell hash in which the shell content decreases with proximity to the reef outcrops only to increase again in the intertidal/coastal zone (Figure 6.17). Diver observations of the granite outcrops reveal the surface to be covered in a thin veneer of biogenic detritus which is derived from the organisms that live on it. Therefore the shell hash around the granite outcrops is the larger biogenic fragments of these dead organisms. Closer inspection of the shell hash reveals it to be composed mainly of cirripede (barnacle) and mollusc fragments with minor amounts of well rounded rock (granite) fragments.

The orientation and morphology of the bedform fields also serve as valuable wave direction indicators. In the shallower nearshore, high energy, wave dominated environment the bedform fields have elongated parallel to the incident wave direction to form sand ribbons (Flemming, 1980), clearly displaying a bimodal wave pattern within the study area of southwest and south, the latter probably due to wave refraction around the Sentinel (Figure 2.4).

The most abundant facies in the study area correlates to fine- to medium grained calcareous quartzose sand (Figure 6.18). The facies is fairly featureless with the amount of living and dead organic matter much higher around reef outcrops than in the more barren parts of the study area (noted while grab sampling). Abundant polycheate worms, prawn/shrimp larvae and burrowing infauna are present in the upper 5 – 10 cm of this facies. Sedimentary statistics have been generated for the entire study area and these better help to describe this facies. These results are discussed in Chapter 9.

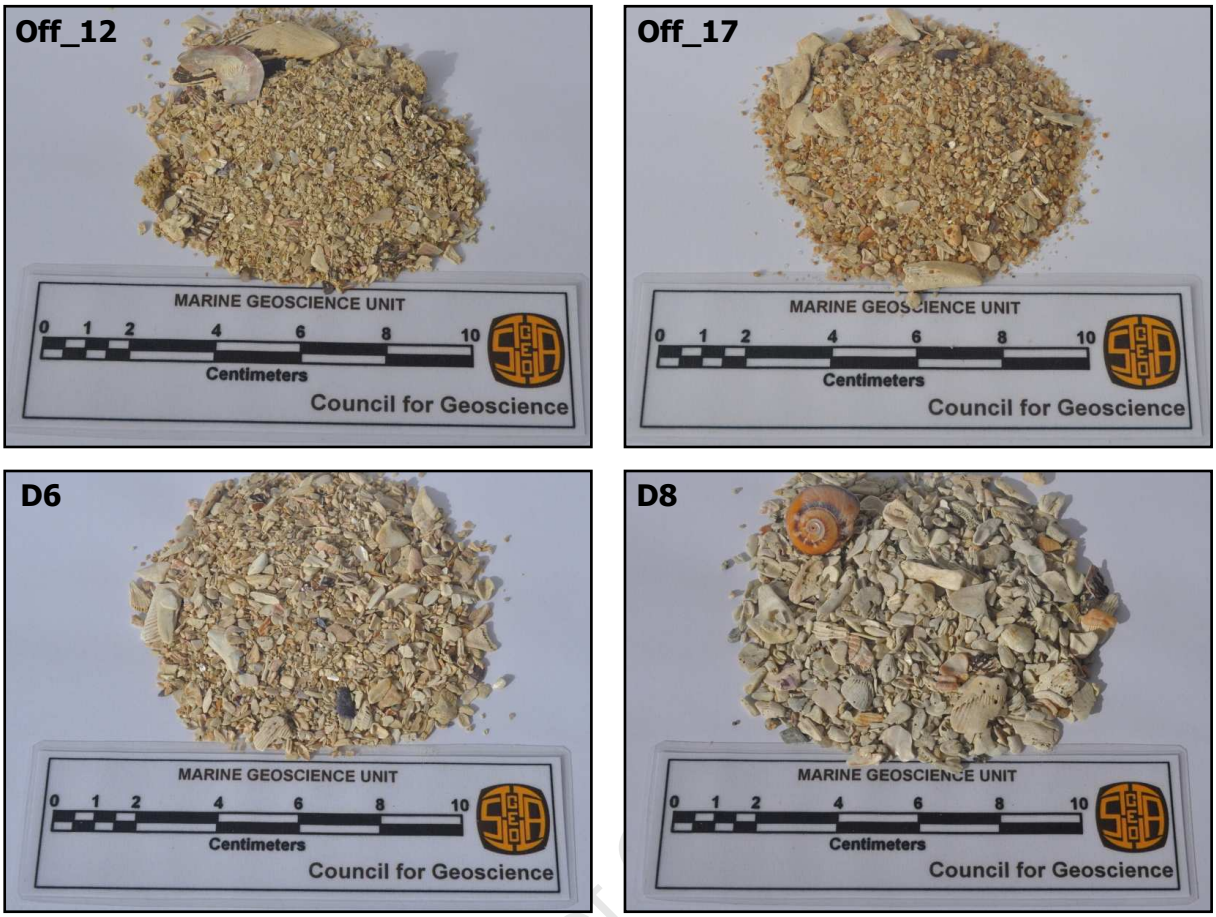

Figure 6.17. Compositional variation within the Bioclastic Gravel facies. Sample numbers are in top left corners of images. For sample positions see Appendix I.

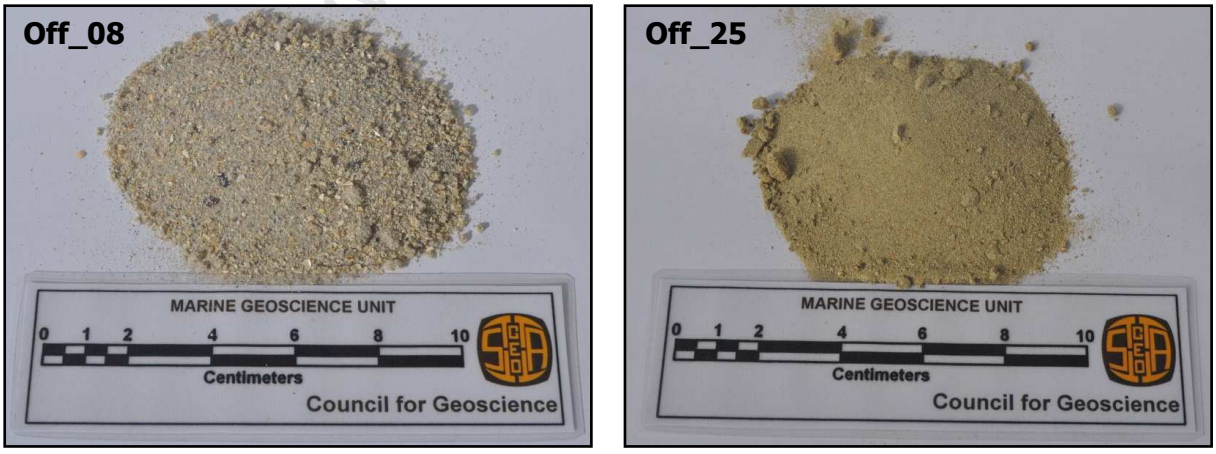

Figure 6.18. Compositional variation within the Shelf Sand facies. Sample numbers are in top left corners of images. For sample positions see Appendix I.

Geophysical and diver observations have delineated that TMG outcrops on the seafloor of Hout Bay. Russel-Cargill (1989) inferred a fault between the TMG and granites at the foot of the Sentinel propagating into the bay in a southeasterly direction (Figure 6.2). There was no surficial expression of the fault line as it was covered by an infilled sediment gully. During this investigation the same transect was swum and observations agreed that there must be a fault due to the juxtaposition of the different lithologies. Another transect was swum further offshore and more to the west of the first and the same relationship between the rock types was observed. It was therefore concluded that a fault block (graben) of TMG must exist to the south of the Sentinel. There is evidence onland of a structural offset between Chapman's Peak and the Sentinel (Figure 6.19). The nonconformity between the Cape Granites and Graafwater Formation on Chapman's Peak exists approximately 50 m above sea-level whereas on the Sentinel this nonconformity is only 1 – 2 m above sea-level. It has been noted by Hartnady and Rogers (1990) that the Sentinel has been downfaulted to the south.

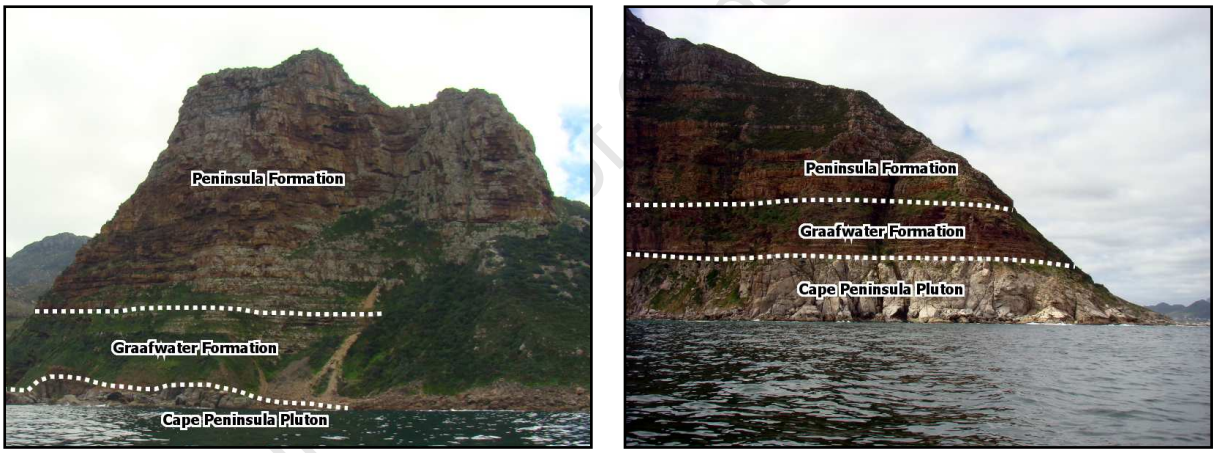

Figure 6.19. Pictures of the Sentinel (left) and Chapman's Peak (right) showing the relationship between Table Mountain Group sediments and Cape Granite Suite granite. Photographs courtesy of Ms. Hayley Cawthra.

One of the limitations of sidescan sonar is that if sediment mantles an outcrop this outcrop not visible on the sidescan record. One of the techniques used to delineate sub-bottom geology is marine magnetics. The next chapter deals with all of the magnetic anomalies encountered in the study area.

7. MAGNETIC DATA

7.1. Introduction

Numerous dykes have intruded the granite and TMG sediments on Chapman's Peak. There was, however, no clear surficial expression of these dykes on the seafloor of Hout Bay. It was therefore decided to acquire magnetic data in the hope that they could delineate if these intrusion extended across the bay in the basement lithologies. The magnetic data acquired for this study was collected with a proton magnetometer that makes use of the Overhauser effect. The principles of magnetometers which utilise this effect and the survey methodology are outlined in Chapter 4.3.

7.2. Results

7.2.1. Raw Magnetic Field Intensity

The raw magnetic field intensity is the magnetic field recorded by the magnetometer as it was towed behind the survey vessel. It has not been corrected for any diurnal variations that could have taken place in the survey area during the day or for the ambient magnetic field surrounding the earth (Figure 4.7). It does however show six distinct linear features which trend at approximately the same orientation of 127º and cut across the entire study area (Figure 7.1 A).

7.2.2. Total Magnetic Field Intensity

The total magnetic field intensity differs from the raw field intensity in that any diurnal variations experienced in the study area have been removed. Diurnal perturbations can be caused by ionosphere variations as a result of sunspot activity (Keary *et al.*, 2002). Normally a base station set up close to the survey area is used to correct for these variations, although it is important for it to be set up in a magnetically "quiet" environment i.e. at

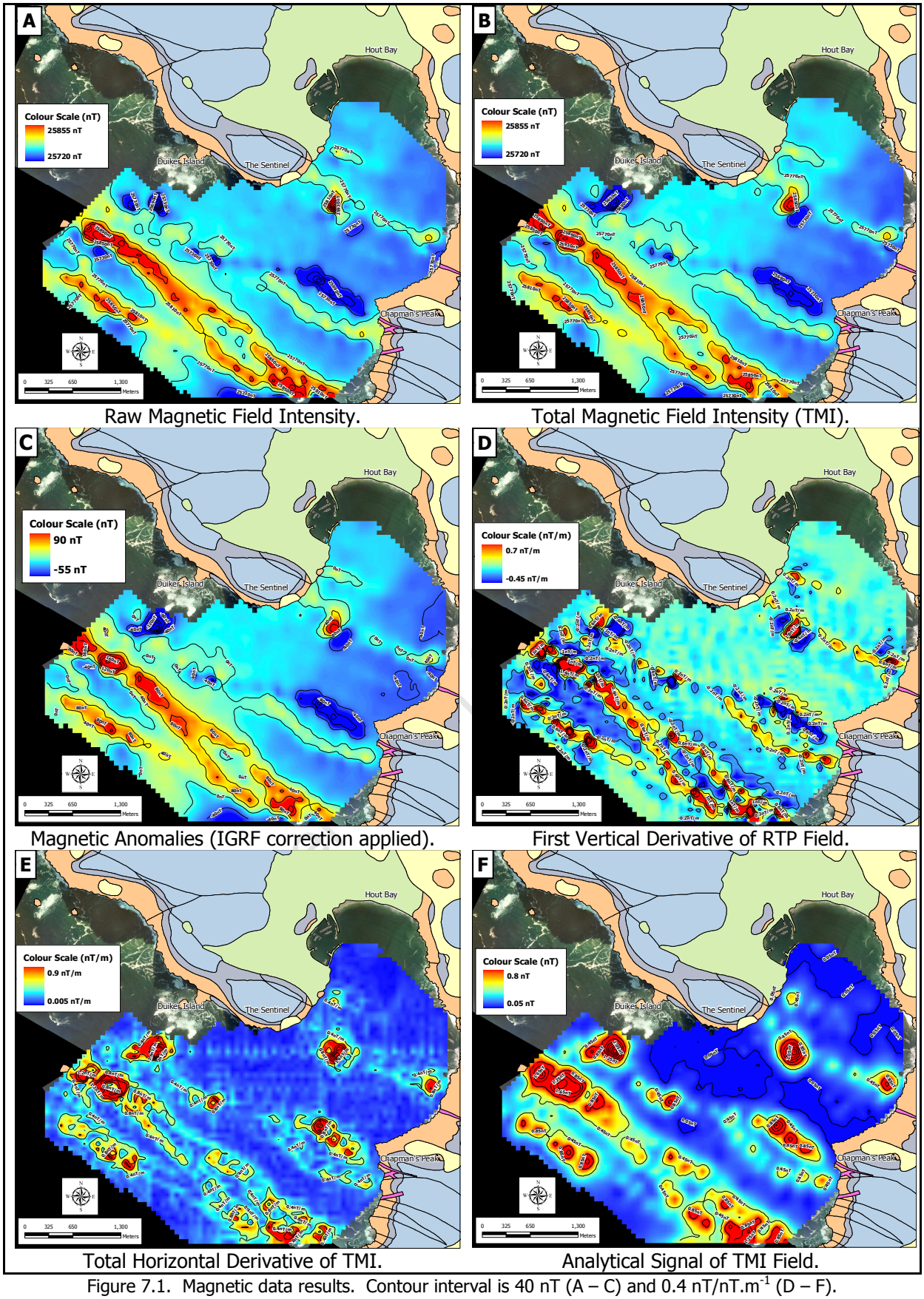

Figure 7.1. Magnetic data results. Contour interval is 40 nT (A – C) and 0.4 nT/nT.m^{-1} (D – F).

least 10 km from any magnetic (human) influence. This was not logistically feasible for the survey area, therefore it was decided to use data obtained from the Hermanus Magnetic Observatory which is within the accepted 100 km of the study area (Keary *et al.*, 2002).The diurnal variation data received are shown in Figure 7.2. For the survey the diurnal variations were at a minimum therefore the resultant chart for Total Magnetic Field Intensity differs very little from that of the Raw Magnetic Field Intensity (Figure 7.1 B).

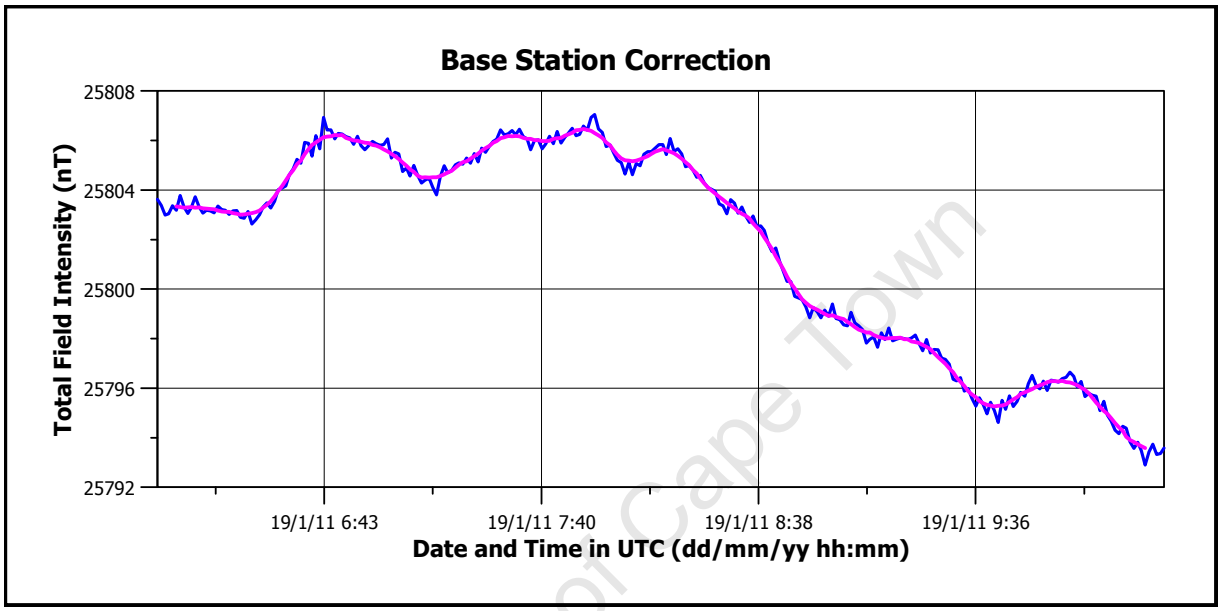

Figure 7.2. Diurnal variation data used to correct raw magnetic field intensity.

7.2.3. Magnetic Anomalies

The magnetic anomalies chart is the final stage in the magnetic data processing (Figure 7.1 C). This chart builds on the total magnetic field intensity chart and removes the effects of the Earth's ambient magnetic field in the study area (Keary *et al.*, 2002) by applying the international geomagnetic reference field (IGRF) correction. It therefore shows only the perturbations of any magnetic body within the pre-existing magnetic field of the Earth. The trends are still the same as the raw and total magnetic field intensity datasets.

7.2.4. Magnetic Derivations

A variety of mathematical operations can be performed on the magnetic anomaly and total magnetic field intensity data to transform and filter the data to accentuate certain features

which ultimately help with interpretation of the magnetic data. By filtering the data one can change the amplitude and/or phase relationships of the collective sine waves that define the recorded data (Milligan and Gun, 1997). Mathematically this is accomplished by transforming the recorded data into its associated frequency domain using Fourier transforms, then by multiplying this result to achieve the desired phase and amplitude alterations, then transforming the modified spectrum back into its original space domain (Milligan and Gun, 1997).

Gun (1975) first described all possible linear transformations, of which only those that could aid in data interpretation by accentuating different magnetic properties have been applied to the acquired data. The first of these is to reduce the total magnetic field data to the pole. This operation is carried out on the total magnetic field intensity using the operator described by Grant and Dodds (1972). The process effectively removes the inclination of the ambient magnetic field (in the study area) to where the magnetic field is vertical (at the pole) (Milligan and Gun, 1997). In geophysical terms, reducing the data to the pole in effect takes the recorded dipolar signal and converts it to a monopolar signal directly over the magnetic body (Milligan and Gun, 1997) (Figure 7.1 C).

The next magnetic data derivation is the first vertical derivative of the reduced to pole data (Figure 7.1 D). The effect of this operation is to accentuate the high frequencies (any vertical changes) in the data relative to low frequencies (Milligan and Gun, 1997) i.e. to accentuate the peaks which define the lineations and the metal shipwrecks. Comparison of the first vertical derivative data with that of the total magnetic field intensity data shows that the lineations have narrowed by effectively removing the "background noise."

The horizontal derivative is an operation performed on the total magnetic intensity field data. Like the vertical derivative, the operation is performed in the frequency domain and is used to identify linear features within the data (Milligan and Gun, 1997) (Figure 7.1 E). Due to the quality of the acquired data the horizontal derivative does not show any new or different trends to any of the other data. It does however show the negative lineation as a positive feature.

The last of the magnetic derivations computed for the acquired data is the analytical signal of the total magnetic field intensity. This idea was first developed by Nabighian (1972, 1984) as the energy envelope around a magnetic anomaly. Roest *et al.*, (1992) showed that

the analytical signal can easily be derived from the three dimensional gradients that comprise the total magnetic field. In principle the analytical signal provides simple, easily understood indications of the magnetic anomaly geometry (Milligan and Gun, 1997). The operation, as with the horizontal derivative, displays the negative anomalies as positive and is used to locate the edges of magnetic source bodies. It is of particular use where remanence and low magnetic latitudes complicate interpretation (Milligan and Gun, 1997). For the acquired data it defines the edges of the lineations more clearly (Figure 7.1 F).

7.2.5. Magnetic Lineations

For the purpose of describing the various lineations within the study area the reduced to pole derivative of the data will be used for the reasons stated above (Figure 7.3). Note that this derivation differs from the magnetic anomaly chart in that the magnetic perturbations show up as monopolar "spikes". On the eastern margin of the study area the coastline forms a relative point. There is a lineation immediately to the west of this point which displays as a negative anomaly. This anomaly is unique in the study area in that all of the other lineations present as positive features, like the one immediately to the south of the negative lineation. If both of these lineations are followed towards the northwest the negative lineation trends towards and cuts across the positive one. This relationship is repeated onland just to the south of the afore mentioned point on Chapman's Peak. In the southern region of the magnetic data (towards the coastal town of Noordhoek) there exists another two lineations. These lineations appear to coalesce, then bifurcate as one traces their axes in a northwestern direction, slightly diverging towards the western margin of the study area. These two (most offshore) lineations are very strongly positive when compared to the other lineations and cut across the entire study area. The positive lineation in the northeastern part of the study area does appear to cut across the whole bay terminating at the foot of the Sentinel. It presents in the data as a much narrower anomaly than the other lineations and does not align with any dykes seen onland. In the vicinity of the lineation previously described near the Sentinel, there appears a large positive "spike". This in not a lineation (like the others described) but rather the location of the two shipwrecks in the study area described in Chapters 5 & 6. To the north of the shipwrecks there is a small lineation which trends 104º and is only laterally extensive for 470 m.

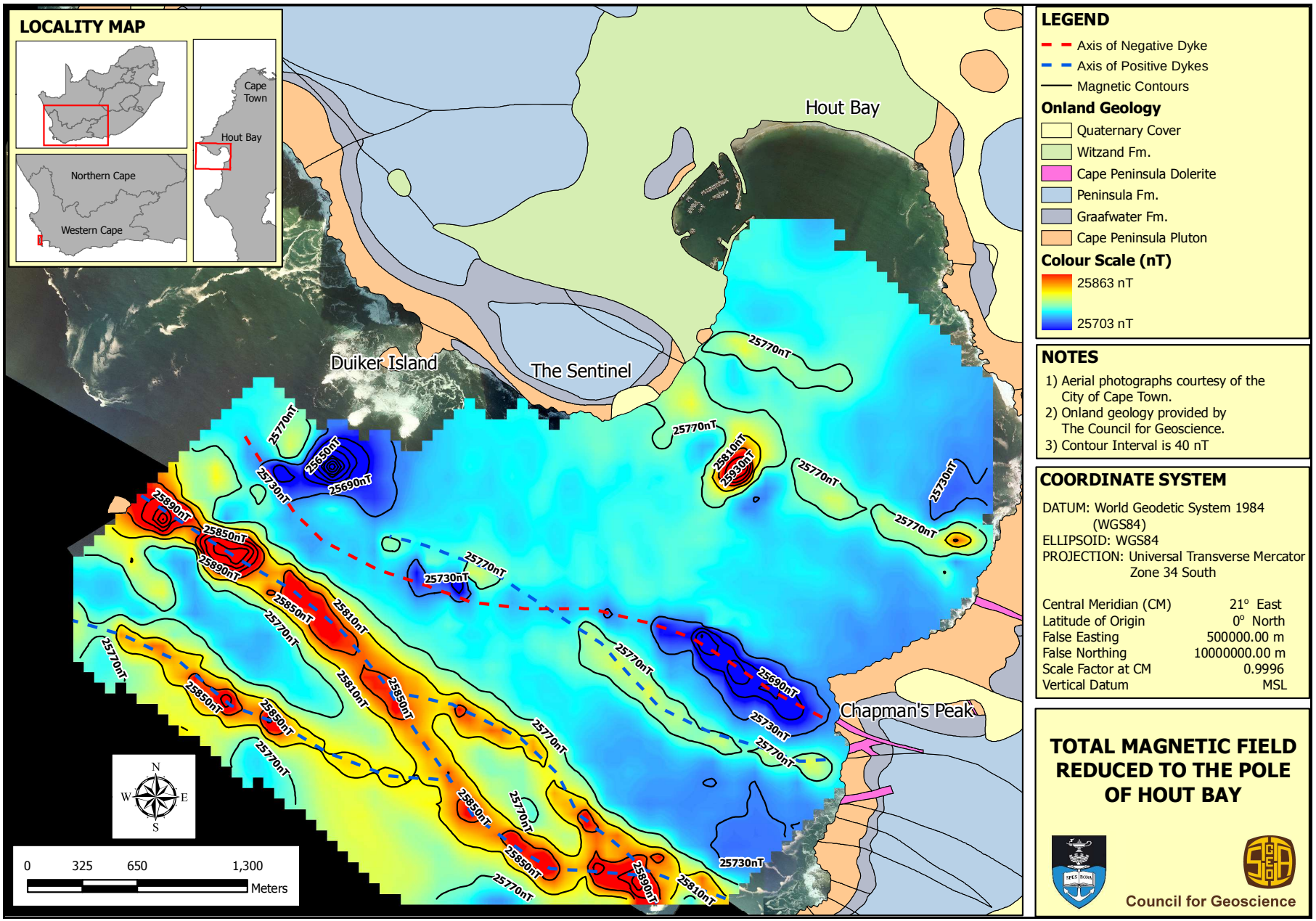

Figure 7.3. Reduced to pole chart of the magnetic anomalies of Hout Bay.

7.3. Discussion

Theron (1984) has shown that six dolerite dykes have intruded the lithologies that comprise the sub-aerial foot of Chapman's Peak. Coupled with these intrusions, numerous faults have been mapped in the same region including the Sentinel. All lineations show approximately the same orientation. Because the magnetic anomalies share the same orientation as the dykes seen onland, and match up almost perfectly in most cases, these lineations are believed to represent the offshore extension of the dykes. Structural relationships seen onland are repeated in the offshore magnetic data, which further reinforces the correlation of the magnetic lineations to the onshore dyke swarm.

The dykes form part of the Cape Peninsula Dolerites (Day, 1986). The overwhelming majority of the dykes within the larger False Bay – Cape Peninsula dyke swarm strike northwest – southeast (Day, 1986; Reid *et al.*, 1991). Day (1986) concluded that there is no correlation between the known extent of the dykes and the distribution of mapped pre-Mesozoic rocks in the area. The dykes appear to have independently intruded the constituent lithologies in the Western Cape without regard. These lithologies include the Malmesbury Group, Cape Granite Suite, Table Mountain and Bokkeveld Groups (Day, 1986). Field evidence shows that these dykes post-date the Cape Orogeny, which implies that they are younger than 210 Ma (Day, 1986). Due to the fact that the larger dyke swarm is closely related to the western continental margin of South Africa, it is believed that they are intimately related to the break up of Gondwana and subsequent rifting of South America from Africa (Martin *et al.*, 1982). Reid *et al.* (1991) sampled all the Chapman's Peak dykes for geochemical analysis with only one of the dykes (CP2) being used to perform K-Ar dating, using techniques similar to Briden *et al.* (1979) (Figure 7.4). From these data an age constraint for this dyke was found to be 131 ± 5 Ma (Reid *et al.*, 1991). This age supports the conclusions of Day (1986) that the dykes were intruded during the Early Cretaceous. It is believed by Reid *et al.* (1991) that the Cape Peninsula Dolerites represent a subprovince of the Lower Cretaceous magmatic activity that was associated with the opening of the South Atlantic Ocean. As a result of this it can be concluded that this dyke swarm is not related to the main Karoo dolerite province which intruded somewhat earlier during the Late Jurassic (Reid *et al.*, 1991).

The aeromagnetic data collected by Day (1986) shows a fairly coarse distribution of dykes in the area around Hout Bay. This study has provided high resolution magnetic data for the area and has the advantage of using a more sensitive measuring and positioning devices than those used by Simpson *et al.* (1970). Although there is no surficial expression of the dykes within the majority of the study area, the gullies with a similar orientation to the dykes that cut across the granites which comprise the Vulcan Rock – Tafelberg Reef complex are believed to represent dykes. SCUBA diving observations done by the author and Marine Geoscience Unit dive team reinforced this observation. Dolerite dykes are exposed within the granite outcrops. Because of prolonged exposure of these outcrops to seawater a halo of alteration has occurred around the dolerite specimens sampled (Figure 6.5).

Figure 7.4. Pictures showing two of the dykes below Chapman's Peak Drive. CP2 was dated by Reid *et al.*, (1991) to 131 ± 5 Ma. Inset maps show image location. Photographs courtesy of Mr. Errol Wiles (left) and Ms. Hayley Cawthra (right).

The magnetic data acquired shows that not all of the dykes within Hout Bay intruded simultaneously. The one dyke presents as a negative magnetic anomaly, in contrast to all the others, which present as positive anomalies. This means that the majority of the dykes intruded when the Earth's magnetic field was similar to the present (modern) field. The date

obtained by Reid *et al.* (1991) implies that the dyke dated could have intruded during one of eleven normal phases of the M-Sequence polarity chron (Ogg *et al.*, 2008) (Figure 7.5). The one dyke which is a negative anomaly intruded when there was a magnetic pole reversal. This "negative" dyke also cuts across the dyke closest to it both offshore and onland which signifies a younger intrusion age. Using the boundaries of the M-Sequence as defined by Ogg *et al.* (2008) this dyke could have intruded during one of 10 phases of magnetic reversals which would give a tentative age of intrusion of 127.5 – 135 Ma. The dyke CP2 dated by Reid *et al.* (1991) represents the majority (positive/normal) anomaly dykes within the study area.

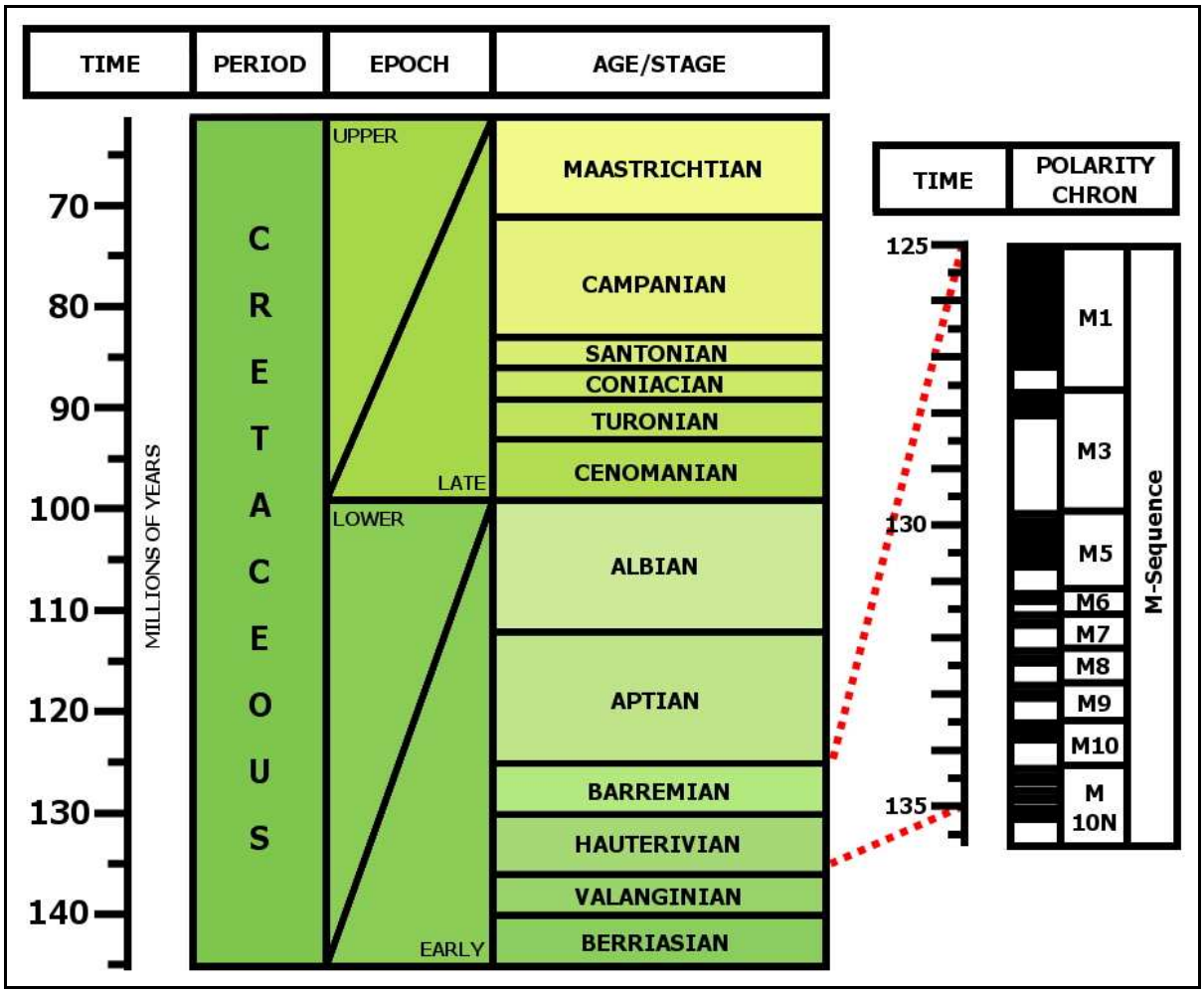

Figure 7.5. Subdivisions of the Cretaceous period modified from Haq (2007). Enlarged portion of M-Sequence Polarity Chron modified from Ogg *et al.* (2008), dark zones represent periods when Earth's magnetic field had same orientation as modern field.

Another technique for delineating sub-bottom geology is by utilising a seismic source. The following chapter deals the seismic data collected in the study area.

8. SUB-BOTTOM PROFILING

8.1. Introduction

Two sub-bottom profiling surveys were carried out in the study area. Both utilised single channel reflection seismics, with the effective operating frequency of the seismic source varying between the two. The first sub-bottom profiling (boomer) survey was performed using a 1 kHz seismic source and the second (pinger) survey utilised a 4 kHz source. The reason for the variation in seismic source is that the lower frequency system allows for increased penetration through the underlying strata, with a slight degradation in vertical resolution in the overlying unconsolidated sediments. The higher frequency system allows for increased vertical resolution with considerably less penetration into the more consolidated basement lithologies. The operating principles behind reflection seismics are outlined in Chapter 4.

8.2. Results

A total of ten boomer seismic lines were collected. Six of these lines were collected within the study area in a northwest southeast orientation. The remaining two lines were collected more or less perpendicular to the others and run as far offshore as the working range of the survey vessel (approximately 27 km) allowed, to a water depth of 200 m. The longer lines have been interpreted to reflect all of the present constituent lithologies (Figure 8.1), whereas the shorter lines have been used to define the thickness of the unconsolidated sediment wedge present in Hout Bay i.e. only to basement. The pinger data were collected along the same boomer lines within the study area yet only over unconsolidated sediment. The purpose of collecting these data was to help better interpret the unconsolidated sediment wedge by providing increased resolution of the internal sediment packets within the wedge.

8.2.1. Long Seismic Lines

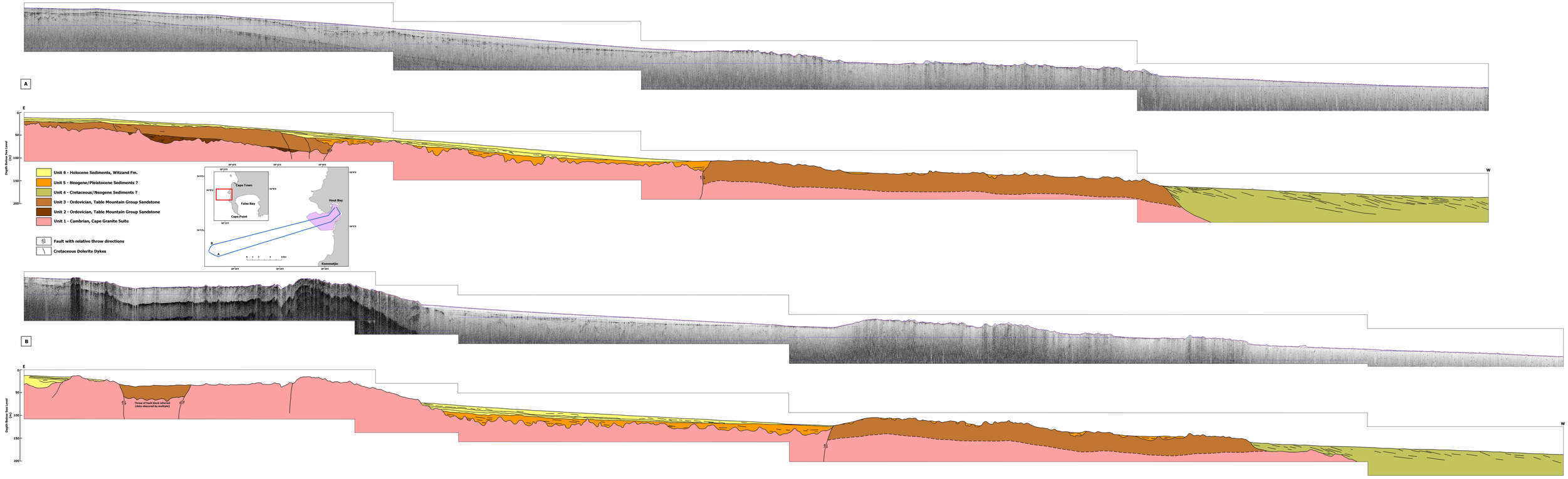

Figure 8.1. Raw and interpreted long boomer lines.

Line B was run out to sea and terminates in water depths of approximately 186 m BSL. Line A started at a similar water depth to the end of Line B and was run towards the shoreline. Between both seismic lines six units have been identified and both show evidence of faulting and intrusion by the dolerite dykes discussed in Chapter 7. The description of each unit is given below.

Unit 1 is the basal of the lithological units. It exhibits a rugged, undulose topography. In places the rugged nature of the unit has been replaced by planed surfaces. On the seismic data the unit presents as being a hard, well-cemented lithology with a strong multiple reflector. In the shallower water depths this multiple obscures the sub-bottom morphology yet for the majority of the line the multiple does not hinder interpretation. Unit 1 does not show any internal reflectors, only structural offsets in places along faults. There is evidence that the unit has been intruded by multiple lineations which represent only those dykes that have intruded sub-vertically.

Unit 2 is only observed on line A. The lack of this unit on line B is possibly due to the strong multiple reflection in the shallower water depths which has obscured it. This unit exhibits parallel to semi-chaotic internal reflectors and is only preserved in the relative depressions of Unit 1 within the study area. Like Unit 1 it is intruded by one of the lineations (dykes).

Unit 3 exhibits a similar internal reflection pattern to that of Unit 2. It forms a cap to Unit 2 on line A, and caps Unit 1 on line B. This unit, like the two below it, is intruded by dykes and bounded by structural offsets. On line B it forms part of a graben fault block in the inshore part of the line, with its shoreward limit not encountered on line A. On both lines the unit is fault bounded in the inshore part of lines in water depths of approximately 120 to 130 m BSL and unconformably overlain distally by a sediment blanket in water depths of approximately 150 m BSL. Both of the upper surfaces of Units 3 and 2 show a much smoother topography than Unit 1.

Unit 4 is found in the distal regions of both lines in water depths in excess of 150 m BSL and exhibits shallow seaward dipping reflectors. There is a notable change in gradient of the seafloor at the contact between Unit 3 and Unit 4.

Unit 5 is found on both lines between water depths of approximately 80 to 150 m BSL. The architecture of its internal reflectors is parallel to sub-parallel with the unit occupying relative

depressions in Units 1 and 3. The unit also appears to infill the structural offset between Units 1 and 3 on line A and truncates against Unit 3. The top of this unit has a strong (dark) reflection on the seismic records.

Unit 6 is the uppermost unit, occurring from 120 m BSL water depth and shallower. The internal reflectors of the unit exhibit downlap onto Unit 5 and onlap onto Unit 3. The unit displays a definite winnowing (pinching out) distally.

8.2.2. Short Seismic Lines

The short boomer lines in conjunction with the pinger lines were interpreted to reveal three different subsurface units. Units 5 and 6 are synchronous with those interpreted from the long boomer lines. The basement is a combination of Units 1, 2 and 3 (Figure 8.2). Unit 4 was not identified in the short boomer lines. From these data the elevation of the sub-bottom basement within the study area was prepared (Figure 8.3). The palaeo-embayment of Hout Bay is clearly emphasised by the data. There is a well defined palaeo-channel which meanders along the western flank of the bay, curving around to appear to link up with the present day Disa River. The channel is fairly deeply incised into the basal strata showing side slopes with a gradient of approximately 6º. The channel appears to open at approximately 50 m BSL which means that the 50 m BSL sub-bottom isobath represents a palaeo-coastline. From the basement elevation it appears as though the palaeo-delta starts opening at approximately 50 m BSL, with the locus of the delta at approximately 65 m BSL. What is immediately evident from the basement surface (Figure 8.3) is the relative flatness of the area adjacent to the Chapman's Peak side of the embayment. The surface would be extremely flat were it not for the incision of the palaeo-channel. To the southwest of the Tafelberg reef complex the sub-bottom basement drops off rapidly.

A consequence of being able to define the basement elevation is that the thickness and volume of unconsolidated sediment within the study area can be calculated. A sediment isopach chart has been generated for the study area (Figure 8.4). From these data two depocentres are immediately evident. The first occurs approximately 850 m southeast of Hout Bay Harbour and shows an accumulation of sediment of between 14 – 20 m thick. The second depocentre coincides with a palaeo-delta at the mouth of Hout Bay. This depocentre exhibits similar sediment thicknesses to that of the more inshore depocentre. Up to 16 m of

sediment has accumulated in the palaeo-channel. The sediment isopach within the channel presents as localised depressions. This is most likely a gridding artefact which could be removed with more (tighter line spaced) seismic data. In reality the base of the channel would be a lot smoother.

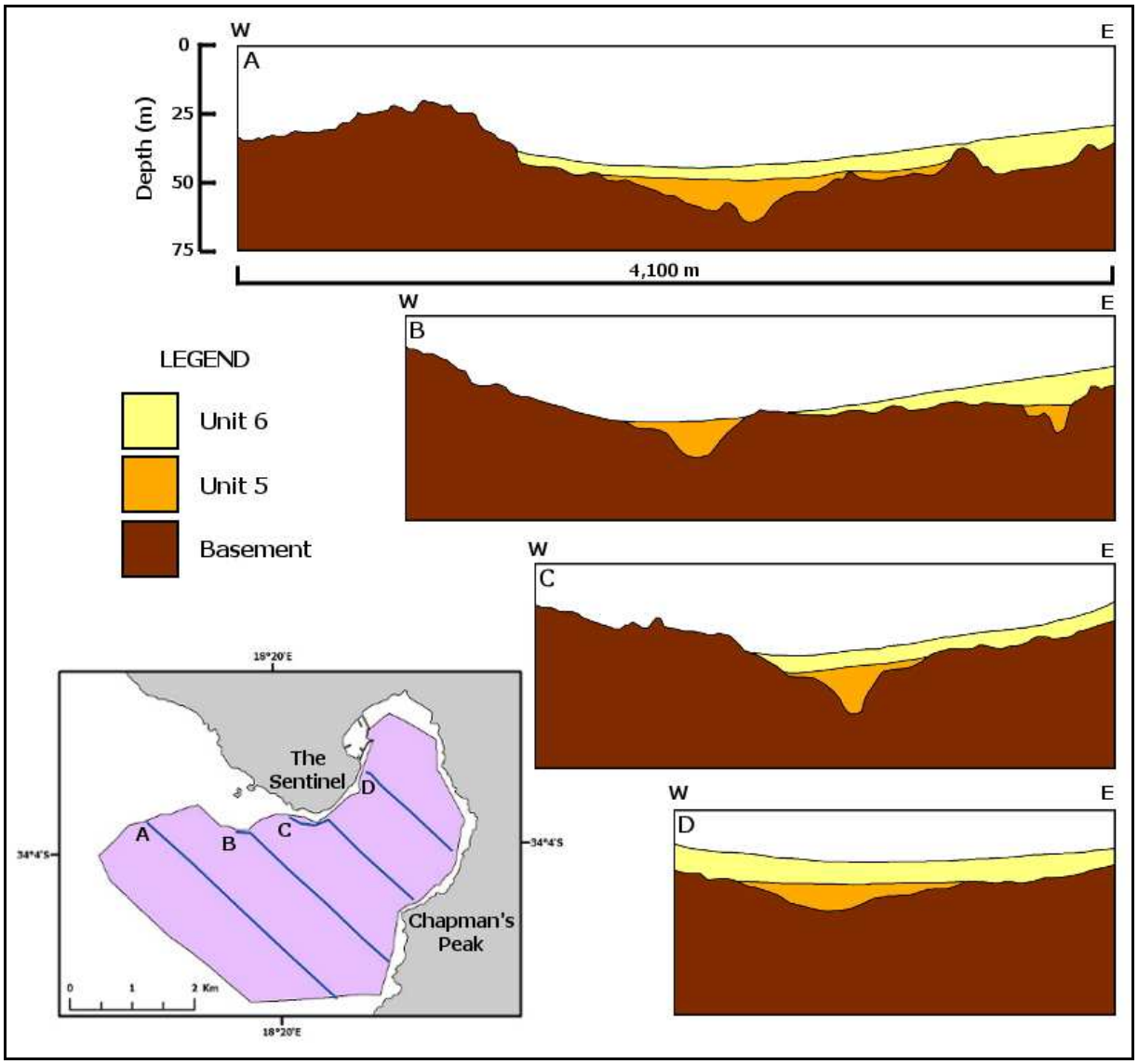

Figure 8.2. Some of the interpreted short seismic lines from the study area.

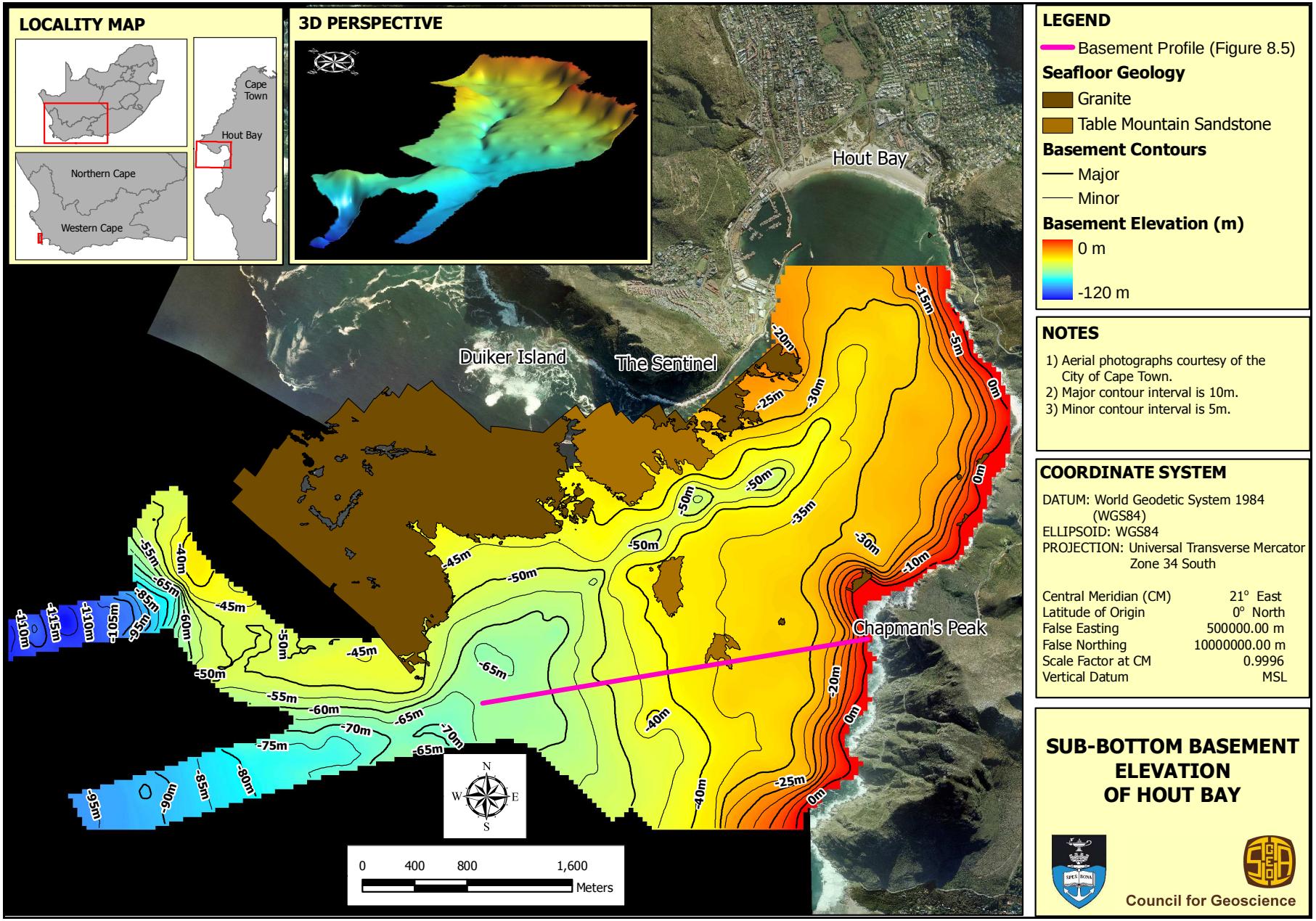

Figure 8.3. Sub-bottom basement elevation of Hout Bay.

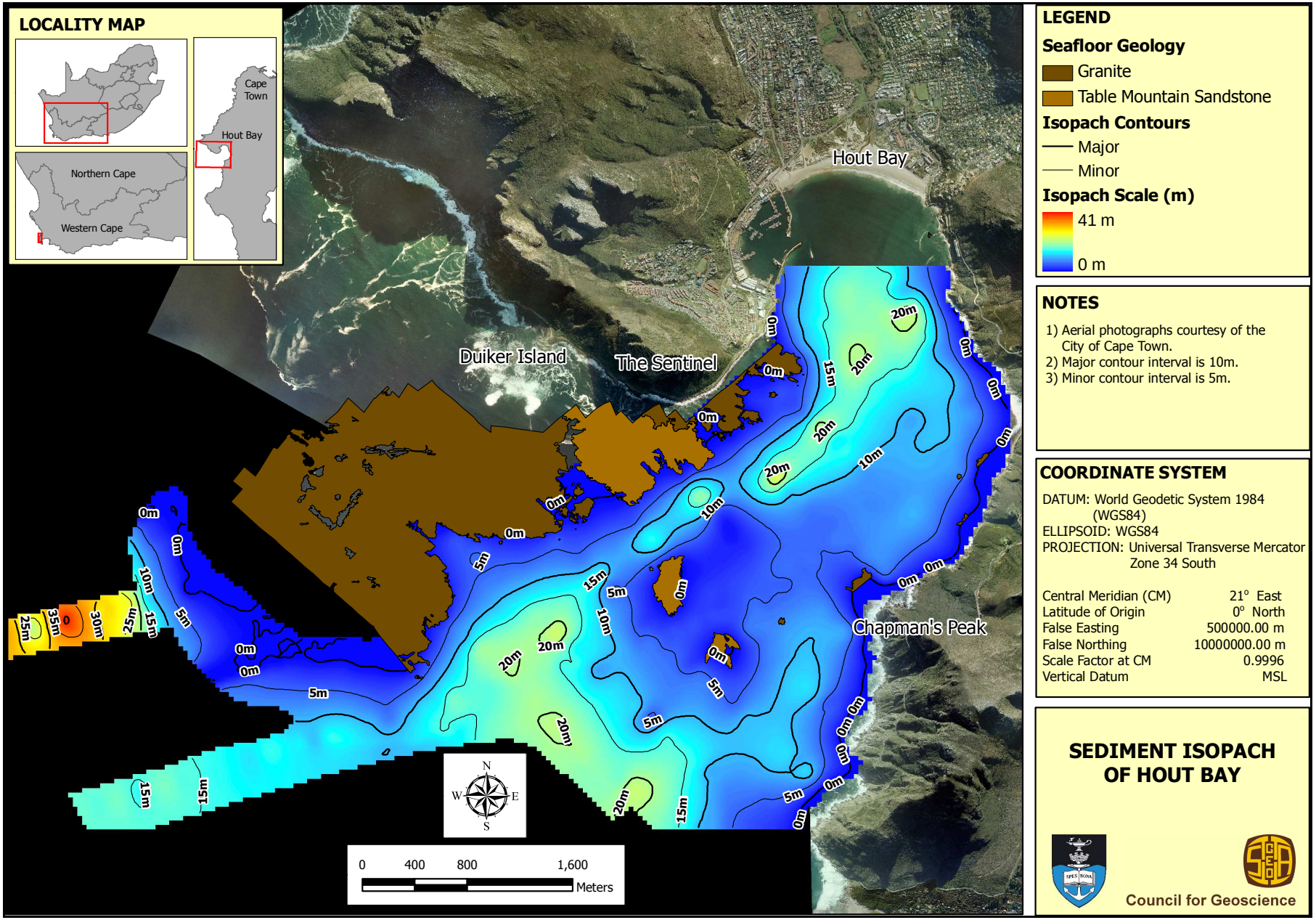

Figure 8.4. Sediment isopach of Hout Bay.

Using the numerical integration algorithm described by Press *et al.* (1988) and referred to as the extended trapezoidal rule, an approximation of the volume of unconsolidated sediment within the study area was calculated. Unlike similar studies (De Decker, 1987; Woodborne, 1991 and Birch *et al.* 1991) who used 1500 m/s, a sub-bottom speed of sound of 1650 m/s (Caufield *et al.*, 2005; Becker, 2007; Whiteley and Stewart, 2007) was used. This faster speed of sound is believed to be a better approximation for the sediments of Hout Bay. The volume of sediment was calculated to be approximately 126 x 10^6 m^3.

8.3. Discussion

Due to the undulose and bulbous morphology of Unit 1 and the fact that it outcrops in the same area as the granite outcrops interpreted from the seafloor acoustic facies, this unit is correlated to the sub-bottom expression of the granites in the study area. Towards the deeper parts of the lines (in water depths in excess of 100 m BSL) the contact between the granite basement and overlying units has been inferred from the relative throw of the faults observed closer inshore. The reason for this is that in the deeper water depths there is more attenuation of the seismic signal and therefore reduced ability to resolve deeper reflectors. The presence of the Columbine/Agulhas Arch however reinforces that the granite basement extends to at least the first shelf break. Unit 2 and 3 have similar internal reflector patterns and crop out in the same area as that of the TMG from the seafloor geology map, therefore these units are correlated to the TMG outcrops seen on Chapman's Peak (Figure 6.19). The basal Unit 2 has been interpreted as a sub-facies of the prominent Unit 3. At first Unit 2 was interpreted as representing the Graafwater Formation yet locally to the study area the Graafwater forms a relatively thick discrete layer and in the seismic data Unit 2 is confined to a small area which is not consistent with the relationship seen onland. Unit 3 represents the Peninsula Formation. The origin of Unit 4 poses conflicting arguments. Superimposing the distal occurrence of Unit 4 with respect to the published offshore sedimentological outcrops (Dingle, 1973; Dingle *et al.*, 1983) and combining the characteristic shallow seaward dipping reflectors (Dingle, 1973), this Unit could represent Upper Cretaceous sediments (Figure 3.9). The extent of offshore Cretaceous sediments near the study area is however extremely localised and interpreted seismic data collected by Dingle (1971) in almost exactly the same area show these sediments to be Neogene in age. Both of these sediments have characteristic shallow seaward dipping reflectors with Neogene reflectors having the

shallower dip of the two. The author therefore has classified Unit 4 as either Cretaceous or Neogene favouring a Neogene origin.

Unit 5 and Unit 6 represent unconsolidated sedimentary units. The boundary between these two units is a dark, highly reflective interface that may represent reworked sediments during a sea-level transgression. Further evidence to support this conclusion is that the reflectors of Unit 6 appear to downlap onto this surface. Coe (2003) defines the maximum flooding surface as the surface onto which the overlying highstand systems tract (HST) clinoforms run tangentially into (downlap). The sediments from the transgressive systems tract (TST) are by definition reworked during this process with the fines winnowed away leaving only the coarser fraction behind. This is why typically the transgressive surface and maximum flooding surface appear as the same reflector (Coe, 2003). Because Unit 6 lies on top of the transgressive surface and the sedimentary packets within the unit appear to prograde seawards (as more accommodation space becomes available during a marine transgression), this unit correlates to Holocene sediments associated with the most recent deglacial transgression when sea-levels rose rapidly from 120 m BSL (Compton, 2001). The relative relationship of Unit 5 to Unit 6 and the transgressive surface leaves the author to assign either a Neogene or Pleistocene age to the sediments of Unit 5. Of these two a Pleistocene age is preferred as the unit is found in relatively shallow depths (inside Hout Bay) which would have been exposed many times since the onset of the Cenozoic with the probability of older sediment being eroded away much greater. The most obvious question is how were these sediments able to be preserved? The seismic nature of the sediment is closer to a consolidated lithology than that of unconsolidated fine- to medium grained sand. Although not encountered around the study area, further to the north near Langebaan, the Neogene Langebaan Formation can be found. This formation is made up of partially cemented aeolian sand which the author is of the opinion Unit 5 represents. Only coring and dating will provide a definitive answer.

From the long seismic lines there is a clear gradient change between the inner and middle shelf. This break occurs at a water depth of approximately 160 m BSL, between the Cambrian basement (which defines the inner shelf) and the Cretaceous strata of the middle shelf. It is interesting to note how the occurrence of this break has migrated over 60 m from the 97 m BSL documented off the Holgat River (just south of the Orange River) (MacHutchon, 2003) to the water depths seen in this study. The morphology of the sub-bottom basement shows evidence of a wave abraded terrace. This terrace occurs between

32 to 35 m BSL (Figure 8.5). The depth of this terrace also conforms to one of the depth ranges of previously published wave abraded terraces off the west coast namely 30 to 35 m BSL (De Decker, 1987) and 33 to 40 m BSL (Woodborne, 1991).

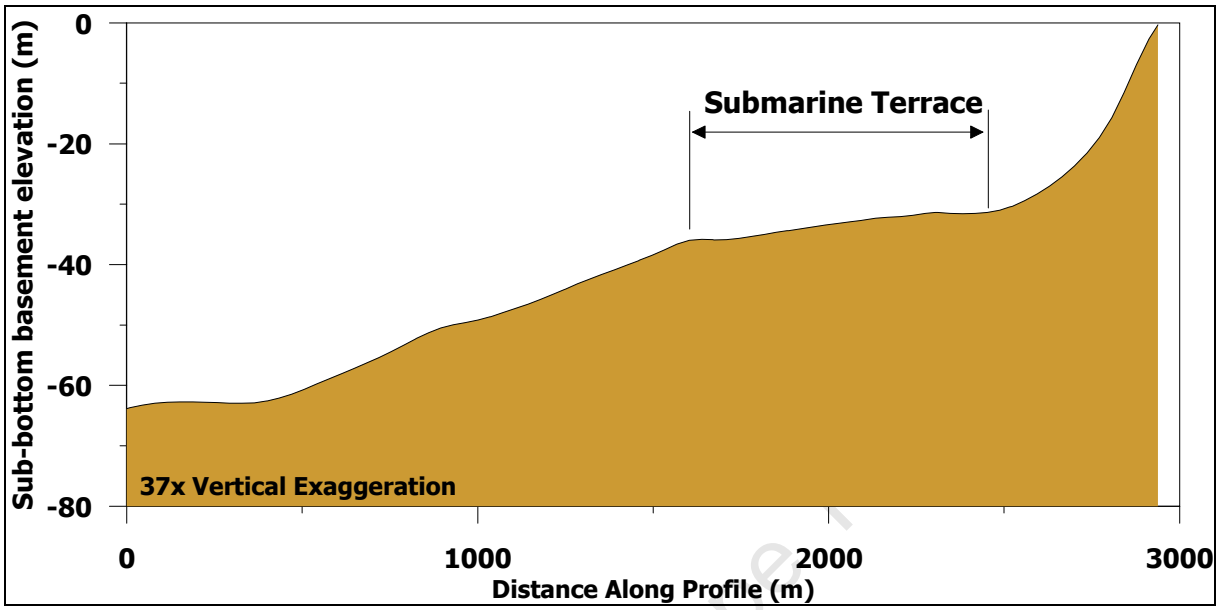

Figure 8.5. Profile across sub-bottom basement of Hout Bay. Profile locality shown on Figure 8.3.

As sea-levels rose and fell in response to changing global volumes of ice the terraces seen in the data would have formed. To infer when these terraces were formed the elevations of the two wave abraded terraces found in the study area have been superimposed on the Pleistocene sea-level curve of Compton and Wiltshire (2009) (Figure 8.6). From these data it is clear that sea-levels have passed both terrace elevations multiple times. When sea-levels are either rising or falling relatively rapidly the amount of erosion is much less, rather when sea-levels experience relative stillstands the erosional ability of wave action is far greater. For the terrace identified in Chapter 6.3 (18 to 20 m BSL) conditions for the formation of a terrace have occurred fifteen times over the last 450 kyr with the most favourable occurring between Marine Isotope Stages (MIS) 8e – 9a and 10 – 11. For the deeper 32 to 35 m BSL terrace favourable conditions were encountered fourteen times with the best of these occurring during MIS 3, between MIS 7a – 7c and during MIS 8c.

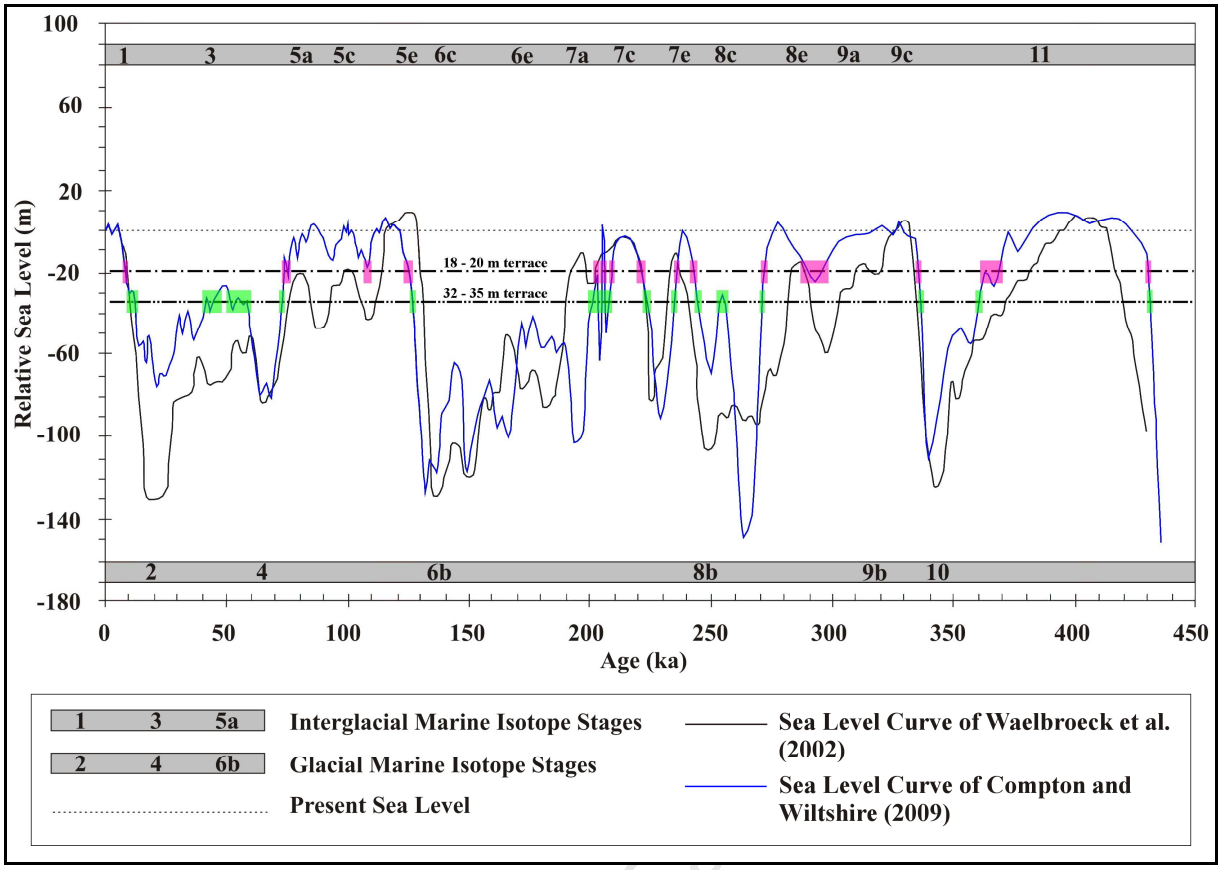

Figure 8.6. Wave abraded terrace elevations encountered in study area, superimposed on Pleistocene sea-level curve of Compton and Wiltshire (2009).

From the sea-level curves it is clear that during glacial maxima the average sea-level was 130 m lower than at present. To help visualise this the 130 m isobath has been plotted on offshore bathymetric DTM of the Cape Peninsula and False Bay (Figure 8.7). Evidence of this lower sea-level in the seismic data can be seen on the seaward margin of the offshore TMG outcrops. On both seismic lines this zone is flatter and more planed with the sediment infills of Unit 5 delineating the 130 m BSL sea-level. From the bathymetric DTM it is evident that the zone inshore of the 130 m isobath is more rugged in nature which is to be expected as rising and falling sea-levels would have caused deposited sediment to be reworked and the majority thereof most probably removed throughout the Quaternary.

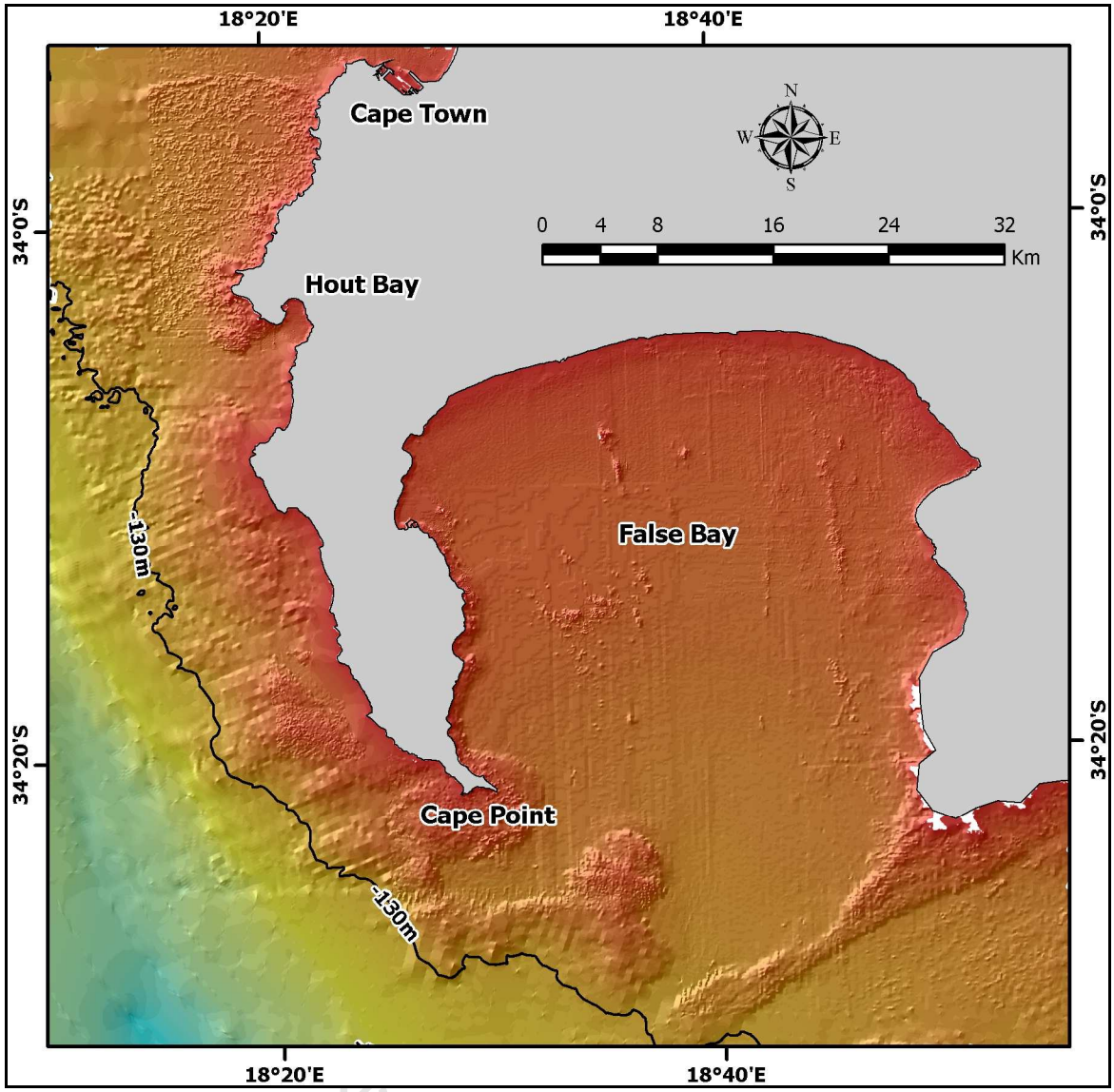

Figure 8.7. Offshore bathymetric DTM of the Cape Peninsula and False Bay. Data digitised from SANHO admiralty charts by Mr. P. Dillon and offshore DTM created by Mr. W. Van Zyl.

The faults depicted on the long seismic lines at depths of approximately 130 m BSL may represent the offshore extension of one of the prominent faults mapped by Theron (1984). If the two surface intersecting points of the fault are connected they exhibit a fault axis with a strike of 114º which is a similar orientation to the dominant faults mapped south of Hout Bay on the Cape Peninsula.

This chapter concludes all of the geophysical datasets collected. The following chapters deal with the physical characteristics of the sediment in the study area and the hydrodynamics effecting the sediment.

9. SEDIMENT ANALYSIS

9.1. Introduction

A total of 57 sediment samples were obtained within the study area (Figure 4.23). These samples were collected to ground truth the geophysical data and to quantify sorting trends within the study area related to sediment dynamics. Where possible the sampling method was based on a predefined grid to ensure statistical accuracy, but while doing underwater observations on SCUBA additional samples were taken which do not conform to the grid spacing. The sediment samples were processed and statistics generated by Environmental Mapping and Surveying (EMS). The methodology employed by EMS to process the sediment samples is outlined in Chapter 4.6. The weight percentage of each sized fraction retained in the sieves was analysed using in-house developed software by EMS to generate the relevant sedimentary statistics for each sample. Selective sub-samples were collected and photographed to help with facies interpretation.

9.2. Results

Classifying the sediments in terms of their texture using the methodology outlined by Folk (1965) reveals that the majority fall between the two ternary end members of gravel and sand (Figure 9.1). This classification however is far too coarse as the relative proportions of the sand size fraction have not been given any weighting. It does, however, serve as a good indication of the general trend.

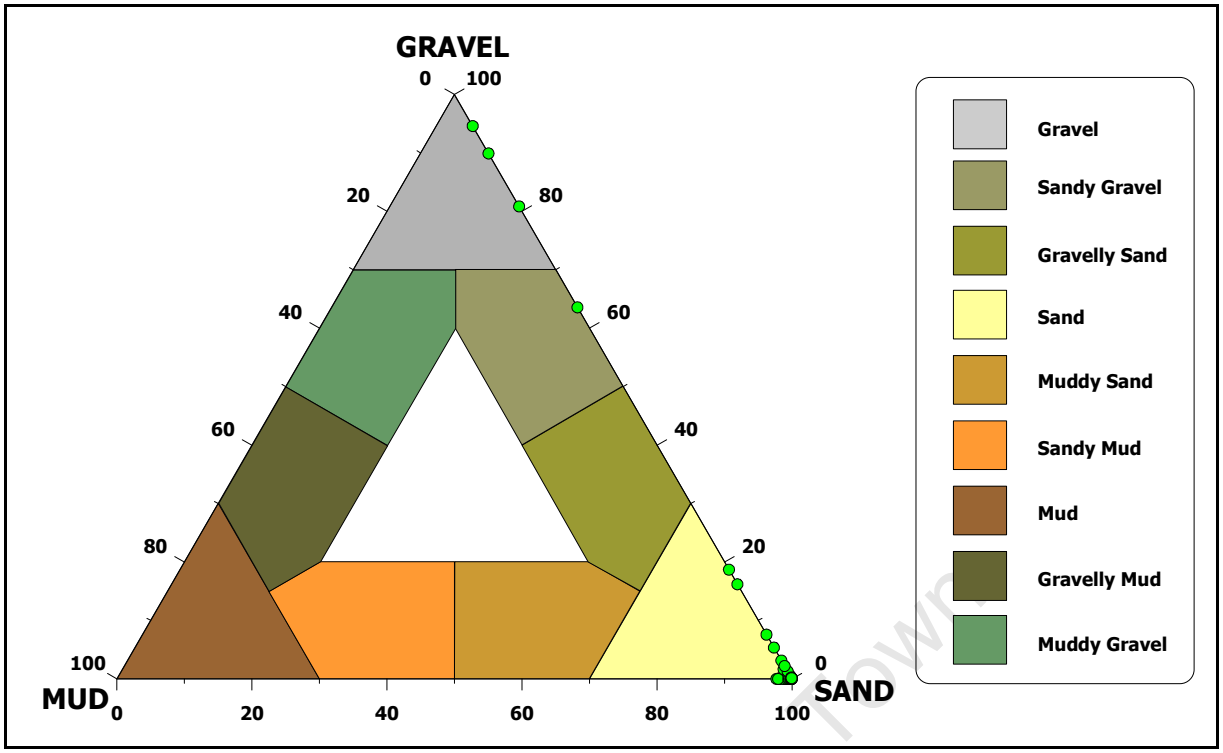

Figure 9.1. Sedimentary texture in terms of Gravel-Sand-Mud. Modified from Folk (1965).

9.2.1. Texture

The sediment samples in the study area have been classified texturally according to the grain size classification of Wentworth (1922). The textural end members of the sediment within the study area are gravel and mud with the sand sized fraction sub-divided into five different textural classes.

The coarsest fraction within these divisions is gravel (clasts > 2 mm). Within the study area the highest percentages of gravel (90%) occur within the granite outcrops that comprise the offshore Vulcan Rock – Tafelberg reef complex (Figure 9.2). High concentrations of gravel are found in the sediment gullies between reef outcrops. Gravel content decreases rapidly with distance from these rock outcrops, reduced to close to 0% for the majority of the study area. It is however not uncommon to find shell rich gravels exposed during storm events along Hout Bay Beach. These gravels represent re-worked shell rich horizons/lenses which are buried during equilibrium conditions within the study area. There is a slight bulge in the percentage gravel adjacent to the Table Mountain Sandstone outcrops associated with the sub-marine toe of the Sentinel.

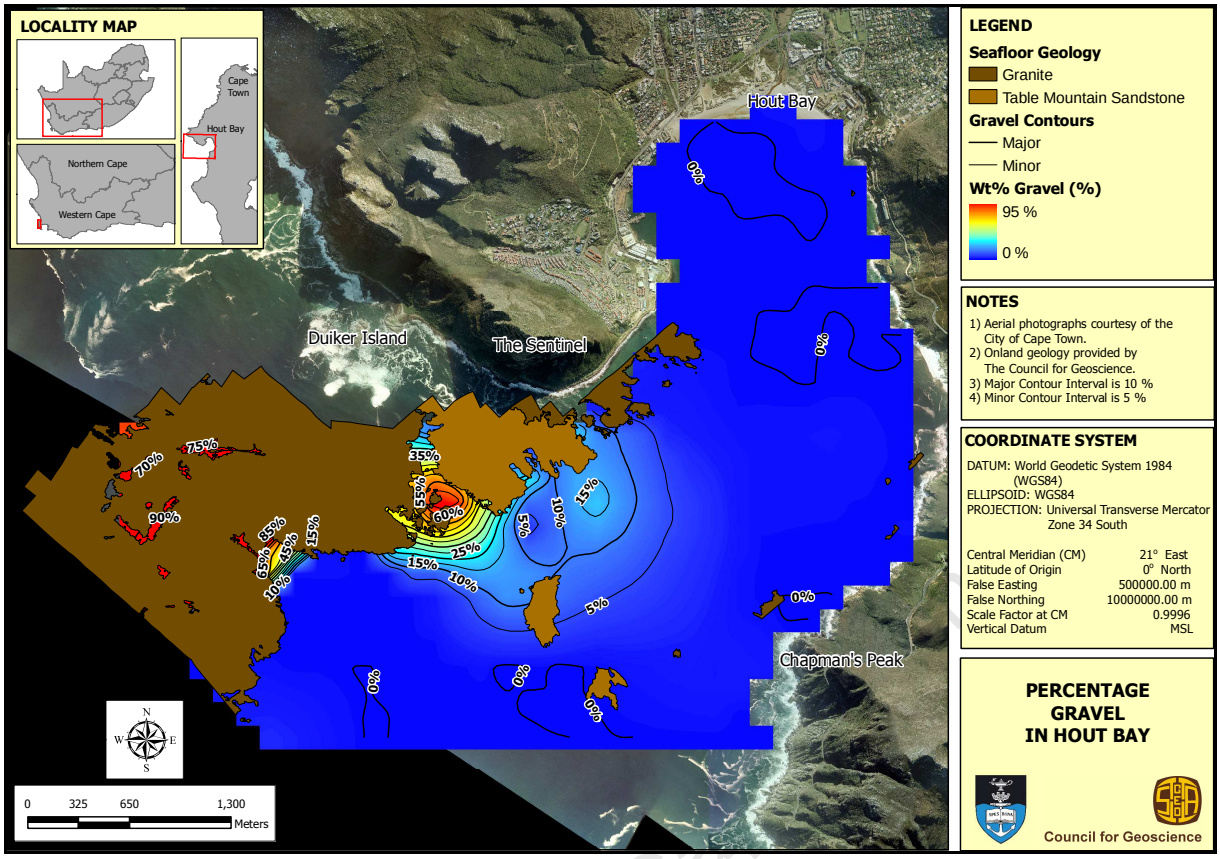

Figure 9.2. Percentage gravel in study area.

The percentages of very coarse- and coarse grained sand exhibit similar trends to one another within Hout Bay (Figure 9.3 & Figure 9.4). Both show relatively high concentrations in the middle of the study area between water depths of 38 to 26 m BSL, slightly seaward of and between the Sentinel and Chapman's Peak viewing point. These relatively high concentrations show a bimodal distribution with elongation along a southwest – northeast and southeast – northwest axis. The coarse sand fraction exhibits this trend more clearly. There is a similar elongating trend of coarse grained sediment off the northeastern edge of the Sentinel parallel to one of the orientations described.

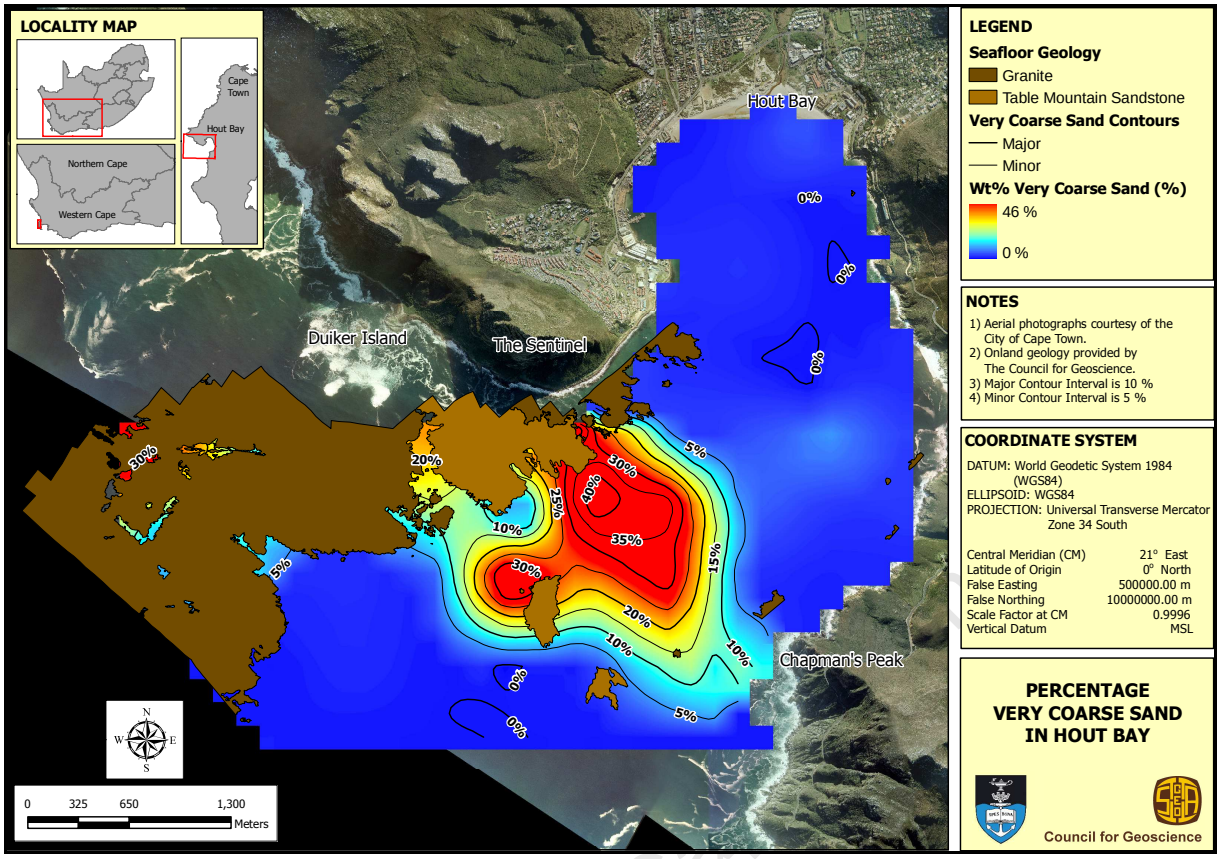

Figure 9.3. Percentage very coarse sand in study area.

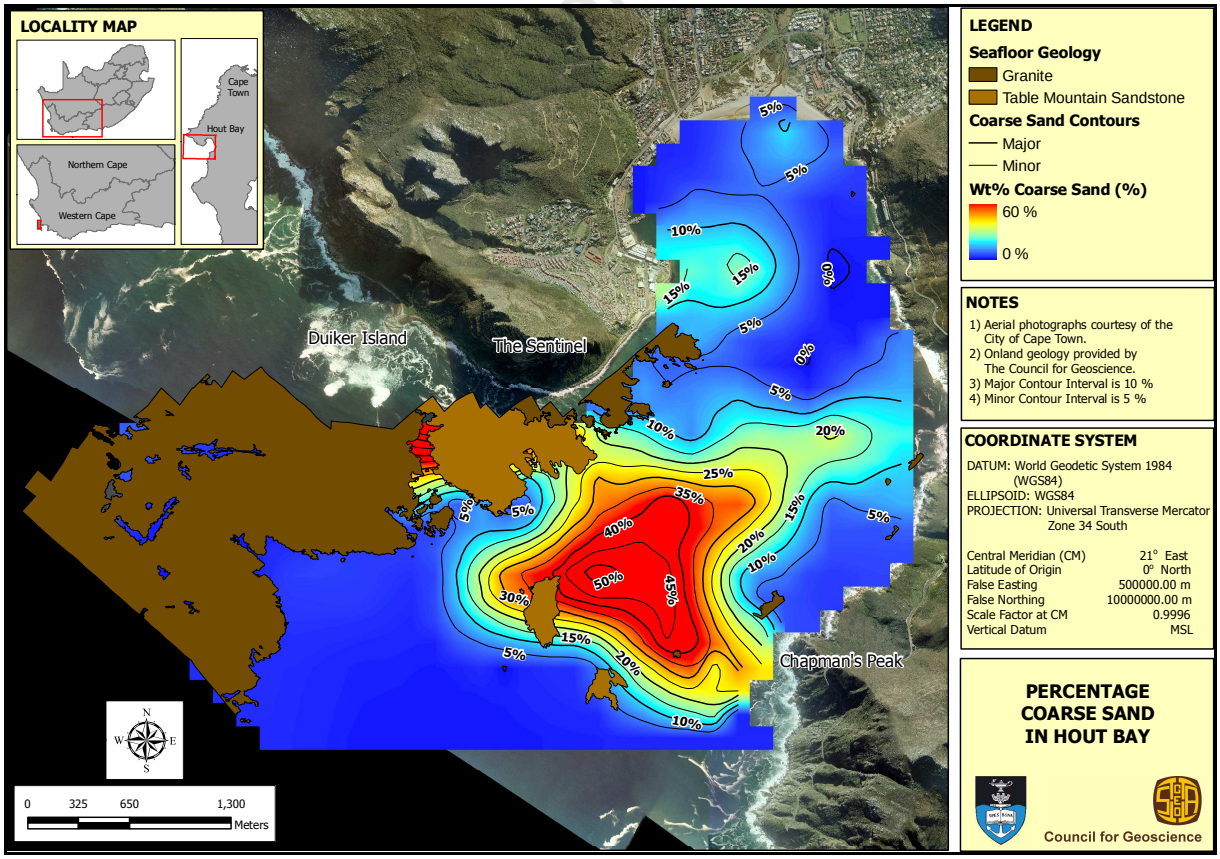

Figure 9.4. Percentage coarse sand in study area.

The locus of medium grained sand differs to that of the two coarser sand fractions in that it is situated slightly more inshore (Figure 9.5). The translation of this locus is along the same orientation as the elongation observed in the coarse grained sediment. Tails of higher relative concentrations reinforce this trend and of those observed in the coarse grained fraction. Another trend observed within the medium grained sand is the relative accumulation of this fraction along the eastern quadrant of Hout Bay Beach and associated littoral zone.

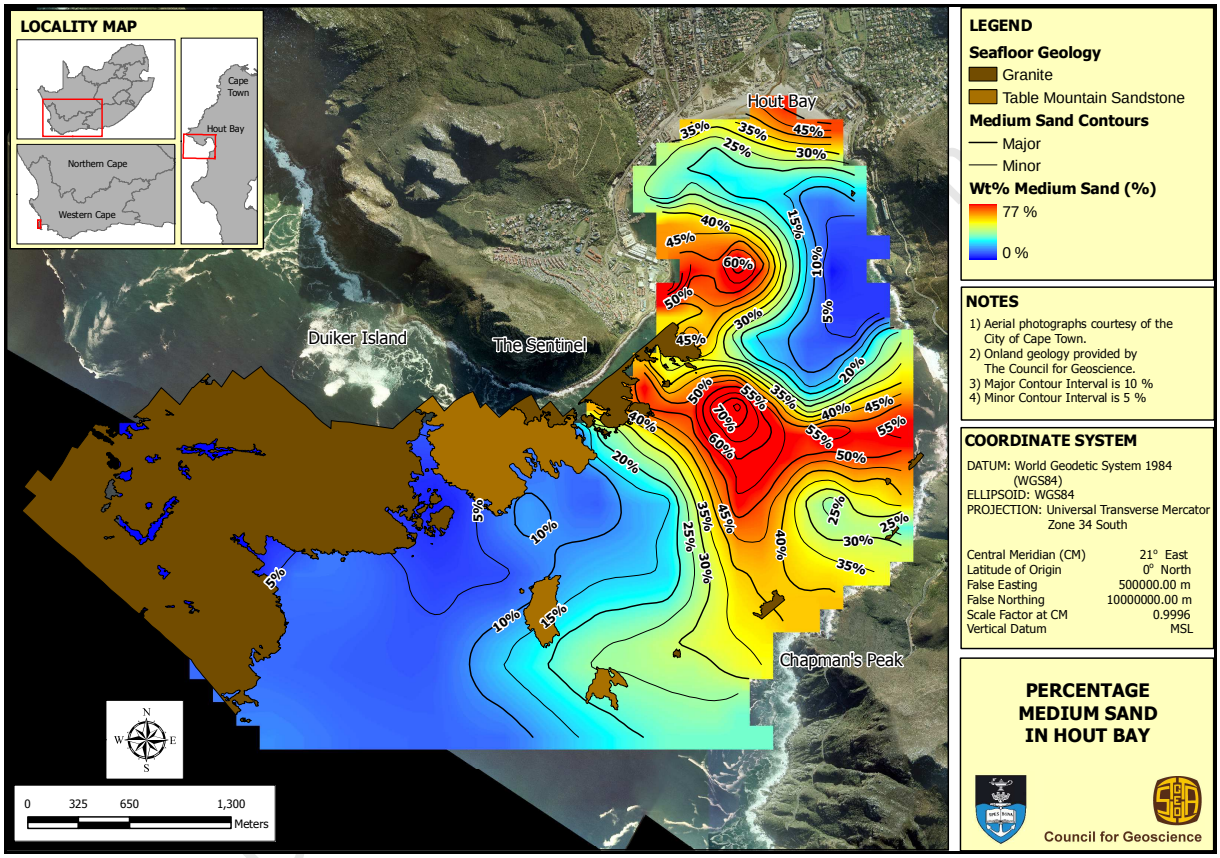

Figure 9.5. Percentage medium sand in study area.

The fine sand fraction is concentrated along the same orientations described above, accumulating up against the foot of Constantiaberg, Chapman's Peak and Hout Bay Harbour (Figure 9.6). To the north of Chapman's Peak viewpoint the fine sand fraction appears to have accumulated in the relative embayment inshore of the prominent sub-marine toe associated with the viewpoint. This accumulation has been separated from that further north by a zone relatively depleted in fine sand which is elongated along the southwest – northeast axis. The largest accumulation of the fine sand fraction can be found between Noordhoek Beach and Tafelberg Reef complex.

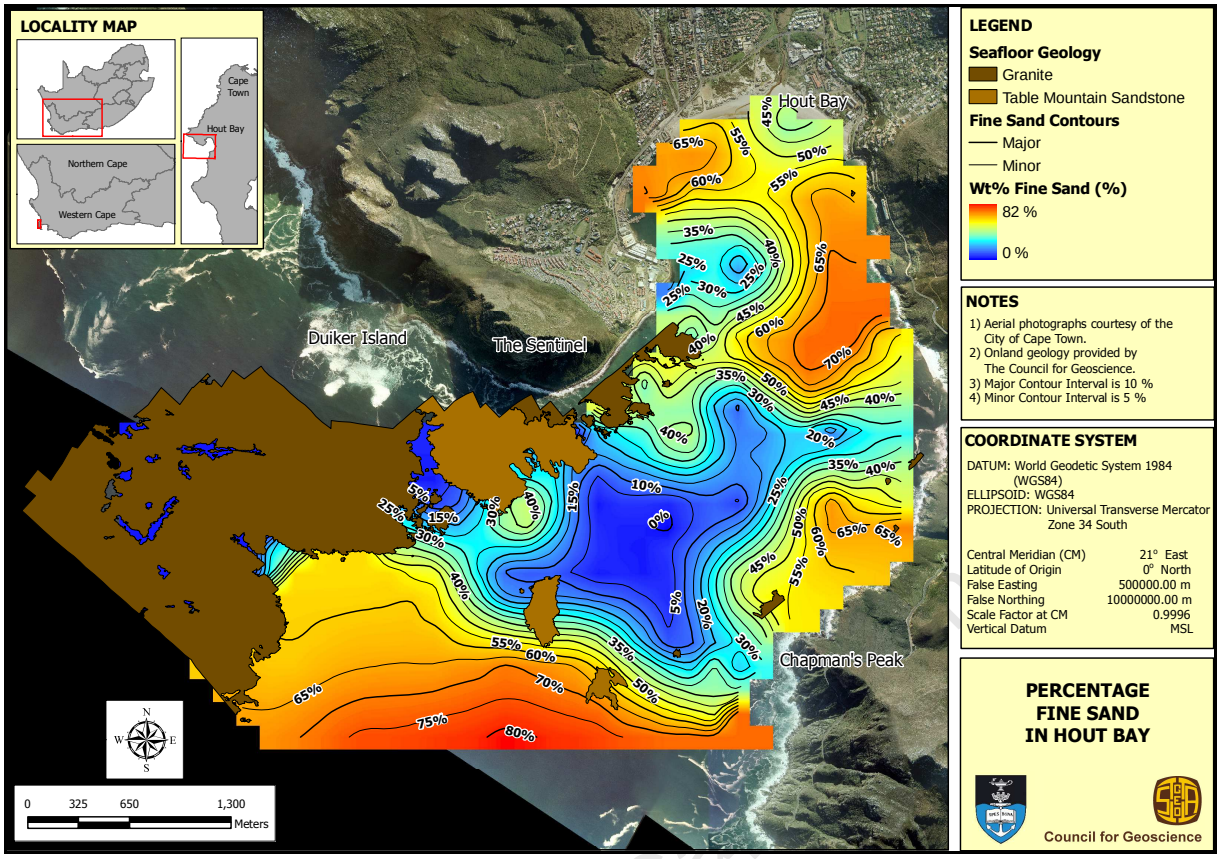

Figure 9.6. Percentage fine sand in study area.

The very fine sand and mud show similar distributions in the study area (Figure 9.7 & Figure 9.8). Both show a bimodal distribution with relative loci in the inshore areas of Hout Bay against the foot of Constantiaberg and adjacent to Tafelberg Reef extending approximately 630 m into the bay.

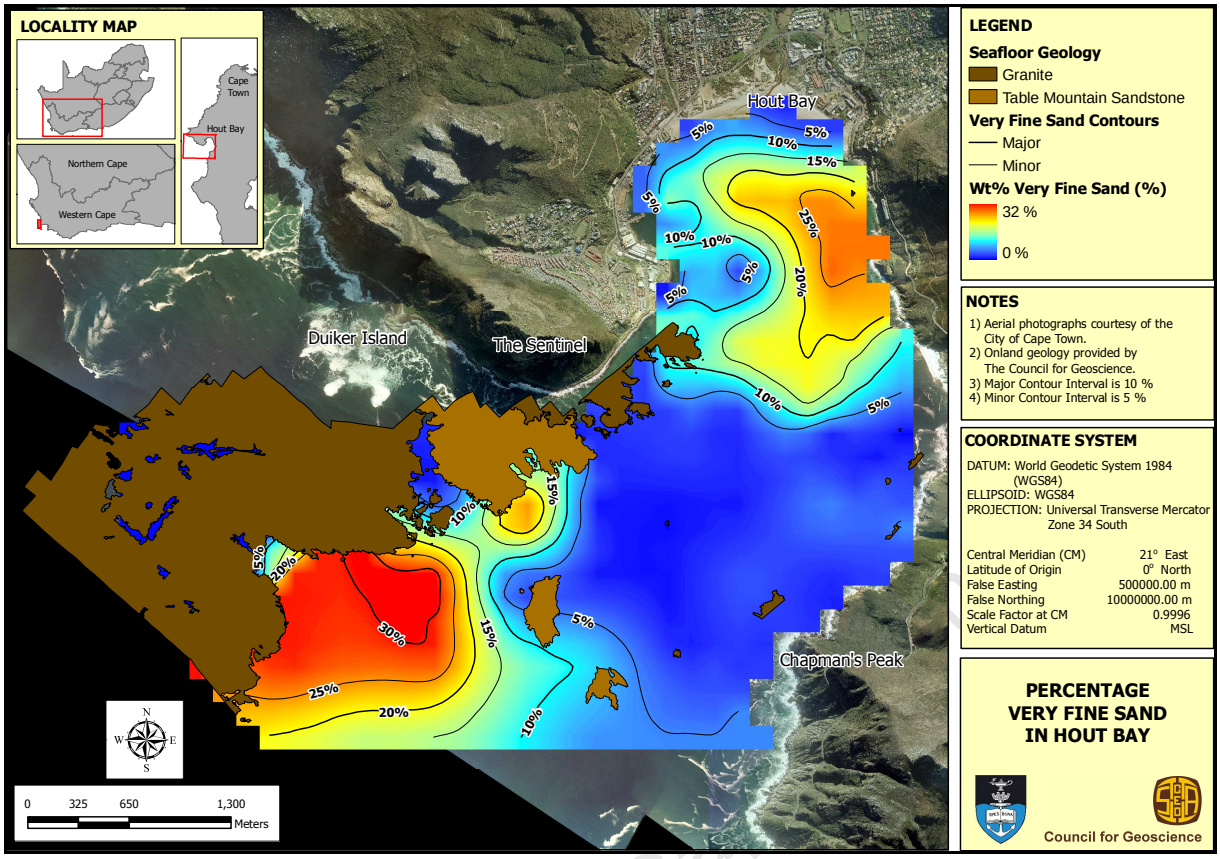

Figure 9.7. Percentage very fine sand in study area.

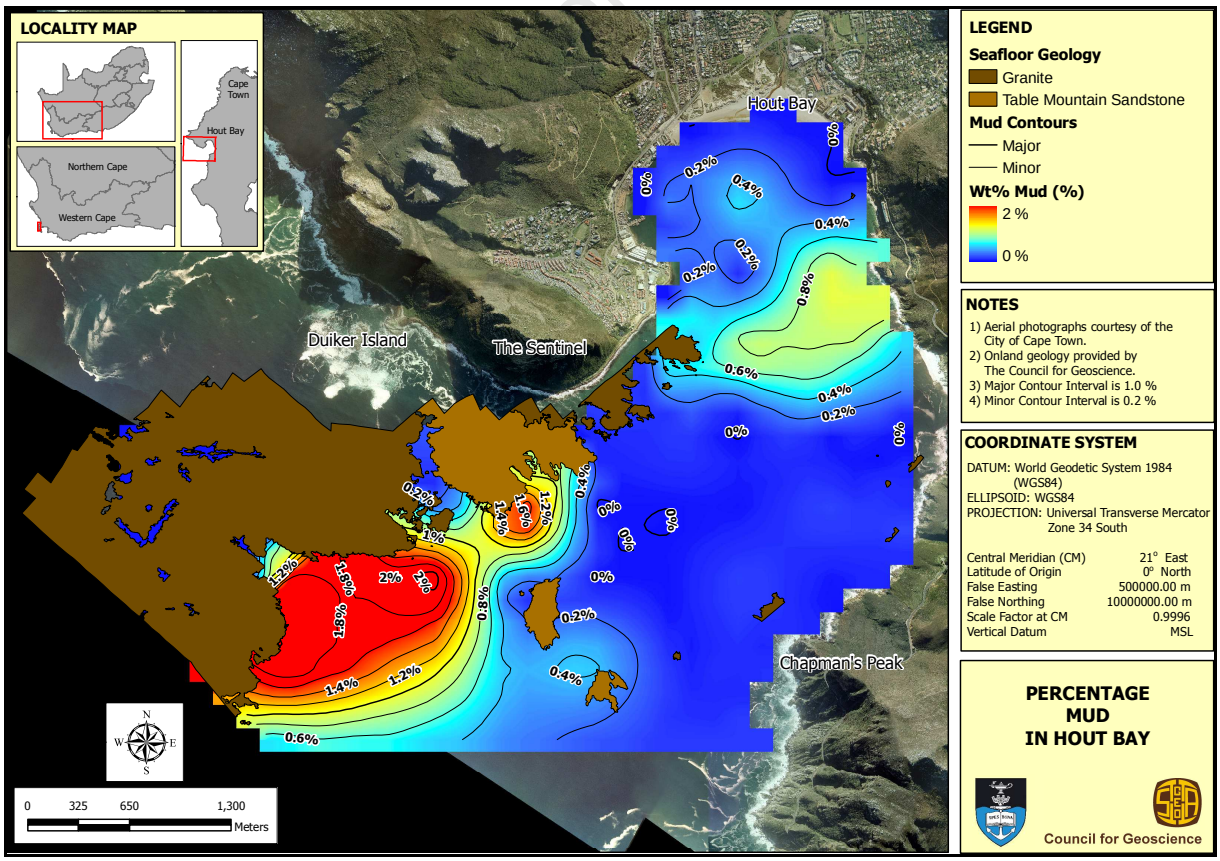

Figure 9.8. Percentage mud in study area.

The mean grain size of the sediment within the study area has been presented in terms of millimetres in Figure 9.9. The data follow the trends seen in the analysis of the different sediment fractions. Larger grain sizes occur on or in the gullies between the surficial reef outcrops or as a halo around these outcrops, decreasing rapidly away from the outcrops for the majority of the study area. In the middle of the bay the mean grain size distribution is focused along two distinct axes orientated approximately perpendicular to one another. There is a relative accumulation of coarser material forming a circular zone to the southeast of the Table Mountain Sandstone forming the sub-marine toe of the Sentinel.

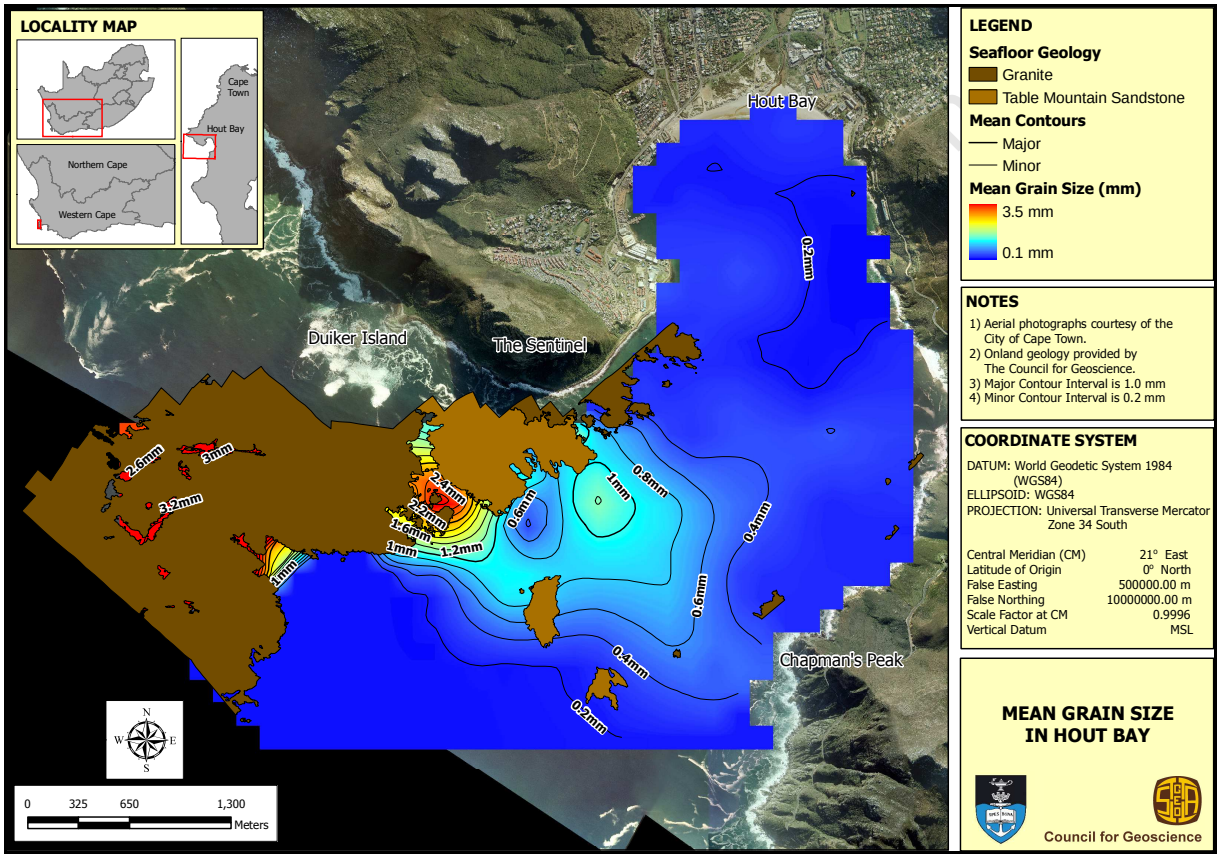

Figure 9.9. Mean grain size (in millimetres) of the sediment in Hout Bay.

The sediments within the study area range from moderately- to very well sorted (Figure 9.10). The locus of moderately sorted sediments occurs in the middle of the bay between the Sentinel and Chapman's Peak viewpoint. This locus shows an elongation along a southwest – northeast axis. There is a small outlier of moderately sorted sediment near the eastern quadrant of the littoral zone of Hout Bay Beach. The remainder of the sediment is well- to very well sorted occurring in two regions namely an inshore area concentrated against the foot of Constantiaberg and an offshore zone extending from Tafelberg Reef towards Noordhoek Beach.

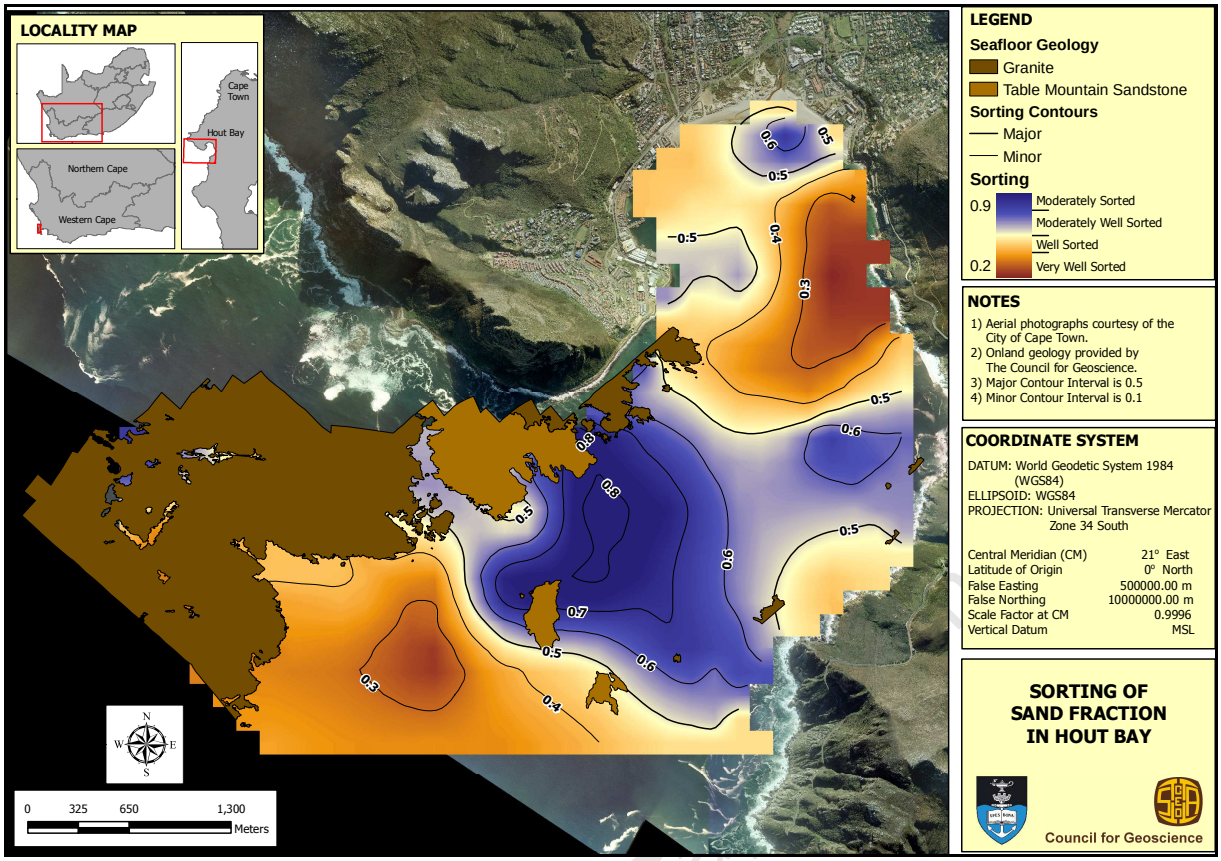

Figure 9.10. Sorting of the sediment in Hout Bay.

The calculated skewness values for the sediment in Hout Bay shows that in close proximity to the reef outcrops the sediment is strongly positively skewed (Figure 9.11). This means that the distribution of grain sizes within the sample has a higher concentration of coarse grained material resulting in a large positive (fine) tail. As one moves away from the dominant lithological outcrops and further into Hout Bay (in a distal direction) the sediment grades into more negatively skewed distributions, which implies higher concentrations of finer grained particles and a larger negative (coarse) tail.

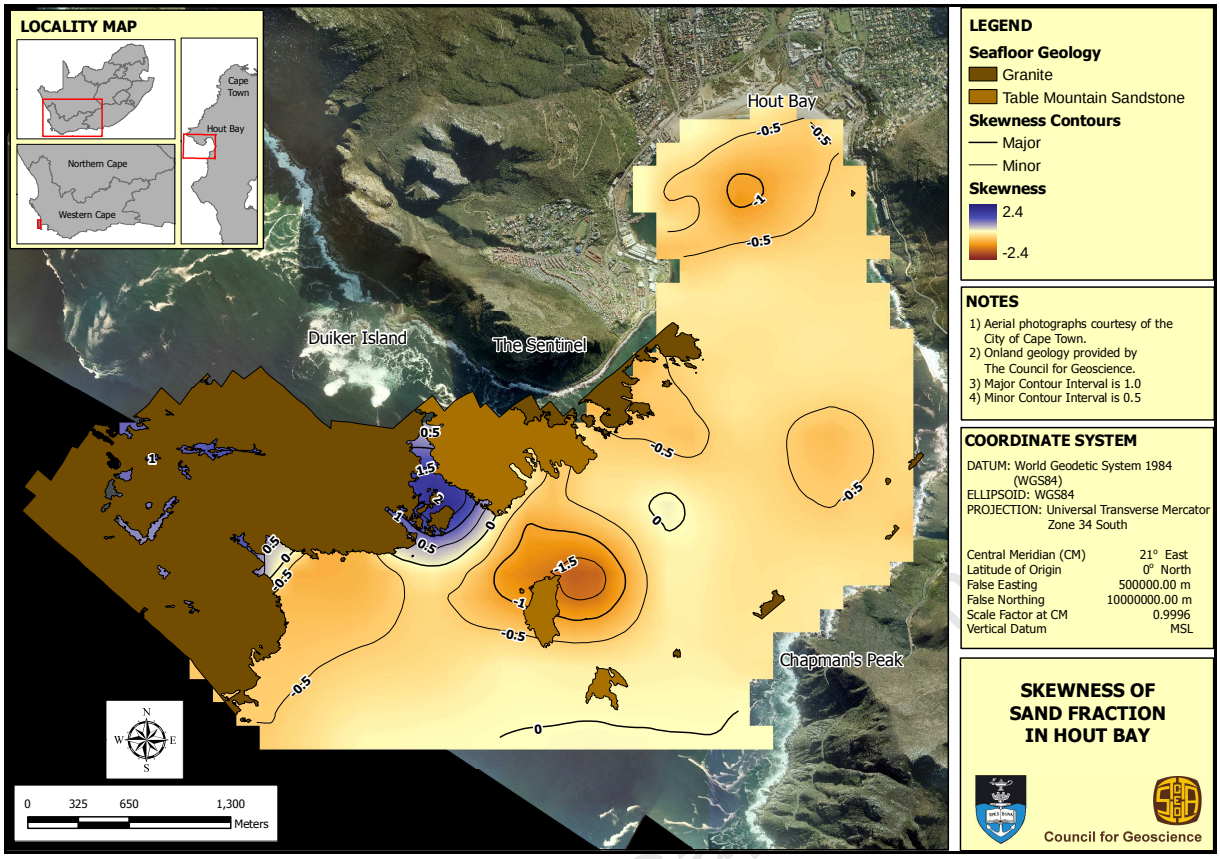

Figure 9.11. Skewness of the sediment in Hout Bay.

9.2.2. Composition

The carbonate content of the sediment samples within the study area reinforces the trends displayed by all of the other physical properties analysed. Around and on the reef outcrops the sediment is comprised almost entirely of calcium carbonate in the form of shell and cirripede fragments (Figure 9.12 & Figure 6.17 (D8)). These carbonate concentrations decrease away from the rock outcrops into the bay along approximately a southwest – northeast orientation. When the extent of the bioclastic gravel is compared to the relative carbonate concentrations it displays similar trends delineated by the sediment samples taken with the largest carbonate accumulation in the middle of the study area, elongating in the direction of Constatiaberg. A relative accumulation of calcium carbonate occurs around the littoral zone associated with Hout Bay Beach. This is as a result of fine- and very fine grained particles of calcium carbonate having a lower specific gravity to that of the quartzose sand and therefore being preferentially transported by wave or wind induced currents within a decreasing energy regime.

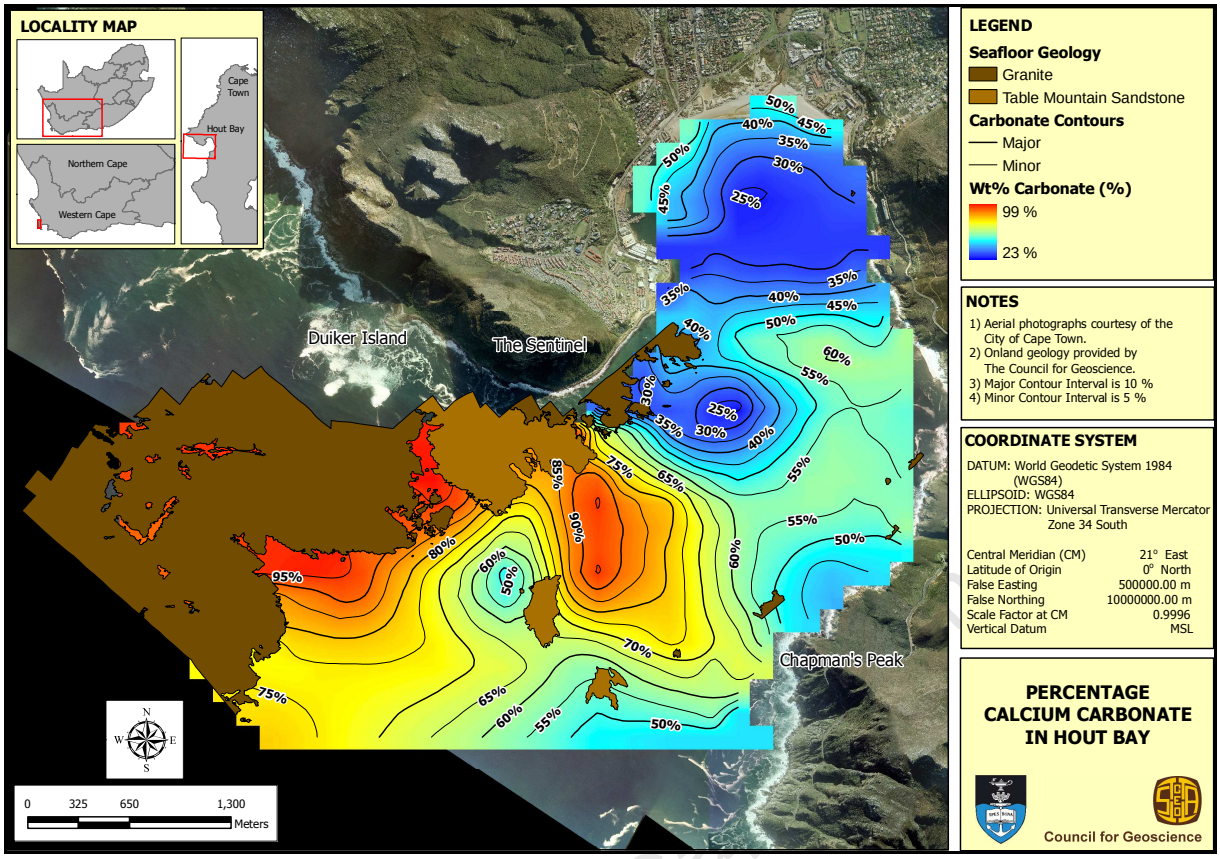

Figure 9.12. Percentage calcium carbonate ($CaCO_3$) in study area.

9.3. Discussion

Comparison of the grain size distributions shows a trend associated with the direction of sedimentation within the bay. The overall axis of sedimentation trends approximately southwest – northeast. This orientation would agree with the dominant incident vector for the wave regime associated with the Atlantic Seaboard of the Cape Peninsula being from the southwest (Rossouw, 1984). The second dominant orientation of sedimentation is approximately perpendicular to the first. A possible mechanism for this trend is the reflection of the incident wave energy against the Sentinel and Chapman's Peak. Other prevailing vectors that could contribute to the observed orientation are the dominant summer and winter wind directions.

The overall direction of sediment transport is from south to north governed by the direction of longshore drift. When the northward directed longshore drift vector encounters the prominent offshore reef complex adjacent to the Sentinel and Karbonkelberg it is forced to bifurcate into Hout Bay and offshore of the Sentinel which in effect causes it to be collinear

with the dominant incident wave vector. When the sediment encounters the prominent bathymetric high of the Vulcan Rock – Tafelberg Reef complex and the sub-marine toe of the Sentinel a large biogenic component is introduced into the system. This is clearly demonstrated by the high calcium carbonate and gravel sized component of the numerous sediment gullies of these outcrops and the halo like appearance around the outcrops of the aforementioned physical properties. The reason for the increase in biogenic carbonate is as a result of the combination of rocky substrate covered in carbonate producing organisms being frequently subjected to the high wave energy regime associated with Hout Bay. The wave energy breaks up the shell fragments to generate abundant shelly gravel (observed) and coarse sand factions. These reef outcrops can be viewed as "carbonate factories". The introduction of this biogenic sediment has the effect of resetting the sediment conveyor. The areas around the reef can therefore be viewed as proximal to the sediment source and those more inshore of the bay as distal. All physical properties of the sediment both analysed and calculated support this observation.

The relative percentages of the various grain size fractions shows sedimentation to be from the southwest, manifested by the dominant incident wave vectors associated with Hout Bay. The sediment fines towards the northeastern margin of Hout Bay which would agree with the declining energy spectrum of an incident wave and the loss of ability to transport large grain sizes. This trend is further supported by the accumulation of fine- to very fine grained sediment in the lowest energy environments within the study area (such as on the protected seaward side of Hout Bay Harbour and the foot of Constantiaberg). The trend of sedimentation displayed by the data is that proximally (near the sediment source) the mean grain size trends towards more coarse and gravelly sediment, whereas distally fine- to very fine grained sediment dominates. Where deviations from this trend are observed is along the littoral zone of the eastern quadrant of Hout Bay beach and a small circular outlier in the mean grain size distribution to the southeast of the Table Mountain Sandstone outcrop of the sub-marine toe of the Sentinel. The littoral zone can be explained by the reworking of the beach deposits by waves breaking onto the beach and the circular outlier as a result of the discharge associated with sub-marine outfall. This discharge causes the finer grained sediments to become re-suspended in the water column and for the coarser gained sediments to become concentrated in the depression associated with the termination point of the outfall.

The sorting data calculated from the sediment grain size distribution supports the overall axis of sedimentation to be from the southwest towards the northeast. Moderately- to moderately well sorted sediment is encountered on the northeastern side of the reef outcrops grading into well sorted and ultimately very well sorted sediment. The skewness data confirms this trend with proximal areas showing positively skewed values which indicate a large fine tail and relatively higher concentrations of coarse grains to the sediment distribution and conversely the distal areas exhibit negatively skewed values indicating a large coarse tail and relatively higher concentrations of fine grains.

The sediment within the study area is imprinted with two different sediment transport regimes. The most dominant of these is a marine regime which is governed by longshore drift and the direction of the dominant incident waves effecting Hout Bay. The fining of the sediment from southwest to northeast is evidence of this and the relative damming (accumulation) of fines along Constantiaberg and in the lower energy environment just to the north of Chapman's Peak viewpoint. Ultimately however these fines are transported to Hout Bay Beach where a portion is entrained into the headland bypass corridor by the prevailing southeasterly winds. One of the ways very fine sand and mud size sediment is introduced into the study area is through the weathering and erosion of the granite which make up the base of Chapman's Peak. The feldspar within these granites has weathered and altered into kaolinite which is easily eroded out of the granite into the bay below. The other sedimentary regime present is an aeolian system derived from Noordhoek Beach. The fines encountered in the deeper parts of the study area appear to dam up against Tafelberg Reef which in keeping with the mechanism of fines accumulating distally to the sediment source would imply the source to be from the southeast (Noordhoek Beach). Once the fines associated with the marine regime accumulate along Hout Bay Beach a small portion will once again be entrained by the strong southeasterly winds that are prevalent along the Cape Peninsula in summer into the headland bypass corridor between Hout Bay and Sandy Bay.

10. SEDIMENT DYNAMICS

10.1. Introduction

Sediment dynamics and the "sediment conveyor" system for any coastal system are crucial to understand, as this has far reaching implications for nourishment and replenishment of beach and dune systems. The system is dominated by the hydrological action of waves and currents and the dynamic interplay between this system and the prevailing wind. If any of the elements within this complex system are altered such as the stabilisation of the foredune with alien dune vegetation it can have far reaching implications for beach erosion both locally or further along the sediment conveyor.

10.2. Hydrodynamics

Most of the data reviewed for the hydrological setting of the study area was relatively dated (circa 1975 – 1984). These data, although not immediately current, describe a system in which changes are relatively slow to manifest, therefore the data described were considered more than adequate for a present day proxy. Although there are a variety of aspects within a typical wave spectrum, for the purpose of this study the most descriptive parameters of wave dynamics are wave height, wave period, wave direction and the wave energy density spectrum. Each of these aspects has been well documented and analysed by Rossouw (1984). There are different descriptive types of wave height, for this study the characteristic wave height H_{mo} is used and is calculated as $H_{mo} = 4.mo^{½}$, where mo is the area under the energy spectrum (Rossouw, 1984). The wave period parameter T_p is defined as the period of the highest wave amplitude, or the wave period at maximum energy (Rossouw, 1984; De Decker, 1987). Rossouw (1984) used a variety of data obtained from different sources namely, wave rider buoys (distributed in an array around the coastline of South Africa), radar and clinometer data (shore-based observations) and voluntary observation ships (VOS) data. Of the aforementioned data types Rossouw (1984) believes the wave rider data to be the most accurate as the others all involve human based measurements.

10.2.1. Wave Height

For the wave height description, only data from a wave rider buoy deployed off Slangkop Point at Kommetjie by the CSIR for the period of October 1978 – February 1981 (Rossouw, 1984) are utilised. These data have a population of 2,318 records spanning 581 days. The location of the buoy was approximately 14 km offshore in a water depth of 170 m (Figure 10.1).

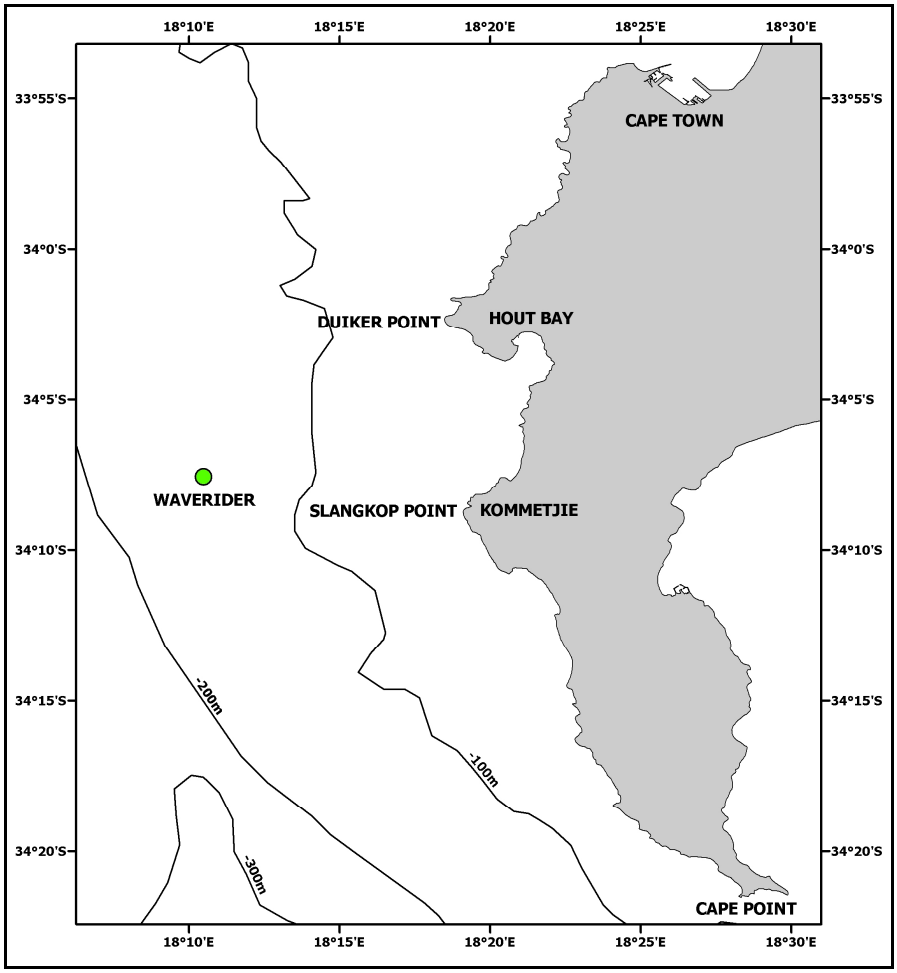

Figure 10.1. Location of Slangkop Waverider buoy, modified from Rossouw (1984). Bathymetric contours from Dingle *et al.* (1987).

From all the recorder data Rossouw (1984) was able to characterise the percentage exceedence of discrete wave heights for the various seasons, autumn (March, April, May), winter (June, July, August), summer (December, January, February) and spring (September, October, November). The recorded data show that the largest wave (8.5 m) occurred during summer, but this result is slightly biased to one large storm that occurred during the summer months. In general consistently larger waves are experienced during winter (Rossouw,

1984). These data, along with similar data analysed by Rossouw (1984) from the western and eastern coastlines of South Africa, show that the Cape Peninsula on average experiences the largest coastal waves in South Africa (MacHutchon, 2008).

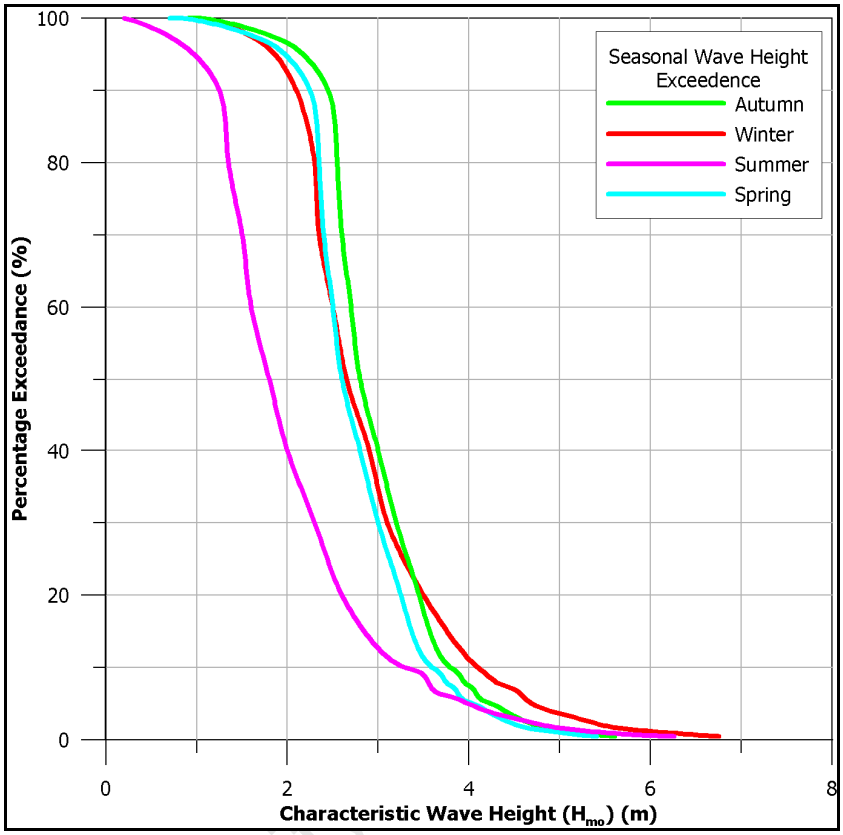

Figure 10.2. Seasonal variation in characteristic wave height for Slangkop, modified from Rossouw (1984).

10.2.2. Wave Period

The calculated wave period for Slangkop Point (Rossouw, 1984) is shown in Figure 10.3. Data for Koeberg have been included to help illustrate that over all of the recording stations the wave period throughout South Africa remains fairly uniform, with the mean period for all the waves being between 11 – 13 s (Rossouw, 1984).

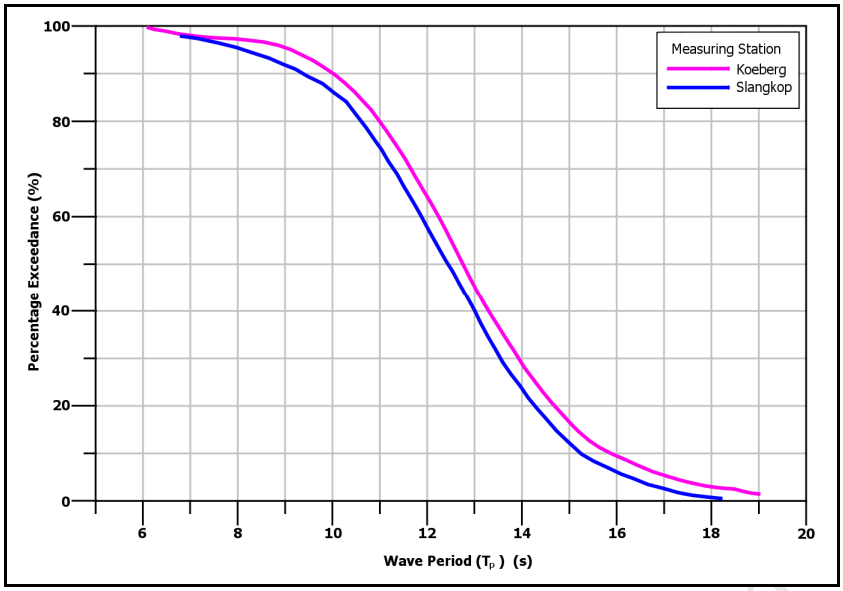

Figure 10.3. Calculated wave periods for Slangkop and Koeberg recording stations, after Rossouw (1984).

10.2.3. Wave Direction

The majority of the wave vector data for the South African coastline have been compiled from a combination of Clinometer, VOS, Radar and direction of swell orthogonals (DOSO) data. A clinometer is a telescope with a graduated lens which is mounted at a fairly high vantage point on the shore (Rossouw, 1984). The DOSO was developed to record the sense of direction of orbital wave motion. It is normally moored in the seafloor (Rossouw, 1984). Retief (1974) has provided a more detailed description of the recording device. Wave direction data collected by the CSIR at Koeberg show that for 88% of the time the dominant wave vectors fall between the southwest and west-southwest direction (Rossouw, 1984). If these data are to be analysed by season Rossouw (1984) shows that during summer 55% of the waves come from the southwest and that during winter the occurrence of westerly waves increases from 5% to 12%. Analysis of the other stations recording wave direction around the southern and southwestern Cape show a similar trend to that of Koeberg (Rossow, 1984) (Figure 10.4). The lack of easterly waves for Koeberg, Saldanha and the study area is primarily due to shielding from the coastal landmass.

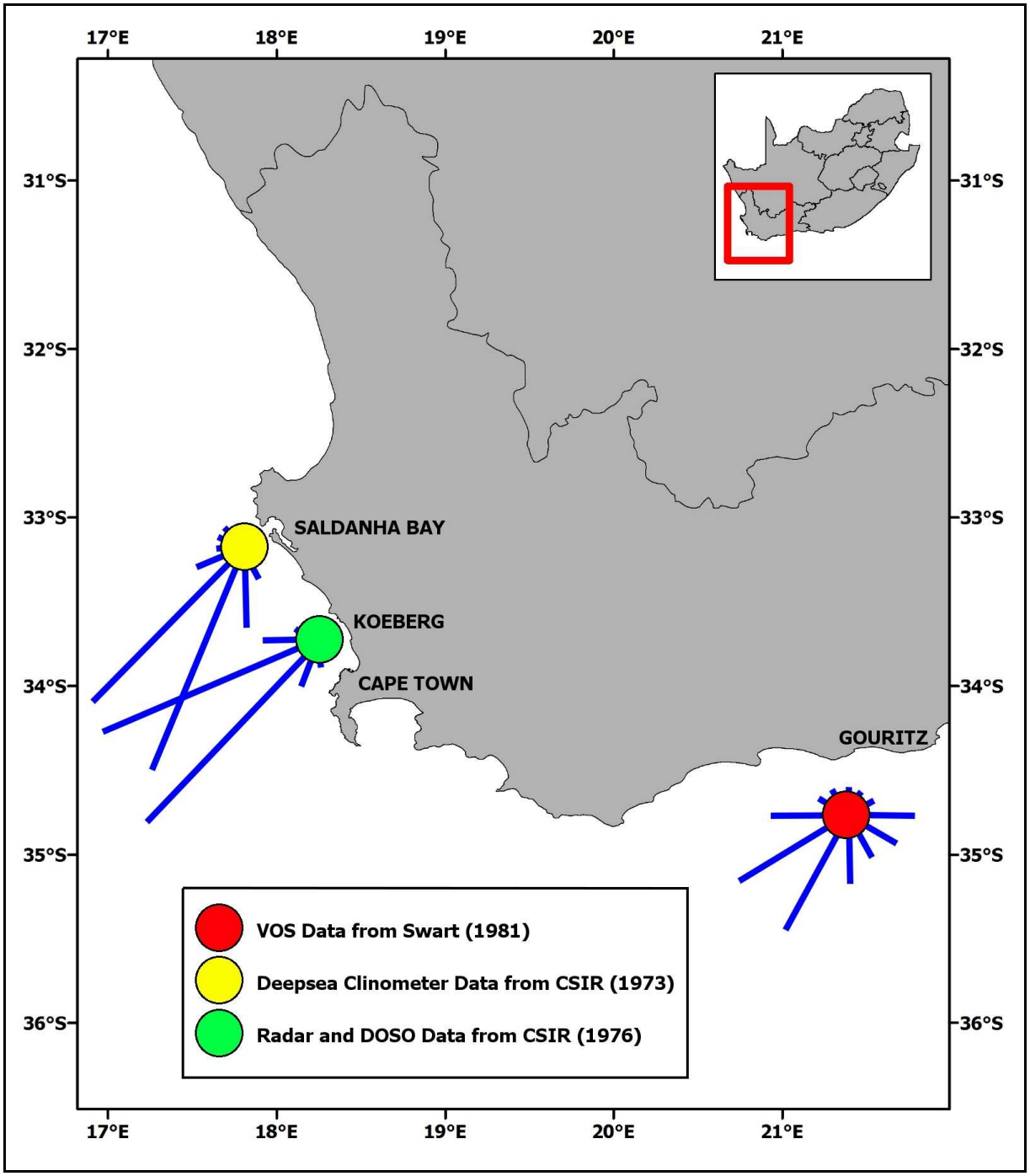

Figure 10.4. Wave vectors for the Southern and South Western Cape from Rossouw (1984).

10.2.4. Wave Energy Spectrum

Rossouw (1984) used 4,412 data points to plot the average energy density spectra for wave height groups (in half metre intervals from 0 – 8 m) for Slangkop. These data were calculated at varying frequencies which the author has converted to wave period by applying the inverse of the frequency. Only selected wave height groups have been represented in

Figure 10.5, though the trend is the same as the full spectrum density shown by Rossouw (1984). Rossouw (1984) concluded that the higher energy levels occurred in wave periods ranging from 10 – 18 s. Rossouw (1984) further goes on to state that the highest energy level that is exceeded for 1% of the time occurs between 10 – 16 s.

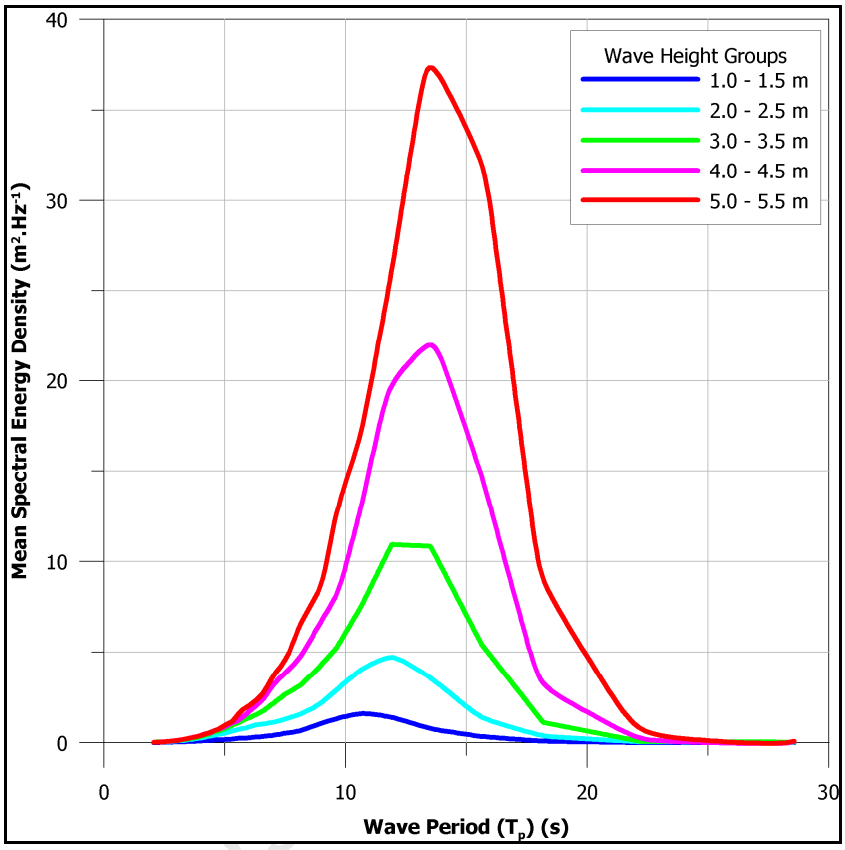

Figure 10.5. Mean wave energy density spectrum for selected wave height groups for Slangkop, modified from Rossouw, (1984).

10.3. Wind Regime

In summer strong southeasterly winds buffet the Cape Peninsula, whereas in winter the pattern is reversed with gale force northwesterly winds common (Figure 2.1). The strong winter winds have higher wind speeds but a lower seasonal frequency than summer winds (Holmes and Luger, 1996).

10.4. Sediment Transport Mechanisms

For any sediment conveyor system there will be a dynamic balance between what volume of sediment is transported as bedload or as suspended fraction, respectively. Within the marine system the dominant factors that will influence suspended load are the wave and bottom current regime (De Decker, 1987), versus the terrigenous and biogenic input. The input determines the degree of sorting of the resultant sediment and therefore to a large extent determines what volume of the sediment is available for suspension and what volume will form part of the bedload. The distribution of the different fractions within the marine system is then controlled by the interplay between bottom and surface currents and local wave conditions. These factors are predominantly controlled by the prevailing wind which controls wave direction and surface currents (MacHutchon, 2008). Storms in the South Atlantic Ocean affect the depth of storm wave base. To accurately assess how often the prevailing weather conditions allow active transportation of sediment one needs to ascertain what wave conditions will produce favourable threshold velocities to facilitate transport (De Decker, 1987).

10.4.1. Horizontal Orbital Velocity

There is no unique equation to accurately describe dynamic ocean wave incidence (De Decker, 1987). The most simple and straight forward model proposed is that waves can be described by a simple sinusoidal curve and is referred to as the linear wave theory (De Decker, 1987). As the wave propagates across the surface of the ocean the water molecules travel in an orbital path. These orbits attenuate in intensity with increasing depth. If one can determine the orbital velocity of the water molecules close to the seafloor, accurate comments can be delivered on the potential to transport sediment.

The horizontal orbital velocity (U_d) is calculated using the following equation (Komar and Miller, 1975):

$$U_d = \frac{\pi H}{T \sinh\left(\frac{2\pi d}{L}\right)} \quad \text{.....(10.1)}$$

Where H = wave height T = wave period
d = water depth L = wavelength

L is determined from equation 10.2:

$$L=(\frac{g}{2\pi})T^2\tanh(\frac{2\pi d}{L}) \quad \text{.....(10.2)}$$

which can be simplified to:

$$L=T\sqrt{g\,d} \quad \text{.....(10.3)}$$

where g is the acceleration due to gravity

The threshold for sediment movement is calculated from equations 10.4 and 10.5 (Komar and Miller, 1975):

$$\frac{\rho U_d^{\,2}}{(\rho_s-\rho)gD}=0.46\pi(\frac{d_0}{D})^{\frac{1}{4}} \quad \text{for D > 0.5 mm .....(10.4)}$$

$$=0.21(\frac{d_0}{D})^{\frac{1}{2}} \quad \text{for D < 0.5 mm .....(10.5)}$$

$$d_0=\frac{U_d T}{\pi} \quad \text{.....(10.6)}$$

Where

ρ = the density of seawater

ρ_s = the density of the sediment

D = is the diameter of the grain size

d_0 = is the orbital diameter of wave motion

From the wave data from Rossouw (1984) (Figure 10.2 & Figure 10.3) the median (50% exceedance) significant wave height for the study area is 1.8 m in summer and 2.7 m in winter. Because the wave period data of Rossouw (1984) are not seasonal, a median value of 12.5 s will be used for both of the dominant seasonal significant wave heights. Using equations (10.1) and (10.3) the orbital velocities at varying depths within the study area have been calculated and the results summarised in Table 10.1.

Table 10.1. Horizontal Orbital Velocities for 50% Exceedance Wave Conditions

H_{mo} (m)	T_p (s)	U_d at different depths (cm/s)				
		10 m	20 m	30 m	40 m	50 m
1.8	12.5	174	84	53	37	27
2.7	12.5	261	126	80	56	41

Using equations (10.4), (10.5) and (10.6) Komar and Miller (1975) produced a series of curves for varying wave periods from which the threshold orbital velocity could be calculated for varying grain sizes (De Decker, 1987) (Figure 10.6). The curves were derived for sediment with a density of 2.65 g.cm^3 (quartz sand).

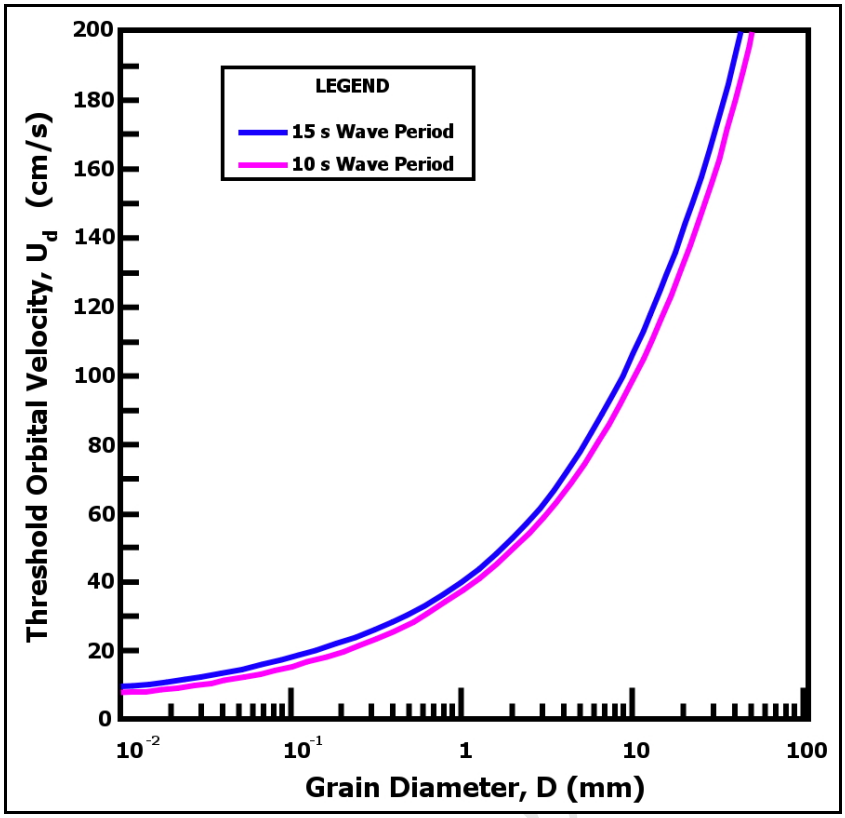

Figure 10.6. Orbital velocity under waves for threshold of sediment motion, modified from Komar and Miller (1975).

Applying the values from Table 10.1 to Figure 10.6 it is evident that during summer the fraction of transportable grain size ranges from medium grained sand (0.35 mm) at 50 m BSL to gravel sized sediment (35 mm) at 10 m BSL. In winter the wave energy is increased which allows the gravel sized sediment to be transported from depths of up to 50 m BSL.

These data describe sediment transport conditions for the median wave height and periods that affect the study area. One could therefore conclude that during storm events the area would be subjected to very intense sediment transport. It must however be taken into consideration that such events are short lived and no cumulative, lasting effects will remain as the milder prevailing conditions will continuously alter any sediment accumulations (De Decker, 1987).

Within the aeolian transport system much the same rules apply with the one exception that the horizontal velocities experienced are a few orders of magnitude higher. During the frequent gales experienced by the Cape Peninsula almost all of the fine- to medium grained unconsolidated sand can be transported as suspended load.

10.5. Results

The results for each of the geophysical surveys have been thoroughly discussed in each chapter. Selected aspects of each will be highlighted in this section with new data (in the form of beach profiling) used to help quantify sediment movement within Hout Bay.

10.5.1. Geophysical Survey Results

From the bathymetric results and the cross sections drawn (Figure 5.5 C, D) it is clear that the morphology of the eastern margin of Hout Bay is the result of a localised sediment wedge that has accumulated against the foot of Chapman's Peak. Seismic data from this study and previous regional seismic surveys (Birch *et al.*, 1991) confirm this accumulation of sediment. From the sidescan sonar data collected, the orientation of the wave ripple crests which define the sub-aqueous bedform fields were determined to be approximately 150º/330º. It is also from these data that the amplitude and profile of the bedforms was quantified. Bioclastic bedform fields form elongated sand ribbons in water depths of less than 15 m BSL.

10.5.2. Beach Profiling Data

Two beach profiling surveys were undertaken for Hout Bay Beach. The first completed in August 2010 is representative of a typical winter beach; the second completed at the end of January 2011 is representative of a typical summer beach. One of the dynamic sediment inputs into Hout Bay Beach is the Disa River. Based on field observations the river has a low discharge and tends to dam landward of the beach berm in summer. During winter however the river manages to breach the berm and discharge into the sea. From the data collected elevation surfaces of the beach at that particular time were developed. From these surfaces the beach profile morphology could be described and volumetric differences between successive surveys calculated, using the extended trapezoidal rule described by Press *et al.* (1988). For the August 2010 survey (Figure 10.7 A) the beach profile had a poorly developed berm towards the eastern side of the beach whereas towards the middle of the beach the berm was much more clearly developed with gradients of approximately 8º. During this survey the Disa River was approximately 3 m wide and meandering in the back

beach towards the centre of Hout Bay Beach. It opened up once past the berm to discharge into the ocean with a water depth of approximately 5 cm. Towards the western part of the beach the dunes were well developed (Figure 10.7 & Figure 10.8) with gradients in the order of 15º.

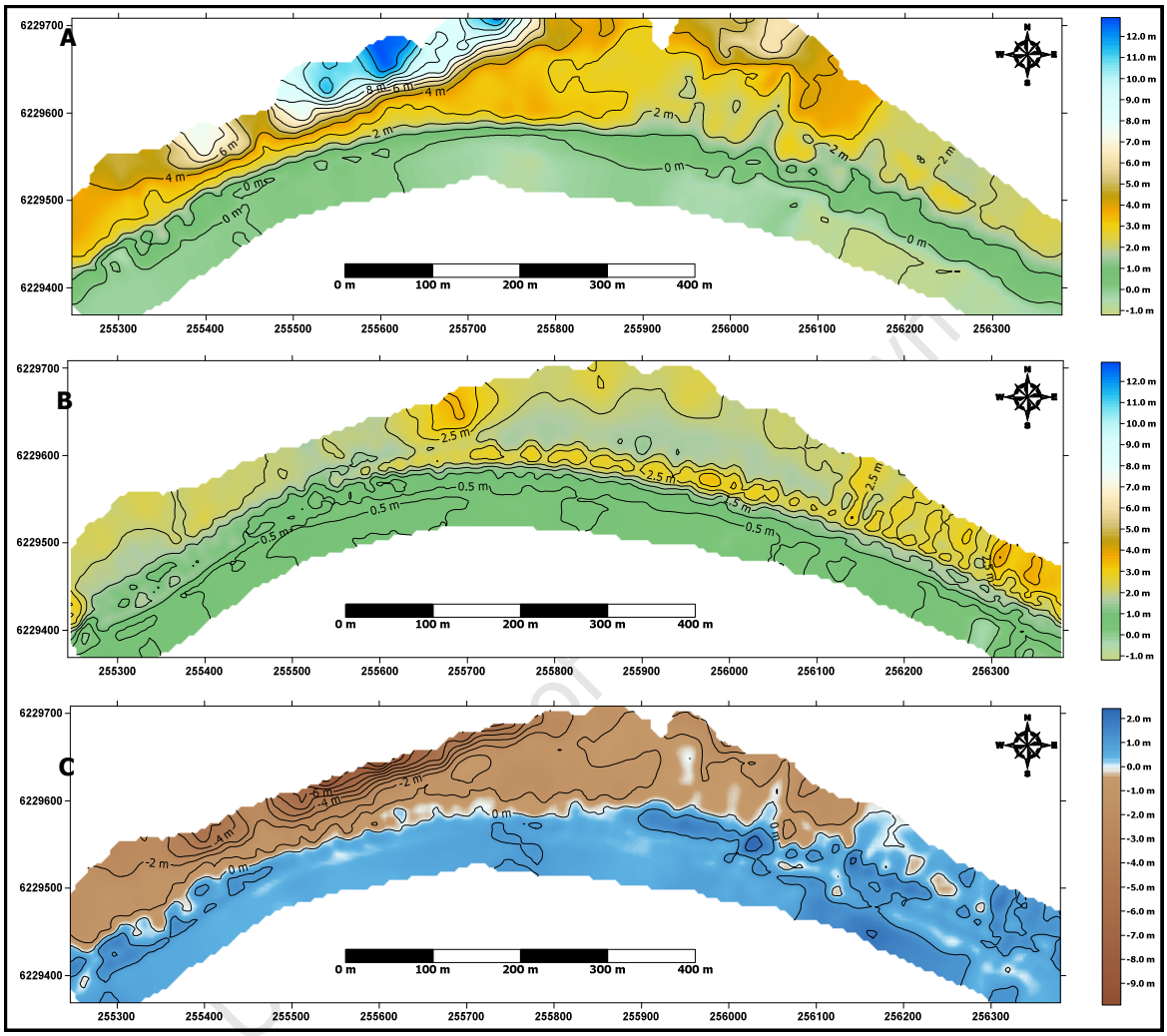

Figure 10.7. Elevation surfaces of Hout Bay Beach. (A) collected in August 2010, (B) in January (2011) and (C) is shows the changes between the two. All elevations have been reduced to Mean Sea Level (MSL).

By January 2011 there had been notable changes (Figure 10.7 B). In the eastern portion of the beach there had been an accumulation of sediment and a well developed berm. The berm continued laterally to the centre of the beach and now the Disa River had developed a back barrier lagoon, damming behind the berm into water depths of approximately 1 m. Towards the western portion of the beach the berm appears to bifurcate. The most marked difference from the previous survey was the denudation of approximately 0.137 x 10^6 m^3 of sediment from the back beach and foredune (Figure 10.7 & Figure 10.8) and the accretion of approximately 0.078 x 10^6 m^3 of sediment along the eastern portion of the beach.

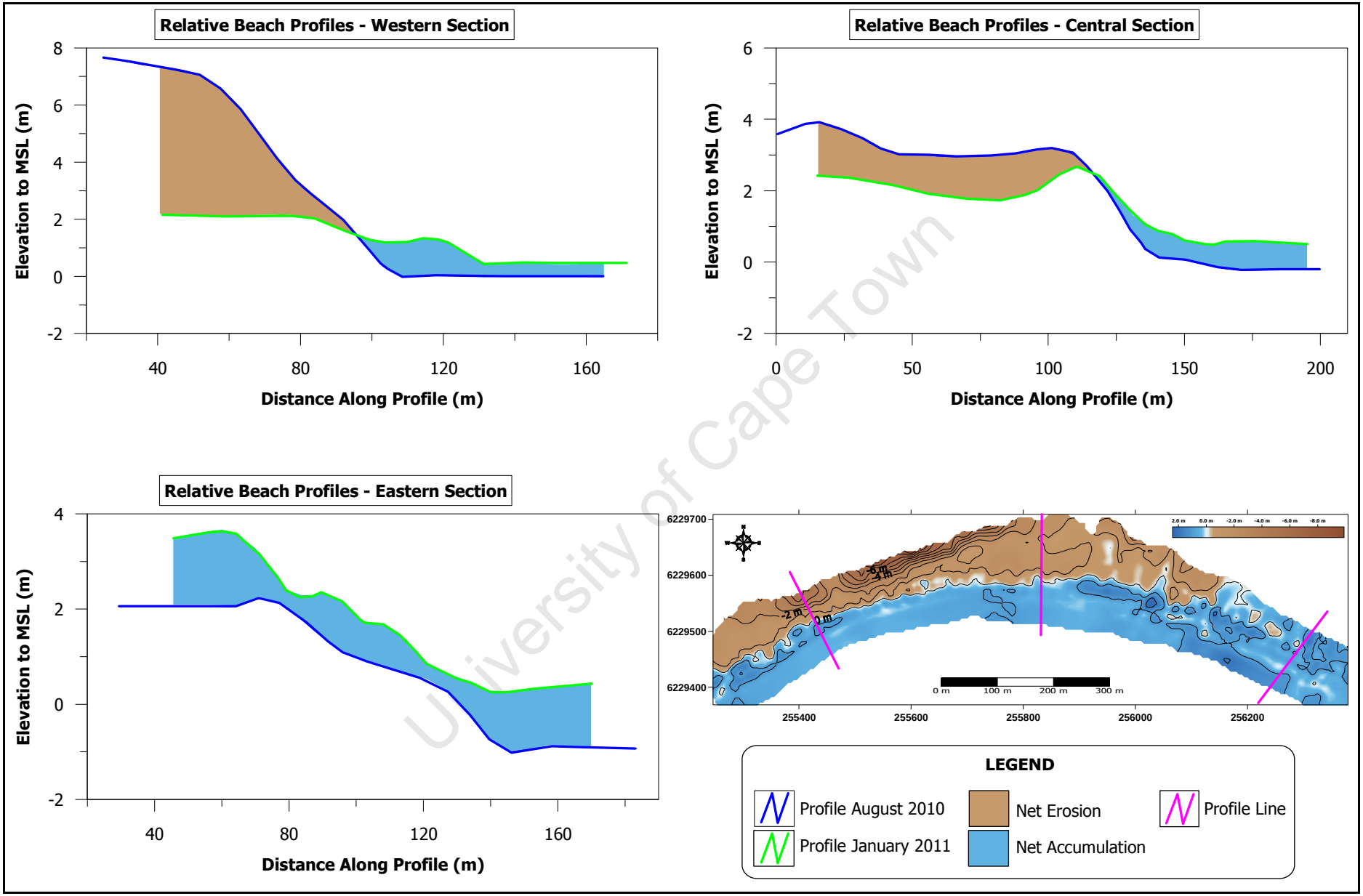

Figure 10.8. Cross sections along the western, eastern and central areas of Hout Bay Beach.

10.5.3. Historical Sand Bypass

From current and historical evidence a headland sand bypass system has existed between Hout Bay and Sandy Bay. This system is referred to as the Karbonkelberg dune field and serves as a clear indicator of the aeolian sediment transport vectors which affect the study area. The axis of the dune field trends southeast – northwest from Hout Bay to Sandy Bay between Karbonkelberg and Klein Leeukop. Historical images show just how extensive the sand corridor was. Images such as Figure 1 in Holmes and Luger (1996), which was taken in 1944, or an even earlier picture from circa 1930 (Figure 10.9) show this. Holmes and Luger (1996) have shown that since 1944 the aerial extent of the dune field has steadily decreased by firstly the introduction of alien plant species such as *Acacia* spp. in 1958, to the fragmentation of the corridor in 1977 as a result of increased residential development. Since 1989 an artificial stabilisation programme was implemented on the dunes of Hout Bay Beach by planting non-invasive alien Marram grass (*Ammophila arenaria*) to arrest sand movement landwards, (Holmes and Luger, 1996).

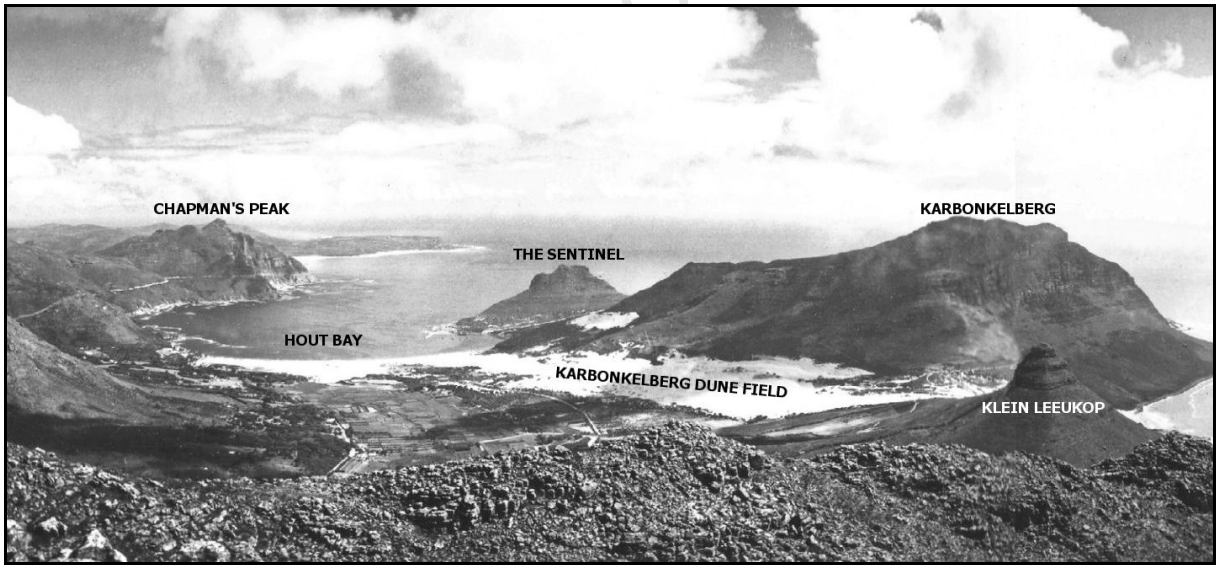

Figure 10.9. Picture of Karbonkelberg dune field from circa 1930 (Flikr, 2011).

Using data from Google Earth (2010) the decrease in areal extend of the sand corridor has been documented from 2001 – 2010. These data supplement that of Holmes and Luger (1996) which spans 1944 – 1991 supporting the sand winnowing trend (Figure 10.10). Since 1944 the areal extent of the dune field has decreased by approximately 1.46 km^2 (90%) from 1.61 km^2.

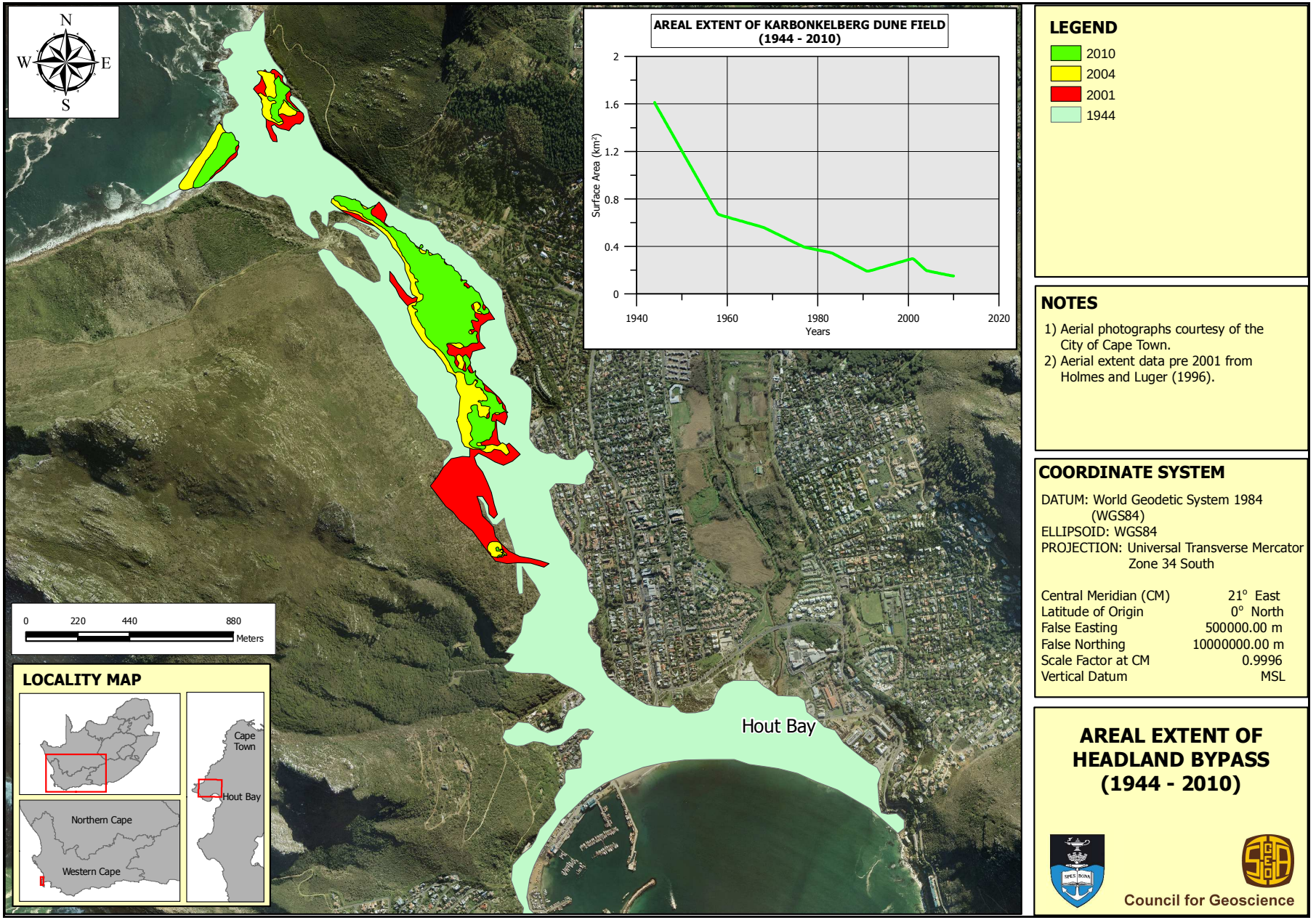

Figure 10.10. Decreasing trend in the aerial extent of the sediment bypass corridor between Hout Bay and Sandy Bay, between 1944 and 2010.

10.6. Discussion

There are a number of factors which control the sediment transport and dispersal for any given area (Flemming, 1981), including sediment supply, seafloor morphology, the wave and wind regime and bottom currents.

There are two types of sediment: terrigenous and biogenic. The terrigenous sediment in Hout Bay is derived from erosion of the lithologies around the study area through coastal processes such as wave action along the coastline, chemical weathering from rain and meteoric water or aeolian erosion of coastal dunes and beaches. Sediment input from rivers could contribute to this although for Hout Bay this influence would have diminished considerably since the construction of dam reservoirs and weirs along the Disa River. The biogenic sediment is derived from marine organisms living in the study area. Consideration should also be made for older Pleistocene sediments. It has been shown by Franceschini and Compton (2006) that sea-level lowstand beach sediment is reworked with rising sea-levels to form part of the modern beach system. Therefore Pleistocene deposits in the study area when sea-levels were lower could now form the core of the unconsolidated sediment seen in Hout Bay.

Birch *et al.* (1991) estimated fluvial discharge and biogenic volumes of Quaternary sediments on the West Coast of South Africa, and grouped the region into three geographic areas. For the Cape Columbine to Hout Bay area Birch *et al.* (1991) reported annual fluvial discharge figures of approximately 0.3×10^6 m^3 (Midgley and Pitman, 1969) and biogenic and terrigenous sediment volume accumulations on the adjacent continental shelf of $2{,}715 \times 10^6$ and $8{,}148 \times 10^6$ m^3, respectively. Birch *et al.* (1991) do not report fluvial discharge figures for the Disa River, figures are however provided for the Riet River (Midgley and Pitman, 1969) which the author is of the opinion represents the present day Diep River. Runoff figures have been reported by the River Health Program (2003) for the Department of Water Affairs and Forestry to be 10.4×10^6 m^3 and 87×10^6 m^3 for the Disa and Diep Rivers, respectively. Milliman and Syvitski (1992) have shown that there is a linear relationship between surface runoff and fluvial discharge. It is therefore assumed by the author that the ratio between runoff figures for the two rivers can be used to calculate the fluvial discharge of the Disa River as both drain similar regional geology. The ratio between the different runoffs of the Disa and Diep Rivers is 12 % therefore the fluvial discharge of the Disa River

has been estimated at 0.024 x 10^6 m^3 which is 12% of the 0.2 x 10^6 m^3 Diep River discharge figures reported by Midgley and Pitman (1969). The dominant mechanism for introducing sediment into Hout Bay is from longshore drift. As longshore drift moves from south to north sediment is continually added to the sediment conveyor by wind blown sand from unconsolidated sediment along the coastline. Standing on Noordhoek beach during a typical summer southeasterly wind, the sediment blown into the sea can easily be observed. This amount however is a small percentage of the total volume of sand which constitutes Noordhoek Beach. Data which support the volumes of sediment transported by the southeasterly wind can be found from the sand bypass corridor which is situated between Hout Bay and Sandy Bay (Figure 10.9 & Figure 10.10). Although the amount of sand within the corridor has decreased by 90% since 1944, this is the result of the introduction of alien dune vegetation and residential expansion (Holmes and Luger, 1996) and the active removal of any sediment not incorporated into the artificially stabilised Hout Bay Beach dunes by the City of Cape Town (observed during a beach profiling survey). This does not negate the fact that the corridor serves as evidence that sand is actively being transported by wind in a southeast to northwest direction along the Cape Peninsula.

The seafloor morphology has a large effect on the sediment movement (Compton and Wiltshire, 2009). The seafloor of Hout Bay and surrounds is characterised by the rugged and irregular Cambrian to Ordovician basement with sediment accumulating in relative basement depressions. This morphology influences the shape of the coastline resulting in Hout Bay being a southward facing embayment. When the longshore drift vector reaches the prominent offshore Vulcan Rock – Tafelberg Reef complex it is forced to bifurcate and a portion of the sediment entrained by it moves into Hout Bay. The bifurcated vector goes into Hout Bay ultimately leaving the bay to merge with the main longshore drift component to the west of the offshore reef complex.

The wind and wave regimes have been clearly defined for the study area in Chapters 10.2 & 10.3. From these data it is clear that the dominant incident wave direction is from the southwest and the dominant wind direction is from the south and southeast. A wave direction from the southwest would result in longshore drift towards the north. Sediment could be blown directly into Hout Bay from Noordhoek, Scarborough and Sun Valley or could derive from wind blown sediment further south along the peninsula which is later entrained by the northward longshore drift to be temporarily deposited in the south facing Hout Bay. It has been shown that horizontal orbital velocities on the seafloor are capable of

transporting up to gravel sized fractions of sediment with storm events having a large potential to transport sediment. The study area falls within a wave dominated environment (Flemming, 1978) and it has been shown that in these shallow depths the wave regime for Hout Bay is more than able to suspend and transport the sediment. During the Holocene highstand when sea-level was approximately 3 m higher than present (Compton, 2001), unconsolidated sand from the base of the headland bypass and Noordhoek would have been added to the sediment accumulation in Hout Bay. Conversely during sea-level lowstands like those experienced during the Pleistocene, the beaches of Hout Bay and Noordhoek would have prograded into the study area which when sea-levels rose would have formed a large majority of the sediment seen in the study area. The volume of sand that moves through the southward facing Hout Bay is not clear but approximations can be offered from the beach profiling data which have revealed that in a six month period up to 2 m of fine- to medium grained marine sand accumulated along the eastern and littoral zones of the beach when during the same time up to 6 m of sediment was eroded from the western backbeach/foredune area of the beach (Figure 10.8). Volumetrically this equates to approximately 0.078 x 10^6 m^3 accumulated and 0.137 x 10^6 m^3 eroded. These figures do not represent net volumes of sediment transported as they do not span a long enough time period. It has been shown by Holmes and Luger (1996) that there exists a potential net movement of sand of 55 m^3/m/year from Hout Bay to Sandy Bay.

With respect to bottom currents, there does not appear to be any evidence in the data to support prolonged bottom current activity. The dominant Benguela current that effects the western margin of South Africa is constrained by the continental shelf and does not appear to have influence as close to shore as the study area. There is however evidence of wave induced bottom currents which are short lived, only active when the seas are rough. The profiles of the ripples formed in the bioclastic bedform fields are symmetrical therefore they formed as the result of wave action and not prolonged bottom currents. The wavelength and amplitude of the bedforms decreases marginally as one moves from deep to shallow water in the study area with the decrease in swell energy. An indicator for wave induced bottom currents are the scour moats on the northern sides of the shipwrecks in the study area and the sand ribbons which form on the leeward cusp of the bioclastic bedform fields in water depths of less than 15 m BSL. These ribbons elongate in the direction of the wave action and show that the dominant wave direction in Hout Bay has a bimodal distribution. There is the dominant southwesterly wave direction and then a wave direction which appears to propagate more from the south which is predominantly as a result of

southwesterly swells being refracted around the foot of the Sentinel (Figure 2.4). As the waves move into the bay friction slows them down and the significant wave height, energy spectrum and bottom orbital velocities decrease rapidly which accounts for the fine- to medium grained accumulation of sediment along Hout Bay Beach. Only a small portion of the accumulated sand is funnelled off by the wind into the headland bypass, the rest will move with longshore drift first out of the bay and then northwards. It has been shown that Hout Bay falls within a microtidal range and that the tidal curve for the study area exhibits asymmetry (Figure 5.1). A result of this asymmetry is that higher flood tide velocities are experienced than during ebb tides which results in increased suspended sediment during the flood tide and favours sedimentation at high slack tide (Brenon and Le Hir, 1999). These effects are localised along the low energy shoreline along the northern margin of the study area and is referred to as tidal pumping (Uncles *et al.*, 1984). Tidal pumping is proposed as a possible mechanism to help move sediment along the western edge of the study area towards the Sentinel where it is re-introduced into the northward flowing longshore drift.

Historical offshore data collected by the Marine Geoscience Unit in the 1990s (Pers. Comm. Mike Woodborne, 2011) shows that there is an accumulation of fine- to medium grained marine sediment extending in a northwesterly direction from the foot of the Vulcan Rock – Tafelberg Reef complex (Figure 10.11). This distribution pattern supports the bifurcation of longshore drift. After considering all of the transport vectors a sediment transport vector chart for the study area has been derived which can be viewed as a proxy for the nearshore zones along the Cape Peninsula. The dominant incident wave vector (from the southwest) causes the northward flowing longshore drift. This vector bifurcates in response to the prominent submarine toe of the Sentinel with fine- to medium grained sediment accumulating along the northern margin of Hout Bay. Some of this sediment is removed from the conveyor introduced into the headland bypass dunefield but the majority continues out of the bay on a northward migration. The amount of sediment entrained by longshore drift is added to from aeolian derived beach sediment to the south of the study area, yet a portion of this will be re-deposited onto the beaches by the incident wave vectors.

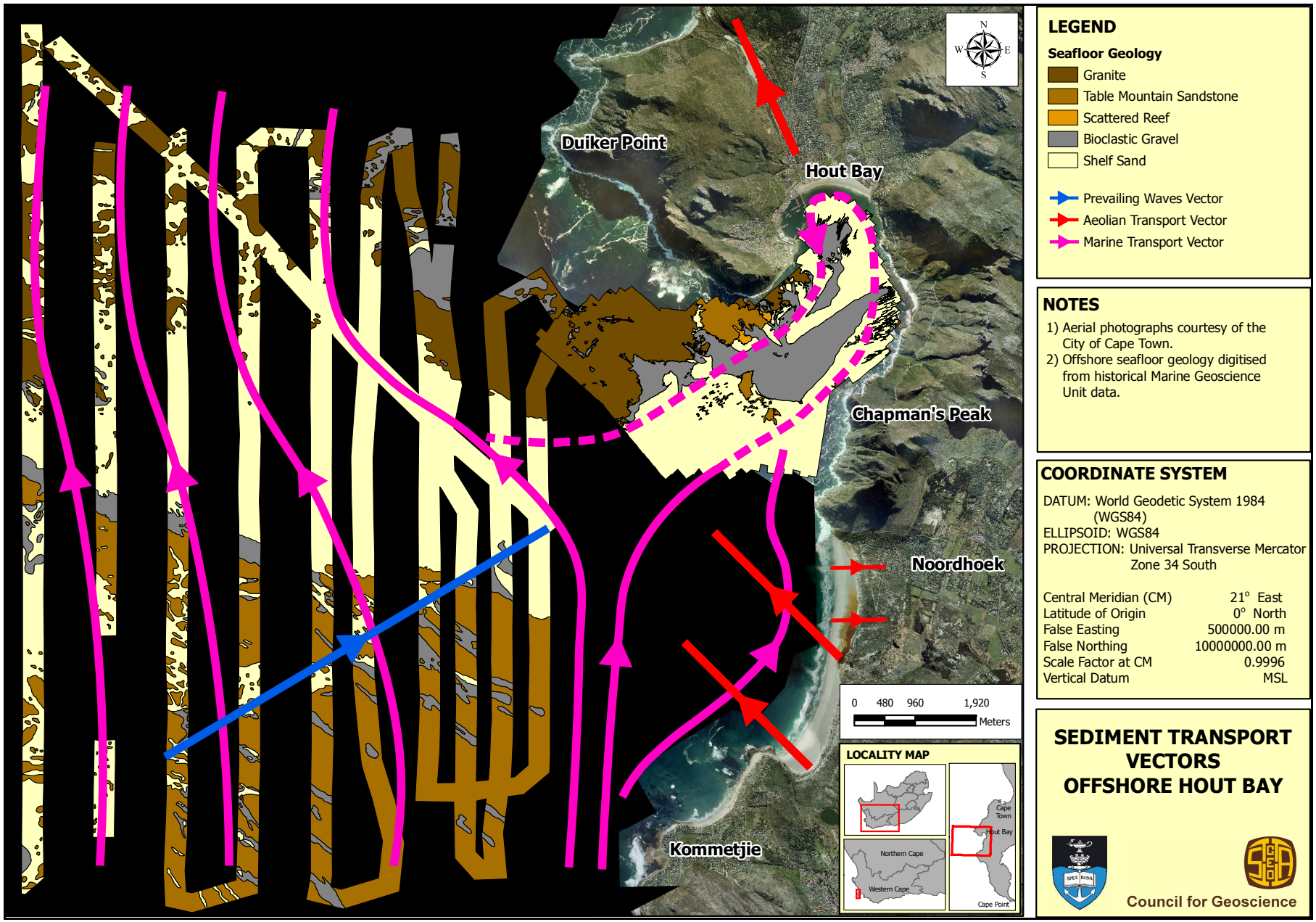

Figure 10.11. Proposed sediment transport vectors for study area.

11. SUMMARY & CONCLUSIONS

This study used the latest in geophysical technology to document the underwater geological environment of Hout Bay and aimed to better understand its geological evolution and by using these data to semi-quantitatively infer sediment dynamics along the Atlantic seaboard of the Cape Peninsula. Over 140 Gigabytes of high-resolution geophysical data were acquired and interpreted, 57 surface sediment grabs were collected to help ground truth the geophysical interpretations and multiple underwater SCUBA investigations were undertaken.

From the bathymetric data it is evident that the most noticeable feature of the study area is the difference in morphology between the eastern and western domains of Hout Bay. The western sector is characterised by rugged and relatively high relief outcrops of granite whereas the eastern is relatively smooth due to a sediment drape over the basement seaward of the rocky surf zone. The western margin exhibits two different lithological units, the first of which has been confirmed by underwater investigations to be granite displaying orthogonal joint sets and a definite underlying fabric as a result of these joints. The granite has been intruded by dykes that trend approximately 127 – 131º. The second consolidated unit shows bedding planes with a slight dip towards the west and has been correlated with Table Mountain Group sandstone. The eastern margin of Hout Bay owes its smooth nature to the accumulation of fine- to medium grained sand. The sediment appears to accumulate against the basement geology which forms the foot of Champan's Peak and Constantiaberg on its longshore path to the north. Longshore drift to the north is in response to the predominant southwest swell direction. The offshore reef complexes cause some of the sediment moving northward by longshore drift to bifurcate into the study area.

Interpretation of the sidescan sonar data revealed seven different acoustic facies. Of the seven, two pairs are related. These include the Prominent- and Sub-aerial Reef, which are both correlated to the same granite bedrock. The Subdued- and Scattered Reef facies are also lithologically related where the latter occurs when the proportion of reef outcrop is subordinate to the sediment veneer that covers it. The most dominant facies in the study area is the fine- to medium grained Shelf Sand facies with the remaining unconsolidated facies being Bioclastic Gravel.

The high-resolution geophysical data allowed measurements of the lineations and joint sets within each facies, all of which were ground truthed and confirmed by underwater SCUBA investigations. The Prominent Reef facies was confirmed to be outcrops of Cape Granite with joint sets trending 100º and 10º. The Subdued Reef facies is Table Mountain Group sandstone (TMG) which outcrops with bedding planes exhibiting a strike of 175º and a dip of 10º to the west. Within the Bioclastic Gravel facies are bedforms which were described after Flemming (1980) and Ashley (1990) as two dimensional, straight crested, small sub-aqueous wave ripples. The orientation of the ripple crests is predominately 150º yet inside the bay trend towards 177º. The reason for this change in orientation is postulated to be as a result of wave refraction taking place around the offshore extension of the Sentinel. There are notable anthropogenic features in the study area which include two shipwrecks, the breakwater armouring and the submarine outfalls pipeline. All of these features have associated erosional depressions.

The magnetic survey helped to quantify the various lineations seen in the granite outcrops. Six lineations were charted that have a general orientation of 127º and run across the whole bay. These lineations represent the submarine expression of the numerous Cretaceous dolerite dykes (Reid *et al.*, 1991) seen intruded into the granite and TMG outcrops on the Chapman's Peak side of the study area. Evidence that supports this is that they shared the same orientation and are all co-linear to the sub-aerial outcrops. Diver observations positively identified the intrusions (amongst the granite outcrops) as dolerite dykes. Samples of dolerite recovered from underwater show an alteration halo around the specimens from chemical alteration by seawater. An unexpected result of these intrusions is that one of them showed evidence of intruding during a magnetic polarity reversal i.e. it presented as a negative anomaly when all the others were positive anomalies. This implies a slightly younger age than the 130 ± 5 Ma normal polarity dykes (Reid *et al.*, 1991). This scenario is definitely plausible, as a very large dyke found less than 5 km to the northwest of the study area in Llandudno shows evidence of being intruded by a younger dyke with identical mineralogy (same magmatic source) to that of the parent dyke (Pers. Comm. Dave Reid, 2011).

Based on correlation between the geophysical data collected and the geological outcrops observed onland a geological map of Hout Bay was produced (Figure 1.1). The sub-bottom profiling data collected provide valuable insight into the geological history of the study area and the relative spatial relationships between the different lithological units.

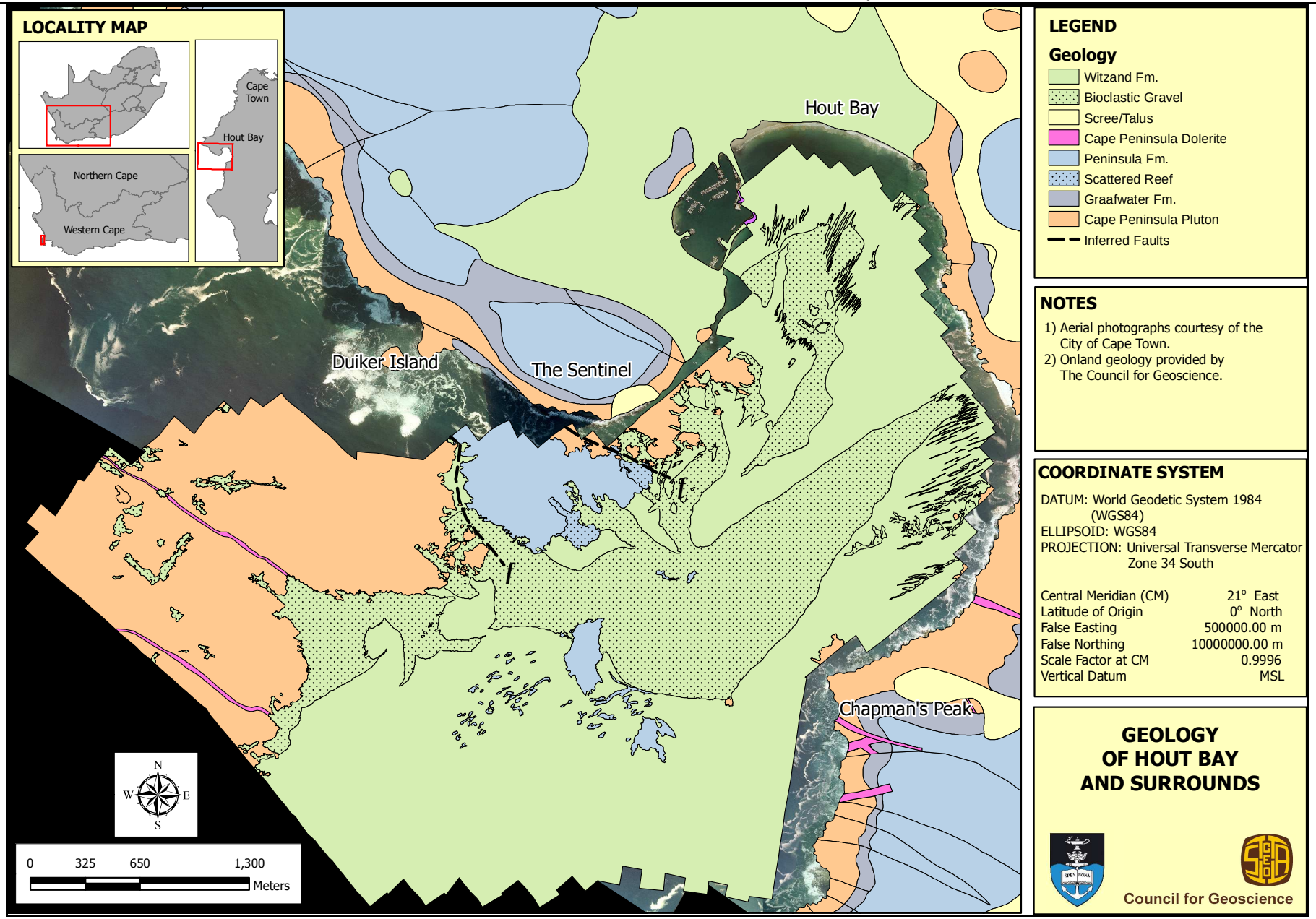

Figure 11.1. Geological map of Hout Bay and surrounds.

These data show that the basement of Hout Bay is composed of Cambrian Cape Granite. Regionally these granites have intruded the Proterozoic metasediments of the Malmesbury Group but no evidence of this exists in the study area or further out onto the inner continental shelf adjacent to Hout Bay. The granites are overlain by the Ordovician Table Mountain Group sandstones. A prominent non-conformity exists between the two groups and is exposed along the flanks of Chapman's Peak and the Sentinel. The basal Graafwater Formation was deposited in a distal fluvial braided plain whereas the overlying Peninsula Formation was deposited in a near coastal environment. The entire Cape Supergroup experienced regional deformation during the Cape Orogeny which culminated in the Jurassic. Evidence of this deformation can be seen in the broad open folds of Constantiaberg and Karbonkelberg. During the Cretaceous Gondwana broke up and South America separated from Africa. A series of faults which can be seen regionally and within the study area formed parallel to the direction of opening, striking northwest – southeast. Basaltic magma intruded along these zones of weakness to form the Cape Peninsula Dyke swarm. It is postulated that some time towards the end of the Cretaceous the floor of Hout Bay would have been downfaulted to the south with a throw in the order of hundreds of metres. During the Palaeogene there was extensive progradation of sediment out onto the continental shelf which during the Neogene was planed off as a result of uplift of the continental landmass and tilting towards the southwest. This re-activated the buoyant basement high of the Columbine/Agulhas Arch removing most of the sediment drape covering the feature.

The morphology of Hout Bay would have looked similar to present day during the Pleistocene with sea-level fluctuations becoming the dominant factor in the further evolution of the bay. Six glacial maxima have been identified during the period when sea-levels were rising and falling in response to water either being "locked up" in ice sheets or released when these sheets melted. Sea-levels fell to as much as 130 m below present day sea-level and rose as high as 10 m above. During lowstand periods the Disa River eroded into the basement lithologies of the study area in response to a more prominent gradient between the head of water feeding it and its base level (sea-level). During glacial periods the Hout Bay and Noordhoek beaches would have prograded out onto the inner shelf to the lowstand strandline. An embayment would have formed between the headlands of Kommetjie and Vulcan Rock – Tafelberg Reef complex. This embayment would have had a generalised east – west orientation bounded to the south by a ridge of TMG and fed from the north by the Disa River. During regressions previously stranded beaches would have been reworked including any low elevated dune deposits such as those found on the Cape Flats or base of

the Karbonkelberg dune field. Coupled with sea-level rise and fall is the formation of wave cut terraces associated with still-stand events. Two such terraces exist in Hout Bay, the first between 32 to 35 m below sea-level and the second 18 to 20 m below sea-level. Sea-levels were at these elevations on multiple occasions during the Pleistocene coinciding with a few relative low- and highstands when the erosive action of the waves would have had a longer period of time over which to carve out the terraces during these relative stillstands of sea-level. Towards the end of the Pleistocene and the onset of the Holocene there was a rapid rise in sea-level as a result of global deglaciation (Rogers, 1977; Compton, 2001). During this transgression the finer sediments were winnowed away leaving behind a coarse lag horizon to mark its position. On top of this transgressive surface the modern Holocene sediments have been deposited, prograding out onto the shelf during the mid-Holocene high of 2 – 3 m above present day sea-level. The hydrodynamics during the Holocene have been the same as those of today with the dominant wave direction from the southwest inducing a longshore drift vector from south to north. Accumulation and deposition of sediment from both fluvial and marine sources are the dominant geological processes taking place during the Holocene highstand. These processes were left undisturbed until the Anthropocene (the introduction of modern humans and how they have impacted on their environment). Up until 1944 there existed a natural sediment headland bypass corridor between Hout Bay and Sandy Bay derived from fine- to medium grained sediment funnelled off from accumulations of sand by hydrological processes along the littoral zones of Hout Bay Beach. The introduction of alien species like *Acacia* sp. meant that by 1977 the dune field had separated from the respective beaches to the point that in 2010 the dune field had decreased in aerial extent by 90%.

Sediment volumes for the study area have been calculated using the extended trapezoidal rule (Press *et al.*, 1988) to reveal the amount of unconsolidated material to be approximately 126×10^6 m^3.

Combining the geophysical data with the hydrodynamics of Hout Bay, more accurate comments can be made about the sediment dynamics within the study area and the regional implications thereof. The first component of any sedimentary dynamic is sediment supply. The terrigenous sediment in Hout Bay is derived from the Disa River and from coastal erosion. The Disa River for most of the year is ephemeral with its path to the sea predominantly blocked off by the berm on Hout Bay beach. Another input is aeolian derived sediment from reworked Pleistocene dunes along the northern margin of False Bay

(Terhorst, 1988) that has been entrained by longshore drift. A small portion of this reworked sediment is deposited along the northwestern margin of False Bay where it is introduced into the headland bypass corridor between Fish Hoek and Noordhoek by the strong southeasterly winds prevalent in summer around the Cape Peninsula ultimately migrating back into the ocean. The bulk of the sediment however follows the path of longshore drift around Cape Point and along the western margin of the Cape Peninsula. A small percentage of the coastal dunes and beaches south of the study area on the Atlantic seaboard are also blown out to sea. Once in the sea the northward flowing longshore drift moves the sediment up the coast towards Hout Bay. The reason for the northward vector of longshore drift is as a result of the dominant southwest incident wave pattern (Rossouw, 1984).

Using wave height and wave period data to identify bottom orbital velocity transport vectors for the study area, it has been shown that during summer gravel sized fractions can only be transported from 10 m below sea-level and medium grained sand from 50 m below sea-level, yet during winter (stormy seas) the threshold for both moves 50 m deeper. Once entrained by longshore drift or accumulated in the relative depression between Hout Bay and Kommetjie the sediment moves northward with the resistant submarine marine terrace and ridge of the Sentinel acting as a bifurcation point. Most of the sediment is transported to the west around the Sentinel yet some deflects into the bay assisted by the southwesterly swell vector. The sediment accumulation offshore of Chapman's Peak Drive is evidence of this deflected sediment transport. The fine- to medium grained sediment is ultimately deposited on the beach at the northern rim of Hout Bay and a portion of this is once again entrained by the strong southeasterly winds into the headland bypass corridor between Hout Bay and Sandy Bay. Beach profiling data show how over a six month period approximately 0.078 x 10^6 m^3 of unconsolidated sediment accreted along the littoral zone of Hout Bay Beach while during the same time 0.137 x 10^6 m^3 was eroded from the foredune/backbeach area. Because these data do not span a full year the values cannot be considered as the net movement of sediment but rather representative of the seasonal winter/summer beach dynamic. Holmes and Luger (1996) have shown that there is a net sand dune transport of 55 m^3/m/year of sediment towards the northwest most of which now accumulates in the artificially planted dunes at Hout Bay Beach.

Using all of the acquired data conclusions can be drawn with respect to calculating the approximate sediment volumes within this contained system and extrapolating these figures to the larger sediment conveyor affecting the Cape Peninsula.

The total sediment volume within the study area above the bedrock (Units 5 and 6 Figure 8.2) was calculated using the method described in Chapter 8 (p. 116) to be 126 x 10^6 m^3. The total sediment volume comprises both Units 5 and 6 which were clearly differentiated from bedrock. It was not possible to calculate the volumes of each unit separately because the contact between the two units was not always well resolved on the seismic lines. The sediment in Unit 5 is interpreted to be older sediment that has filled the lowstand palaeo Disa River channel. The data from this study suggests that Unit 5 sediment has been stable and was not mobilised during the present interglacial highstand. The sediment of Unit 6 is interpreted to have been deposited since the last marine transgression when the study area was inundated by the sea approximately 13 ka years ago when sea-level was 40 m below present level. The sediment of this unit is interpreted to represent both sediment that has migrated inland with the rise in sea-level and Holocene sediment derived from river input, coastal erosion, wind blown sediment and biogenic production (mollusc shells).

Numerous assumptions have been made based on the data collected. The first assumption is that the sediment inputs into Hout Bay are roughly equal to the outputs. This assumption is supported by the comparison of aerial photographs of Hout Bay Beach from 1944 (Holmes and Luger, 1996) and present which show that there has been no significant beach erosion or progradation (Figure 10.10). The lack of beach movement implies no net accumulation or denudation of beach sediment. Another indication of sediment stability is the unchanged sediment thickness at several sites in Hout Bay mentioned by Birch *et al.* (1991) and those recorded for this investigation. The total sediment volume reflects the current dynamic interplay of sediment input and output (Figure 11.2).

The sediment inputs identified in the study area include the fluvial discharge from the Disa River system, coastal erosion, aeolian derived sediment from Noordhoek Beach, biogenic sediments created from the marine organisms present in the study area and from longshore drift of sand from the south. The outputs identified include longshore drift to the north, sediment entrained into the Karbonkelberg headland bypass dunefield and biogenic sediments created in the study area entrained by the predominately northward flowing longshore drift.

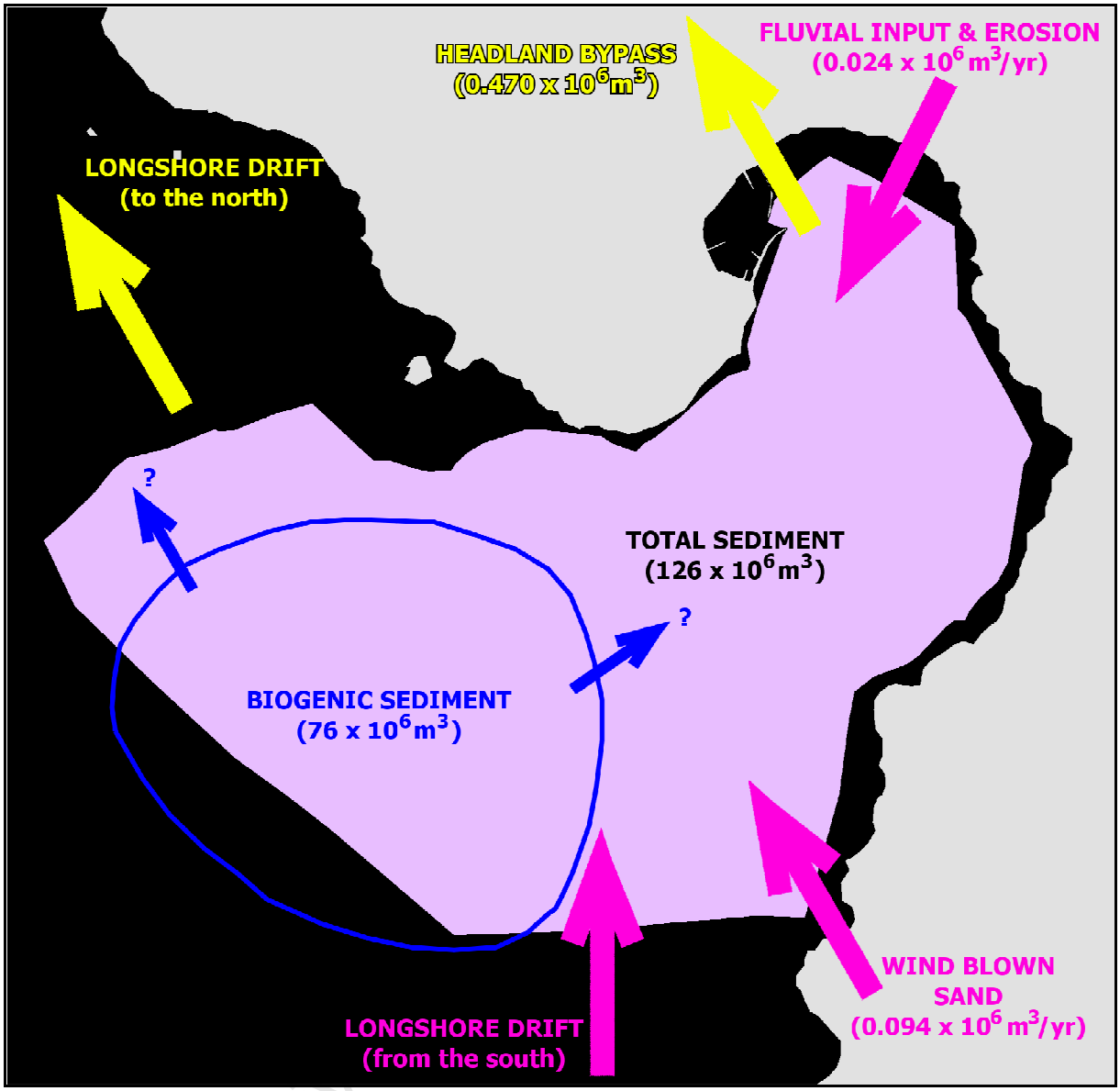

Figure 11.2. Diagrammatic representation of the sediment volumes and their respective inputs and outputs to Hout Bay.

The fluvial discharge from the Disa River was calculated to be 0.024 x 10^6 m^3/yr of sediment with the aeolian input from Noordhoek Beach postulated as 20% of the volume of sediment moving through the Karbonkelberg headland bypass dunefield. The remaining 80% of these aeolian sediments would be re-deposited onto Noordhoek Beach by wave action. The volume of sediment transported by longshore drift from the south was postulated to be the accretion observed along the beach minus the sum of 90% of the fluvial discharge of the Disa River and the aeolian sediment introduced from Noordhoek Beach. The volume of sediment entrained by the headland bypass corridor was calculated to be approximately 0.47 x 10^6 m^3, assuming approximated dimensions observed from the 1944 aerial extent and the thickness of sand to be 0.5 m (Figure 10.10). The volume of sediment entrained by

longshore drift to the north could not be accurately calculated but one would expect it to be similar to that of the longshore drift from the south as the relative inputs from the Disa River and Noordhoek Beach are comparatively negligible to the total volume of sediment in the study area.

One of the components of the sediment budget is the biogenically derived sediment in the study area, composed primarily of mollusc shell fragments. Birch *et al.* (1991) reported biogenic sediment volumes equivalent to 33% of the total sediment accumulated on the continental shelf adjacent to the study area. From the sediment samples collected for this study the average biogenic carbonate content is significantly higher at around 60% indicating a total biogenic carbonate sediment volume of 76 x 10^6 m^3). A possible reason for the high biogenic carbonate content is that a large portion of the study area includes shallow rocky to sandy substrates within the highly productive photic zone, which would facilitate increased biological activity. The relative volumes of biogenic material available for the inputs and outputs are unknown, yet the amounts are postulated to be similar in order to achieve the state of sediment equilibrium postulated. The conclusion which can be drawn from these data is that the rate of biogenic production of carbonate grains is much greater than the introduction of quartz grains from longshore, aeolian, fluvial and coastal erosion sources.

From the evidence above it has been demonstrated that the sediment budget for the study area is dominated by the production of biogenic material. The amount of terrigenous sediment introduced to the system is negligible in comparison. Net accumulation of sediment is limited to the eastern areas where accommodation space and bottom wave energy levels are low enough to allow for sediment accumulation. Other areas lack accommodation space having been infilled by relict lowstand fluvial and dune sediment. Applying these relationships to the larger Cape Peninsula sediment conveyor it can be inferred that the majority of sediment on the inner shelf found within the conveyor is derived from sea-level lowstands. Very little modern sediment is accumulating currently; rather it is transported within the conveyor from south to north with temporary accumulations found in southward facing embayments like Hout Bay. The longshore drift component is expected to increase marginally to the north as the fluvial inputs along the western margin of the Cape Peninsula are not very substantial. The amount of sediment moving in and out of the study area is volumetrically small when compared to the total unconsolidated sediment reservoir it contains.

12. REFERENCES

Ashley, G. M. (1990). Classification of large-scale subaqueous bedforms: A new look at an old problem. *Journal of Sedimentary Petrology*, **60 (1)**. 160 – 172.

Armstrong, R., De Wit, M.J., Reid, D., York, D. and Zartman, R. (1998). Cape Town's Table Mountain reveals rapid Pan-African uplift of its basement rocks. *Journal of African Earth Science*, **27 (1A)**, 10 – 11.

Backeberg, N.R. (2009). Petrogenesis of the False Bay Dyke Swarm. *11th SAGA Biennial Technical Meeting and Exhibition Swaziland, 16 – 18 September 2009*, p. 545.

Bang, N.D. (1970) Dynamic interpretation of a detailed surface temperature chart of the Agulhas Current retroflexion and fragmentation area. *South African Geographic Journal*, **52**, 67 – 76.

Beal, L.M. and Bryden, H.L. (1999) The velocity and vorticity structure of the Agulhas Current at 32ºS. *Journal of Geophysical Research*, **104**, C3, 5151 – 5176.

Becker, K.M. (2007). Geoacoustic Inversion for spatially and temporally varying shallow water environments. *ONR special research awards in Underwater Acoustics: Entry level faculty award.* The Pennsylvania State University/Applied Research Laboratory. 6 pp.

Belderson, R.H., Kenyon, N.H., Stride A.H., and Stubbs, A.R. (1972) *Sonographs of the Sea Floor: A Picture Atlas*. Elsevier, Amsterdam.

Birch, G.F., Rogers, J., Bremner, J.M. and Moir, G.J. (1976) Sedimentation controls on the continental margin of Southern Africa. *Proceedings of the 1st interdisciplinary conference for marine and freshwater research in South Africa (Port Elizabeth)*, **Fiche 20A**, C1 – D12.

Birch, G.F. (1979). The Karbonat-Bombe: a precise, rapid and cheap instrument for determining calcium carbonate in sediment and rocks. *Technical Report Joint Geological Survey University of Cape Town Marine geoscience Unit.* **11**, 122 – 126.

Birch, G.F, Day, R.W. and Du Plessis, A. (1991). Nearshore Quaternary sediments on the west coast of southern Africa. *Bulletin of the Geological Survey of South Africa*, **101**, 14 pp.

Boebel, O., Rae, C.D., Garzoli, S., Lutjeharms, J.R.E., Richardson, P., Rossby, T., Schmid, C. and Zenk, W. (1998) Float experiment studies interocean exchanges at the tip of Africa. *EOS*, **79**, 1, 1, 7 – 8.

Boggs, S, Jr. (2001). *Principles of Sedimentology, third Edition*. New Jersey, Prentice Hall, 726 pp.

Boyer, D., Cole, J. and Bartholome, C. (2000) Southwestern Africa: Northern Benguela Current region. *Marine Pollution Bulletin*, **41**, 123 – 140.

Brenon, I and Le Hir, P. (1999). Modelling the turbidity maximum in the Seine Estuary (France): identification of formation processes. *Estuarine, Coastal and Shelf Science*, **49**, 525 – 544.

Briden, J.C., Rex, D.C., Faller, A.M. and Tomblin, J.F. (1979). Geochronology and paleomagnetism of volcanic rocks in the Lesser Antilles island arc. *Philosophical Transactions of the Royal Society of London*, **291**, 485 – 528.

Broquet, C.A.M. (1990). Tace fossils and ichno- sedimentary facies from the lower Palaeozoic Peninsula Formation, Cape Peninsula, South Africa. *Abstracts, Geocongress '90, Geological Society of South Africa, Cape Town*, 64 – 67.

Broquet, C.A.M. (1992). The sedimentary record of the Cape Supergroup: A review. In: De Wit, M.C.J and Ransome, I. (Editors), *Inversion Tectonics of the Cape Fold Belt, Karoo and Cretaceous Basins of Southern Africa*. A.A. Balkema, Rotterdam, 159 – 183.

Bryden, H.L., Beal, L.M. and Duncan, L.M. (2003) Structure and transport of the Agulhas Current and its temporal variability. Submitted to the *Journal of Oceanography*.

Caufield, D.D., Ballard, R. and Leist, R.L. (2005). Analytical techniques for shallow marine near-surface geotechnical parameter estimation. *In* Butler, D.W. (ed), *Near Surface Geophysics*, Society of Exploration Geophysicists, **Ch. 31**, 707 – 725.

Cawthra, H.C. (2010). The Cretaceous to Cenozoic Evolution of the Durban Bluff and Adjacent Continental Shelf. *Unpublished MSc Thesis, University of Kwazulu-Natal*. 241 pp.

Chappell, B.W. and White, A.J.R. (1974). Two contrasting granite types, *Pacific Geology*, **8**, 173 – 174.

Cocks, L.R.M. and Fortey, R.A. (1986). New evidence on the South African Lower Palaezoic: age and fossil reviewed. *Geological Magazine*, **123**, 437 – 444.

Coe, A.L. (*Ed*) (2003). *The sedimentary record of sea-level change.* Cambridge University Press, Cambridge, 286 pp.

Compton, J.S. (2001). Holocene sea-level fluctuations inferred from the evolution of depositional environments of the southern Langebaan Lagoon salt marsh, South Africa. *The Holocene*, **11(4)**, 395 – 405.

Compton, J.S. (2006). *The Rocks and Mountains of Cape Town*. Double Storey Books. 112 pp.

Compton, J.S. and Wiltshire, J.G. (2009). Terrigenous sediment export from the western margin of South Africa on glacial to interglacial cycles. *Marine Geology*, **266**, 212 – 222.

Cole, D.I. (2003). The metallogeny of the Cape Town Area. Explanation of Metallogenic Map Sheet 3318, Scale 1:250 000. *Council for Geoscience, South Africa*. 80 pp.

Cole, D.I. and Roberts, D.L. (2000). Lignite potential of the western coast, Western Cape Province. South Africa. *Memoir, Council for Geoscience, South Africa*, **89**, 50 pp.

Cooper, J.A.G. (2001). Geomorphological variability among microtidal estuaries from wave-dominated South African coast. *Geomorphology*, **40**, 99 – 122.

Cramez, C. and Jackson, M.P.A. (2000). Superposed deformation straddling the continental-oceanic transition in deep water Angola. *Marine and Petroleum Geology*, **17**, 1095 – 1109.

CSIR. (1973). Deep-sea Wave Clinometer data from 1967 to 1972. *CSIR Report,* **ME 1263**, Pretoria.

Da Silva, L.C., McNaughton, N.J., Hartmann, L.A., Fletcher, I.R., Gresse, P.G. and Scheepers, R. (1997). U-Pb (SHRIMP) isotopic constraints for the evolution of the Brazilian granitic province, and some correlated South African Pan-African plutons. *Abstract Second International Symposium On Granites and Associated Mineralizations, Salvador*, 276 – 277.

Davies, J.H. (1980). *Geographical variation in coastal development*. Oliver and Boyd, Edinburgh.

Day, R.W. (1986). Magnetometric mapping of the False Bay dolerites. *Joint Geological Survey/University of Cape Town Marine Geoscience Unit*, **Technical Report 16**, 217-227.

De Decker, R.H. (1987) The geological setting of diamondiferous deposits on the inner shelf between the Orange River and Wreck Point, Namaqualand. *Bulletin of the Geological Survey of South Africa*, **86**, 99 pp.

De Moustier, C. (1988) State of the Art in Swath Bathymetry Survey Systems. *International Hydrographic Review*, **Volume 65 (2)**, 25-54.

De Ruijter, W. (1982) Asymptotic analysis of the Agulhas and Brazil Current systems. *Journal of Physical Oceanography*, **12**, 361 – 373.

De Ruijter, W.P.M., Ridderinkhof, H., Lutjeharms, J.R.E., Schouten, M.W. and Vetch, C. (2002) Observations of the flow in the Mozambique Channel. *Geophysical Research Letters*, **29**, 140.1 – 140.3.

De Wet, L.W. (1979). Die invloed van die Suid-Afrikaanse Hoogland op die ontwikkeling en voorplanting van atmosferiese druk and sirkulasiestelsels. *Unpublished MSc thesis, University of Pretoria*, 79 pp.

Dingle, R.V. (1970). Bathymetry. *Technical Report of the Joint Geological Survey/University of Cape Town Marine Geology Program*, **3**, 11 – 12.

Dingle, R.V. (1971). Tertiary sedimentary history of the continental shelf off Southern Cape province, South Africa. *Transactions of the Geological Society of South Africa*, **Vol. 74, No. 3**, 173 – 186.

Dingle, R.V. (1973). The geology of the continental shelf between Lüderitz and Cape Town (Southwest Africa), with special reference to Tertiary strata. *Journal of the Geological Society of London*, **129**, 337 – 363.

Dingle, R.V., Siesser, W.G. and Newton, A.R. (1983). Mesozoic and Tertiary Geology of South Africa. A.A. Balkema/Rotterdam. 375 pp.

Dingle, R.V., Birch, G.F., Bremner, J.M., De Dekker, R.H., Du Plessis, A., Engelbrecht, J.C., Fincham, M.J., Fitton, T., Flemming, B.W., Gentle, R.I., Goodlad, S.W., Martin, A.K., Mills, E.G., Moir, G.J., Parker, R.J., Robson, S.H., Rogers, J., Salmon, D.A., Siesser, W.G., Simpson, E.S.W., Summerhayes, C.P., Westall, F., Winter, A.,Woodborne, M.W. (1987) Deep-sea sedimentary environments around southern Africa (south-east Atlantic and south-west Indian Oceans). Annals of the South African Museum 98, 1 – 27 2 separate maps.

Donohue, E.A., Firing, E. and Beal, L (2000) Comparison of the three velocity sections of the Agulhas Current and the Agulhas Undercurrent. *Journal of Geophysical Research*, **105**, C12, 28585 – 28593.

Duncan, C.P. (1965) An eddy in the subtropical convergence southwest of South Africa. *Journal of Geophysical Research*, **73**, 531 – 534.

Du Plessis, A. and Glass, J.G. (1991). The geology of False Bay. *Transactions of the Royal Society of South Africa*, **47**, 495 – 517.

Eby, G.N. (1992). Chemical subdivision of the A-type granitoids and tectonic implications. *Geology*, **2**, 641 – 644.

Edgerton, H.E. and Haywood, G.G. (1964) The "Boomer" sonar source for seismic profiling. *Journal of Geophysical Research*, **66**, 2917 – 2927.

Farr, H.K. (1980) Multi-beam Bathymetric Sonar: SeaBEAM and HYDROCHART. *Marine Geodesy*, **Volume 4 (2)**, 7 – 10.

Flemming, B.W. (1978). Underwater sand dunes along the southeast African continental margin – observations and implications. *Marine Geology*, **26**, 177 – 198.

Flemming, B.W. (1980). Sand transport and bedform patterns on the continental shelf between Durban and Port Elizabeth (south-east African continental margin). *Sedimentary Geology*, **26**, 179 – 205.

Flemming, B.W. (1981). Factors controlling shelf sediment dispersal along the southeast African continental margin. *Marine Geology*, **42**, 259 – 277.

Folk, R.L. (1965). *Petrology of sedimentary rocks*. Hemphills, Austin, Texas, 246 pp.

Folk, R. L. and Ward, W. C. (1957). Brazos River bar, a study in the significance of grain-size parameters. *Journal of Sedimentary Petrology*, **27**, 3-27.

Franceshini, G. and Compton, J.S. (2006). Holocene evolution of the sixteen mile beach complex, Western Cape, South Africa. *Journal of Coastal Research*, **Vol 22, No. 5**, 1158 – 1166.

Fuller, A.O. (1985). A contribution to the conceptual modelling of pre-Devonian fluvial systems. *Transactions of the Geological Society of South Africa*, **88**, 189 – 194.

Fuller, A.O. and Broquet, C.A.M. (1990). Aspects of the Peninsula Formation – Table Mountain Group. *Abstracts from Geocongress 1990, Geological Society of South Africa*, 169 – 172.

Galway, R.S. (2000) Comparison of Target Detection Capabilities of the Reson Seabat 8101 and Reson Seabat 9001 Multibeam Sonars. (unpublished term paper).

Garzoli, S.L., Gordon, A.L., Vamenkovich, V., Pillsbury, D. and Duncombe-Rae, C. (1996) Variability and sources of the south eastern Atlantic circulation. *Journal of Marine Research*, **54**, 1039 – 1071.

Geological Survey of South Africa. (1990). 3318 Cape Town 1:250 000 geological sheet. Government Printer, Pretoria (Compiler J.N. Theron).

Gibbard, P. and Kolfschoten, T. (2004). The Pleistocene and Holocene epochs. *In*: Gradstein, F.M., Ogg, J.G. and Smith, A.G. (Eds), *A geological time scale*. Cambridge University Press, Cambridge, **22**, 441 – 452.

Gibbard, P., Cohen, K. and Ogg, J.G. (2008). Quaternary Period. In: Ogg, J.G., Ogg, G. and Gradstein, F.M., (Eds), *A concise geologic time scale*. Cambridge University Press, Cambridge, **15**, 149 – 159.

Gordon, A.L. (1985) Indian – Atlantic transfer of thermocline water at the Agulhas Retroflection. *Science,* **227**, 1030 – 1033.

Grant, F.S. and Dodds, J. (1972). MAGMAP FFT processing system development notes. Paterson Grant and Watson Limited.

Gründlingh, M.L. (1978) Drift of a satellite-tracked buoy in southern Agulhas Current and Agulhas Return Current. *Deep-Sea Research*, **25**, 1209 – 1224.

Gunn, P.J. (1975). Linear transformations of gravity and magnetic fields. *Geophysical Prospecting*, **23**, 300 – 312.

Gyory, J., Beal, L.M., Bischof, B., Mariano, A.J. and Ryan, E.H (2004) "The Agulhas Current". Ocean Surface Currents. http://oceancurrents.rsmas.miami.edu/atlatic/agulhas.html. Accessed 13/01/2010.

Hartnady, C.J.H., Newton, A.R., and Theron, J.N. (1974). The stratigraphy and structure of the Malmesbury Group in the Southwestern Cape. *Bulletin Precambrian Research Unit, University of Cape Town*, **15**, 193 – 214.

Hartnady, C.J.H. and Rogers, J. (1990). The scenery and geology of the Cape Peninsula. *Guidebook Geocongress '90 Geological Society of South Africa*, M1: 1 – 67.

Harris, T.F.W., Legeckis, R. and van Foreest, D. (1978) Satellite infrared images in the Agulhas Current system. *Deep-Sea Research*, **25**, 543 – 548.

Haq, B.U. (2007). The Geological Time Scale, sixth revised and enlarge edition. *Elsevier*, 1 A0 Poster.

Hobday, D.K. and Tankard, A.J. (1978). Transgressive-barrier and shallow-shelf interpretation of the lower Palaeozoic Peninsula Formation, South Africa. *Bulletin of the Geological Society of America*, **89**, 1733 – 1744.

Holmes, P. and Luger, A. (1996). Geomorphic implications of the stabilisation of a headland bypass dune system in the Cape Peninsula, South Africa. *Z. Geomorph. N.F.*, **107**, 63 – 77.

Horton, J.W. (1959) *Fundamentals of Sonar*. United States Naval Institute, Annapolis.

Hrvoic, D. (2007) SeaSPY Technical Application Guide rev 1.4. *Internal Report of Marine Magnetics Corporation*, *Onterio, Canada*, 13 pp.

Hughes-Clark, J.E. (1999) Provisional Swath Sonar Survey Specifications. *TH Technical Report #2, National Topographic and Hydrographic Authority, Land Information New Zealand*. http://www.omg.unb.ca/~jhc/LINZ_spec.html, Ocean Mapping Group, Department of Geodesy and Geomatics Engineering, University of New Brunswick, Federicton.

Hutchings, L., van der Lingen, C.D., Shannon, L.J., Crawford, R.J.M., Verheye, H.M.S., Bartholomae, C.H., van der Plas, A.K., Louw, D., Kreiner, A., Ostrowski, M., Fidel, Q., Barlow, R.G., Lamont, T., Coetzee, J., Shillington, F., Veitch, J., Currie, J.C. and

Monteiro, P.M.S. (2009). The Benguela Current: an acosystem of four components. *Ocenography*, **83**, 15 – 32.

Ingham, A.E. (Editor) (1975) *Sea Surveying*. John Wiley, London.

Jackson, S.P. (1947). Air masses and the circulation over the plateau and coast of South Africa. *South African Geological Journal*, **29**, 1 – 15.

Johnson, D.W. (1919). *Shore processes and shoreline development, (1st edition):* New York, Wiley, 584 pp.

Johnson, M.R. (1976). *Stratigraphy and sedimentology of the Cape and Karoo Sequences in the eastern Cape Province*. M.Sc. thesis (unpublished), Rhodes University, Grahamstown, 336 pp.

Jones, E.J.W. (1999) *Marine Geophysics*. John Wiley, London

Keary, P., Brooks, M. and Hill, I. (2002) *An Introduction to Geophysical Exploration, Third Edition*. Blackwell Science, London.

Komar, P.D. and Miller, M.C. (1975). On the comparison of the threshold of sediment movement under waves and unidirectional currents with a discussion of the practical evaluation of threshold. *Journal of Sedimentary Petrology*, **45**, 362 – 367.

Koornhof, A. (2000). Dive Guide South Africa. New Holland Publishing (Pty) Ltd., London, 183 pp.

Krumbein, W.C. (1944). Shore processes and beach characteristics. *U.S. Army Corps Engineers Beach Erosion Board Technical Memorandum*, **3**, 1 – 35.

Lavier, L.L., Steckler, M.S. and Brigaud, F. (2001). Climatic and tectonic control on the Cenozoic evolution of the West African margin. *Marine Geology*, **178**, 63 – 80.

Leygonie, F.E. (1977). Die graniete van Langebaan, Kaapprovinsie. *Annals University of Stellenbosch*, **A1**, 33 – 106.

Loiselle, M.C. and Wones, D.R. (1979). Characteristics and origin of anorogenic granites, *Memoirs of the Geological Society of America*, **174**, 225 – 236.

Lutjeharms, J.R.E and van Ballegooyen, R.C. (1984) Topographic control in the Agulhas Current system. *Deep-Sea Research*, **31**, 1321 – 1337.

Lutjeharms, J.R.E and van Ballegooyen, R.C. (1988) The Retroflection of the Agulhas Current. *Journal of Physical Oceanography*, **18**, 11, 1570 – 1583.

Lutjeharms, J.R.E., Boebel, O., and Rossby, H.T. (2003) Agulhas cyclones. *Deep-Sea Research II*, **50**, 13 – 34.

Lutjeharms, J.R.E., and Roberts, H.R. (1988) The Natal Pulse: an extreme transient on the Agulhas Current. *Journal of Geophysical Research*, **93**, 631 – 635.

MacHutchon, K.R. (2008). The characterisation of South African sea storms. *Unpublished MSc Thesis, Department of Civil Engineering, University of Stellenbosch*, 142 pp.

MacHutchon, M.R. (2003). Depositional history of the Holocene mudbelt offshore of the Buffels River, South Africa. *Unpublished honours project, Department of Geological Sciences, University of Cape Town*, 36 pp.

MacHutchon, M.R. (2009) Geophysical Survey of Hout Bay and Surrounds for Stat Project ST-2010-1095. *Internal Report of the Council for Geoscience, South Africa*, **2010-0126**. Private Bag X112, Pretoria, 26 pp.

MacHutchon, M.R. and Cawthra, H.C. (2009) Survey of Simons Town Harbour Walls using Multibeam Echosounder and Scuba Diving Methods. *Commercial Report of the Council for Geoscience, South Africa*, **2009-0222**. Private Bag X112, Pretoria, 153 pp.

Martin, A.K., Goodlad, S.W., Hartnady, C.J.H., and Du Plessis, A. (1982). Cretaceous paleopositions of the Falkland Plateau relative to southern Africa using Mesozoic seafloor spreading anomalies. *Geophysical Journal of the Royal Astronomical Society*, **71**, 567 – 579.

Mayer, L. and Hughes-Clark, J.E. (1995) STRATAFORM Cruise Report: R/V Pacific Hunter, Multibeam Survey, July 14 – 28, 1995.

Mazel, C. (1985) Side Scan Sonar Training Manual – Klein Associates, Inc, **11230001 Rev 01.**

McQuillin, R and Ardus, D.A. (1977) Exploring the Geology of Shelf Seas. Graham and Trotman, London.

Midgley, D.C. and Pitman, W.V. (1969). Surface water resources of South Africa: *University of Witwatersrand Hydrological Research Unit*, **Report No. 2/69**, Johannesburg.

Milligan, P.R. and Gun, P.J. (1997). Enhancement and presentation of airborne geophysical data. *Journal of Australian Geology and Geophysics*, **17(2)**, 63 – 75.

Milliman, J.D. and Syvitski, J.P.M (1992). Geomorphic/Tectonic Control of Sediment Discharge to the Ocean: The Importance of Small Mountainous Rivers. *The Journal of Geology*, **100**, 525 – 544.

Murray, L.G., Joynt, R.H., O'Shea, D.O'C., Foster, R.W. and Kleinjan, L. (1970). The geological environment of some diamond deposits off the west coast of South West Africa. *In*: Delany, F.M. (*ed*). The Geology of the East Atlantic Continental Margin. *Report of the Institute for Geological Science*, **70(16)**, 119 – 141.

Nabighian, M.N. (1972). The analytical signal of two-dimensional magnetic bodies with polygonal cross-section: Its properties and use for automated anomaly interpretation. *Geophysics*, **37**, 507 – 517.

Nabighian, M.N. (1984). Toward the three-dimensional automatic interpretation of potential field data via generalised Hilbert transforms: Fundamental relations. *Geophysics*, **53**, 957 – 966.

Nell, G. and Brink, W.C. (1944). The petrology of the Western Province dolerites. *Annals of the University of Stellenbosch*, **22(A)**, 27 – 62.

Nelson, G. and Hutchings, L. (1983) The Benguela upwelling area. *Progressive Oceanography*, **12**, 333 – 356.

Ogg, J.G., Ogg, G. and Gradstein, F.M. (2008). *The Concise Geological Time Scale*. Cambridge University Press. United Kingdom. 177 pp.

Olsen, D.B. and Evans, R.H. (1986) Rings of the Agulhas Current. *Deep-Sea Research*, **Vol. 33, No. 1**, 27 – 42.

Partridge, T.C. (1998). Of diamonds, dinosaurs and diastrophism: 150 million years of landscape evolution in South Africa. *South African Journal of Geology*, **101 (3)**, 167 – 184.

Partridge, T.C. and Maud, R.R. (1987). Geomorphic evolution of Southern Africa since the Mesozoic. *South African Journal of Geology*, **90 (2)**, 179 – 208.

Partridge, T.C. and Maud, R.R. (2000). Macro-scale geomorphic evolution of Southern Africa. *In*: Partridge, T.C. and Maud, R.R. (*eds*). *The Cenozoic of Southern Africa*. Oxford University Press, Inc., New York, 3 – 18.

Peterson, R.G. and Stramma, L. (1991) Upper-level circulation in the South Atlantic Ocean. *Progress in Oceanography*, **26**, 1 – 73.

Pethick, J. (1984). *An introduction to coastal geomorphology*. Edward Arnold, London, Great Britain, 260pp.

Press, W.H., Flannery, B.P., Teukolsky, S.A., and Vetterling, W.T. (1988)*, Numerical Recipes in C*, Cambridge University Press.

Price, J.F., Weller, R.A. and Schudlich, R.R. (1987). Wind-driven ocean currents and Ekman transport. *Science*, **238 (4833)**, 1543 – 1538.

Quartly, G.D. and Srokosz, M.A. (1993) Seasonal variations in the region of the Agulhas Retroflection: Studies with Geosat and FRAM. *Journal of Physical Oceanography*, **23**, 2107 – 2124.

Ramsay, P.J. (1995). 9000 Years of sea-level change along the Southern African coastline. *Quaternary International*, **31**, 71 – 75.

Ramsay, P.J. and Cooper, J.A.G. (2002). Late Quaternary sea-level change in South Africa. *Quaternary Research*, **57**, 82 – 90.

Reid, D.L., Erlank, A.J. and Rex, D.C. (1991). Age and correlation of the False Bay dolerite dyke swarm, south-western Cape, Cape Province. *South African Journal of Geology*, **94**, 155-158.

Renard, V. and Allenou, J-P. (1979) Sea beam, multi-beam echo-sounding in "Jean Charcot": description, evaluation and first results. *International Hydrographic Review*, **LVI**, 35 – 67.

Retief, G de F. (1974). Low cost inshore wave direction indicator. *Proceedings 14th International Conference on Coastal Engineering*, Copenhagen.

River Health Program (2003). State-of-rivers report: Diep, Hout Bay, Lourens and Palmiet River systems. *Department of Water Affairs and Forestry*, Pretoria, 1 – 41.

Roberts, D.L. (1999). The geology of Melkbosstrand and environs. Explanation, Sheet 3318CB (1:50 000), *Council for Geoscience*, 36 pp.

Roberts, D.L. (2006). Lithostratigraphy of the Sandveld Group. *South African Committee for Stratigraphy*. **Lithostratigraphic Series 9**, 25 – 26.

Roberts, D.L., Mathews, T., Herries, A.I.R., Boulter, C., Scott, L., Dondo, C., Mtembi, P., Browning, C., Smith, R.H., Haarhoff, P. and Bateman, M.D. (2011). Regional and global context of the Late Cenozoic langebaanweg (LBW) palaeontological site: West Coast of South Africa. *Earth Science Reviews*, **106**, 191 – 214.

Robinson, A.R., editor (1983) *Eddies in Marine Science*. Springer-Verlag, Berlin, 609 pp.

Roest, W.R., Verhoef, V. and Pilkington, M. (1992). Magnetic interpretation using the 3-D analytical signal. *Geophysics*, **57**, 116 – 125.

Rogers, J. (1977) Sedimentation of the Continental Margin off the Orange River and the Namib Desert. *Bulletin of the Geological Survey of South Africa/University of Cape Town Marine Geoscience Unit*, **7**, 210 pp.

Rogers, J. (1980). First report on the Cenozoic sediments between Cape Town and Eland's Bay: Open-file report, *Geological Survey of South Africa*, **1980-0136**, 64 pp.

Rogers, J. (1982). Lithostratigraphy of Cenozoic sediments between Cape Town and Eland's Bay. *Palaeoecology of Africa*, **15**, 121 – 137.

Rogers, J. and Bremner, J.M. (1991). The Benguela Ecosystem. Part VII. Marine-Geological Aspects. *Oceanography and Marine Biology: An Annual Review*, **29**, 1 – 85.

Rogers, J. and Rau, A.J. (2006). Surficial sediments of the wave-dominated orange river delta and the adjacent continental margin off south-western Africa. *African Journal of Marine Science*, **28**, 511 – 524.

Rogers, J., Pether, J., Molyneux, R., Hill, R.S., Kilham, J.L.C., Cooper, G. and Corbett, I.B. (1990). Cenozoic geology and mineral deposits along the west coast of South Africa and the Sperrgebiet: Guidebook PR2, *Geocongress '90, Geological Society of South Africa*, 111 pp.

Rossouw, J. (1984). Review of existing wave data, wave climate and design waves for South African and South West African (Namibian) coastal waters. *CSIR Report*, **T/Sea 8401**, Stellenbosch. 66 pp.

Russel-Cargill, W.G.A (1989). Extracts from a Report on the Geotechnical Studies Undertaken for the Proposed Marine Outfall Sewer Pipeline at Hout Bay. *Report Number MD265/1 June 1989,* Prepared on Instruction from Kapp Prestedge & Retief for the Western Cape Regional Services Council, 121 pp.

Rust, I.C. (1967) On the sedimentation of the Table Mountain Group in the Western Cape Province: Unpublished Doctoral dissertation, University of Stellenbosch, South Africa.

Rust, I.C. (1973) The Evolution of the Palaeozoic Cape Basin, Southern Margin of Africa. In: Nairn, A.E.M. and Stehli, F.G. (eds), *The Ocean Basins and Margins Volume 1. The South Atlantic*. New York, Plenum Press, 247 – 276.

Rust, I.C. (1977). Evidence of shallow marine and tidal sedimentation in the Ordovician Graafwater Formation, Cape Province, South Africa. *Sedimentary Geology*, **18**, 123 – 133.

Rust, I.C. (1981). Lower Palaeozoic rocks of southern Africa. In: Holland, C.H. (Editors), *Lower Palaeozoic of the Middle East, Eastern and Southern Africa, and Antarctica*. Wiley and Sons Ltd., New York, 165 – 187.

Scheepers, R. (1990). *Magmatic associations and radioelement geochemistry of selected Cape Granites with special reference to subalkaline and leucogranitic phases* (in Afrikaans), Ph. D. thesis (unpublished), University of Stellenbosch.

Scheepers, R. (1995). Geology and petrogenisis of the Late Precambrian S-, I- and A-type granitoids in the Saldania belt, Western Cape Province, South Africa. *Journal of African Earth Science*, **21**, 35 – 58.

Scheepers, R. and Armstrong, R. (2002). New U-Pb SHRIMP zircon ages on the Cape Granite Suite: implications for magmatic evolution of the Saldania Belt. *South African Journal of Geology*, **105**, 241 – 256.

Scheepers, R. and Cuney, M. (1992). Hydrothermal breccia-related Cu-Mo-Au mineralization in Late Precambrian granites, Western Cape Province, South Africa. *Ore Geological Review*, **7**, 1 – 23.

Scheepers, R. and Schoch, A.E. (2006). The Cape Granite Suite. In: Johnson, M.R., Anhaeusser, C.R., and Thomas, R.J. (Eds), The Geology of South Africa. Geological Society of South Africa, Johannesburg/Council for Geoscience, Pretoria, 421-432.

Schink, J.C., Stockwell, J.H. and Ellis, R. A. (1979). An improved device for gasometric determination of carbonate in sediment. *Journal of Sedimentary Petrology*, **48**, 651-653.

Schoch, A.E. (1975). The Darling granite batholith. *Annals of the University of Stellenbosch*, **A1 (1)**, 1 – 104.

Schoch, A.E. (1976). Die geografiese posisie van die Colensoverskuiwing in die Vredenburg-Saldanha-gebied. *Suid Afrikaanse Geograaf*, **5**, 303 – 309.

Schoch, A.E., Leterrier, J. and De La Roche, H.D. (1977). Major element geochemical trends in the Cape granites. *Transactions of the Geological Society of South Africa*, **80**, 197 – 209.

Scholtz, D.L. (1946). On the younger Pre-Cambrian granite plutons in the Cape granites. *Proceedings of the Geological Society of South Africa*, **49**, 35 – 82.

Schultze, B.R. (1965) Climate of South Africa. Part 8. General Survey. *Weather Bureau, Department of Transport South Africa*, **WB 28**, 1 – 330.

Schwartz, B.L. (2005). *Encyclopaedia of coastal science.* Springer. 1211 pp.

Scrutton, R.A. and Dingle, R.V. (1973). Basement control over sedimentation on the continental margin west of South Africa. *Transactions of the Geological Society of South Africa*, **77**, 253 – 260.

Shannon, L.V. (2009) Benguela Current. In: Steele, J.H., Thorpe, S.A., Turekian, K.K. (eds), *Encyclopedia of Ocean Sciences*. Academic Press, 255 – 267.

Shannon, L.V. and Anderson, F.P. (1982). Applications of satellite ocean colour imagery in the study of the Benguela Current system. *South African Journal of Photogrammetry Remote Sensing and Cartography*, **13(3)**, 153 – 169.

Shannon, L.V. and Nelson, G. (1996). The Benguela: Large scale features and processes and system variability. *In*: Wefer, G., Berger, W.H., Siedler, G. and Webb, D.J. (*eds*). *The South Atlantic: Present and Past Circulation*. Springer-Verlag, Berlin Heidelberg, 163 – 210.

Siesser, W.G. and Dingle, R.V. (1981). Tertiary sea-level movements around Southern Africa. *Journal of Geology*, **89**, 83 – 96.

Simpkin, P.G. and Davis, A. (1993) For seismic profiling in very shallow water, a novel receiver. *Sea Technology*, September, 21 – 28.

Simpson, E.S.W., Du Plessis, A. and Forder, E. (1970). Bathymetric and magnetic traverse measurements in False Bay and west of the Cape Peninsula. *Transactions of the Royal Society of South Africa*, **39**, 113 – 116.

Skogen, M.D. (1999) A biophysical model applied to the Benguela upwelling system. *South African Journal of Marine Science*, **21**, 235 – 249.

Smith, W.H.F (1993) On the accuracy of digital bathymetric data. *Journal of Geophysical Research*, **98**. 9591 – 9603.

Smith, W.H.F and Sandwell, D.T (1994) Bathymetric prediction from dense satellite altimetry and sparse shipboard bathymetry. *Journal of Geophysical Research*, **99**. 21 803 – 21 824.

Stramma, L. and Lutjeharms, J.R.E. (1997) The flow field of the subtropical gyre in the South Indian Ocean into the Southeast Atlantic Ocean: a case study. *Journal of Geophysical Research*, **99**, 14053 – 14070.

Swart, D.H. and Serdyn, J de V. (1981). Statistical analysis of visually observed wave data from voluntary observing ships for South African east coast. *Unpublished CSIR Report*, Stellenbosch.

Tankard, A.J. and Hobday, D.K. (1977). Tide-dominated back-barrier sedimentation, Early Ordovician Cape Basin, Cape Peninsula, South Africa. *Sedimentary Geology*, **18**, 135 – 159.

Terhorst, A. (1988). The seafloor environment off Simon's Town in False Bay, revealed by side-scan sonar, bottom sampling, diver observations and underwater photography. *Bulletin of the Geological Survey of South Africa/University of Cape Town Marine Geoscience Unit*, **22**, 98 pp.

Thamm, A.G. and Johnson, M.R. (2006). The Cape Supergroup. *In*: Johnson, M.R., Anhaeusser, C.R., and Thomas, R.J. (Eds), The Geology of South Africa. Geological Society of South Africa, Johannesburg/Council for Geoscience, Pretoria, 443-460.

Theron, J.N. (1970) A stratigraphical study of the Bokkeveld Group (Series): Second I.U.G.S. Symposium on the stratigraphy and palaeontology of the Gondwana System. Cape Town, South Africa, July 1970, (preprint).

Theron, J.N. (1972). *The stratigraphy and sedimentation of the Bokkeveld Group*. Unpublished Doctoral dissertation, University of Stellenbosch, 175 pp.

Theron, J.N. (1984). The geology of Cape Town and environs. Explanation of sheets 3318 CD and DC, and 3418 AB, AD and BA, Scale 1:50 000. *Geological Survey of South Africa*, 77 pp.

Theron, J.N. (1984). 1:50 000 Geological series, Sheet 3418 AB & AD Cape Peninsula. *Geological Survey of South Africa*, A0 Map.

Theron, J.N. (1984). 1:50 000 Geological series, Sheet 3418 BA Mitchells Plain. *Geological Survey of South Africa*, A0 Map.

Theron, J.N. (1984). 1:50 000 Geological series, Sheet 3418 AB & AD Cape Peninsula. *Geological Survey of South Africa*, A0 Map.

Theron, J.N. (1984). 1:50 000 Geological series, Sheet 3318 CD Cape Town. *Geological Survey of South Africa*, A0 Map.

Theron, J.N. (1984). 1:50 000 Geological series, Sheet 3318 DC Bellville. *Geological Survey of South Africa*, A0 Map.

Theron, J.N., Gresse, P.G., Siegfried, H.P. and Rogers, J. (1992). The geology of the Cape Town area. Explanation, Sheet 3318 (1:250 000), *Geological Survey of South Africa*, 140 pp.

Toole, J.M. and Warren, B.A. (1993) A hydrographic section across the subtropical South Indian Ocean. *Deep-Sea Research I*, **40**, 10, 1973 – 2019.

Turner, B.R. (1990). Continental sediments in South Africa. *Journal of African Earth Science*, **10**, 139 – 149.

Turner, M. (1997) *Shipwrecks & Salvage In South Africa*, C. Struik, Cape Town, 224 pp.

Uncles, R.J., Stephens, J.A. and Barton, M.L. (1984). Observation of fine-sediment concentrations and transport in the turbidity maximum region of an estuary. In *Prandle, D (ed), Coastal and Estuarine Studies. Dynamics and Exchanges in Estuaries and the Coastal Zone*, American Geophysical Union, 255 – 276.

Van Leeuwen, P.J., De Ruijter, W.P.M. and Lutjeharms, J.R.E. (2000) Natal pulses and the formation of Agulhas Rings. *Journal of Geophysical Research*, **105**, 6425 – 6436.

Veronis, G. (1973) Model of world ocean circulation: I. Wind-driven, two-layer. *Journal of Marine Research*, **31**, 228 – 288.

Von Veh, M.W. (1983). Aspects of sedimentation, structure and tectonic evolution in the Tygerberg terrane, southwestern Cape Province. *Bulletin of Precambrian Research Unit, University of Cape Town*, **32**, 88 pp.

Waelbroeck, C., Labeyrie, L., Michel, E., Duplessy, J.C., McManus, J.F., Lambeck, K., Balbon, E. and Labracherie, M. (2002). Sea-level and deep water temperature changes derived from benthic foraminifera isotopic records. *Quaternary Science Reviews*, **21**, 295 – 305.

Wedepohl, P.M., Lutjeharms, J.R.E. and Meeuwis, J.M. (2000) Surface drift in the south-east Atlantic Ocean. *South African Journal of Marine Science*, **22**, 71 – 79.

Wentworth, C.K. (1922). A scale of grade and class terms for clastic sediments. *Journal of Geology*, **30**, 377 – 392.

Whiteley, R.J. and Stewart, S.B. (2007). Shallow marine investigations in Australia with advanced underwater seismic refraction (USR). *Exploration Geophysics*, **39(1)**, 34 – 40.

Whittle, C., Lutjeharms, J.R.E., Duncombe Rae, C.M. and Shillington, F.A. (2008). Interaction of Agulhas filaments with mesoscale turbulence: a case study. *South African Journal of Science*, **104**, 135 – 139.

Wigley, R.A. (2005). Sedimentary facies from the head of the Cape Canyon: insights into the Cenozoic evolution of the western margin of South Africa. *Unpublished PhD thesis, Department of Geological Sciences, University of Cape Town*, 289 pp.

Wigley, R.A. and Compton, J.S (2006). Late Cenozoic evolution of the outer continental shelf at the head of the Cape Canyon, South Africa. *Marine Geology*, **226**, 1 – 23.

Woodborne, M.W. (1991) The geology of the diamondiferous inner shelf off Namaqualand between Stompneus Bay and White Point, just north of the Buffels River. *Bulletin of the Geological Survey of South Africa*, **99**, 68 pp.

1stweather (2010)

http://www.1stweather.com. Accessed 15 January 2010

Flikr (2011)

http://www.flikr.com/photos/hilton-t). Accessed 10 February 2011.

NOAA (2010)

http://www.ngdc.noaa.gov/mgg/topo/pictures/AFRICAcolshade.jpg. Accessed 06 April 2010

NOAA (2011)

http://www.pmel.noaa.gov/ocs/ARC/. Accessed 20 September 2011

Redbull BWA (2008)

http://www.redbullbwa.com/photos.php. Accessed 28 June 2011.

Wavescapes (2009)

http://www.wavescape.co.za/photos/old-slideshows/dungeons-the-third-session-in-10-days.html. Accessed 28 June 2011.

Wikitravel (2009)

http://wikitravel.org/en/Diving_the_Cape_Peninsula_and_False_Bay/MV_Aster. Accessed 20 November 2009.

Wikitravel (2009)

http://wikitravel.org/en/Diving_the_Cape_Peninsula_and_False_Bay/MV_Katsu_Maru. Accessed 20 November 2009.

Windfinder (2010)

http://www.windfinder.com. Accessed 16 January 2010

Pers. Comm. Reid, D.L. (2011)

Pers. Comm. Woodborne, M.W. (2011)

13. APPENDIX I – SEDIMENTARY STATISTICS

Sample	Position		Weight Percentages								
	Easting	Northing	$CaCO_3$	Gravel	Vcs	Cs	Ms	Fs	Vfs	Sand	Mud
D2	253783	6227578	96.57	0.16	23.55	67.64	6.41	1.23	0.84	99.68	0.16
D3	251986	6226901	90.1	94.59	5.41	0.00	0.00	0.00	0.00	5.41	0.00
D4	255342	6227473	33.62	1.21	1.21	5.50	41.72	48.08	2.21	98.71	0.08
D5	256172	6227723	48.34	0.00	0.00	0.85	12.45	66.10	20.17	99.57	0.43
D6	251799	6227338	94.71	63.57	32.86	3.57	0.00	0.00	0.00	36.43	0.00
D8	252380	6227022	95.78	89.91	9.97	0.12	0.00	0.00	0.00	10.09	0.00
Off_01	255720	6229068	23.15	0.00	0.44	3.94	13.53	55.89	25.66	99.46	0.54
Off_02	256224	6229068	29.18	0.00	0.00	0.76	6.20	66.77	26.27	100.00	0.00
Off_03	256223	6228568	27.11	0.00	0.00	0.00	2.25	69.83	26.89	98.97	1.03
Off_04	255725	6228568	29.66	0.00	0.87	17.95	68.72	12.20	0.25	100.00	0.00
Off_05	255725	6228066	56.71	0.00	0.00	0.49	9.55	67.34	21.65	99.02	0.98
Off_06	256223	6228068	64.78	0.00	0.05	0.23	4.28	75.38	19.24	99.17	0.83
Off_07	256224	6227564	57.51	0.51	5.72	24.36	62.56	6.52	0.33	99.49	0.00
Off_08	256721	6227563	53.01	0.00	1.25	12.34	56.88	29.25	0.29	100.00	0.00
Off_09	256220	6227062	58.37	0.11	0.90	3.94	20.23	69.35	5.35	99.77	0.11
Off_10	255722	6227068	56.23	0.17	3.11	35.71	58.06	2.73	0.22	99.83	0.00
Off_11	255222	6227070	80.94	5.36	36.92	43.39	13.57	0.70	0.06	94.64	0.00
Off_12	254730	6227068	96.92	18.69	45.96	29.58	5.08	0.42	0.28	81.31	0.00
Off_13	254303	6226993	68.24	0.00	0.22	1.41	12.54	53.62	30.22	98.00	2.00
Off_14	253818	6227095	98.21	80.84	15.84	3.00	0.27	0.05	0.00	19.16	0.00
Off_15	253223	6226563	96.84	0.10	0.67	2.05	7.83	57.78	29.79	98.11	1.79
Off_16	253728	6226569	71.13	0.00	0.00	0.54	3.93	58.78	34.44	97.69	2.31
Off_17	254225	6226566	44	16.18	41.33	38.33	3.82	0.20	0.14	83.82	0.00
Off_18	254723	6226565	96.6	7.57	21.35	55.57	14.35	0.83	0.32	92.43	0.00
Off_19	255224	6226565	79.89	3.14	33.72	47.92	15.22	0.00	0.00	96.86	0.00
Off_20	255724	6226565	55.88	0.00	0.44	4.24	40.07	51.97	3.17	99.89	0.11
Off_21	256225	6226566	40.42	0.00	0.11	1.41	40.54	57.51	0.43	100.00	0.00
Off_22	254721	6226069	56.2	0.00	0.28	1.71	26.23	61.59	9.70	99.51	0.49
Off_23	254226	6226066	68.85	0.00	0.00	0.35	16.89	69.12	13.29	99.65	0.35
Off_24	253728	6226067	74.95	0.00	0.00	0.21	5.14	63.77	29.71	98.83	1.17
Off_25	253229	6226065	75.05	0.00	0.48	0.32	5.76	63.39	28.38	98.32	1.68
Off_26	252780	6226010	72.78	0.00	0.00	0.86	6.78	60.13	30.17	97.94	2.06
Off_27	252726	6225561	78.54	1.64	0.12	0.79	9.60	68.10	19.32	97.93	0.43
Off_28	253228	6225568	72	0.00	0.00	0.14	7.13	76.17	16.02	99.46	0.54
Off_29	253723	6225568	64.93	0.00	0.00	0.15	6.61	77.66	15.14	99.56	0.44
Off_30	254223	6225566	56.34	0.00	0.00	0.13	7.26	81.75	10.61	99.74	0.26
Off_31	254723	6225567	47.91	0.00	0.00	0.28	15.86	78.13	5.59	99.86	0.14
Off_32	255633	6227712	19.62	0.04	0.97	11.19	82.59	4.53	0.69	99.96	0.00
Off_33	255275	6226201	77.69	1.28	18.64	49.04	29.29	1.64	0.11	98.72	0.00
Off_34	255228	6225560	45.78	0.00	0.00	0.58	21.82	72.32	5.21	99.92	0.08
01	255981	6229528	41.5	0.00	2.12	11.63	49.15	34.72	2.38	100.00	0.00
02	255989	6229554	45	0.05	1.10	5.22	35.36	54.26	4.02	99.95	0.00
03	255996	6229572	57.78	0.00	0.17	0.89	52.58	45.72	0.64	100.00	0.00
04	256003	6229588	62.65	2.20	1.30	3.50	58.95	33.83	0.22	97.80	0.00
05	256011	6229609	51.9	0.25	10.05	16.53	51.25	21.75	0.18	99.75	0.00
06	256013	6229646	52.24	0.14	0.28	0.60	54.59	44.01	0.39	99.86	0.00
07	256236	6229509	51.56	0.04	0.92	2.42	61.10	35.27	0.25	99.96	0.00
08	256235	6229492	60.6	0.00	0.00	0.11	41.71	57.71	0.47	100.00	0.00
09	256233	6229473	37.14	0.16	2.07	6.34	46.66	42.58	2.20	99.84	0.00

Sample	Position		Weight Percentages								
	Easting	Northing	$CaCO_3$	Gravel	Vcs	Cs	Ms	Fs	Vfs	Sand	Mud
10	255449	6229479	37.16	0.00	0.14	1.00	21.30	70.53	7.02	100.00	0.00
11	255441	6229494	56.11	0.00	0.00	1.69	49.01	48.07	1.22	100.00	0.00
12	255430	6229512	59.07	0.03	0.00	0.48	42.39	55.74	1.36	99.97	0.00
13	255421	6229525	52.38	0.00	0.09	1.21	49.07	48.51	1.12	100.00	0.00
14	255413	6229538	53.05	0.00	0.00	1.13	51.30	46.41	1.16	100.00	0.00
15	255330	6229448	63.02	0.00	0.00	0.03	34.66	63.60	1.71	100.00	0.00
16	255316	6229473	59.48	0.00	0.00	0.19	29.92	66.34	3.54	100.00	0.00
17	255305	6229502	45.58	0.12	0.08	0.87	35.87	60.39	2.66	99.88	0.00

Sample	Calculated Sedimentary Statistics					
	Mean (Φ)	Mean (mm)	Median (Φ)	Median (mm)	Sorting (σ)	Skewness (sk)
D2	0.33	0.79	0.32	0.80	0.54	0.20
D3	-1.80	3.49	-2.00	4.00	0.31	0.72
D4	1.93	0.26	2.00	0.25	0.62	-0.73
D5	2.45	0.18	2.45	0.18	0.36	-0.34
D6	-1.30	2.46	-1.41	2.66	0.67	1.00
D8	-1.72	3.30	-2.00	4.00	0.41	1.20
Off_01	2.39	0.19	2.53	0.17	0.45	-1.31
Off_02	2.52	0.17	2.64	0.16	0.28	-0.47
Off_03	2.55	0.17	2.69	0.15	0.22	-0.32
Off_04	1.42	0.37	1.42	0.37	0.56	-0.13
Off_05	2.45	0.18	2.45	0.18	0.32	-0.32
Off_06	2.52	0.17	2.55	0.17	0.27	-0.18
Off_07	1.21	0.43	1.28	0.41	0.68	-0.78
Off_08	1.65	0.32	1.66	0.32	0.59	-0.33
Off_09	2.20	0.22	2.23	0.21	0.54	-0.52
Off_10	1.09	0.47	1.13	0.46	0.56	-0.32
Off_11	0.18	0.88	0.15	0.90	0.76	0.12
Off_12	-0.33	1.26	-0.31	1.24	0.86	-0.30
Off_13	2.47	0.18	2.70	0.15	0.44	-0.93
Off_14	-1.61	3.06	-2.00	4.00	0.57	2.41
Off_15	2.48	0.18	2.67	0.16	0.41	-0.86
Off_16	2.59	0.17	2.83	0.14	0.28	-0.33
Off_17	-0.21	1.16	-0.13	1.10	0.83	-1.32
Off_18	0.34	0.79	0.42	0.74	0.82	-2.03
Off_19	0.26	0.83	0.26	0.83	0.71	-0.07
Off_20	1.98	0.25	2.06	0.24	0.56	-0.31
Off_21	2.03	0.24	2.07	0.24	0.41	-0.18
Off_22	2.23	0.21	2.21	0.22	0.46	-0.20
Off_23	2.41	0.19	2.32	0.20	0.40	-0.08
Off_24	2.53	0.17	2.70	0.15	0.22	-0.40
Off_25	2.51	0.18	2.68	0.16	0.30	-0.46
Off_26	2.51	0.18	2.71	0.15	0.33	-0.58
Off_27	2.48	0.18	2.50	0.18	0.37	-0.47
Off_28	2.50	0.18	2.42	0.19	0.34	-0.07
Off_29	2.50	0.18	2.41	0.19	0.34	-0.02
Off_30	2.44	0.18	2.36	0.19	0.34	0.01
Off_31	2.35	0.20	2.29	0.20	0.39	0.05

Sample	Calculated Sedimentary Statistics					
	Mean (Φ)	Mean (mm)	Median (Φ)	Median (mm)	Sorting (σ)	Skewness (sk)
Off_32	1.44	0.37	1.42	0.37	0.43	-0.18
Off_33	0.61	0.66	0.63	0.64	0.71	-0.15
Off_34	2.29	0.20	2.27	0.21	0.45	0.01
01	1.74	0.30	1.79	0.29	0.70	-0.45
02	2.06	0.24	2.10	0.23	0.60	-0.54
03	1.97	0.26	1.96	0.26	0.41	0.01
04	1.87	0.27	1.84	0.28	0.50	-0.66
05	1.36	0.39	1.60	0.33	0.87	-2.20
06	1.96	0.26	1.94	0.26	0.36	0.05
07	1.88	0.27	1.85	0.28	0.42	-0.08
08	2.05	0.24	2.08	0.24	0.35	0.00
09	1.86	0.28	1.92	0.27	0.64	-0.58
10	2.32	0.20	2.31	0.20	0.45	-0.14
11	1.99	0.25	1.99	0.25	0.46	0.01
12	2.05	0.24	2.07	0.24	0.41	0.05
13	1.99	0.25	2.00	0.25	0.43	0.02
14	1.98	0.25	1.97	0.25	0.43	0.05
15	2.10	0.23	2.14	0.23	0.38	0.04
16	2.20	0.22	2.19	0.22	0.44	0.09
17	2.11	0.23	2.14	0.23	0.46	-0.04

14. APPENDIX II – CUMULATIVE GRAIN SIZE CURVES

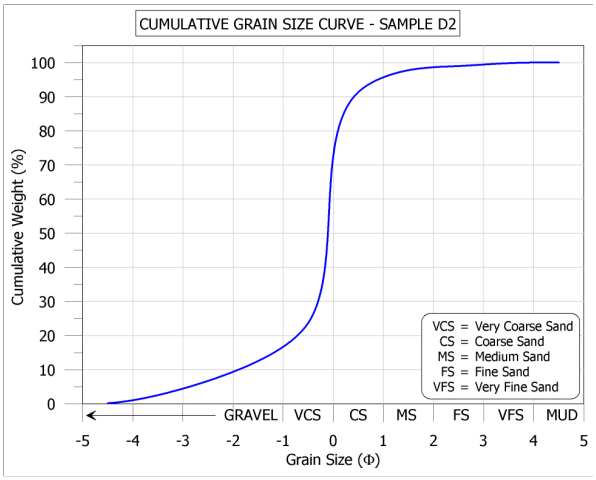
CUMULATIVE GRAIN SIZE CURVE - SAMPLE D2
Cumulative Weight (%)
Grain Size (Φ)
GRAVEL VCS CS MS FS VFS MUD
VCS = Very Coarse Sand
CS = Coarse Sand
MS = Medium Sand
FS = Fine Sand
VFS = Very Fine Sand

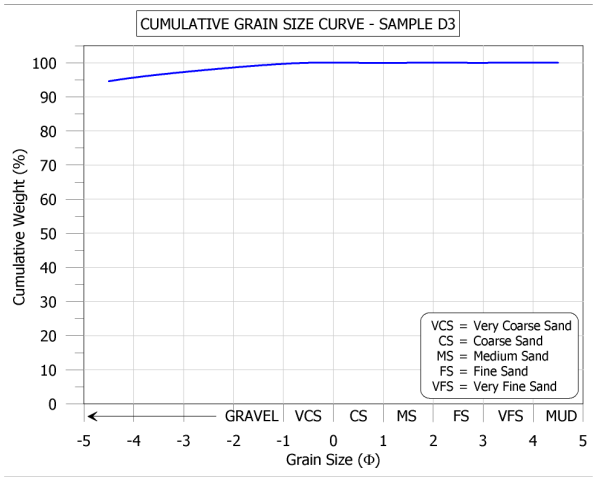
CUMULATIVE GRAIN SIZE CURVE - SAMPLE D3
Cumulative Weight (%)
Grain Size (Φ)
GRAVEL VCS CS MS FS VFS MUD
VCS = Very Coarse Sand
CS = Coarse Sand
MS = Medium Sand
FS = Fine Sand
VFS = Very Fine Sand

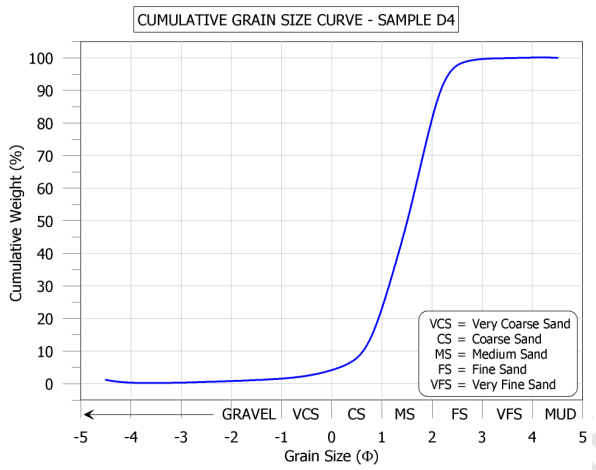
CUMULATIVE GRAIN SIZE CURVE - SAMPLE D4
Cumulative Weight (%)
Grain Size (Φ)
GRAVEL VCS CS MS FS VFS MUD
VCS = Very Coarse Sand
CS = Coarse Sand
MS = Medium Sand
FS = Fine Sand
VFS = Very Fine Sand

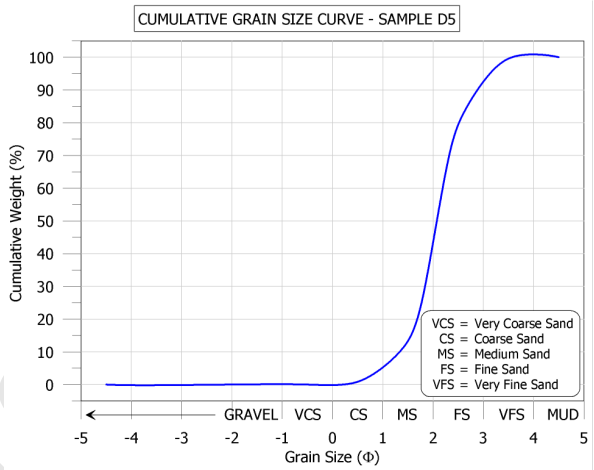
CUMULATIVE GRAIN SIZE CURVE - SAMPLE D5
Cumulative Weight (%)
Grain Size (Φ)
GRAVEL VCS CS MS FS VFS MUD
VCS = Very Coarse Sand
CS = Coarse Sand
MS = Medium Sand
FS = Fine Sand
VFS = Very Fine Sand

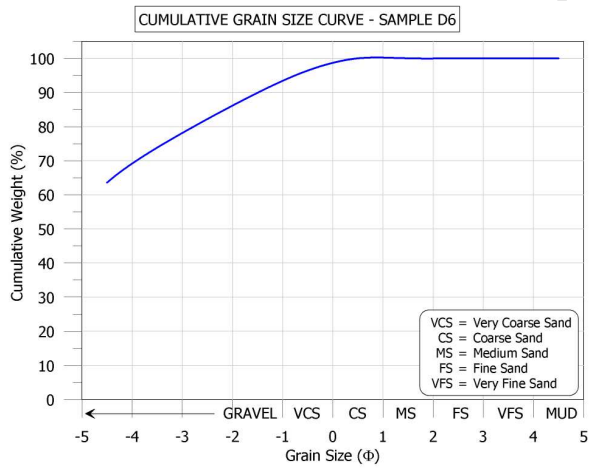
CUMULATIVE GRAIN SIZE CURVE - SAMPLE D6
Cumulative Weight (%)
Grain Size (Φ)
GRAVEL VCS CS MS FS VFS MUD
VCS = Very Coarse Sand
CS = Coarse Sand
MS = Medium Sand
FS = Fine Sand
VFS = Very Fine Sand

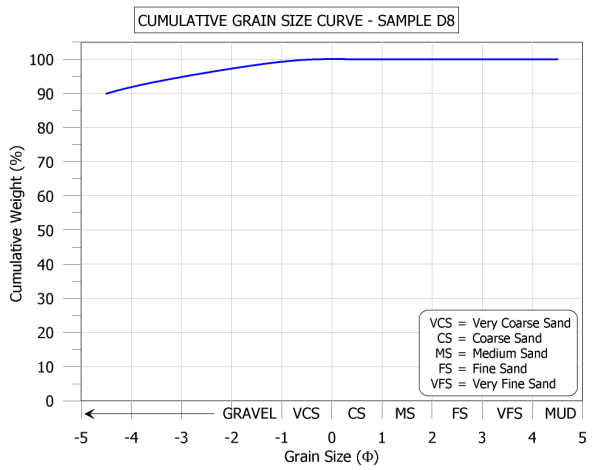
CUMULATIVE GRAIN SIZE CURVE - SAMPLE D8
Cumulative Weight (%)
Grain Size (Φ)
GRAVEL VCS CS MS FS VFS MUD
VCS = Very Coarse Sand
CS = Coarse Sand
MS = Medium Sand
FS = Fine Sand
VFS = Very Fine Sand

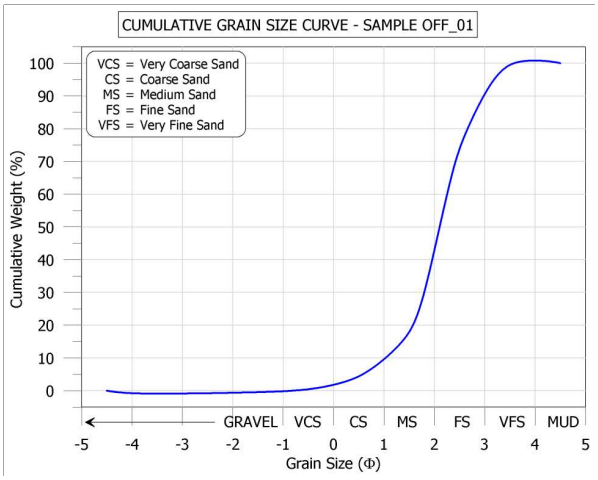
CUMULATIVE GRAIN SIZE CURVE - SAMPLE OFF_01
VCS = Very Coarse Sand
CS = Coarse Sand
MS = Medium Sand
FS = Fine Sand
VFS = Very Fine Sand
Cumulative Weight (%)
GRAVEL VCS CS MS FS VFS MUD
Grain Size (Φ)

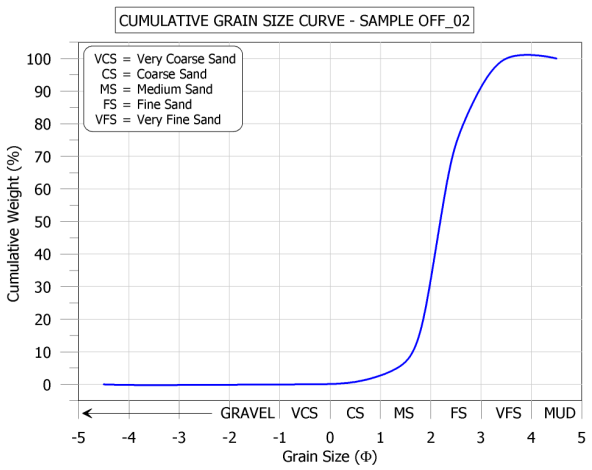
CUMULATIVE GRAIN SIZE CURVE - SAMPLE OFF_02
VCS = Very Coarse Sand
CS = Coarse Sand
MS = Medium Sand
FS = Fine Sand
VFS = Very Fine Sand
Cumulative Weight (%)
GRAVEL VCS CS MS FS VFS MUD
Grain Size (Φ)

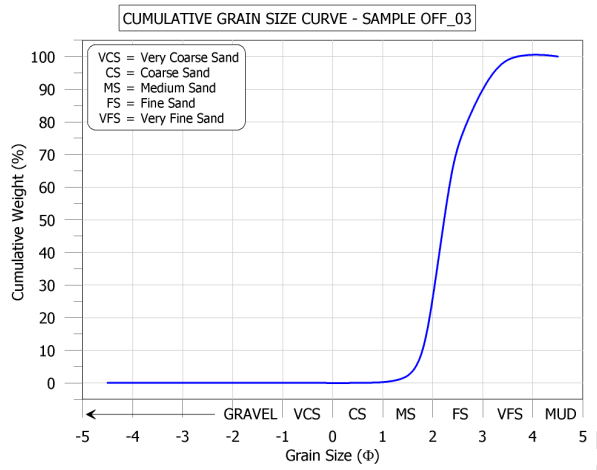
CUMULATIVE GRAIN SIZE CURVE - SAMPLE OFF_03
VCS = Very Coarse Sand
CS = Coarse Sand
MS = Medium Sand
FS = Fine Sand
VFS = Very Fine Sand
Cumulative Weight (%)
GRAVEL VCS CS MS FS VFS MUD
Grain Size (Φ)

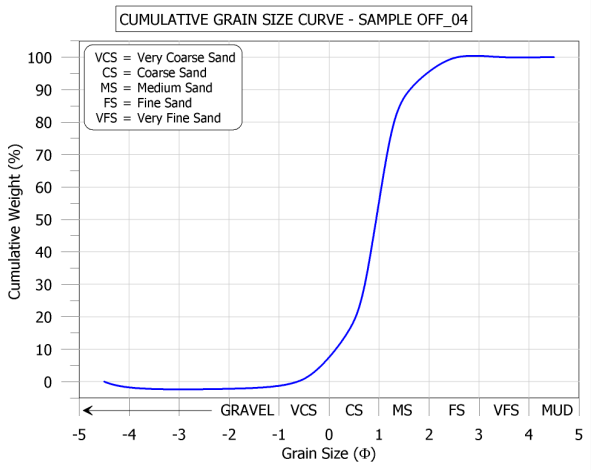
CUMULATIVE GRAIN SIZE CURVE - SAMPLE OFF_04
VCS = Very Coarse Sand
CS = Coarse Sand
MS = Medium Sand
FS = Fine Sand
VFS = Very Fine Sand
Cumulative Weight (%)
GRAVEL VCS CS MS FS VFS MUD
Grain Size (Φ)

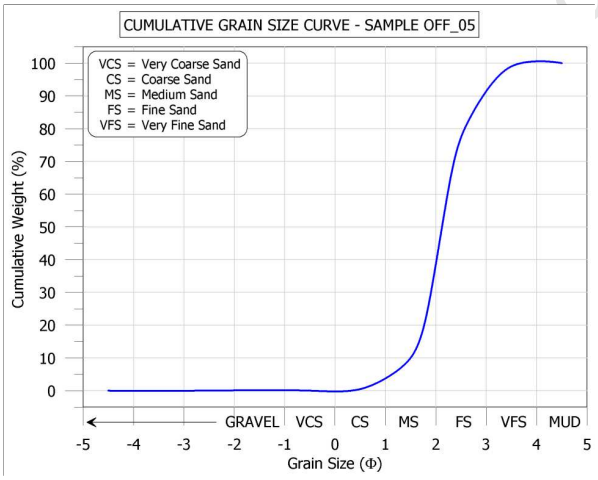
CUMULATIVE GRAIN SIZE CURVE - SAMPLE OFF_05
VCS = Very Coarse Sand
CS = Coarse Sand
MS = Medium Sand
FS = Fine Sand
VFS = Very Fine Sand
Cumulative Weight (%)
GRAVEL VCS CS MS FS VFS MUD
Grain Size (Φ)

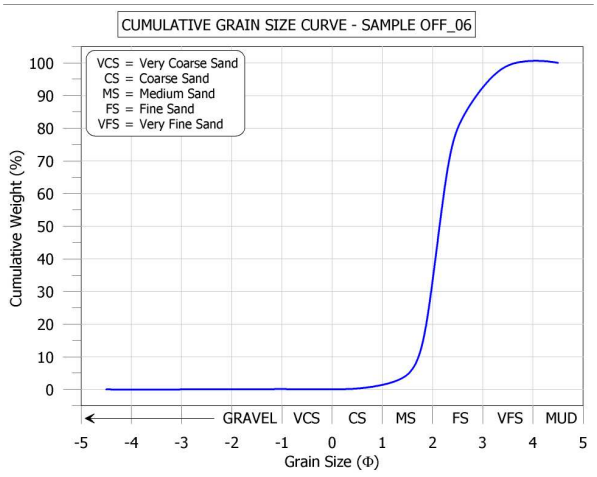
CUMULATIVE GRAIN SIZE CURVE - SAMPLE OFF_06
VCS = Very Coarse Sand
CS = Coarse Sand
MS = Medium Sand
FS = Fine Sand
VFS = Very Fine Sand
Cumulative Weight (%)
GRAVEL VCS CS MS FS VFS MUD
Grain Size (Φ)

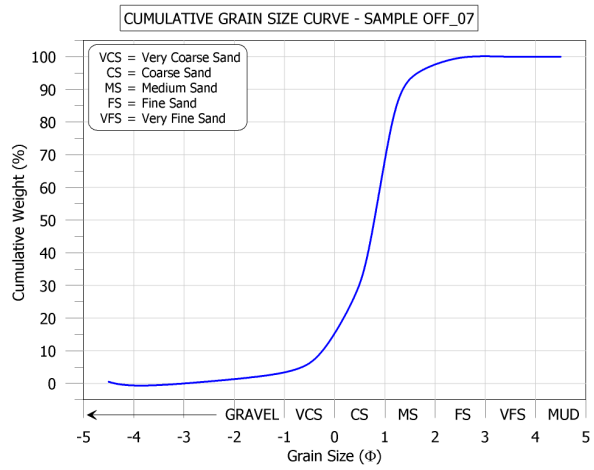
CUMULATIVE GRAIN SIZE CURVE - SAMPLE OFF_07
VCS = Very Coarse Sand
CS = Coarse Sand
MS = Medium Sand
FS = Fine Sand
VFS = Very Fine Sand
Cumulative Weight (%)
GRAVEL VCS CS MS FS VFS MUD
Grain Size (Φ)

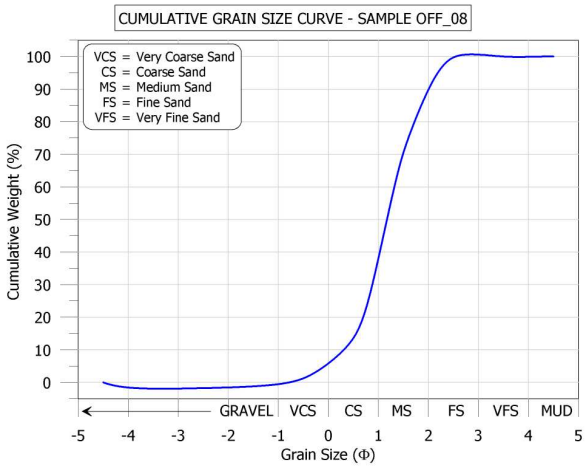
CUMULATIVE GRAIN SIZE CURVE - SAMPLE OFF_08
VCS = Very Coarse Sand
CS = Coarse Sand
MS = Medium Sand
FS = Fine Sand
VFS = Very Fine Sand
Cumulative Weight (%)
GRAVEL VCS CS MS FS VFS MUD
Grain Size (Φ)

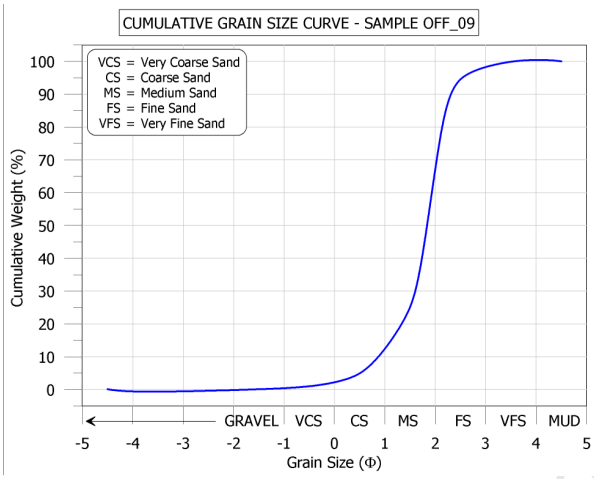
CUMULATIVE GRAIN SIZE CURVE - SAMPLE OFF_09
VCS = Very Coarse Sand
CS = Coarse Sand
MS = Medium Sand
FS = Fine Sand
VFS = Very Fine Sand
Cumulative Weight (%)
GRAVEL VCS CS MS FS VFS MUD
Grain Size (Φ)

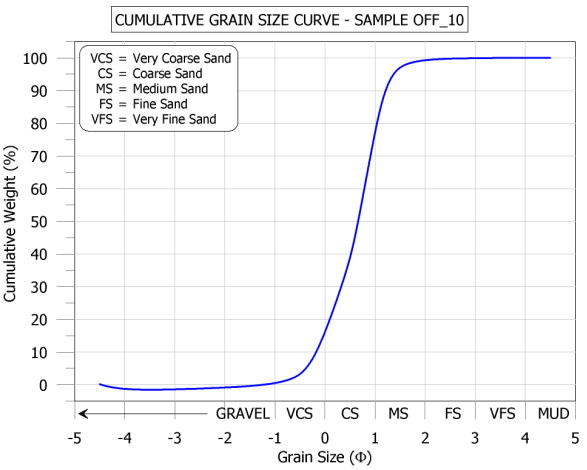
CUMULATIVE GRAIN SIZE CURVE - SAMPLE OFF_10
VCS = Very Coarse Sand
CS = Coarse Sand
MS = Medium Sand
FS = Fine Sand
VFS = Very Fine Sand
Cumulative Weight (%)
GRAVEL VCS CS MS FS VFS MUD
Grain Size (Φ)

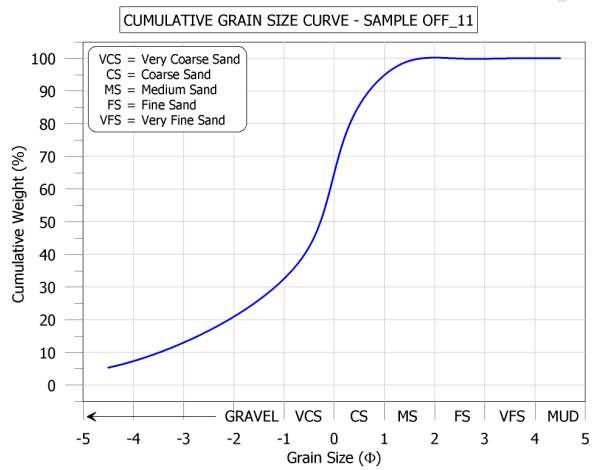
CUMULATIVE GRAIN SIZE CURVE - SAMPLE OFF_11
VCS = Very Coarse Sand
CS = Coarse Sand
MS = Medium Sand
FS = Fine Sand
VFS = Very Fine Sand
Cumulative Weight (%)
GRAVEL VCS CS MS FS VFS MUD
Grain Size (Φ)

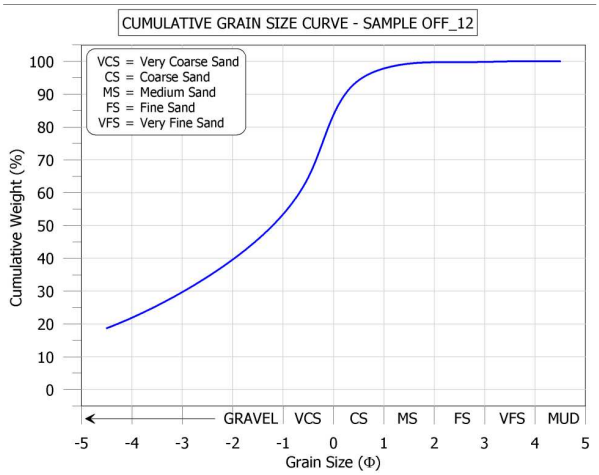
CUMULATIVE GRAIN SIZE CURVE - SAMPLE OFF_12
VCS = Very Coarse Sand
CS = Coarse Sand
MS = Medium Sand
FS = Fine Sand
VFS = Very Fine Sand
Cumulative Weight (%)
GRAVEL VCS CS MS FS VFS MUD
Grain Size (Φ)

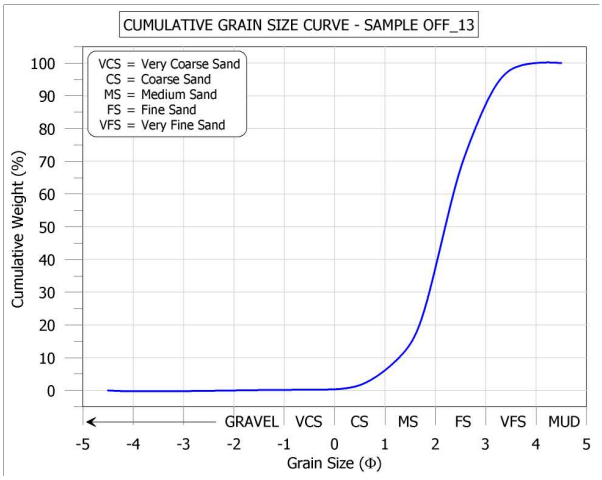
CUMULATIVE GRAIN SIZE CURVE - SAMPLE OFF_13
VCS = Very Coarse Sand
CS = Coarse Sand
MS = Medium Sand
FS = Fine Sand
VFS = Very Fine Sand
Cumulative Weight (%)
GRAVEL VCS CS MS FS VFS MUD
Grain Size (Φ)

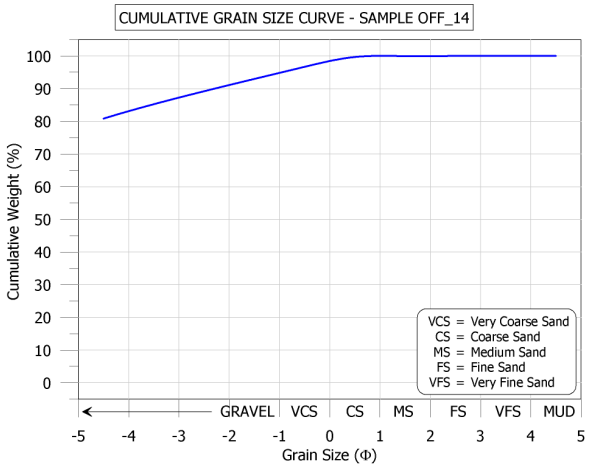
CUMULATIVE GRAIN SIZE CURVE - SAMPLE OFF_14
VCS = Very Coarse Sand
CS = Coarse Sand
MS = Medium Sand
FS = Fine Sand
VFS = Very Fine Sand
Cumulative Weight (%)
GRAVEL VCS CS MS FS VFS MUD
Grain Size (Φ)

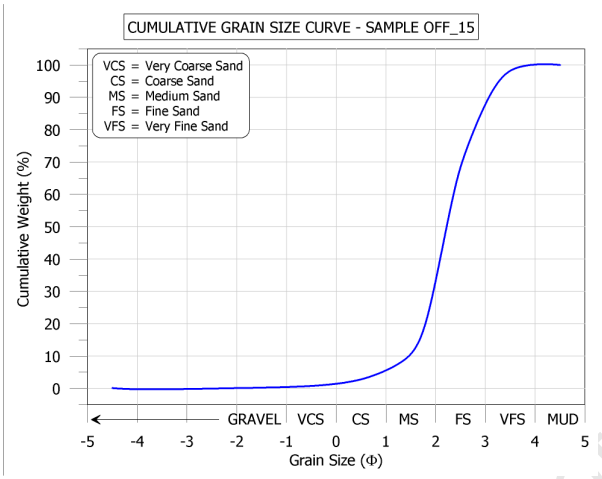
CUMULATIVE GRAIN SIZE CURVE - SAMPLE OFF_15
VCS = Very Coarse Sand
CS = Coarse Sand
MS = Medium Sand
FS = Fine Sand
VFS = Very Fine Sand
Cumulative Weight (%)
GRAVEL VCS CS MS FS VFS MUD
Grain Size (Φ)

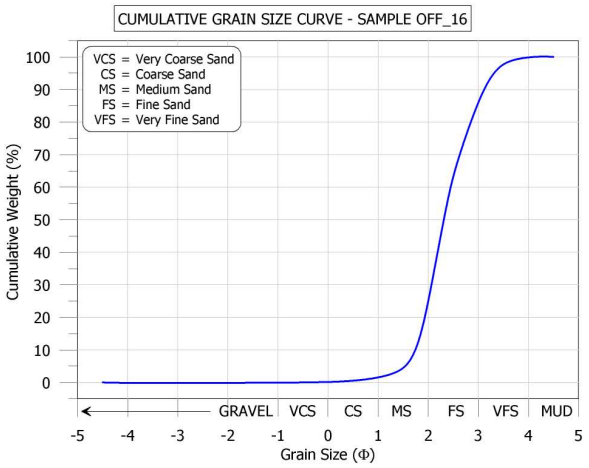
CUMULATIVE GRAIN SIZE CURVE - SAMPLE OFF_16
VCS = Very Coarse Sand
CS = Coarse Sand
MS = Medium Sand
FS = Fine Sand
VFS = Very Fine Sand
Cumulative Weight (%)
GRAVEL VCS CS MS FS VFS MUD
Grain Size (Φ)

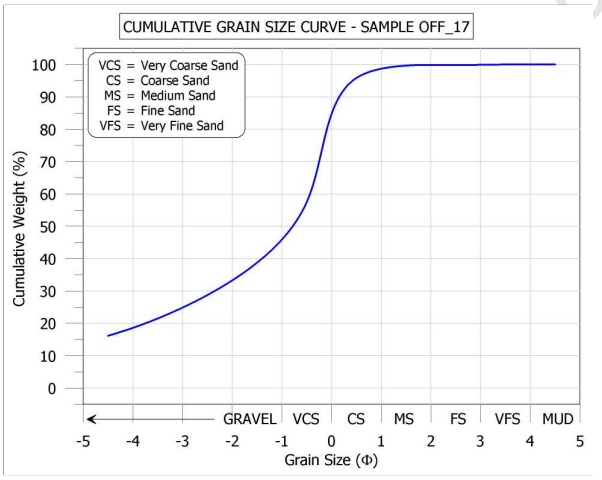
CUMULATIVE GRAIN SIZE CURVE - SAMPLE OFF_17
VCS = Very Coarse Sand
CS = Coarse Sand
MS = Medium Sand
FS = Fine Sand
VFS = Very Fine Sand
Cumulative Weight (%)
GRAVEL VCS CS MS FS VFS MUD
Grain Size (Φ)

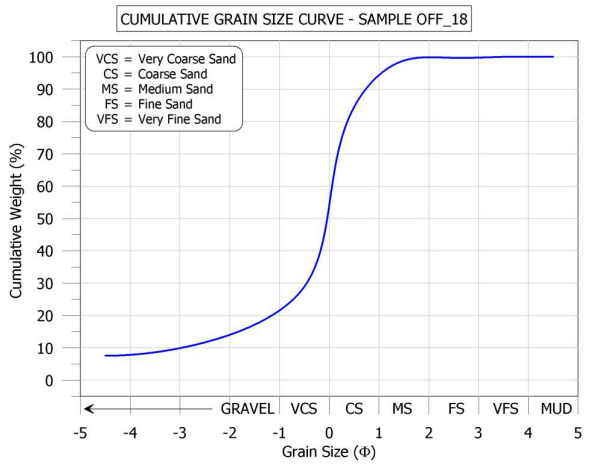
CUMULATIVE GRAIN SIZE CURVE - SAMPLE OFF_18
VCS = Very Coarse Sand
CS = Coarse Sand
MS = Medium Sand
FS = Fine Sand
VFS = Very Fine Sand
Cumulative Weight (%)
GRAVEL VCS CS MS FS VFS MUD
Grain Size (Φ)

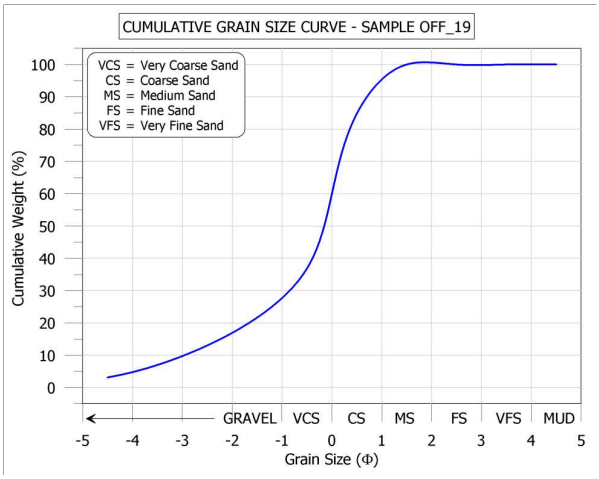
CUMULATIVE GRAIN SIZE CURVE - SAMPLE OFF_19
VCS = Very Coarse Sand
CS = Coarse Sand
MS = Medium Sand
FS = Fine Sand
VFS = Very Fine Sand
Cumulative Weight (%)
GRAVEL VCS CS MS FS VFS MUD
Grain Size (Φ)

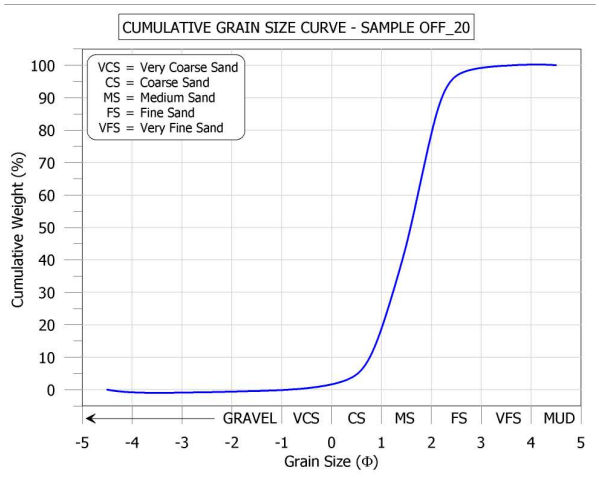
CUMULATIVE GRAIN SIZE CURVE - SAMPLE OFF_20
VCS = Very Coarse Sand
CS = Coarse Sand
MS = Medium Sand
FS = Fine Sand
VFS = Very Fine Sand
Cumulative Weight (%)
GRAVEL VCS CS MS FS VFS MUD
Grain Size (Φ)

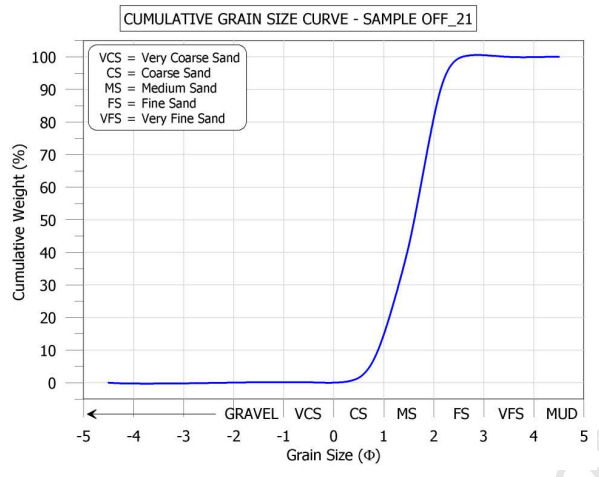
CUMULATIVE GRAIN SIZE CURVE - SAMPLE OFF_21
VCS = Very Coarse Sand
CS = Coarse Sand
MS = Medium Sand
FS = Fine Sand
VFS = Very Fine Sand
Cumulative Weight (%)
GRAVEL VCS CS MS FS VFS MUD
Grain Size (Φ)

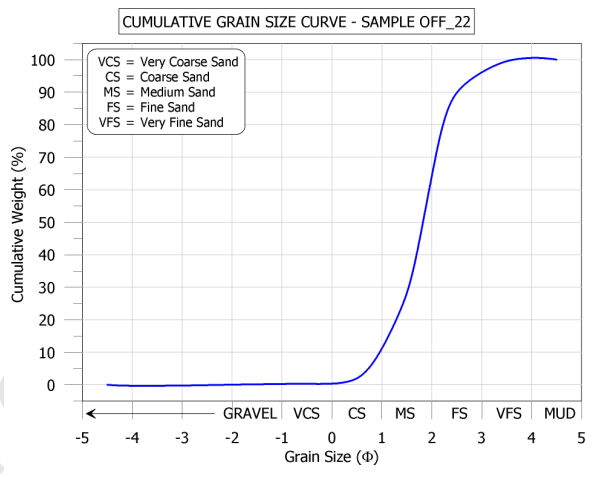
CUMULATIVE GRAIN SIZE CURVE - SAMPLE OFF_22
VCS = Very Coarse Sand
CS = Coarse Sand
MS = Medium Sand
FS = Fine Sand
VFS = Very Fine Sand
Cumulative Weight (%)
GRAVEL VCS CS MS FS VFS MUD
Grain Size (Φ)

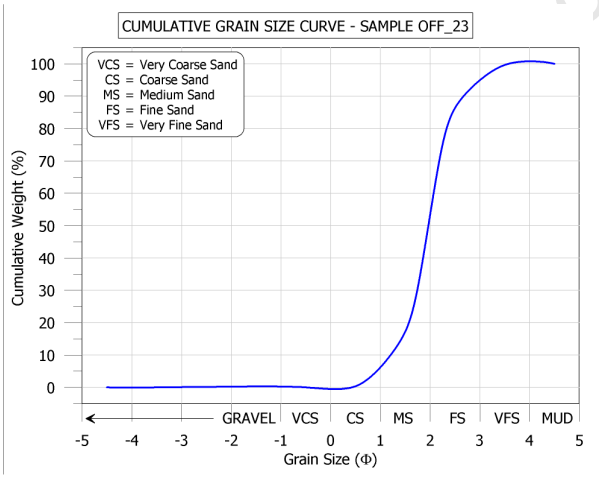
CUMULATIVE GRAIN SIZE CURVE - SAMPLE OFF_23
VCS = Very Coarse Sand
CS = Coarse Sand
MS = Medium Sand
FS = Fine Sand
VFS = Very Fine Sand
Cumulative Weight (%)
GRAVEL VCS CS MS FS VFS MUD
Grain Size (Φ)

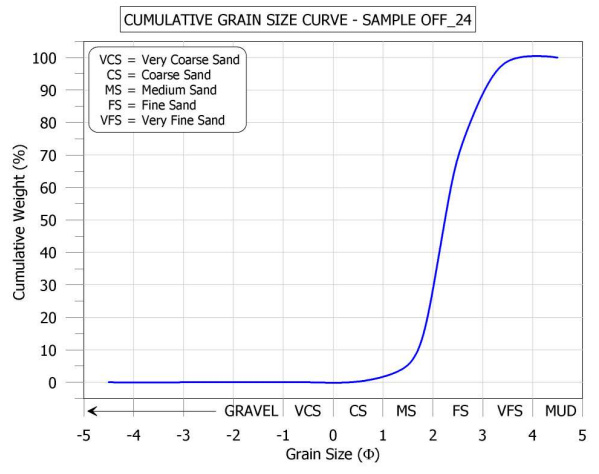
CUMULATIVE GRAIN SIZE CURVE - SAMPLE OFF_24
VCS = Very Coarse Sand
CS = Coarse Sand
MS = Medium Sand
FS = Fine Sand
VFS = Very Fine Sand
Cumulative Weight (%)
GRAVEL VCS CS MS FS VFS MUD
Grain Size (Φ)

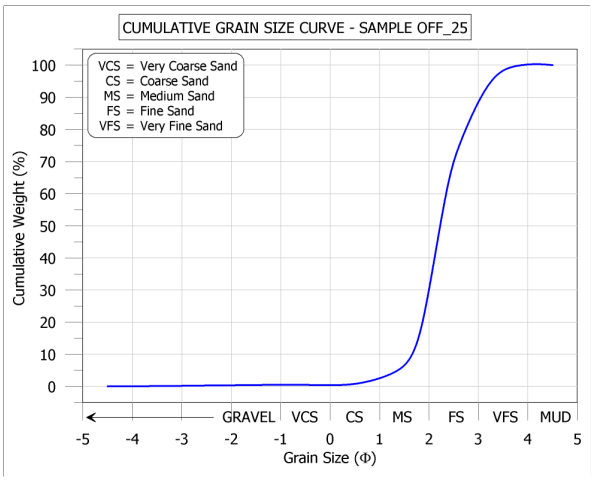
CUMULATIVE GRAIN SIZE CURVE - SAMPLE OFF_25
VCS = Very Coarse Sand
CS = Coarse Sand
MS = Medium Sand
FS = Fine Sand
VFS = Very Fine Sand
Cumulative Weight (%)
GRAVEL VCS CS MS FS VFS MUD
Grain Size (Φ)

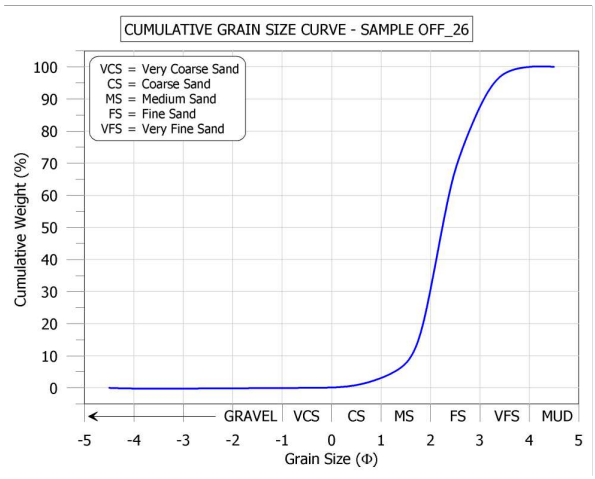
CUMULATIVE GRAIN SIZE CURVE - SAMPLE OFF_26
VCS = Very Coarse Sand
CS = Coarse Sand
MS = Medium Sand
FS = Fine Sand
VFS = Very Fine Sand
Cumulative Weight (%)
GRAVEL VCS CS MS FS VFS MUD
Grain Size (Φ)

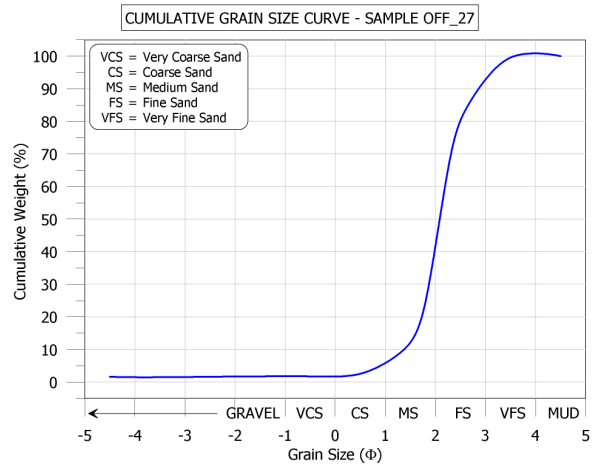
CUMULATIVE GRAIN SIZE CURVE - SAMPLE OFF_27
VCS = Very Coarse Sand
CS = Coarse Sand
MS = Medium Sand
FS = Fine Sand
VFS = Very Fine Sand
Cumulative Weight (%)
GRAVEL VCS CS MS FS VFS MUD
Grain Size (Φ)

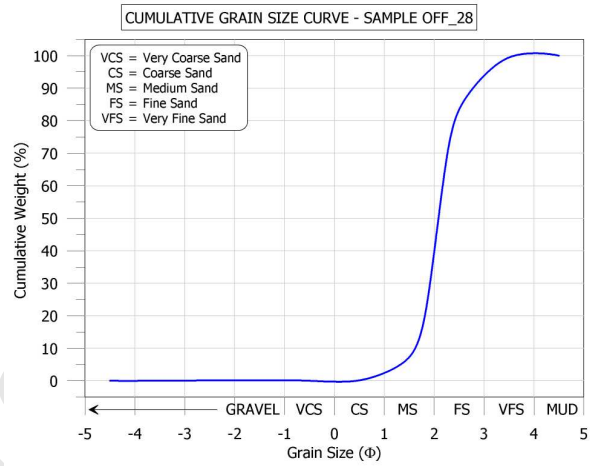
CUMULATIVE GRAIN SIZE CURVE - SAMPLE OFF_28
VCS = Very Coarse Sand
CS = Coarse Sand
MS = Medium Sand
FS = Fine Sand
VFS = Very Fine Sand
Cumulative Weight (%)
GRAVEL VCS CS MS FS VFS MUD
Grain Size (Φ)

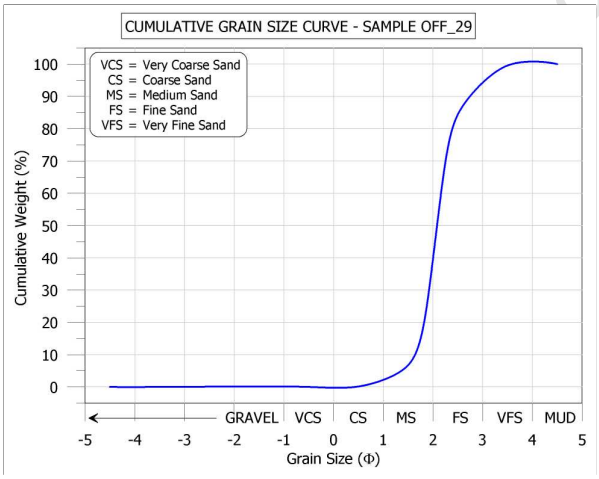
CUMULATIVE GRAIN SIZE CURVE - SAMPLE OFF_29
VCS = Very Coarse Sand
CS = Coarse Sand
MS = Medium Sand
FS = Fine Sand
VFS = Very Fine Sand
Cumulative Weight (%)
GRAVEL VCS CS MS FS VFS MUD
Grain Size (Φ)

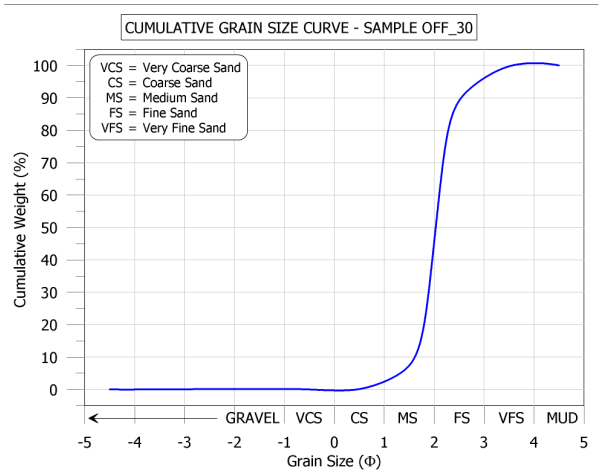
CUMULATIVE GRAIN SIZE CURVE - SAMPLE OFF_30
VCS = Very Coarse Sand
CS = Coarse Sand
MS = Medium Sand
FS = Fine Sand
VFS = Very Fine Sand
Cumulative Weight (%)
GRAVEL VCS CS MS FS VFS MUD
Grain Size (Φ)

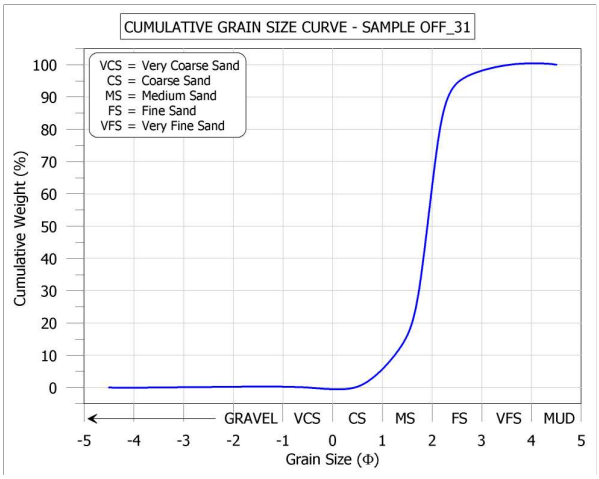
CUMULATIVE GRAIN SIZE CURVE - SAMPLE OFF_31
VCS = Very Coarse Sand
CS = Coarse Sand
MS = Medium Sand
FS = Fine Sand
VFS = Very Fine Sand
Cumulative Weight (%)
GRAVEL VCS CS MS FS VFS MUD
Grain Size (Φ)

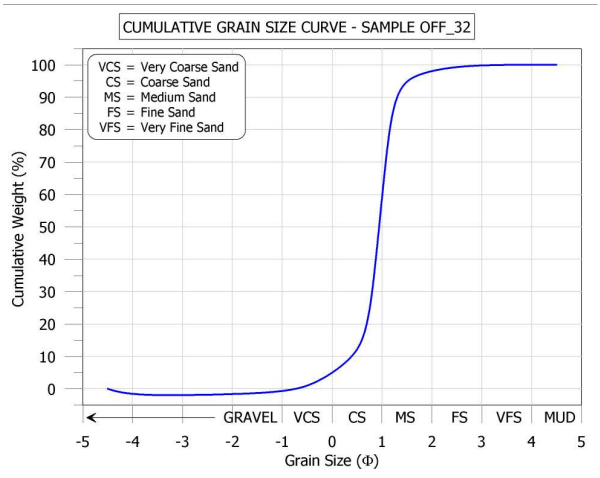
CUMULATIVE GRAIN SIZE CURVE - SAMPLE OFF_32
VCS = Very Coarse Sand
CS = Coarse Sand
MS = Medium Sand
FS = Fine Sand
VFS = Very Fine Sand
Cumulative Weight (%)
GRAVEL VCS CS MS FS VFS MUD
Grain Size (Φ)

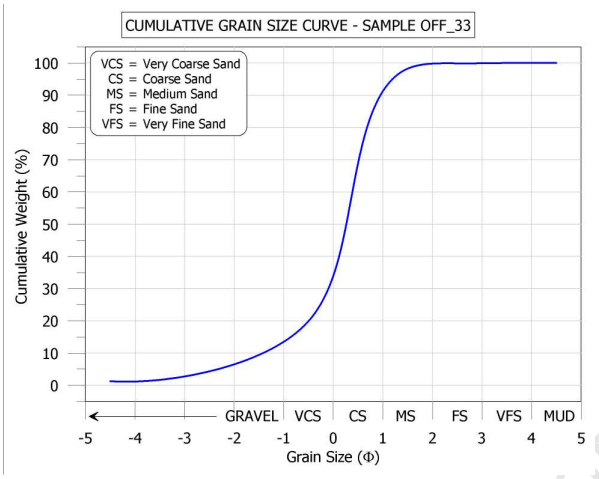
CUMULATIVE GRAIN SIZE CURVE - SAMPLE OFF_33
VCS = Very Coarse Sand
CS = Coarse Sand
MS = Medium Sand
FS = Fine Sand
VFS = Very Fine Sand
Cumulative Weight (%)
GRAVEL VCS CS MS FS VFS MUD
Grain Size (Φ)

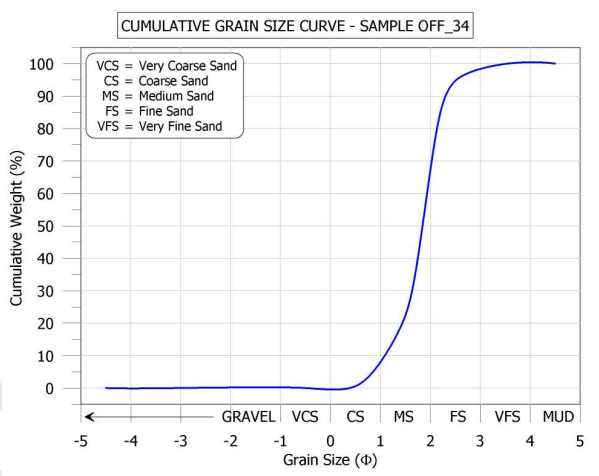
CUMULATIVE GRAIN SIZE CURVE - SAMPLE OFF_34
VCS = Very Coarse Sand
CS = Coarse Sand
MS = Medium Sand
FS = Fine Sand
VFS = Very Fine Sand
Cumulative Weight (%)
GRAVEL VCS CS MS FS VFS MUD
Grain Size (Φ)

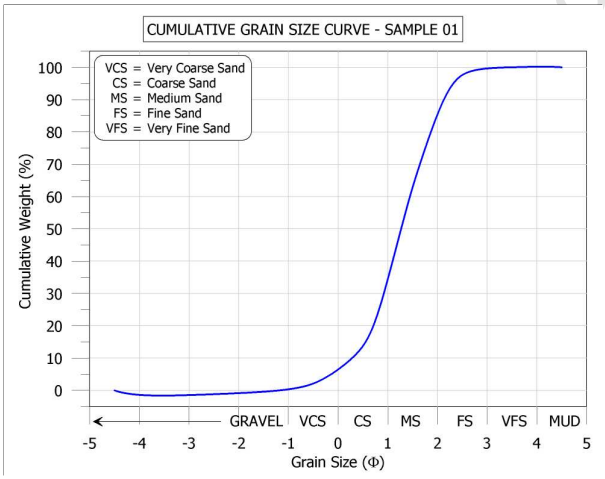
CUMULATIVE GRAIN SIZE CURVE - SAMPLE 01
VCS = Very Coarse Sand
CS = Coarse Sand
MS = Medium Sand
FS = Fine Sand
VFS = Very Fine Sand
Cumulative Weight (%)
GRAVEL VCS CS MS FS VFS MUD
Grain Size (Φ)

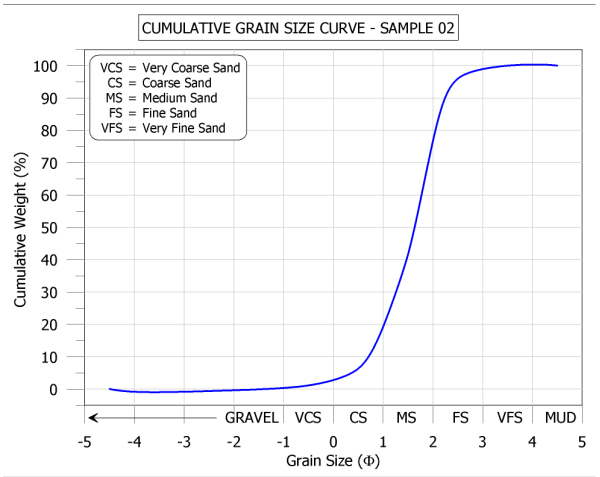
CUMULATIVE GRAIN SIZE CURVE - SAMPLE 02
VCS = Very Coarse Sand
CS = Coarse Sand
MS = Medium Sand
FS = Fine Sand
VFS = Very Fine Sand
Cumulative Weight (%)
GRAVEL VCS CS MS FS VFS MUD
Grain Size (Φ)

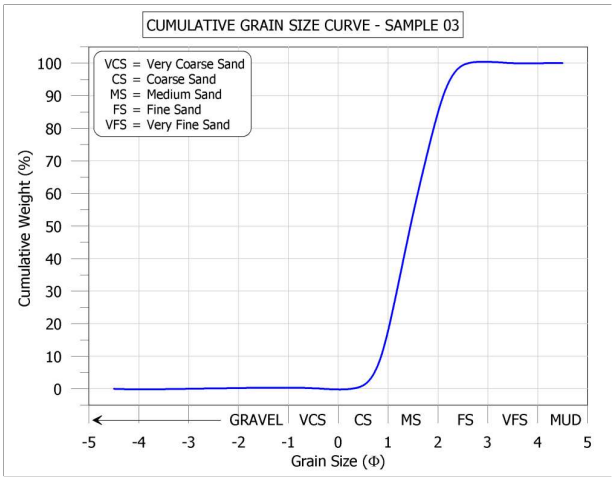
CUMULATIVE GRAIN SIZE CURVE - SAMPLE 03
VCS = Very Coarse Sand
CS = Coarse Sand
MS = Medium Sand
FS = Fine Sand
VFS = Very Fine Sand
Cumulative Weight (%)
GRAVEL VCS CS MS FS VFS MUD
Grain Size (Φ)

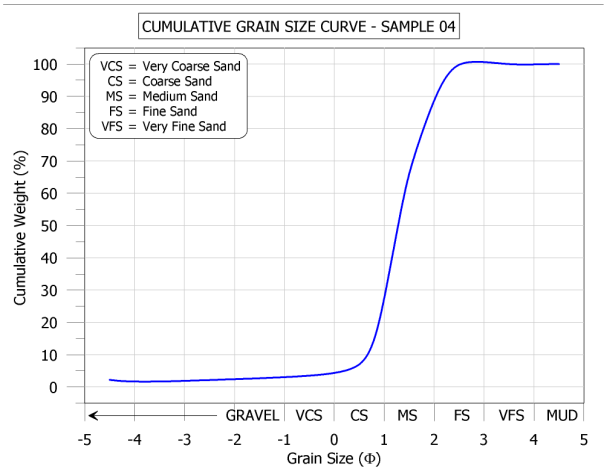
CUMULATIVE GRAIN SIZE CURVE - SAMPLE 04
VCS = Very Coarse Sand
CS = Coarse Sand
MS = Medium Sand
FS = Fine Sand
VFS = Very Fine Sand
Cumulative Weight (%)
GRAVEL VCS CS MS FS VFS MUD
Grain Size (Φ)

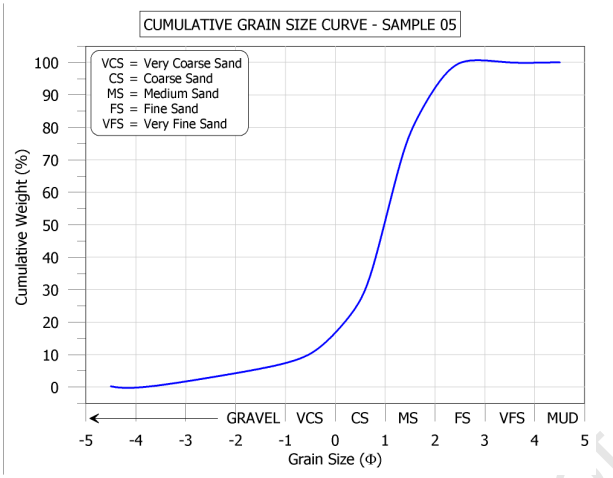
CUMULATIVE GRAIN SIZE CURVE - SAMPLE 05
VCS = Very Coarse Sand
CS = Coarse Sand
MS = Medium Sand
FS = Fine Sand
VFS = Very Fine Sand
Cumulative Weight (%)
GRAVEL VCS CS MS FS VFS MUD
Grain Size (Φ)

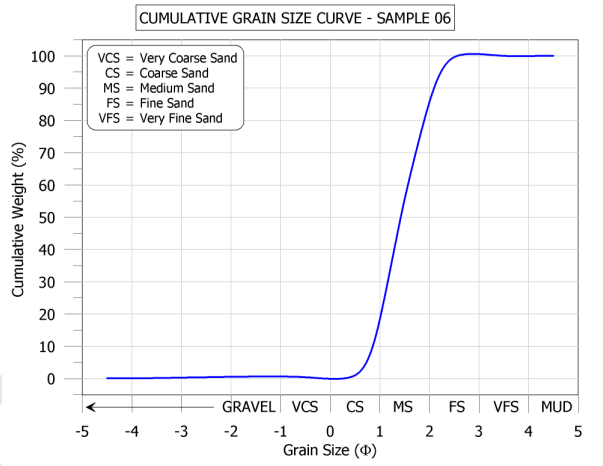
CUMULATIVE GRAIN SIZE CURVE - SAMPLE 06
VCS = Very Coarse Sand
CS = Coarse Sand
MS = Medium Sand
FS = Fine Sand
VFS = Very Fine Sand
Cumulative Weight (%)
GRAVEL VCS CS MS FS VFS MUD
Grain Size (Φ)

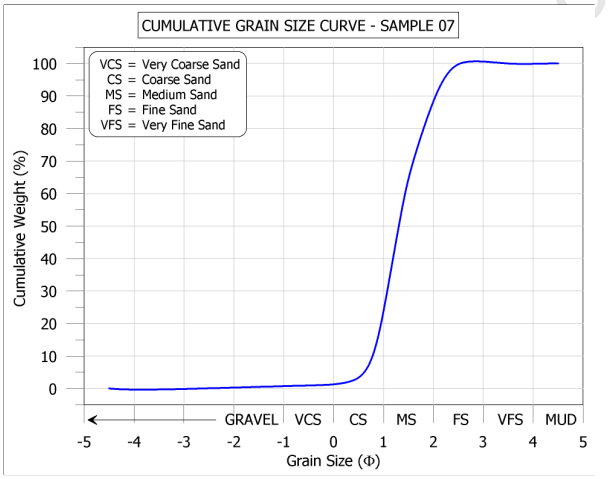
CUMULATIVE GRAIN SIZE CURVE - SAMPLE 07
VCS = Very Coarse Sand
CS = Coarse Sand
MS = Medium Sand
FS = Fine Sand
VFS = Very Fine Sand
Cumulative Weight (%)
GRAVEL VCS CS MS FS VFS MUD
Grain Size (Φ)

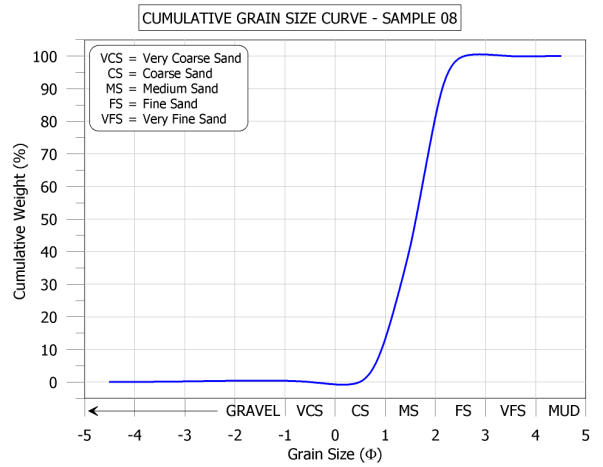
CUMULATIVE GRAIN SIZE CURVE - SAMPLE 08
VCS = Very Coarse Sand
CS = Coarse Sand
MS = Medium Sand
FS = Fine Sand
VFS = Very Fine Sand
Cumulative Weight (%)
GRAVEL VCS CS MS FS VFS MUD
Grain Size (Φ)

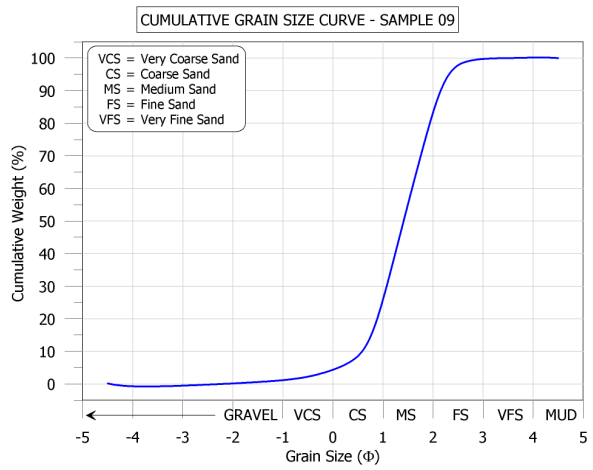
CUMULATIVE GRAIN SIZE CURVE - SAMPLE 09
VCS = Very Coarse Sand
CS = Coarse Sand
MS = Medium Sand
FS = Fine Sand
VFS = Very Fine Sand
Cumulative Weight (%)
GRAVEL VCS CS MS FS VFS MUD
Grain Size (Φ)

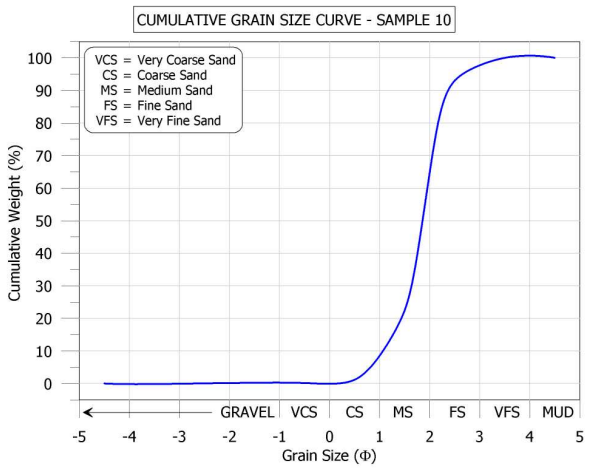
CUMULATIVE GRAIN SIZE CURVE - SAMPLE 10
VCS = Very Coarse Sand
CS = Coarse Sand
MS = Medium Sand
FS = Fine Sand
VFS = Very Fine Sand
Cumulative Weight (%)
GRAVEL VCS CS MS FS VFS MUD
Grain Size (Φ)

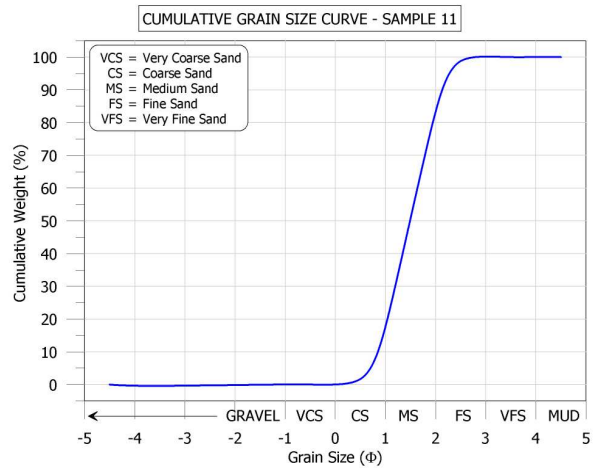
CUMULATIVE GRAIN SIZE CURVE - SAMPLE 11
VCS = Very Coarse Sand
CS = Coarse Sand
MS = Medium Sand
FS = Fine Sand
VFS = Very Fine Sand
Cumulative Weight (%)
GRAVEL VCS CS MS FS VFS MUD
Grain Size (Φ)

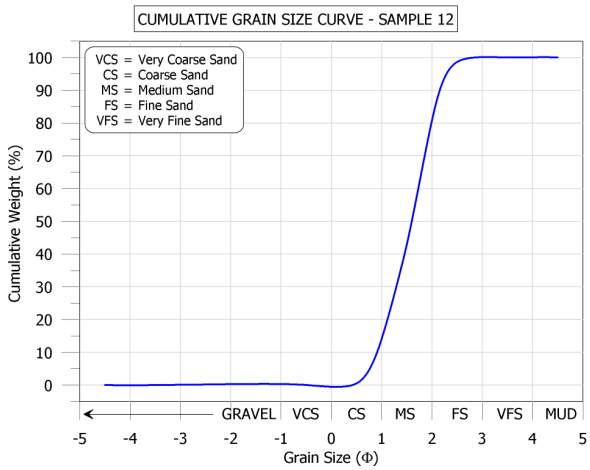
CUMULATIVE GRAIN SIZE CURVE - SAMPLE 12
VCS = Very Coarse Sand
CS = Coarse Sand
MS = Medium Sand
FS = Fine Sand
VFS = Very Fine Sand
Cumulative Weight (%)
GRAVEL VCS CS MS FS VFS MUD
Grain Size (Φ)

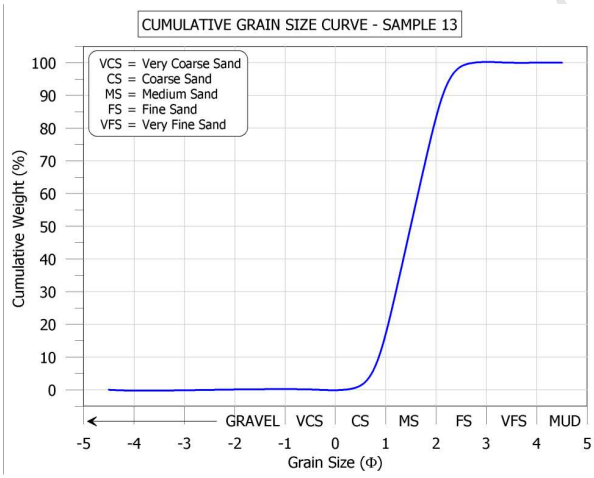
CUMULATIVE GRAIN SIZE CURVE - SAMPLE 13
VCS = Very Coarse Sand
CS = Coarse Sand
MS = Medium Sand
FS = Fine Sand
VFS = Very Fine Sand
Cumulative Weight (%)
GRAVEL VCS CS MS FS VFS MUD
Grain Size (Φ)

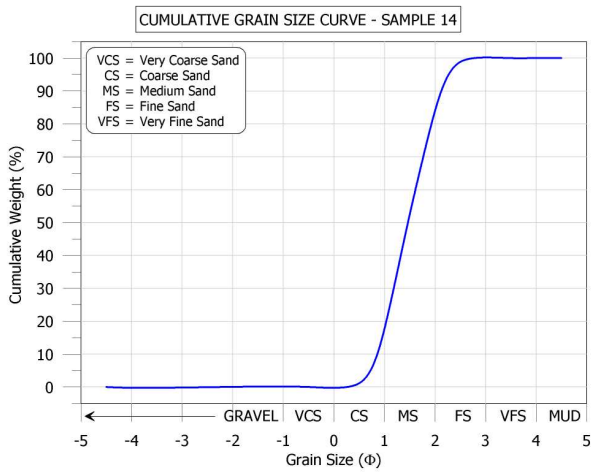
CUMULATIVE GRAIN SIZE CURVE - SAMPLE 14
VCS = Very Coarse Sand
CS = Coarse Sand
MS = Medium Sand
FS = Fine Sand
VFS = Very Fine Sand
Cumulative Weight (%)
GRAVEL VCS CS MS FS VFS MUD
Grain Size (Φ)